THE KINETICS OF PHOTO-COLLOIDAL SYSTEMS

A thesis submitted for the degree of DOCTOR OF PHILOSOPHY of the University of London and for the DIPLOMA OF MEMBERSHIP of Imperial College.

By

ESMAIEL SAIEVAR-IRANIZAD B.Sc., M.Sc.

Chemistry Department

Imperial College

London SW7 2AY

August 1987

ABSTRACT

This thesis is concerned with the photophysical and photoelectrochemical behaviour of colloidal semiconductors such as cadmium sulfide. CdS can absorb a significant fraction of the solar spectrum and is an efficient photosensitiser for various chemical reactions.

The kinetics study of the semiconductor/solution interface demonstrated a complex kinetic behaviour of electron transfer reaction, which was explained by the "Gaussian Model". This model provided a valuable explanation of the kinetics of heterogeneous systems which are not simple firts-order or second-order but result from a distribution of first-order rate constants. In the case of colloidal semiconductors, a relationship was obtained between the dispersed kinetics and the dispersed radii of colloidal particles.

Our studies in photocolloidal systems extended to wide band gap semiconductor colloids such as zinc sulfide (ZnS). The photophysical and photochemical behaviour of doped and undoped-zinc sulfide were investigated in more detail.

In the case of CdS colloids particular features of its surface chemistry using time-resolved techniques, the desorption of the dimer of cationic radical methyl viologen, $(MV^{+})_2$, from the surface of CdS particles into the bulk of solution and the deramatic effect of cysteine concentration, as an electron donor, on the yield of methyl viologen photoreduced by the conduction band electrons of CdS colloids are investigated.

A new method has been developed for the synthesis of CdS

particles in inexpensive matrices such as Dialysis Membrane. Using this system, we produced small CdS particles (diameter < 5nm) immobilised within the DM to keep them from coagulating. This system enables us to remove CdS film from solution for analysis of the reaction product and regeneration of the uniform semiconductor particles. The studies of both photophysical properties, such as quantisation effect, and photochemical behaviour, such as photoreduction of methyl viologen, photo-oxidation of methyl orange, photocorrosion and stabilisation of CdS film using steady-state and photolysis techniques, have revealed that the method is an excellent media for studying photo(-electro)chemical reactions and the factors which control the rate of interfacial charge transfer.

Finally attempt to immobilise CdS on an electrode modified by polypyrrole as a conducting polymer are discussed.

LEARN THE KNOWLEDGE FROM CRADLE TO THE GRAVE

PROPHET MOHAMMED (S.A.A)

TO:

IMAM ROUHOLLAH

ACKNOWLEDGEMENTS

I would like to thank the following people for their help in various aspects of this thesis.

Professor W J Albery, FRS, and Dr J R Darwent for all their tolerant supervision, guidance and encouragement.

All the members of the research groups in Imperial College and Birkbeck College, particularly Dr A F Geins, G P Brown and A Lepre in BC and C Boxall and Dr B Verity in IC for their assistance and interesting discussions.

Dr B Verity for his proof reading.

Miss D Dobson for producing the typed manuscript.

The Islamic Republic of IRAN (TABRIZ UNIVERSITY) for their financial support to enable me to pursue my higher degree.

Unilever Research plc for their six months CASE Award.

Finally, my wife, children and parents for their unquestioning support, constant encouragement and patience.

Abbreviations

A^{o}	Angstrom
CB	Conduction band
CLS	Conventional light scattering
CTAB	Cetyltrimethylammonium bromide
cys	Cysteine
DDW	Double distilled water
DLS	Dynamic light scattering
DM	Dialysis membrane
EDTA	Ethylenediaminetetra acetic acid
E_F	Fermi level
E_{gap}	Energy of band gap
FP	Flash photolysis
L_D	Debye length
M	mol dm^{-3}
MO	Methyl Orange
MV^{2+}	Methyl Viologen
NHE	Normal hydrogen electrode
OD	Optical density (Absorbance)
PAA	Polyacrylamide
PPy	Polypyrrole
PVA	Polyvinyl alcohol
PVP	Poly(2-vinyl)pyridine
SCE	Saturated calomel electrode
SEM	Scanning electron microscope
SHMP	Sodium hexametaphosphate
SS	Steady state

TBAT	Tetrabutylammoniumtetrafluoroborate
TEM	Transmission electron microscope
V	Volt, vacancy
VB	Valence band
$\bar{e}_t$	Trapped electron
h^+_t	Trapped hole
λ	Wavelengths
ε	Extinction coefficient, dielectric constant
χ	Electron affinity
$\bar{e}_{CB}$	Electron of conduction band
h^+_{VB}	Hole of valence band

TABLE OF CONTENTS

	Page No.
ABSTRACT	2
ACKNOWLEDGEMENTS	5
ABBREVIATIONS	6
LIST OF FIGURES	15
LIST OF TABLES	26
LIST OF APPENDICIES	27
CHAPTER 1: INTRODUCTION	
1.1. The Nature of Colloids	29
1.1.1 Classification of Colloidal Systems	30
1.1.2 Preparation of Colloidal Dispersion	33
1.1.2.1 Condensation Methods	35
1.1.2.2 Dispersion Methods	35
1.2 The Optical Properties of Colloids	37
1.2.1 Light Absorption	37
1.2.2 Light Scattering	38
1.2.2.1 Conventional Light Scattering (CLS)	39
1.2.2.2 Dynamic Light Scattering (DLS)	40
1.3 The Electrical Properties of Colloids	43
1.3.1 Electrical Properties of Colloids	43
1.3.2 Electrophoresis	47
1.4 Colloidal Semiconductors	47
1.4.1 Energy Bands	50

1.4.2 The Types of Semiconductors 51

1.4.3 The Fermi Level 55

1.4.4 Macroscopic and Microscopic Semiconductor Electrodes 57

1.4.5 Flat Band Potential 62

1.4.6 Semiconductor/Electrolyte Interface 66

1.4.7 Photo-Induced Electron Transfer Reactions 69

1.4.8 Solar Conversion Efficiency 70

1.5 Conclusion 74

1.6 Outline of This Thesis 75

CHAPTER 2: EXPERIMENTAL 76

2.1 Instrumentation 76

2.1.1 Steady-State Techniques 76

2.1.2 Conventional Flash Photolysis 76

2.1.3 Laser Flash Photolysis 79

2.1.4 Dynamic Light Scattering 82

2.1.5 Absorption Spectroscopy 82

2.1.6 Emission Spectroscopy 85

2.1.7 Electron Microscope 89

2.1.7.1 TEM 89

2.1.7.2 SEM 90

2.1.8. The RRDE Apparatus 90

2.1.8.1 Electrodes 91

2.1.8.2 Electronics 91

2.1.8.3 Rotation System 97

2.1.8.4 Electrochemical cell 101

2.1.9 Light Source 101

2.2 Sample Preparation 104

2.2.1 Colloidal CdS 104

2.2.2 Colloidal CdS/pt 104

2.2.3 CdS Film 104

2.2.3.1 Polymers 104

2.2.3.2 Dialysis Membrane 105

2.2.4 Colloidal ZnS 105

2.3 Materials 106

CHAPTER 3: TIME-RESOLVED PHOTOREDOX REACTIONS OF COLLOIDAL CdS

INTRODUCTION 108

3.1 Photoabsorption in CdS 108

3.2 Photoluminescence of CdS 112

3.2.1 the quenching effect 117

3.2.1.1 Fe^{3+} Ions 118

3.2.1.2 Pt Colloids 118

3.2.1.3 Sonicating Effect 122

3.2.1.4 Doping Effect 123

3.3 Photobleaching 123

3.4 Kinetics of Electron Transfer Reactions 129

3.5 Photoreduction of MV^{2+} and O_2 140

3.6 Conclusion 146

CHAPTER 4: TIME-RESOLVED SURFACE EFFECTS IN CdS COLLOIDS

INTRODUCTION 147

4.1 Desorption of Dimer From CdS Surface 148

4.2 Cysteine Effect on the Yield of MV^+ 164

4.3 pH Effect 165

4.4 Pt Effect 168

4.5 Flash Intensity Effect 172

4.5.1 At Various pH 172

4.5.2 Photodegradation 174

4.6 Conclusion 175

CHAPTER 5: PHOTOCHEMISTRY OF ZnS COLLOIDS

INTRODUCTION 178

5.1 Photophysical Properties of Undoped ZnS 179

5.1.1 Absorption Spectrum 179

5.1.2 The Fluorescence of ZnS 180

5.1.2.1 Quenching Effect 183

5.1.2.2 The Kinetics of Quenching 186

5.2 Photophysical Properties of Doped ZnS 188

5.2.1 Absorption Spectrum 188

5.2.2 Fluorescence Spectrum 190

5.2.3 Aging Effect 194

5.2.4 Photodegradation 197

5.3 Kinetics Study 199

5.4 Conclusion 200

CHAPTER 6: PHOTOPHYSICAL AND PHOTOCHEMICAL PROPERTIES OF CdS IMMOBILISED WITHIN DIALYSIS MEMBRANE

INTRODUCTION 201

6.1 CdS in Polymer 203

6.2 CdS in Dialysis Membrane 204

6.3 Photophysical Properties 208

6.3.1 Absorption 208

6.3.1.1 The Effect of Concentration 211

6.3.1.2 The Effect of Preparation Method 211

6.3.2. Emission 217

6.3.2.1 The Effect of Water 220

6.4 Photochemical Properties 222

6.4.1 Luminescence Quenching 222

6.4.2 Flash Photolysis Experiments 226

6.4.3 Steady-State Experiments 232

6.4.3.1 Photoreduction of MV^{2+} 232

6.4.3.2 Photocorrosion of CdS film 238

6.4.3.3 Quantisation Effect 241

6.4.3.4 Stabilisation of CdS film 244

6.4.3.5.1 Cysteine effect 246

6.4.3.5.2 MV^{2+} Effect 251

6.4.3.5.3 Both MV^{2+} and Cysteine Effect 252

6.4.3.5.4 Polyphosphate Effect 252

6.4.3.5.5 Both Polyphosphate and MV^{2+} Effect 253

6.5 Conclusion 254

CHAPTER 7: MODIFIED ELECTRODE

INTRODUCTION 258

7.1 Chemical Modification of Electrodes 258

7.2 Preparation Techniques 259

7.2.1 Chemisorption 259

7.2.2 Covalent Attachment 261

7.2.3 Polymer Film 261

7.3 Characterisation 263

7.3.1 Electrochemical Method 264

7.3.2 Spectroscopic Techniques 264

7.3.3 Other Methods 264

7.4 Applications 266

7.4.1 Electrocatalysis 266

7.4.2 Electronic Devices 267

7.4.3 Batteries 267

7.4.4 Photoelectrochemical Applications 268

7.5 Experimentals 269

7.5.1 Electrodes 269

7.5.2 Cell Assembly 270

7.5.3 Purification 270

7.6 Incorporation of CdS in Polypyrrol Modified Electrode 270

7.6.1 Coating Procedure 271

7.6.2 Results 274

7.7 Conclusion 276

Appendicies

Appendix 1 277

Appendix 2 281

Appendix 3 286

Appendix 4 290

Appendix 5 295

References 296

LIST OF FIGURES

Page No.

CHAPTER 1

Fig. 1.1 Cross section of a spherical or cylindrical micelle with counterions. 34

Fig. 1.2 Schematic diagram of nucleation process C_s: solubility, C^*: critical supersaturation. 36

Fig. 1.3 Decay of the autocorrelation function $g(\tau)$, in dynamic light scattering experiments. 44

Fig. 1.4 The model of double layers.
a) Helmholtz Model
b) Gouy-Chapman Model
c)Stern Model. 48

Fig. 1.5 Energy bands of solid particles (a represents an atom). 50

Fig. 1.6 Diagram of bands in metals and semiconductors. 52

Fig. 1.7 The CdS lattice at T=0 and T>0 K (Formation of conduction band electrons, e^-_{CB}, and valence band holes, h^+_{VB}. 53

Fig. 1.8 Formation of electron donor (ED) and electron acceptor (EA) levels with the forbidden region. 56

Fig. 1.9 Schematic Fermi level (E_F) of semiconductors. 58

Fig. 1.10 Potential distribution and Fermi levels in a macroscopic planar electrode and spherical particle (microscopic colloidal electrode). 60

Fig. 1.11 Schematic diagram of Energy levels for semiconductor-electrolyte junction

V_H: potential drop at Helmholtz layer

E_g: the semiconductor band gap

χ: electron affinity

ϕ_{sc}: semiconductor work function

V_B: Band bending

E_{FB}: Flat band potential. 63

Fig. 1.12 Experimental Flat band potential for CdS $V_{FB}=-(0.47\pm0.02)V$. 65

Fig. 1.13 Schematic potential distribution at a metal macroscopic semiconductor and colloidal semiconductor/electrolyte interface. 67

Fig. 1.14 The distribution of the solar spectrum outside the Earth's atmosphere (AM=0) and at normal incidence to the Earth's surface (AM=1). 71

Fig. 1.15 Theoretical conversion efficiency as a function of band gap energy. 73

CHAPTER 2

Fig. 2.1 Microsecond Flash Photolysis Apparatus. 78

Fig. 2.2 Analysis of transients. 80

Fig. 2.3 The Cr^{3+} energy levels in the ruby laser (3-level laser). 81

Fig. 2.4 Schematic of Dynamic Light Scattering (DLS). 83

Fig. 2.5 Energy levels of diatomic molecule. 84

Fig. 2.6 Schematic diagram of absorption spectroscopy. 86

Fig. 2.7 Schematic diagram of luminescence spectroscopy. 87

Fig. 2.8 Cross section of a RRDE. 92

Fig. 2.9 The three electrode system. 93

Fig. 2.10 An Op-amp. 95

Fig. 2.11 Voltage follower. 95

Fig. 2.12 Voltage inverter. 95

Fig. 2.13 Summing inverter amplifier. 96

Fig. 2.14 A potentiostat. 97

Fig. 2.15a A Triangular Wave Generator. 98

Fig. 2.15b A Power supply for Triangular Wave Generator. 99

Fig. 2.16 Voltage Source. 100

Fig. 2.17 Schematic diagram of the electrochemical cell. 102

Fig. 2.18 A light source. 103

CHAPTER 3

Fig. 3.1 The electronic transitions upon the absorption of a photon by the semiconductor. 110

Fig. 3.2 Absorption spectrum of colloidal CdS (5.10^{-4} M)/SHMP(10^{-3} M) at pH=7.5. 111

Fig. 3.3 Luminescence emission from CdS colloids (a) prepared from H_2S(———) and (b) prepared from Na_2S(------); CdS 5.10^{-3} M, SHMP 10^{-2} M. 114

Fig. 3.4 Luminescence quenching of CdS(5.10^{-4} M)/SHMP (10^{-3} M) by Fe^{3+}(5.10^{-5} M). 119

Fig. 3.5 Luminescence quenching of CdS(5.10^{-4} M)/SHMP (10^{-3} M) by Pt($1.5.10^{-5}$ M) colloids. 121

Fig. 3.6 Sonicating effect on the luminescen of CdS colloids. 124

Fig. 3.7 (a) Ground state absorption spectrum (———) and derived transient spectrum 10 ms after photoflash(------), (b) Transient difference spectrum 10 ms after photoflash for N_2 purged CdS(5.10^{-4} M), SHMP 10^{-3} M at pH 7.5. 125

Fig. 3.8 Variation in initial absorption (ΔA_o) with flash intensity for CdS (5.10^{-4} M), SHMP 10^{-3} M at pH 7, (a) alone (—●—) and (b) with 5.10^{-2} m cysteine (—○—). 128

Fig. 3.9 Recovery of absorption at 485nm for CdS, (A) for CdS alone: (ΔA_o) was -0.09 (○), -0.13 (●), -0.19 (◒) and (B) for CdS plus cysteine (10^{-2} M): (ΔA_o) was -0.08 (○), -0.13 (●), -0.17 (◒). The curve was calculated from equation (3.31) with $\gamma=2x\varrho$ 2x0.7 for (A) and $\gamma = 2x\varrho = 2x0.8$ for (B). 130

Fig. 3.10 Oscilloscope traces for formation of MV^+ at 605nm (A) and recovery of absorbance at 485nm (B) for a colloid containing CdS (5.10^{-3} M), cys (10^{-2} M) and MV^{2+} (5.10^{-6} M). 135

Fig. 3.11 Decay of the autocorrelation function of G(t) from Dynamic laser light scattering for CdS. The curve was calculated from equation (3.35) with $\rho = \gamma = 0.7$. 138

Fig. 3.12 Variation in rate constants for recovery at 485nm with O_2 (—○—) and MV^{2+} (—●—) ;concentrations and conditions as for Figure 3.7 plus 10^{-2} M cysteine. 141

CHAPTER 4

Fig. 4.1 Photoreduction of MV^{2+} (10^{-6} M) by CdS(5.10^{-4} M)/SHMP(10^{-3} M) as a function of flash intensity. 150

Fig. 4.2 Transient absorption spectrum of photoreduced MV^{2+}(4.10^{-3} M) by CdS (10^{-3} M) immediately after photoflash (O) and again 3 ms later (●). 152

Fig. 4.3 Oscilloscope traces of A) absorbance of photoreduced MV^{2+} at 605 nm and B) recovery of absorbance at 485 nm for a colloid containing CdS(5.10^{-4} M) and MV^{+2} (4.10^{-3} M). 154

Fig. 4.4 Desorption of dimers, $(MV^{+})_2$, from CdS surface, CASE I & CASE IV. 160

Fig. 4.5 Desorption of dimers, $(MV^{+})_2$, from CdS surface, CASE II. 162

Fig. 4.6 Desorption of dimers, $(MV^{+})_2$, from CdS surface, CASE III. 163

Fig. 4.7 Cysteine effect on the yield of photo-reduced MV^{2+}. 166

Fig. 4.8 Oscilloscope trace of photoreduced MV^{2+} after adding cysteine. 167

Fig. 4.9 pH-effect on the yield of photoreduced MV^{2+}. 169

Fig. 4.10 The effect of flash intensity on the yield of MV^{+}. 173

Fig. 4.11 The effect of platinum on the yield of photodegradation of CdS colloids. 176

CHAPTER 5

Fig. 5.1 Absorption spectrum of undoped ZnS ($5x10^{-3}$M). 181

Fig. 5.2 Fluorescence spectrum of undoped ZnS. 182

Fig. 5.3 Fluorescence quenching of ZnS. 184

Fig. 5.4 The effect of MV^{2+} on the fluorescence intensity. 185

Fig. 5.5 Stern-Volmer plot (●) and Poisson plot (O) of ZnS fluorescence quenching by MV^{2+}. 187

Fig. 5.6 Absorption spectrum of ZnS (5×10^{-3} M) doped with 10% Mn^{2+}. 189

Fig. 5.7 Fluorescence spectrum of ZnS (5×10^{-3} M) doped with 10% Mn^{2+}. 191

Fig. 5.8 Luminescence mechanism for colloidal ZnS emission. 193

Fig. 5.9 Aging effects on the emisson spectrum of ZnS doped with 2% Tb^{3+}/10% Mn^{2+}. 195

Fig. 5.10 Irradiation effect on the fluorescence intensity of 2% Tb^{3+}-doped ZnS. 198

CHAPTER 6

Fig. 6.1 (a) Absorption and (b) emission spectra of CdS (5×10^{-3} M) incorporated into 1% PVA. 205,206

Fig. 6.2 Absorption spectrum of CdS (10^{-2} M) immobilised in the DM. 209

Fig. 6.3 The concentration effect on the absorption onset of CdS film. 212

Fig. 6.4 The effect of preparation method on the absorption spectrum of CdS film. (b) prepared by H_2S, (a) by Na_2S. 215

Fig. 6.5 Emission spectrum of CdS film (5×10^{-2} M). 218

Fig. 6.6 Water effect (---) on the emission spectrum of dry(——) CdS film. 221

Fig. 6.7 Water effect (---) on the absorption spectrum of dry(——) CdS film. 223

Fig. 6.8 Poisson plot of quenching effect on the red emission of CdS film. 225

Fig. 6.9 Oscilloscope traces of MV^{+}, photoreduced from MV^{2+}(4×10^{-3} M) by CdS film(10^{-2} M) at (a) 395 and (b) 605nm using nanosecond laser flash photolysis. 228

Fig. 6.10 Absorption transient of MV^{+}, photoreduced from MV^{2+}(10^{-2} M) by CdS film(10^{-2} M) using microsecond flash. 230

Fig. 6.11 The yield of MV^{+}, photoreduced from MV^{2+} (4×10^{-3} M) by CdS film(10^{-2} M) immediately after microsecond flash as a function of methyl viologen concentration. 233

Fig. 6.12 Absorption spectrum of MV^{+}, photoreduced from MV^{2+} (1.5×10^{-4}M) by CdS film(10^{-2} M) as a function of time using steady-state techniques (900W Xenon lamp). 235

Fig. 6.13 The yield of MV^{+}, photoreduced from MV^{2+} by CdS film(10^{-2}M) as a function of time in SS techniques. 237

Fig. 6.14 Absorption spectrum of MV^{+}, photoreduced from MV^{2+}(10^{-3}moldm^{-3}) by CdS film (10^{-2} M) using 450nm monochromatic irradiation. 239

Fig. 6.15 Photodegradation of CdS film(10^{-2} M) in the presence of oxygen. 240

Fig. 6.16 The effect of O_2 on the yield of MV^{+}, photoreduced from MV^{2+} (10^{-3} M) by CdS film(10^{-2} M). 242

Fig. 6.17 Cysteine (10^{-2} M) effect on the photo-corrosion of CdS film (0.1 M). 245

Fig. 6.18 Absorption spectrum of methyl orange (5×10^{-5} M). 247

Fig. 6.19 Photo-oxidation of methyl orange(5×10^{-5} M) by CdS film(10^{-2} M). 248

Fig. 6.20 Absorption change of photo-oxidised methyl orange (4×10^{-5} M) as a function of time. CdS within film (10^{-3} M) and ZNO colloids(7.5×10^{-3} M). 250

Fig. 6.21 Poly phosphate (SHMP = 10^{-2} M) effect on the photo-oxidation of methyl orange by

CdS film(10^{-2} M) in the presence of MV^{2+} ($6x10^{-4}$ M). 255

Fig. 6.22 Supported CdS effect on the photo-oxidation of MO($5x10^{-5}$ moldm^{-3}). 256

CHAPTER 7

Fig. 7.1 Schematic diagram of mediated electron transfer at a chemically-modified electrode. 260

Fig. 7.2 Schematic diagram of an electrode modified by covalent attachment techniques. 262

Fig. 7.3 The ideal cyclic voltammogram of a monolayer of material. 265

Fig. 7.4 The structure of polypyrrole. 272

Fig. 7.5 Cyclic voltammogram of Pt-electrode modified by PPy. 275

APPENDICES

Fig. A3.1 Plotting log y vs log t. 289

Fig. A4.1 Calculation of dimer extinction coefficient. 292

LIST OF TABLES

1.1 Types of colloidal systems. 31

1.2 Properties of some important semiconductors. 54

2.1 Materials. 107

3.1 Decay constants (k_z) for recovery at 485 nm. 139

6.1 The effect of Cd^{2+} ions and preparation method on λ_{th}. 214

6.2 The emmision spectra maximum of different CdS film. 219

APPENDICIES

1. Sinclair Basic programme used to analayse the kinetics data in terms of first and second order reactions using a least squares fit. 277

2. Sinclair Basic programme used to fit two exponentials to the kinetics data in chapter 3. 281

3. Homogeneous dimer equiliberium case (Transport Model). 286

4. Homogeneous dimer case (using absorbance). 290

5. Calculation of the dimer extinction coefficient. 295

REFERENCES 296

CHAPTER 1

INTRODUCTION

Since it is clear that our fossil and nuclear fuel reserves are limited and must eventually be consumed; much attention has been focussed over the past ten to fifteen years on renewable energy resources.

Solar energy is one of these resources and its application in different ways dates back to the period of thousands of years before Christ.[1] While it is true that many energy sources such as hydroelectric, tidal, wave and wind energy are indirectly related to the solar energy, this thesis is concerned with the direct trapping of solar radiation.

The sun as a "furnace" radiates large amounts of energy into space every day through thermonuclear fusion of hydrogen atoms; the earth receives approximately 10^{19}kj per day which is one billionth of the sun's total energy. This enormous amount of energy will in a few days equal the total known reserves of conventional energy on the earth's surface. However, if we can trap only a small fraction of this energy flux, the world's critical energy problem would be solved.

Solar energy has many advantages in comparison with other energy sources, it is free, easily available and clean. Its exploitation is a field that involves many branches of science and technology including physics, chemistry, biology, mathematics; mechanical, electrical, chemical engineering;

agriculture and economics.

In recent years the promotion of photochemical and photoelectrochemnical reactions by colloidal particles[2-6] and their application in conversion of solar energy into electrical and chemical energy[7-16] has received much attention. It is worthwhile studying the nature of colloids as a neglected dimension[17] to increase our understanding about these systems and their exploitation in future technology.

1.1 The Nature of Colloids[18-21]

A dispersion of small particles of one substance in another is called a colloid. The word colloid (Greec Koll, glue; - oeides, like) was introduced first by Graham[22] in 1861 to refer to material that diffused slowly and would not pass through parchment. Graham from the slow diffusion and the lack of crystallinity of all colloidal systems concluded that colloid particles are larger than 1nm and from the fact that the same colloid solutions under normal gravity sediment very slowly if at all argued that the size of particles can not be larger than 1μm. For instance Michael Faraday[23] reduced a gold chloride solution with phosphorus to produce colloidal gold sol (Faraday sols), whose particles had a radius of about 3nm.

Colloidal systems, in which the particles are aggregates of many atoms or particles, are too small to see with the eye or with the ordinary optical microscope, and can easily pass through most filters. But they can be detected by electron microscopy,

light scattering, sedimentation and osmosis. Particles smaller than 1 nm approach true solution, such as sugar or salt in water, where the particles consist of individual molecules or ions. On the other hand particles larger than 1μm, which consist of more than one molecule, are colloidal suspensions and can be seen at least by ordinary microscope. A sharp distinction between true solutions, colloidal dispersions and suspensions cannot be drawn.

The most important feature of colloidal systems is the large ratio of surface area to volume. For example, a 1cm cube of material has a surface area of $6cm^2$; but when it is dispersed into small cube of side 10nm, typical of colloidal systems, 1cm cube = $(10^6)^3$ 10nm cubes and 10nm square = $(10^{-6})^2$cm square, therefore the total surface area of 10^{18} small cubes is $10^{18}x6x10^{-12} = 6x10^6 cm^2$. This simple calculation shows that the surface area has increased by a factor of one million. Owing to this large area, surface effects are very important in determining colloidal properties such as the surface potential and adsorption.

1.1.1 Classification of Colloidal Systems

A true solution is a one phase system, since the solute particles are individual molecules or ions; but a simple colloidal dispersion is a two-phase system, since each particle contains a definite separation surface between its dispersed phase (the phase formed by particles) and dispersion medium (the medium, in which the particles are dispersed). The name given to

the colloid depends on the nature of both phases, which may be gaseous, liquid or solid.

Since gases are completely miscible, it is impossible to have a gas-in-gas colloid, but all other combinations are possible and eight different colloids are listed in Table 1.1 with general names and examples for each colloidal system.

TABLE 1.1: TYPES OF COLLOIDAL SYSTEMS

Dispersed Phase	Dispersion Medium	Name of System	Examples
Gas	Liquid	Foam	Soap solution, whipped cream
Gas	Solid	Solid Foam	Pumice, floating soap, expanded polystyrene
Liquid	Gas	Liquid aerosol	Fog, mist, liquid spray
Liquid	Liquid	Emulsion	Milk, mayonnaise
Liquid	Solid	Solid emulsion	Opal, pearl, jelly
Solid	Gas	Solid aerosol	Smoke, dust
Solid	Liquid	Sol, colloidal suspension	Gold in water, toothpaste
Solid	Solid	Solid suspension	Ruby glass, pigmented plastic

In this classification the most important types of colloidal systems are sols and emulsions. Sols are dispersion of solids in liquid.

Colloids with a liquid dispersison medium can also be classified as solvent attracting (Lyophilic) or solvent repelling (Lyophobic). The term hydrophobic was first used by Jean Baptiste persin in 1905 to denote a dispersed phase, such as gold or cadmium sulphide, which has a low affinity for water; but it is now applied in surface chemistry to a water-repellent surface. Lyophilic (liquid loving) sols have a strong affinity between the dispersed phase and dispersion medium and are therefore thermodynamically much more stable. They behave as a true solution of macromolecular material (natural or synthetic), and are reversible, in the sense that after separations of solute from solvent they can easily be reconstituted.

Lyophobic (Greek: solvent-fearing) sols are thermodynamically unstable owing to their low affinity for water (high surface free energy). They are irreversible systems, in that they are not easily converted to the same state after phase separation.

It is possible to change the Lyophilic surface to Lyophobic and vice versa. For example by coating wax on the surface of clean glass, one may convert a hydrophilic surface into a hydrophobic one. Alternatively by the addition of proteins to an oil-in-water emulsion, a hydrophobic system can be changed to a hydrophilic one; this is achieved by the protein molecules adsorbing on the oil droplet surfaces.

The last class of colloidal systems are Association colloids (sometimes called colloidal electrolytes) which are thermodynamically stable. These types of colloids consist of

soap solutions and other amphipolar substances. These are molecules which contain both a non-polar part (such as a hydrocarbon or fluorocarbon) and a water-compatible polar part. The polar substance may be anionic, as in $C_{12}H_{25}OSO_3^-Na^+$, or cationic, as in $C_{16}H_{33}N(CH_3)_3^+\ Br^-$ or non-ionic, as in $C_9H_{19}(C_6H_4)O(CH_2CH_2O)_8H$. Above a certain concentration in aqueous solution a number of these molecules (20 or more) aggregate and form micelles which are association colloids, and shown in Figure 1.1. The non-polar (hydrocarbon) parts of antipolar micelles are insoluble in water and thus come together and form a separate phase, the nucleus of the micelle. The growth of particles stops when the polar groups have surrounded the non-polar nucleus, thereby minimizing the contact of water to hydrocarbon. Inverse micelles can be made from the same substances in non-polar solvents, but in this case the polar parts form the nucleus of the micelle.

When micelles or inverse micelles take up other molecules inside, we have the phenomenon of stabilization. If a relatively large droplet with radius of 10nm or more is formed, this is called a microemulsion.

1.1.2 Preparation of Colloidal Dispersions

Colloidal dispersions can be made by a variety of methods. They can be classified as intrinsic or extrinsic colloids. Intrinsic colloids are usually soluble substances which readily form dispersion colloids such as sols in contact with a suitable dispersion medium. For example a colloidal solution of starch

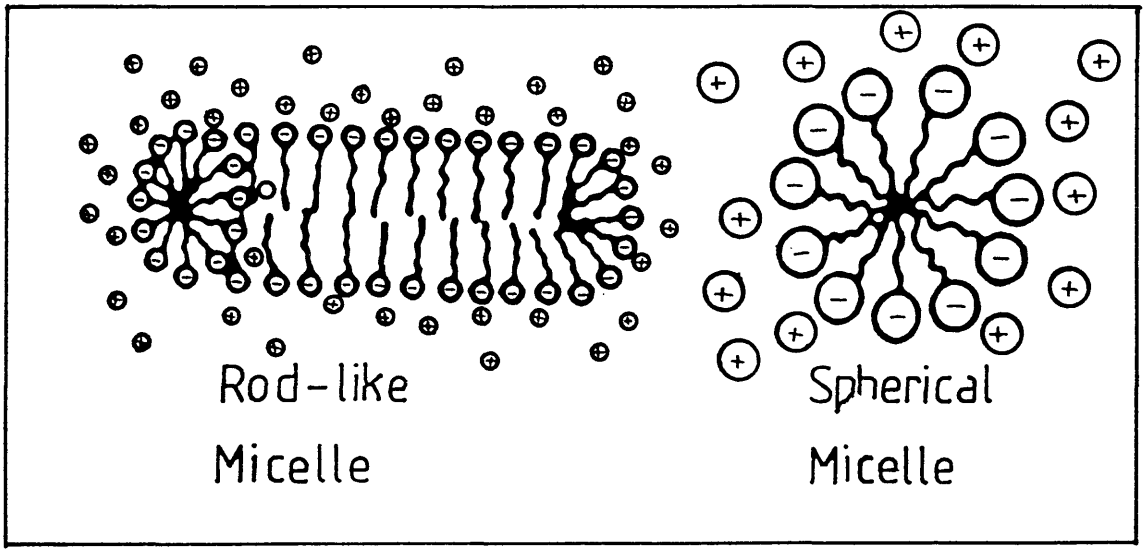


Fig. 1.1 Cross section of a spherical or cylindrical micelle with counterions.

can be prepared simply by introducing starch into boiling water. This kind of colloid is usually Lyophilic being either long chain molecules with polar end groups forming micelles (such as soaps and other detergents) or macromolecules (such as proteins). Extrinsic colloids are often insoluble substances and do not easily form colloidal dispersions. This type of colloid is usually Lyophobic and must be prepared by special methods. There are two major categories of these:

1.1.2.1 Condensation Methods

In this method the insoluble substance is precipitated from a true solution (small molecules or ions) under circumstances in which a high rate of nucleation is combined with a fairly slow rate of growth of these nuclei. Figure 1.2 shows this process schematically. Sometimes, the nucleation process is carried out in a very short time, whereas the growth of the nuclei to larger particles occurs in a long time without further nucleation. In these conditions all particles have the same size which leads to mono-disperse systems. In this method care should be taken, such as concentration controlling, to prevent the growth of the particles and therefore precipitation, such as in the preparation of various oxide sols carried out by hydrolysis of salts.

1.1.2.2 Dispersion Methods

The simplest method used to make a colloidal dispersion is

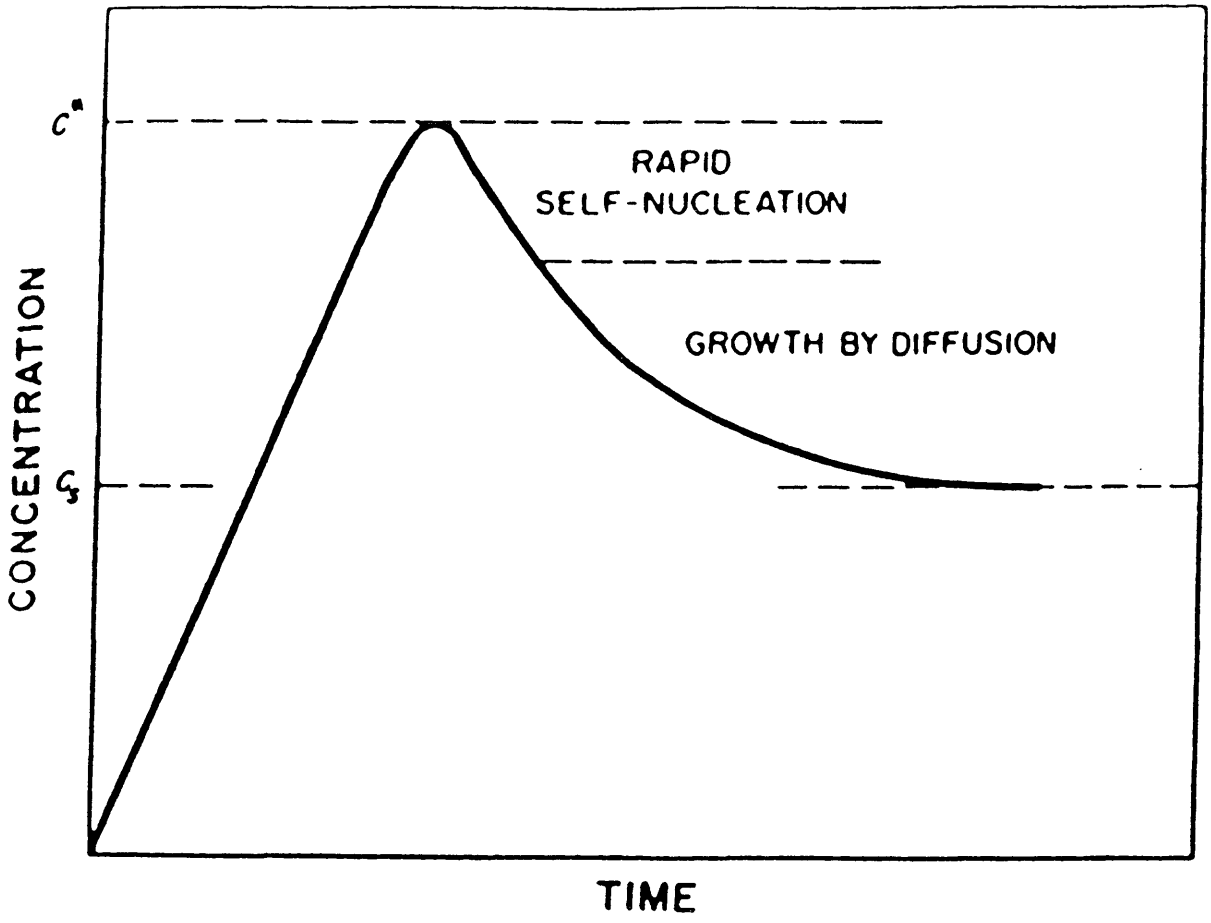
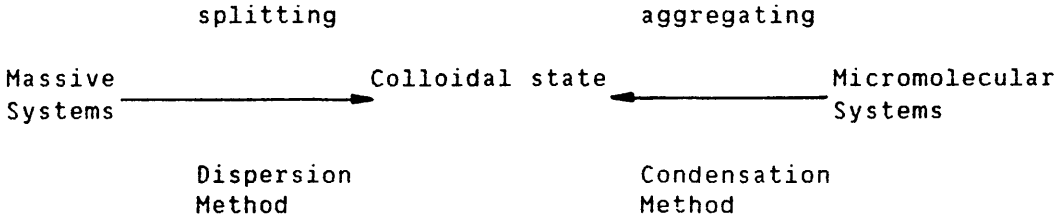


Fig. 1.2 Schematic diagram of nucleation process C_s: solubility, C^*: critical supersaturation (Ref.24, 25).

mechanical grinding. This can also be done by irradiation of the substance with ultrasonic waves which are essentially mechanical. An electrical dispersion method, called Bredig's method, is performed by dispersion of the electrode material. Another variation of this method is known as peptization (Greek: pepticos, promoting digestion). Peptization is the process of dispersing precipitated substances into colloidal systems by chemical reaction. For example, precipitates of certain metal hydroxides in water can be peptized by dilute alkali hydroxides. These methods are illustrated in the following scheme:



1.2 The Optical Properties of Colloids

This section is only concerned with light absorption and light scattering as follows:-

1.2.1 Light Absorption

Lambert's law states that the amount of light (-dI) absorbed by a medium of thickness dx is directly proportional to the intensity of the incident light.

$$dI = - k I dx \qquad (1.1)$$

or

$$\int_{Io}^{Ix} \frac{dI}{I} = k \int_{o}^{l} dx \qquad (1.2)$$

and hence

$$\log \frac{I_o}{I} = kl/_{2.303} = A \qquad (1.3)$$

where I_o is the intensity of light before passage through the medium, A is the absorbance and l is the light path in cm.

The transmittance T is the ratio of the intensities of transmitted to incident light:

$$T = \frac{I}{I_o} = \exp \frac{1}{A} \qquad (1.4)$$

Beer has formulated the law for solutions. The Lambert-Beer Law therefore is written as follows:

$$A = \varepsilon cl \qquad (1.5)$$

where c is the concentration of solution (mol dm^{-3}) and ε is the extinction coefficient in $dm^3 mol^{-1} cm^{-1}$.

1.2.2 Light Scattering[26,27]

This phenomenon was first investigated in 1871 by John Tyndall, and is known as Tyndall effect[28]. Light scattering results from the periodic oscillation of the electron clouds of the atoms, which is induced by the field of the incident light. Analysis of the scattered light provides valuable information

about the numbers, sizes, shapes and interactions of colloidal particles. The light scattering increases with an increase in the number and size of particles. The intensity of transmitted radiation is governed by $I = I_o e^{-\tau l}$ where τ is the turbididy, given in 1871 by Lord Rayleigh[29] as:

$$\tau = \frac{32\pi^3 n_2[(n_1-n_2)/C]^2 CM}{3\lambda^4 L} \qquad (1.6)$$

where n_1 and n_2 are the refractive indices of the particle and solution respectively, C is the concentration of the scattering particles, M is the molar mass for spherical macromolecules and L is Avagadro's constant.

Conventional (or time averaged) light scattering measures the absolute intensity of light scattered as a function of scattering angle. It started around 1940. An important advance in light scattering was in 1961, when the laser was invented. Since that time a new technique called dynamic light scattering (DLS) has been developed. This technique provides information about the dynamics (i.e. the Brownian motion) of colloidal particles.

1.2.2.1 Conventional Light Scattering (CLS)

There are three classes of CLS as follows:-

(i) Rayleigh Scattering - When the frequency of the scattered light is the same as that of the incident light, that is the scattering particles are small enough relative to the

wavelength of light, λ: $R/\lambda \ll 1$, where R is the particle radius.

(ii) Debye Scattering - The particles are large, but the difference between the refractive indices of Particle and solution is small ($R/\lambda \ll 1/(n_1-n_2)$).

(iii) Mie Scattering - When the dimension of the particles are not small compared to λ and the particles are not spherical. The theory is very complicated ($R/\lambda \gtrsim 1/(n_1-n_2)$).

Important theories have been described by Mie[30] in 1908, and in more recent years by Zimm[31] and Doty[32].

1.2.2.2 Dynamic Light Scattering (DLS)[33-38]

Since 1970, analysis of the intensity fluctuations in a DLS experiment has been performed by the technique of "Photon Correlation Spectroscopy" (PCS). The function, $g(\tau)$, is the temporal correlation function of the scattered light field and τ is the "correlation delay time". For a dilute suspension of identical spheres, correlation between the positions and motions of different particles can be neglected. In this case the $g(\tau)$ quantity which is measured by DLS, takes its simplest form:

$$g(\tau) = \exp\ (-\tau/\tau_c) \qquad (1.7)$$

where τ_c is the fluctuation time, the time which is taken by a particle to diffuse a distance equal to the wavelength of light, λ. It is given by equation (1.8):

$$\tau_c = \frac{1}{DQ^2} \qquad (1.8)$$

where D is the translational diffusion coefficient of a particle and Q is the scattering vector:

$$Q = (4n/\lambda) \sin(\theta/2) \qquad (1.9)$$

D is given by the Stokes-Einstein relationship

$$D = kT/6\pi\eta R_H \qquad (1.10)$$

where k is Boltzman's constant, T, the temperature, η, the viscosity of the liquid and R_H the hydrodynamic radius of the particles.

Since Q, T and η are all mensurable quantities, use of equations (1.8) and (1.10) then gives the particles hydrodynamic radius R_H. For particles smaller than one micron, τ_c is in the microsecond to millisecond range. In many cases R_H is close to the actual particles radius R. The DLS technique is a good method of measuring particle sizes in the range of 20A to 1μm.

For polydisperse colloids, the equations for $g(\tau)$ and τ_c are generalised to:

$$g(\tau) = \frac{\int F(R), I(R, \theta) \exp[-D(R)\, Q^2 \tau] dR}{\int F(R)\, I(R, \theta)\, dR} \qquad (1.11)$$

where F(R) is the distribution of particle ratii. The intensity of light scattered at an angle θ by a suspension of N identical particles is given by equation (1.12).

$$I(R,\theta) = I_R \times P(\theta) \qquad (1.12)$$

$$I_R = \frac{16\pi^4 R^6}{r^2\lambda^4}\left[\frac{n_1^2-n_2^2}{n_1^2+n_2^2}\right]^2 \qquad (1.13)$$

$$P(\theta) = [3\,(\mathrm{Sin}QR - QR\,\mathrm{cos}QR)/(QR)^3]^2 \qquad (1.14)$$

where I_R is the intensity of light scattered by an isolated particle of much smaller size than λ (Wavelength of light in the suspension), and n_1, n_2 are the refractive indices as before. The subscript R indicates a "Rayleigh" or point scatterer. $P(\theta)$ is a shape factor with the properties

$$P(0) = 1 \qquad P(\theta)<1 \quad \text{for } \theta>0$$

For narrower distributions the exponential term in equation (1.11) may be expanded to give:

$$\mathrm{lng}(\tau) = -AQ^2\tau + \frac{B}{2}Q^4\tau^2 + \ldots. \qquad (1.15)$$

By assuming R_H=R for spherical Rayleigh scatterers,

$$A = \frac{KT}{6n\zeta(\bar{R^6}/\bar{R^5})} \qquad (1.16)$$

and

$$B = \frac{\bar{R^6}\,\bar{R^4}}{\bar{R^5}^2} - 1 \qquad (1.17)$$

where $\bar{R^n}$ is the n'th moment of F(R). By measuring $g(\tau)$ and putting it in equation (1.15), it is possible to obtain an average

radius and a measure, B/A^2, of the width of the particle size distribution. Figure 1.3 shows a plot of equation (1.15), measured by DLS, as ln $g(\tau)$ against delay time τ.
The average size of the particles can be calculated from the slope of the diagram.

1.3 The Electrical Properties of Colloids

The electrical double layer and electrophoresis measurements are the important aspects of colloidal systems.

1.3.1 Electrical Double Layers

Electrical double layers play an important role in the understanding of stability of colloids. The double layer (e.g. in sols and suspensions) consists of a charge on the particle, the surface charge σ_o, and an equal but opposite charge in the solution, the countercharge. Double layers as a whole are electrically neutral. But this does not mean that the potential difference ϕ_o, known as the surface potential, between the interior of a particle and the bulk of the solution is zero. The separation of the electrochemical potential, $\bar{\mu}_i$, into $(Z_i F\phi_o)$ and chemical potential, μi, terms according to:

$$\bar{\mu}_i = \mu_i + Z_i F \phi_o \qquad (1.18)$$

is useful only if one of the two terms is generally accepted as being fixed. If for example $Z_i F\phi_o$, the binding energy, is a purely coulombic term, all remaining terms are then defined as μ_i,

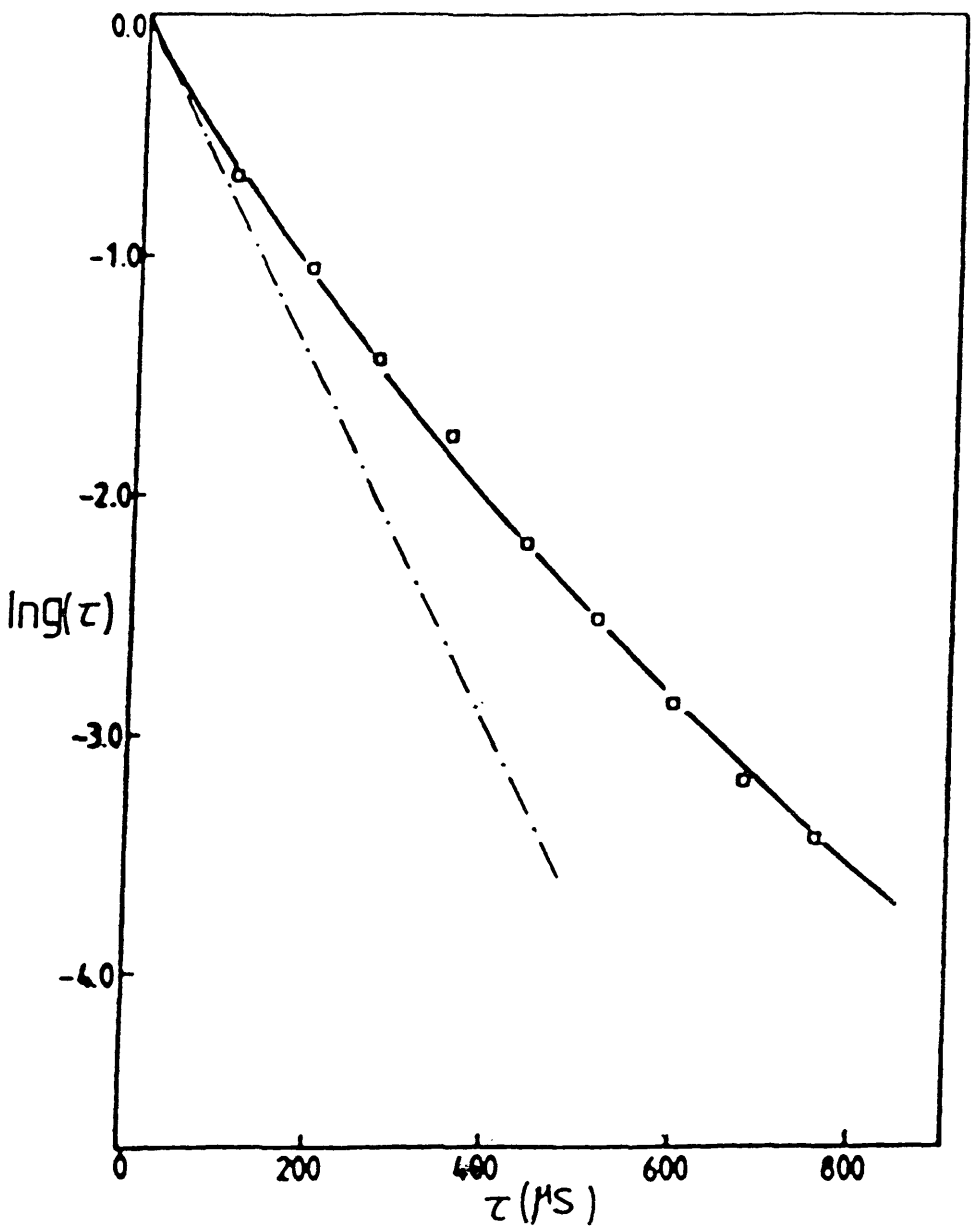


Fig. 1.3 Decay of the autocorrelation function g(τ), in dynamic light scattering experiments.

where Z is the valancy of the ion with the sign included, and F is the Faraday constant.

The simplest theory for the electric double layer was given first by Helmholtz[39] in 1879. According to this model the surface of the suspensions particles can be positive or negative. A single layer of counter charge will be attached to the surface from the solution. As in Figure 1.4.a shown, a fixed double layer is formed. This will correspond to an electric capacitor. By using electrostatic theory, the potential difference between the two layers is:-

$$\phi_o = \frac{\sigma_o a}{\varepsilon_o \varepsilon} \qquad (1.19)$$

where a is the distance between the layers of charge and countercharge, ε is the dielectric constant of the solution, and $\varepsilon_o = 8.854 \times 10^{-12} cv^{-1} m^{-1}$ is the permittivity of free space.

There are two different capacitances: The integral capacitance:-

$$K = \frac{\sigma_o}{\phi_o} \qquad (1.20)$$

and the differential capacitance:-

$$C = \frac{d\sigma_o}{d\phi_o} \qquad (1.21)$$

Equation (1.21) is more commonly used for two reasons:
(i) ϕ_o is inaccessible to direct measurements but $d\phi_o$ is not;
(ii) in various experimental techniques the variation of σ_o due

to a given change of surface charge is measured.

The two capacitances are related through the expression:-

$$K = \frac{1}{\phi_o} \int C d\phi_o \qquad (1.22)$$

$$C = K + \phi_o \frac{dK}{d\phi_o} \qquad (1.23)$$

The Helmholtz model was modified by G. Gouy[40] and D. L. Chapman[41] in 1910. According to their model, the theory of Helmholtz is unsatisfactory in that it neglects the Boltzman distribution of the ions. They suggest a diffuse double layer as represented in Fig.(1.4.b). Thermal agitation in solution permits the free movement of the ions, but the distribution of positive and negative ions is not uniform. The idea behind this theory is very similar to the Debye-Hückel theory of the ionic atmosphere surrounding an ion.

In Chapman's theory as x becomes very large, ϕ_o approaches zero, when x=a, the potential is:-

$$\phi_a = \frac{\sigma_o}{\varepsilon_o \varepsilon K} = \frac{\sigma_o d}{\varepsilon_o \varepsilon} \qquad (1.24)$$

where d=1/k is the effective thickness of the double layer.

The potential ϕ_a with respect to the bulk solution is known as the electrokinetic potential or ζ potential and is given by:-

$$\zeta = \frac{\sigma_o d}{\varepsilon_o \varepsilon} \qquad (1.25)$$

The Gouy-Chapman theory was modified by O.Stern[42] in 1924.

The Stern model, shown in Fig. (1.4.c), combined the fixed double layer and diffuse double layer models.

1.3.2 Electrophoresis

If particles are suspended in a solution to which an electric potential is applied, the particles often move towards one of the electrodes. This process is known as electrophoresis. This phenomenon was discovered in 1807 by Reuss. The first important experiment on electrophoresis was carried out by A. Wilhelm Kaurin Tiselius in studying mixtures of proteins[43]. The electrophoretic velocity of a cylindrical particle along its axis is:-

$$v_o = \frac{\xi \varepsilon_o \varepsilon}{\zeta} \qquad (1.26)$$

where ζ is the viscosity of the liquid. This equation (1.26) was formulated by Debye and Hückel in 1924 for spherical particles by:-

$$v_o = \frac{2\xi \varepsilon_o \varepsilon}{3\zeta} \qquad (1.27)$$

The technique of electrophoresis supplements the ultracentrifuge, which separates the molecules according to sizes and shapes.

1.4 Colloidal Semiconductors

During the past few years considerable interest has been

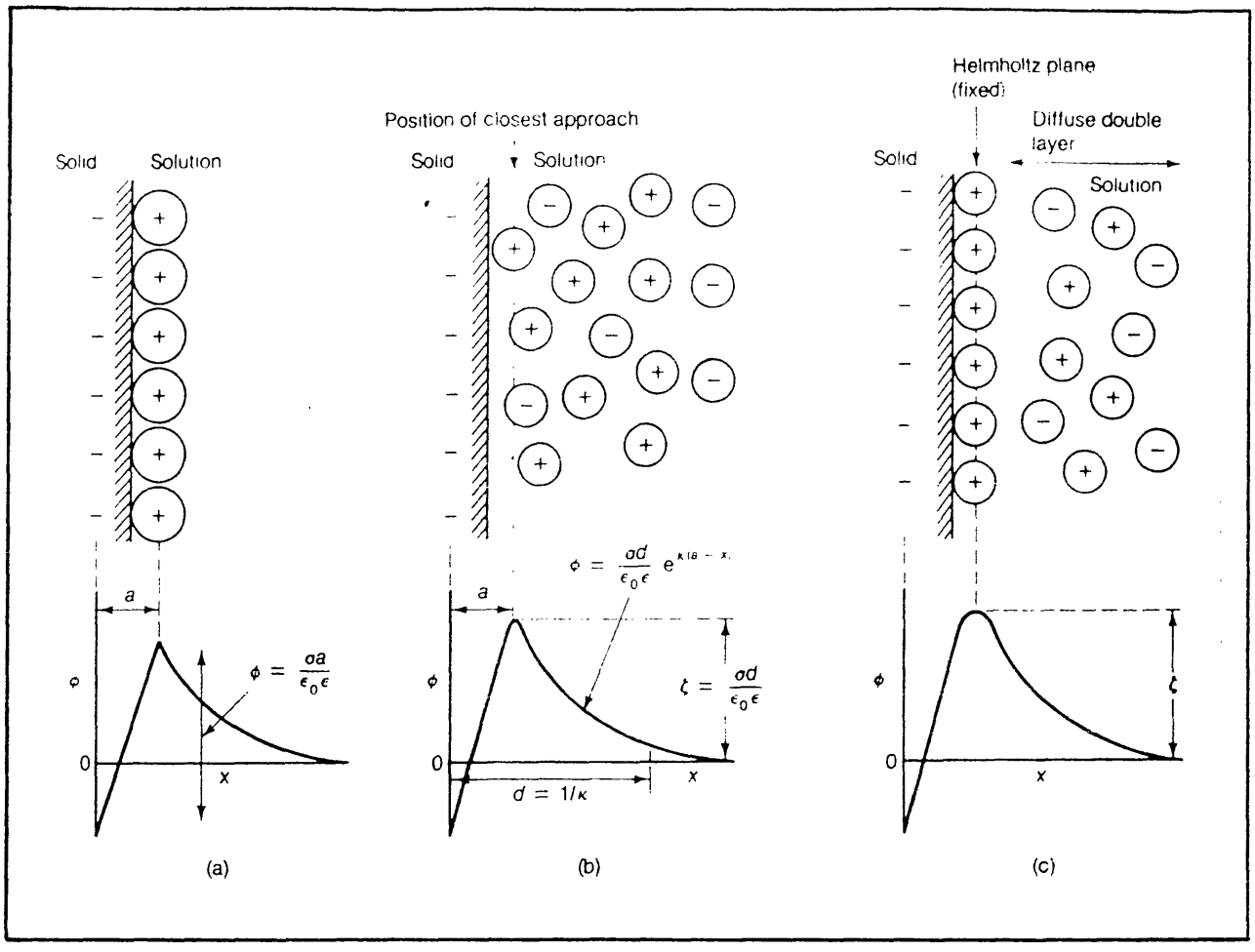


Fig. 1.4 The model of double layers.

a) Helmholtz Model

b) Gouy-Chapman Model

c)Stern Model.

(Ref. Laidler,K.J.; Meiser,J.H. Physical Chemistry 1982)

focused on photo-induced electron transfer reactions in colloidal semiconductors[44-90]. From the solar energy conversion view they exhibit several advantages as follows:-

(i) high absorption coefficient;

(ii) optimal exploitation of the solar energy by suitable choice of material;

(iii) high quantum yield for electron-hole (e^-h^+) pairs separation following band gap excitation;

(iv) very fast charge diffusion to the interface in comparison with (e^-h^+) recombination;

(v) possibility of surface modification of semiconductor particles by chemisorption, chemical deriviation or catalyst.

However, before discussing more about these systems a review of electronic properties of semiconductors could help in the understanding of the photo(electro)chemical process occurring at the colloidal semiconductor/electrolyte interface.

1.4.1 Energy Bands

An isolated atom has a set of discrete energy levels. In a solid, which is a lattice containing ca. $5x10^{22}$ atoms/cm^3, the energy levels are split due to interatomic interactions. Therefore electrons occupy energy bands rather than energy levels (Fig. 1.5).

In the language of solid state physics the highest occupied energy band is called the valence band (VB) and the lowest empty energy band the conduction band (CB). These bands are separated

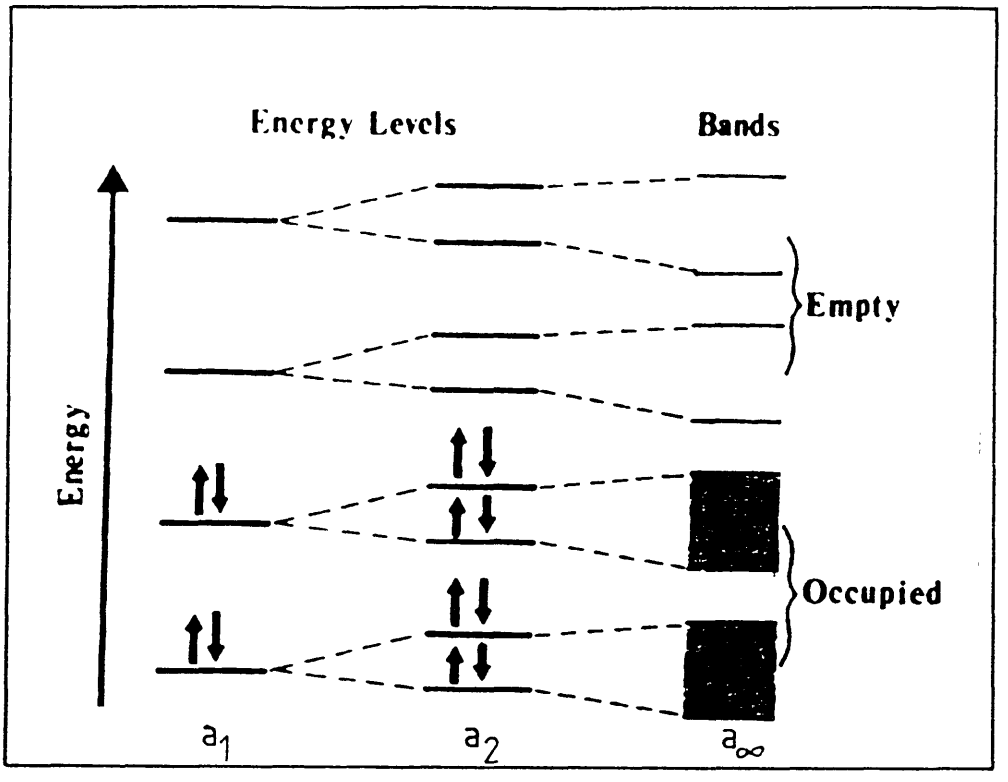


Fig. 1.5 Energy bands of solid particles

(a represents an atom)

by a forbidden region, called the band gap, and the difference in their energies is known as the band gap energy (E_{gap}).

In metals $E_{gap} << kT$, i.e. ca. 0.26 eV at 298K. Then the conduction bands and valence bands overlap and electrons have enough thermal energy to move from VB to CB. However, if $4eV > E_{gap} >> kT$, the specific resistance would be between 10^{-2} to 10^{9} Ω-cm, and materials with these properties, are called semiconductors. Insulators have band gap energies over 4eV (Fig.1.6).

1.4.2 Types of Semiconductors

At T=0 K semiconductors behave as insulators. But at temperatures higher than absolute zero, thermal activation can excite VB electrons into the CB and holes (the vacancies caused by the removal of electrons) are created in the VB. Such a material is called an Intrinsic Semiconductor (Fig. 1.7). For an intrinsic semiconductor the density of electrons and holes in CB and VB respectively can be calculated as below.[91]

$$n_i = P_i \approx 2.5 \times 10^{19} \exp \frac{(-E_{gap})}{(2KT)} \ cm^{-3} \text{ at } \sim 298K \qquad (1.28)$$

For example, Silicon with E_{gap} = 1.1 eV posesses $n_i = P_i = 1.4 \times 10^{10} cm^{-3}$. The mobilities of electrons, μ_n and holes, μ_p, in semiconductors are larger than ions in solution. The properties of some important semiconductors are listed in Table 1.2.

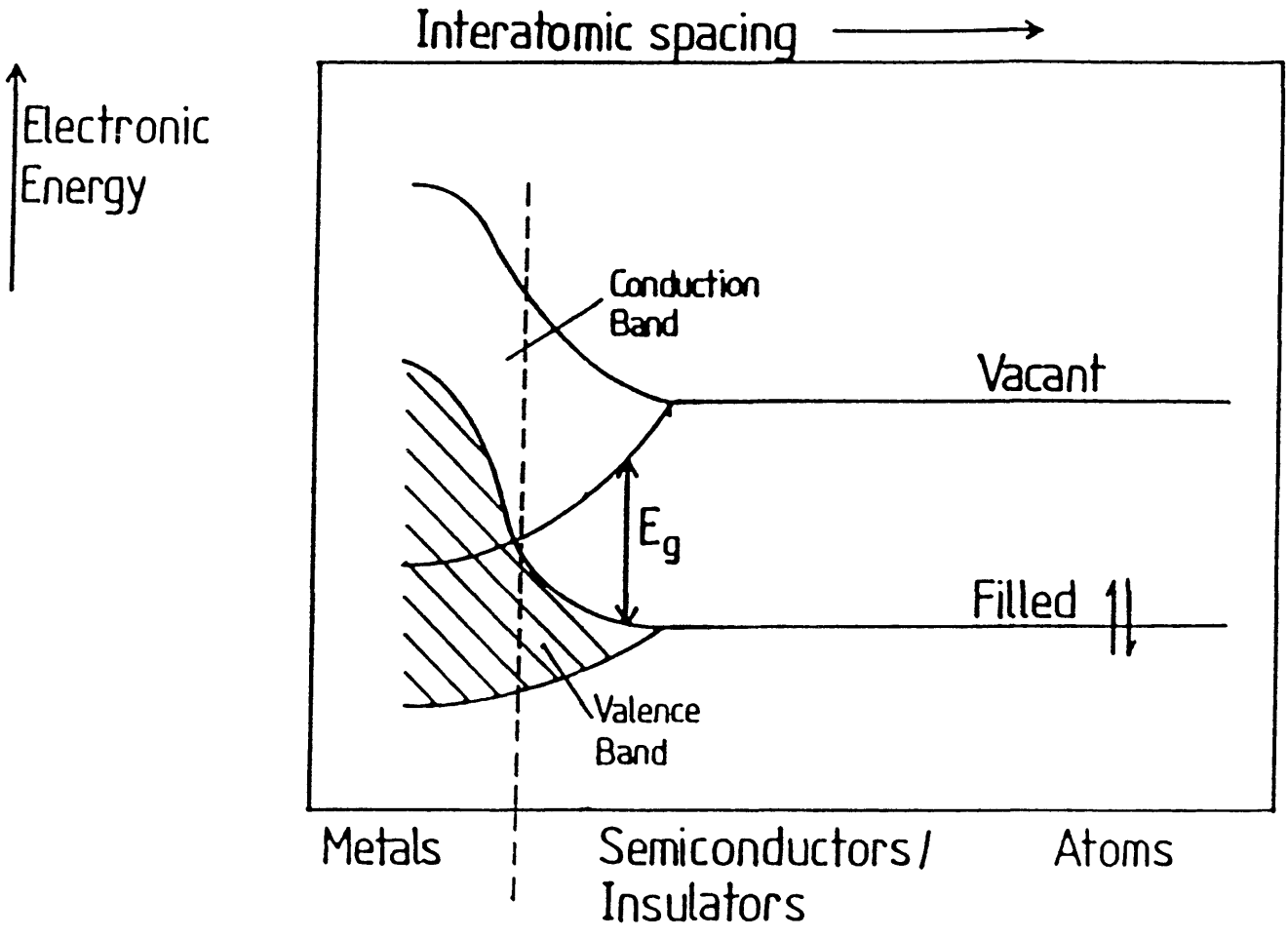


Fig. 1.6 Diagram of bands in metals and semiconductors.

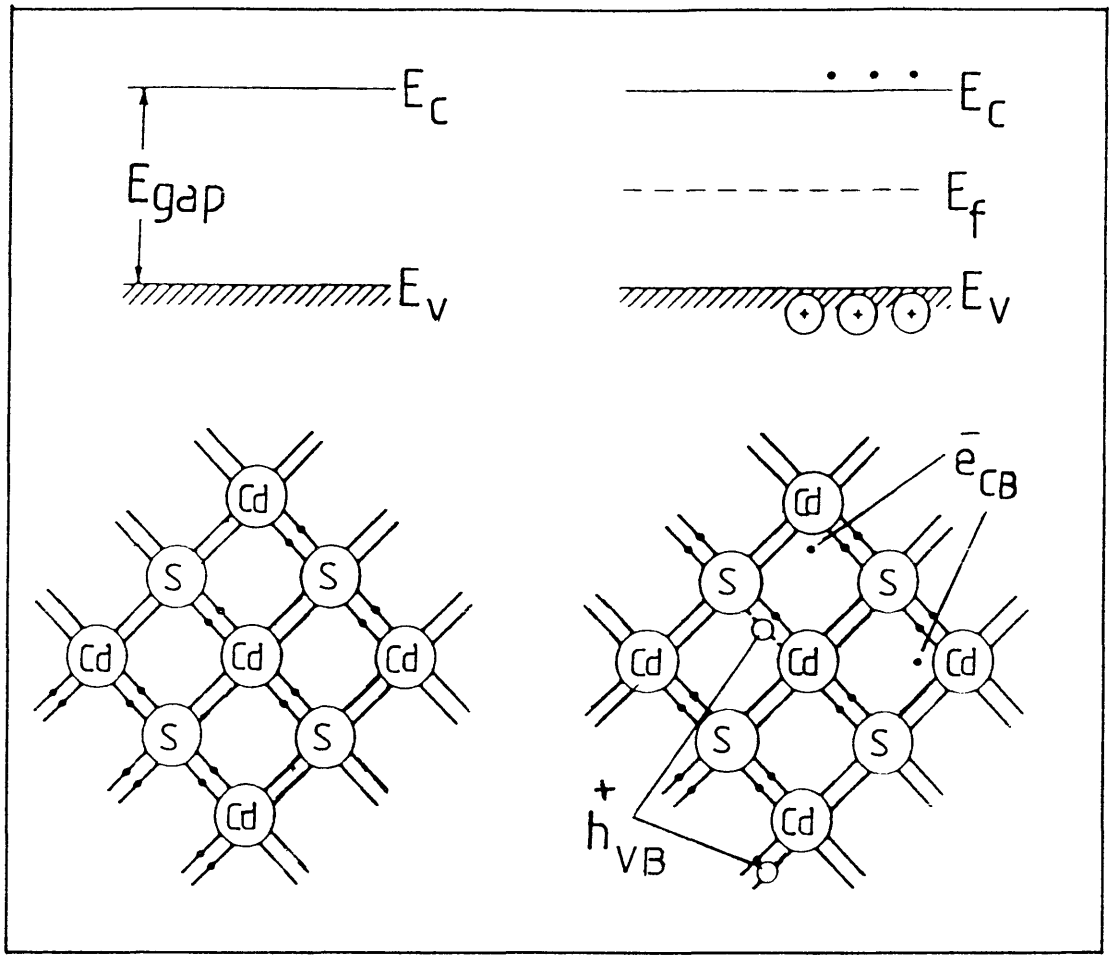


Fig. 1.7 The CdS lattice at T=0 and T>0 K (Formation of conduction band electrons, e^-_{CB}, and valence band holes, h^+_{VB}).

Table 1.2 Properties of Some Important Semiconductors

	Semiconductors	Band gap (eV)	μ_n (cm^2/V-sec)	μ_p (cm^2/V-sec)	σ ≈Ω-cm)
Element	C	5.47	1800	1200	
	Ge	0.66	3900	1900	43
	Si	1.12	1500	450	2.5×10^5 *
	Sn	0.082[a]	1400	1200	
IV-IV	α-SiC	2.996	400	50	10^{10}
III-V	Al Sb	1.58	200	420	5
	Ga Sb	0.72	5000	850	0.04
	Ga As	1.42	8500	400	4×10^8 *
	Ga P	2.26	110	75	1
	In Sb	0.17	80000	1250	0.06
	In AS	0.36	33000	460	0.03
	In P	1.35	4600	150	
II-VI	Cd S	2.42	340	50	
	Cd Se	1.70	800		10^{15}
	Cd Te	1.56	1050	100	10^{10}
II-VI	Zn O	3.35	200	180	
	Zn S	3.68	165	5	10^{10}
	Zn Se	2.7	600		10^9
	Zn Te	2.25		100	100
IV-VI	Pb S	0.41	600	700	5×10^{-3}
	Pb Si	0.27	1000	1000	10^{-3}
	Pb Te	0.31	6000	4000	10^{-2}
	Ti O_2	3.0			

(a) at T = 300K

* Intrinsic Resistivity

By doping foreign atoms into the crystal lattice of a semiconductor additional energy levels form within the energy spectrum of crystal.[91] These materials are called extrinsic semiconductors. An extrinsically doped CdS lattice with electron donor, E_D, and electron acceptor, E_A is represented in Fig. 1.8.

Semiconductors doped with E_D and E_A are called n-type and p-type extrinsic semiconductor respectively. Conduction in n-type semiconductor occurs via electrons promoted from the donor sites to the CB, while in p-type semiconductor it is due to hole migration throughout the VB.

1.4.3 The Fermi Level

For semiconductors, the chemical potential of electrons is represented by the Fermi level in the semiconductor. The Fermi level is the energy (E_F) at which the probability of occupation by an electron is exactly 1/2. This probability is given by the Fermi-Dirac distribution:

$$F(E) = \text{probability of occupation} = \{1+[\exp(E-E_F)/kT]\}^{-1} \qquad (1.29)$$

when $E = E_F$, $F(E) = 1/2$. Therefore the Fermi level for an intrinsic semiconductor lies very close to the middle of the band gap.

For a doped material, the location of E_F depends on the doping level, N_A or N_D given by[92]:

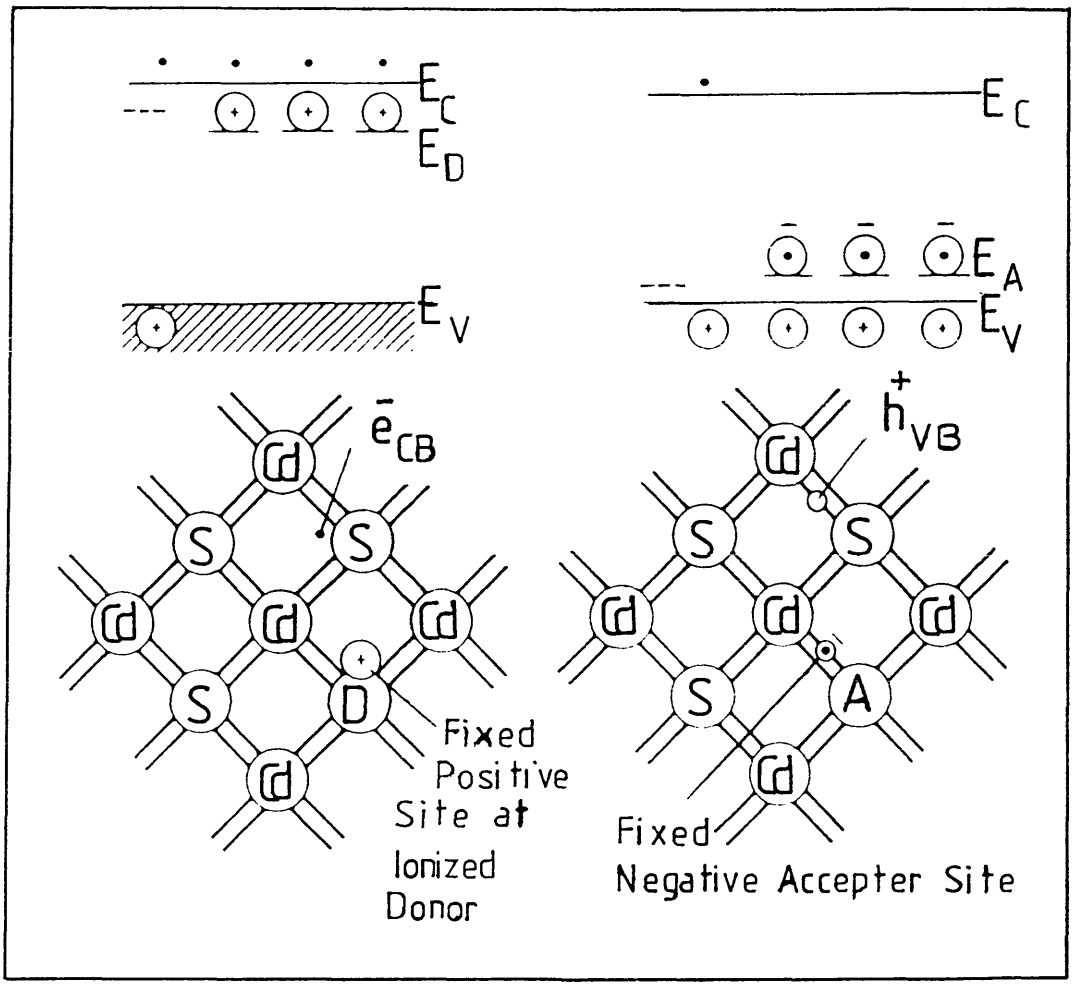


Fig. 1.8 Formation of electron donor (ED) and electron acceptor (EA) levels with the forbidden region.

$$N_A = N_A^- \left[1+g \exp \frac{(E_A - E_F)}{kT}\right] \qquad (1.30)$$

$$N_D = \frac{N_D^+ \exp \frac{E_D - E_F}{kT}}{g + \exp \frac{(E_D - E_F)}{kT}} \qquad (1.31)$$

Where N_A^- and N_D^+ are the number of ionised acceptors and donors respectively and g is their ground state degeneracy.

For n-type semiconductor ($N_D > 10^{17} cm^{-3}$), E_F lies slightly below the CB and for p-type semiconductors, E_F lies just above the VB as shown in Fig. 1.9. Since we are dealing with electron transfer across the semiconductor solution interface it is convenient to identify an equivalent Fermi level in the solution. Since the Fermi level of a phase, α, E_F, can be identified as the electrochemical potential of an electron in α, μ_e^α [93,94]:

$$E_F = \overline{\mu_e^\alpha} = \mu_e^\alpha - e\phi n \,(eV) \qquad (1.32)$$

where ϕ is the work function of semiconductors. This is simply the electrochemical potential of whatever is present in the solution.

1.4.4 Macroscopic and Microscopic Semiconductor Electrode[95-97]

One of the important points in the semiconductor electrodes with which we will be concerned is the crucial difference between macroscopic electrodes and colloidal semiconductors which are

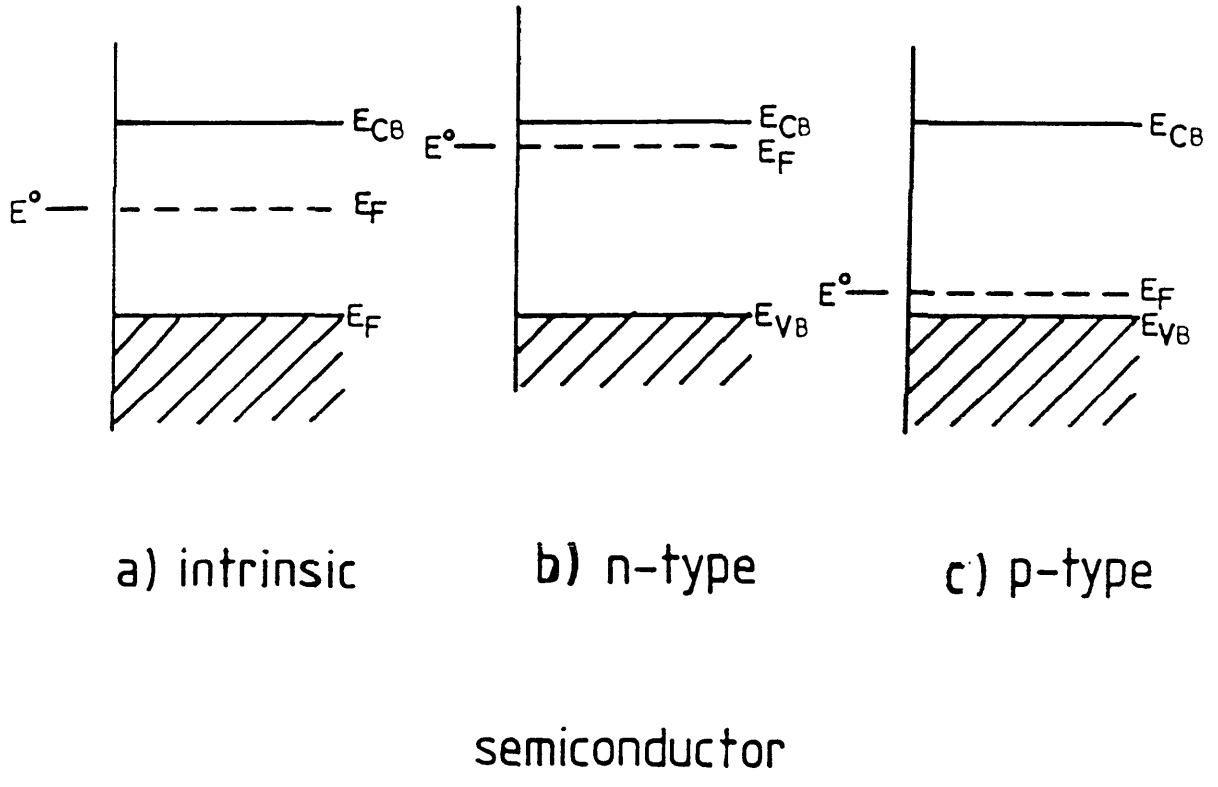


Fig. 1.9 Schematic Fermi level (E_F) of semiconductors.

microscopic. Most authors such as Grazel and Frank[55] have assumed that microscopic semiconductor particles behave in a similar fashion to the macroscopic semiconductor electrodes. However, Albery and Bartlett[97] have analysed the recombination and transport kinetics of carriers and the kinetics of their reactions at the surface of the particle and concluded that the behaviour of particles is very different from that of their macroscopic analogues. According to their model, the comparison of potential distributions and Fermi levels for a macroscope planar electrode and for spherical particle is given in Fig. 1.10.

By solving the poisson-Boltzmann equation for the depletion layer of a spherical particle one can obtain

$$\theta = \frac{1}{6} (\varrho-\varrho_w)^2(1+2\varrho_w/\varrho) \qquad (1.33)$$

where

$$\varrho = \frac{r}{L_D}$$

and

$$\theta = \phi F/RT$$

are dimensionless variables, r is the distance from the centre of the particle, L_D is the Debye length and ϕ is potential measured with respect to the centre of the particle so that $\phi = 0$ at $r = 0$.

In large particles the width of the depletion layer, ϱ_w, is small compared to the radius of the particle (at $\theta = 0$, $\partial\theta/\partial\varrho = o$, $\varrho = \varrho_w$) equation (1.33) simplifies for a macroscopic semiconductor planar electrode (eq. 1.34) to

$$\theta = 1/2 (\varrho-\varrho_w)^2 \qquad (1.34)$$

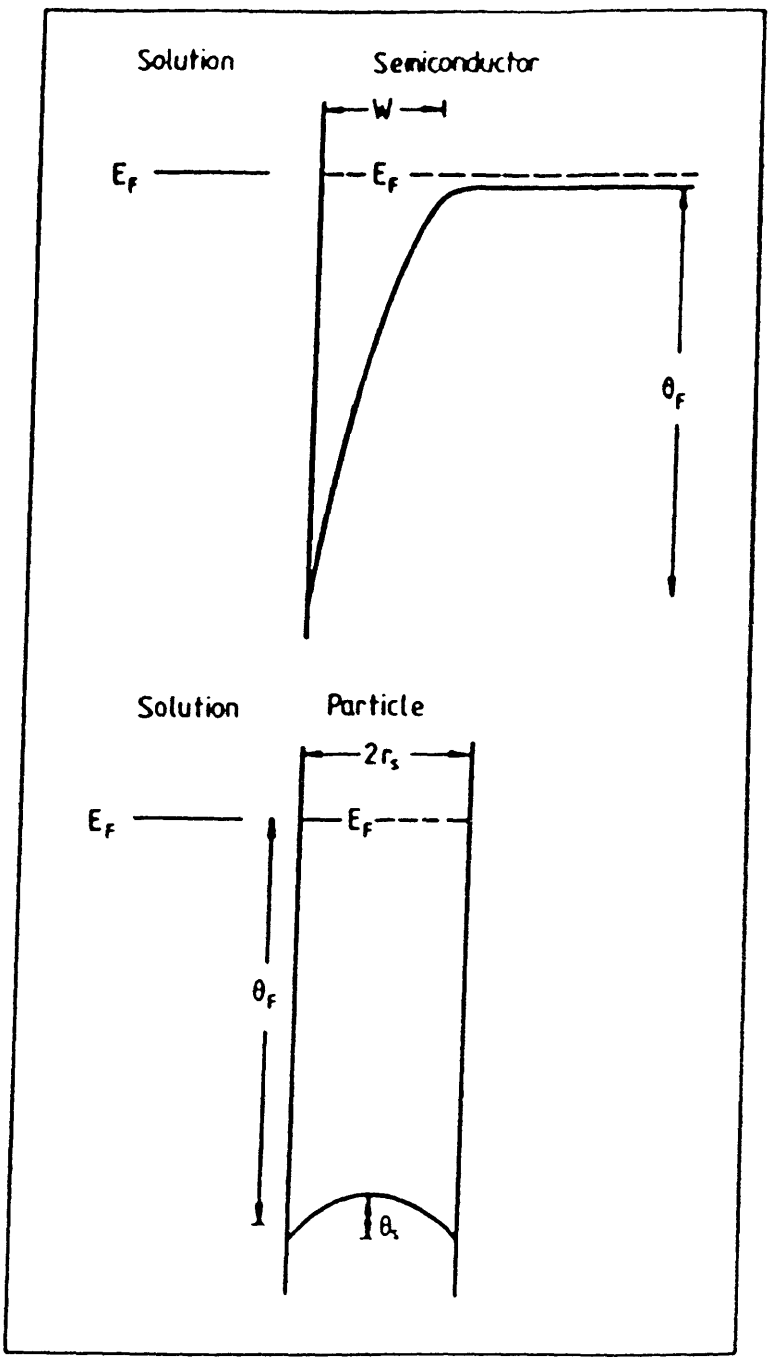


Fig. 1.10 Potential distribution and Fermi levels in a macroscopic planar electrode and spherical particle (microscope).

For a small colloidal particle, $r_s \sim 10^{-6}$ cm, the radius of the particle may be smaller than the width of depletion layer; therefore equation (1.33) simplifies to

$$\theta = \frac{\rho^2}{6} \tag{1.35}$$

As shown in Fig. 1.10, the whole of the particle is depleted of majority carriers and there is no field free region. Equation (1.35) expresses a major difference between the small colloidal particle and the macroscopic electrode. The conditions under which eq. (1.35) will hold are given by

$$\frac{1}{6}\left(\frac{r_s}{L_D}\right)^2 = \theta_s < \theta_F = \frac{1}{2}\left(\frac{w}{L_D}\right)^2$$

or

$$r_s < 3^{1/2} w = (6\theta_F)^{1/2} L_D \tag{1.36}$$

where θ_s is the maximum value of θ from equation (1.35) for too small particles and θ_F is the shifting of Fermi level from its position at flatband. In a planar electrode θ_F describes the potential drop across the depletion layer of width w. For colloidal particles where $r_s < 10^{-6}$ cm, equation (1.36) will be satisfied, that is, the particle is completely depleted of its majority carriers and the potential distribution will be given by equation (1.33).

When $\theta_s < \theta_F$ there is much less potential difference within the particle than within the macroscopic depletion layer. Under conditions

$$r_s > 6^{1/2} L_D \quad \text{for} \quad \theta_s < 1,$$

the particle can be treated as being field free.

θ_F is an important parameter and (from equation (1.37)) it plays the same role for semiconductor particles as the electrode potential does for the macroscopic electrode:

$$\theta_F = \ln P^D_{FB} - \ln P^D_S \qquad (1.37)$$

where P^D_{FB} is the concentration of majority carriers in the dark at flat band and is equal to the carrier density of the macroscopic material.

1.4.5 Flat Band Potential[98-105]

The flat-band potential is the electrode potential at which the semiconductor bands are flat (zero space charge in the semiconductor). It is measured with respect to a reference electrode, either the normal H^+/H_2 redox potential (NHE) or the saturated calomel electrode (SCE). The band bending is given by

$$V_B = E_F - E_{FB} \qquad (1.38)$$

At equilibrium in the dark, E_F is the same as the potential of the redox couple in the electrolyte (Fig. 1.11).

It should be mentioned that the Helmholtz layer does usually change upon variation of the pH of solution[98] and adsorption of ions on the semiconductor surface.

By experimental methods one can determine the position of energy bands at the surface. This is achieved by capacity

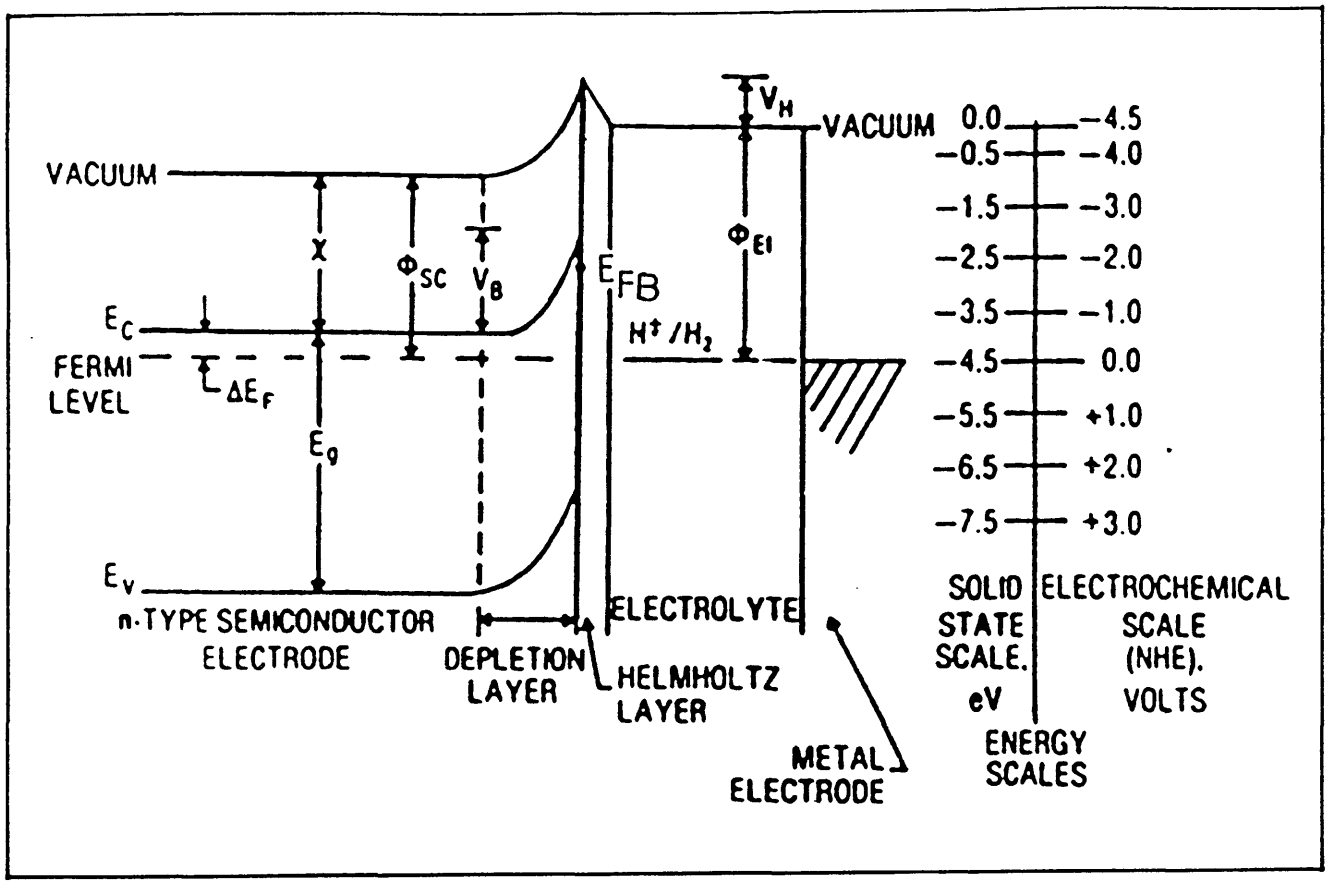


Fig. 1.11 Schematic diagram of Energy levels for semiconductor-electrolyte junction:

V_H: potential drop at Helmholtz layer

E_g: the semiconductor band gap

χ: electron affinity

Φ_{sc}: semiconductor work function

V_B: Band bending

E_{FB}: Flat band potential

measurements of the semiconductor liquid interface.[98] The interface is usually determined by two capacities in series, Helmholtz capacity C_H and space charge capacity C_{SC}. To obtain a relation between the space charge capacity C_{SC} and the potential drop across the space charge layer V_{SC} one can use the Mott-Schottky relation as given by

$$1/C_{SC}^2 = \frac{(2L_D^*)^2}{(\varepsilon\varepsilon_o)_2}\left(\frac{V_{SC}}{kT} - 1\right) \qquad (1.39)$$

where L_D^* is the effective Debye length given by

$$L_D^* = \frac{(\varepsilon\varepsilon_o kT)}{2n_o e^2}^{1/2} \qquad (1.40)$$

where ε is the dielectric constant and n_o the majority carrier density. By plotting $1/C_{SC}^2$ versus the electrode potential V_E one can obtain information on the potential distribution across the interface by comparison of the slope of the experimental curve with that of the theoretical relation of $1/C_{SC}^2$ vs. V_{SC} (eq.1.39). It is found that any change of V_E can be ascribed completely to V_{SC}, so that E_{FB} can be found from the value of V_E when $1/C_{SC}^2 = 0$ Fig. 1.12 represents the experimental flat band potential which is found for CdS[139], and it is pH-independent[105]. However, Gomes and Gordon[104] reported a change consistent with equation (1.41).

$$E_{FB}(SCE) = \chi + \Delta E_F + V_H - 4.5 = \phi_{SW} + V_H - 4.5 \qquad (1.41)$$

In which χ is the electron affinity of the semiconductor, ΔE_F is

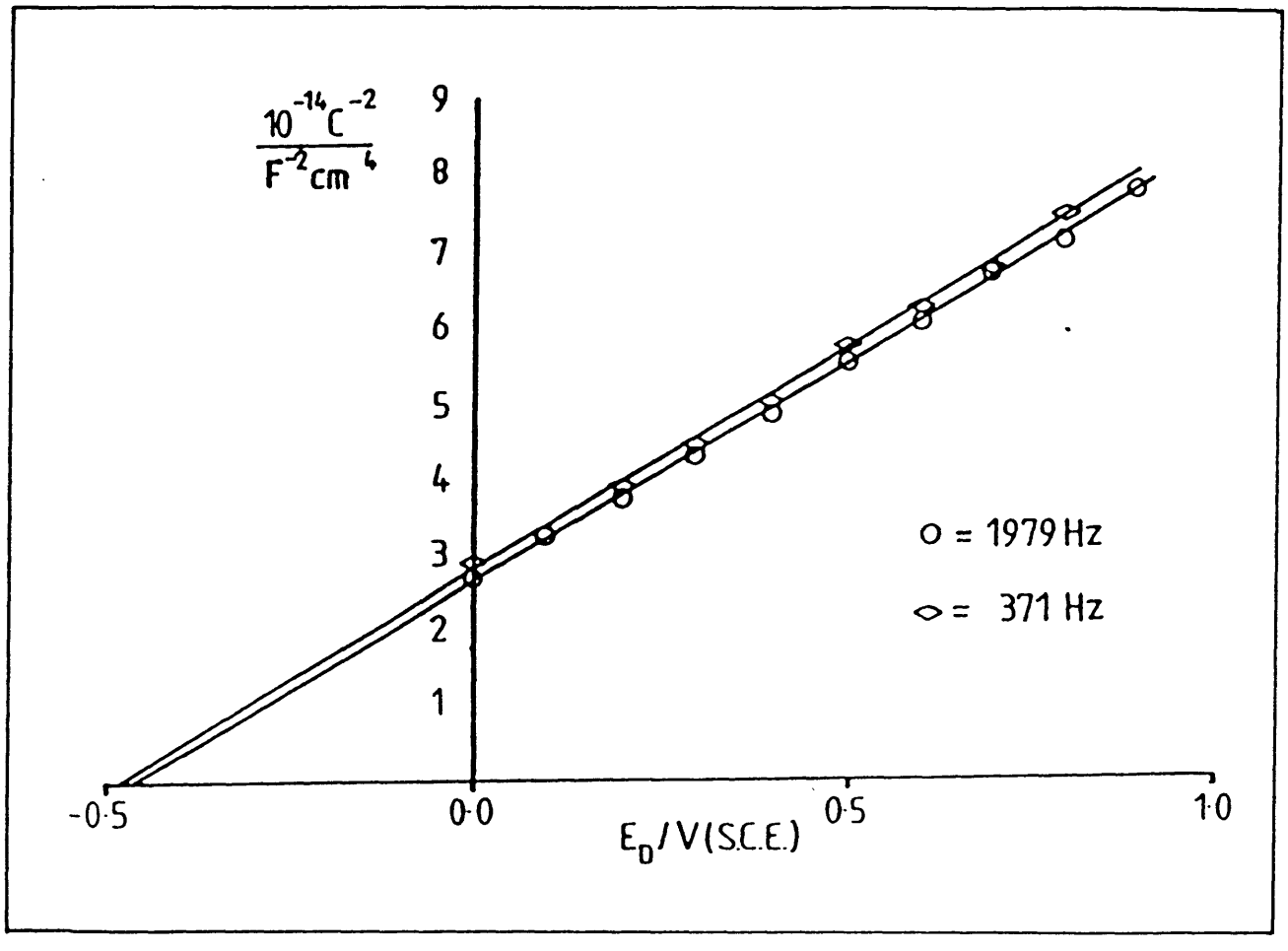


Fig. 1.12 Experimental Flat band potential for CdS

$V_{FB} = -(0.47 \pm 0.02)V.$ [139]

the difference between the Fermi level and majority carrier band edge of the semiconductor and ϕ_{SC} is the semiconductor work function. V_H is the potential drop across the Helmholtz layer. V_H can be obtained from the point of zero zeta potential (PZZP) where the numbers of adsorbed positive and negative ions are equal, so that $V_H=0$. For many semiconductors in aqueous electrolytes, the change of V_H with pH follows a simple equation (1.41) and therefore

$$V_H(\text{volts}) = 0.059\ (pH_{PZZP} - pH) \qquad (1.42)$$

pH_{PZZP} can be obtained experimentally by a simple potentiometric titration of an aqueous suspension of a powder of the semiconductor in a solution of known ionic strength.

1.4.6 Semiconductor Electrolyte Interface[93-95, 97]

The semiconductor/electrolyte junction plays an important role in photoelectrochemical systems as a means of solar energy conversion. The great difference between the electrolyte junctions of a metal, macroscopic semiconductor electrode and a small colloidal semiconductor particle are shown in Fig. 1.13. In a semiconductor the charge carrier density is smaller than that in the electrolyte and much smaller than that in the metal. Thus, according to expression (1.43) we can say that[96]

$$1/L_D(\text{Debye Length}) \propto (C_q \text{ carrier concentration})^{1/2} \qquad (1.43)$$

and

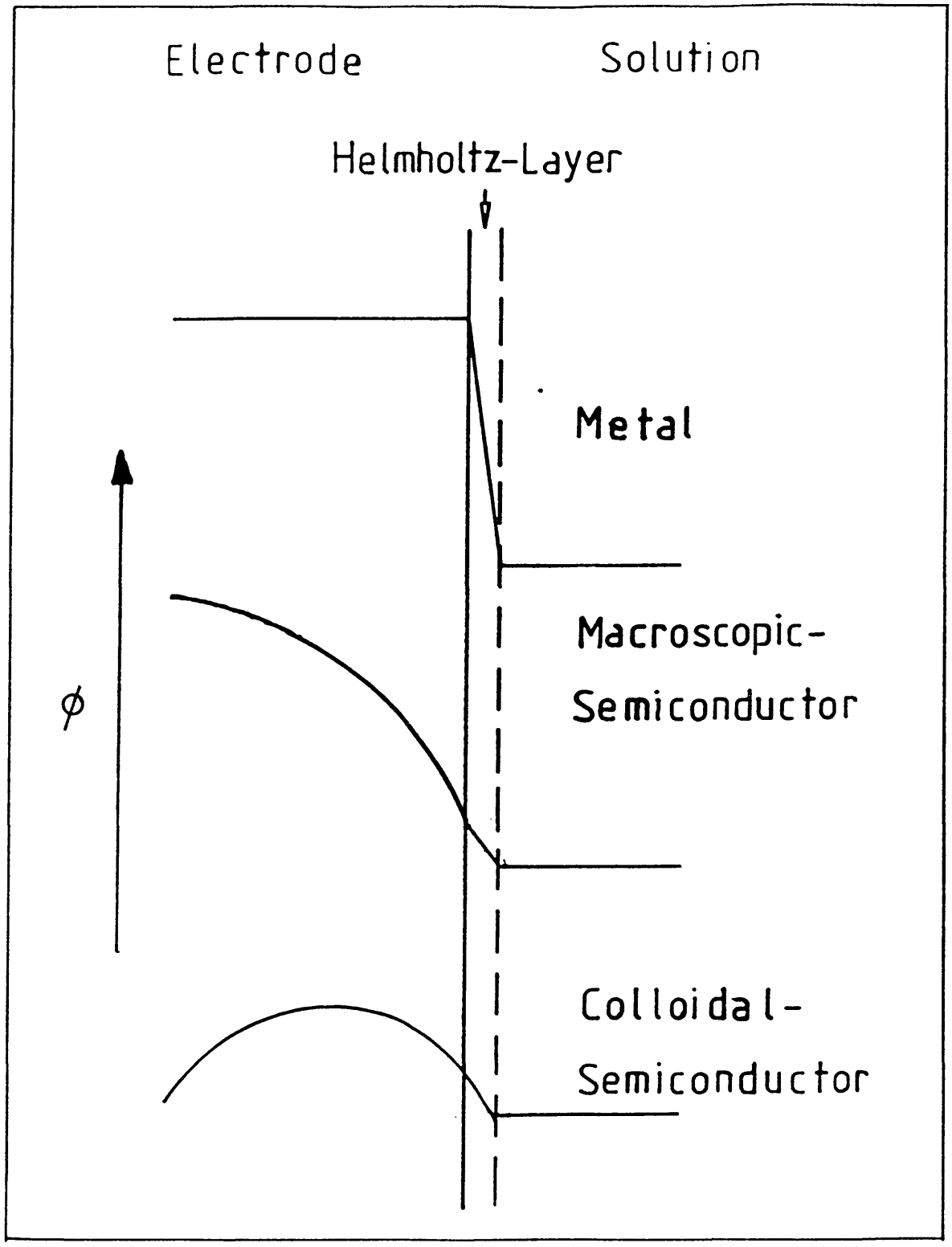


Fig. 1.13 Schematic potential distribution at a metal macroscopic semiconductor and colloidal semiconductor/electrolyte interface.

(L_D) semiconductor > (L_D) electrolyte > (L_D)metal (1.44)

Therefore the charge distribution for a semiconductor/electrolyte interface is the reverse of the metal/electrolyte system (Fig. 1.13).The lower charge carrier density in the semiconductor leads to a charge distribution over a distance of between 100Å and several microns in the bulk of the macroscopic semiconductor, which is called the space charge region or depletion layer. There is an analogue between the semiconductor/electrolyte interface and the conventional diffuse double layer,[96] except in the macroscopic semiconductor the positive charges are fixed on the lattice sites and only negative charges are free to move. In a small colloidal semiconductor the radius of the particle may be smaller than the width of the depletion layer, therefore the whole of the particle may be depleted of majority carriers as shown in Fig. 1.13.

A charged layer also exists in the electrolyte in contact with the solid phase, called the Helmholtz layer. This layer may consist of dipoles at the interface or ions adsorbed from the solution to the solid electrode surface; these ions are of opposite sign to the charge induced in the solid electrode. The width of the Helmholtz layer is generally of the order of a few A^o. Applying a potential to the macroscopic semiconductor/electrolyte interface from an external source causes more potential drop in the space charge region than in the Helmholtz layer, while in a metal/electrolyte system the potential drop occurs more rapidly in the Helmholtz layer (Fig. 1.13). This is an important point in electron transfer process.

1.4.7 Photo-Induced Electron Transfer Reactions

Light-induced electron transfer reactions in colloidal semiconductor dispersion have become an exciting and rapidly growing area of research in the field of solar energy conversion over the last few years. Photochemists and photoelectrochemists are nowadays trying to develop a cyclic system for solar energy collection and storage in the form of chemical and electrical potential.

Natural photosynthesis in green plants is an example in the field of energy storage process. The challenge facing photochemists is to find an artificial cycle, which produces a storable fuel from readily available, plentiful and inexpensive material.[106-108] Amongst the numerous systems, the following have been extensively considered by several groups all over the world[109-114]:

(i) photosplitting of water into H_2 and O_2

(ii) photo reduction of CO_2

(iii) photo reduction of N_2 to hydrazine or ammonin

(iv) photodecomposition of hydrogen halides and sulfide

(v) photochemical treatment of natural and industrial wastes.

The common features of all photoconversion systems are a photoredox reaction and fuel production such as:-

$$A + D \xrightarrow{h\nu} (AD)^* \longrightarrow A^- + D^+ \qquad (1.45)$$

$$2A^- + 2H_2O \longrightarrow 2A + 2OH^- + H_2 \qquad (1.46)$$

$$4D^{+} + 2H_2O \longrightarrow 4D + 4H^{+} + O_2 \qquad (1.47)$$

The overall photoredox reaction (1.45) to cyclic photodecomposition of water (1.46,1.47) can be performed either in dye-based-systems[124, 125] or semiconductor-based systems:[73,89,115-123] Because of the small fraction of solar radiation absorbed in dye-based systems the engineering efficiency of H_2 formation will be lower. This problem can be solved by using colloidal semiconductor dispersions as a light harvesting unit.

1.4.8 Solar Conversion Efficieny[126-131]

The spectra of sunlight in space (AM=0) and at the surface of the earth (AM=1) are shown in Figure 1.14[127,132] Absorption by a dye solution corresponds to this absorption spectrum, whilst a semiconductor absorbs only radiation of higher energy than the band gap energy (threshold absorber). The efficiency of solar energy conversion into redox energy for any threshold absorber is given by equation (1.48):-

$$\zeta = \frac{E_{stor}\int_{E_{th}}^{E_{th}+\Delta E} A(E)N(E)dE}{\int_{o}^{\infty} N(E)dE} \qquad (1.48)$$

In a semiconductor the threshold energy E_{th} is the band gap energy and E_{stor} is the cell voltage (less than E_{th} due to entropy production upon absorption and band bending)[133]. A(E) is

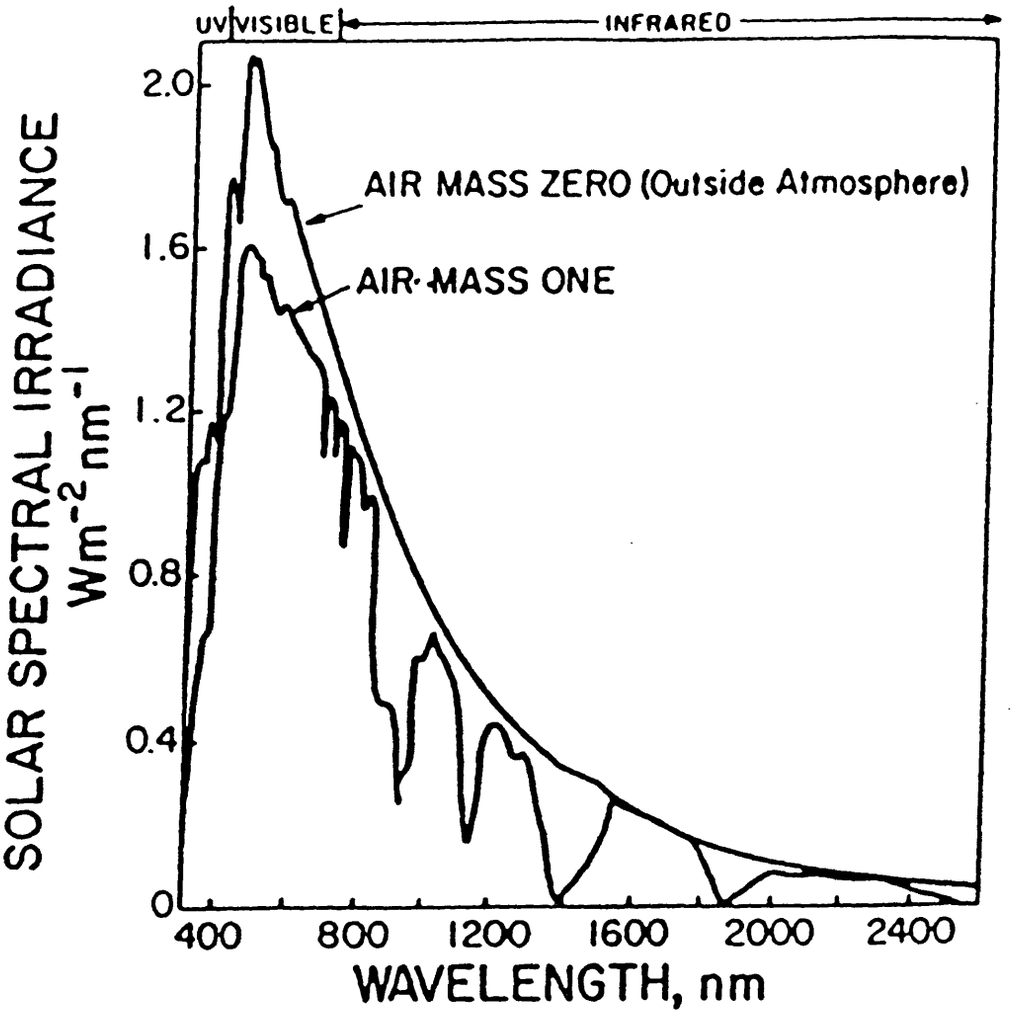


Fig. 1.14 The distribution of the solar spectrum outside the Earth's atmosphere (AM=0) and at normal incidence to the Earth's surface (AM=1/sinθ=1).

the fraction of the photons energy absorbed by the dye or semiconductor. N(E) is the incident photon flux density.

The maximum possible solar conversion efficiency has been calculated by a number of authors[127,128,131] to be 1.1eV giving a maximum value of η = 45%. Albery and Bartlett[97] calculated the optimum value for solar energy conversion which corresponds to a band gap of 1.5eV.Memming's[134] calculation gives a maximum around 1.6ev with 28% maximum theoretical efficieny (Fig. 1.15). However smaller band gap semiconductors produce larger maximum conversion efficiency.

It is necessary to mention that the theoretical conversion efficiency for photoelectrolysis cells has not yet been achieved. Because of basic differences between photoelectrolysis (one-step process for water clearage) and photovoltaic cell (two-step process), a separate and independent efficiency calculation for photoelectrolysis cells is essential.[135]

1.5 Conclusion

In recent years photochemical (PC) and photoelectrochemical (PEC) systems for the generation of either electricity or fuel using sun light have generated considerable interest. Solar-hydrogen production from photodecomposition of water is one of the new ideas for supplying the future energy requirement.

Side reaction limitation in organic, inorganic dye based systems caused attention to be directed towards semiconductors, particulate and colloidal systems as a light harvesting unit. Colloidal semiconductors have many advantages from a solar energy

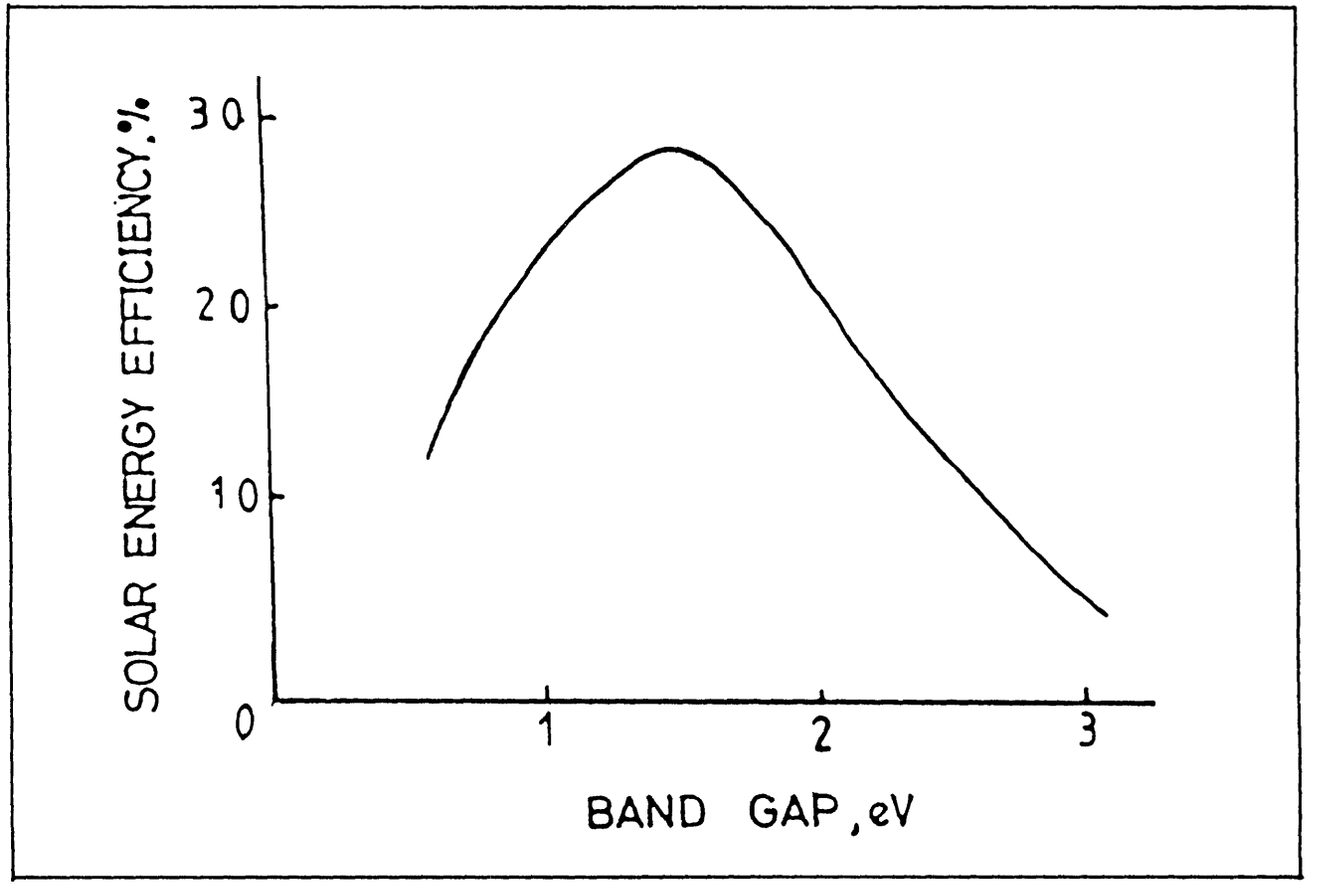


Fig. 1.15 Theoretical conversion efficiency as a function of band gap energy.

conversion view point. A number of disadvantages such as stability, efficiency, production and maintenance costs are investigated.

Colloidal CdS has been chosen in photo(electro)chemical reactions by the author for several reasons.

(i) CdS with E_{gap} = 2.42eV (corresponding to light of wavelength 520nm or less) absorbs approximately half of the visible spectrum of sunlight.

(ii) It can be prepared easily to produce relatively small (nm diameters) particles.

(iii) Colloidal CdS particles have a ratio of large surface area to volume, therefore can be expected to produce a high yield.

(iv) From the economic point it is much cheaper than expensive semiconductors, such as, silicon, GaP and so on.

1.6 Outline of this Thesis

The second chapter is concerned with the experimental equipment which was used in this work. The third chapter describes the photochemical reactions at the surface of Cds and developes a new method to study the kinetics of colloidal semiconductors. The surface chemistry of CdS is dealt with in Chapter 4. Some photophysical and photochemical aspects of ZnS are discussed in Chapter 5. Chapter 6 deals with immobilized Cds particles in Dialysis Membrane and organic compounds. Finally, the study of modified electrodes using immobilised CdS colloids within an electronically conducting polymer such as Polypyrrole is discussed in Chapter 7.

CHAPTER 2

Experimental Apparatus

Numerous experimental techniques were employed in this thesis as below.

2.1 Instrumentation

2.1.1 Steady-State Technique

Steady-state experiments were carried out with an Applied photophysics Clincial Photoirradiator system using a 900w Xenon lamp. Experiments with very intense light were carried out and using the 900W Xenon lamp filtered by a 5cm quartz cell filled with water to remove infrared wavelengths (Chapter 6). Experiments with low intensity monochromatic light were performed by passing white light through a high radiance monochromator. Light intensities of the 900 watt Xenon lamp were measured with a calibrated thermopile.

2.1.2 Conventional Flash Photolysis

The flash photolysis method is an important technique for studying fast reactions. Porter and Norris[136] showed that a large number of reactions can be initiated by a very intense flash of light. The excited state lifetimes of chemical compounds vary from less than a picosecond (10^{-12} sec) to tens of seconds.

Microsecond flash photolysis experiments were made at pH 7.5

in a 10cm quartz cell using an Applied Photophysics K200 system as described in Reference [137]. Data analysis was performed on a Sinclair ZX spectrum microcomputer, which was interfaced to the flash photolysis system.

The excitation of colloidal CdS particles was carried out by using two flash lamps as shown in Figure (2.1). The change in the solution's transmittance was monitored continuously at a fixed wavelength using light from a tungsten halogen lamp which passed through the sample and then through a high radiance monochromator. A photomultiplier detected any transmittance change and displayed it on a Gould type OS4100 digital storage oscilloscope. It is triggered by a photodiode connected to a quartz fibre optic from the excitation cavity. The excitation beam was filtered with quartz jackets containing the appropriate solution on the front of flush lamps and monitoring beam by glass or appropriate plastic filters.

The samples were in a 10cm cylindrical quartz cell bubbled with N_2 to remove O_2 before any experiment. The kinetics of reactions were analysed with two microcomputer programs (Appendicies 1 and 2) and traces were transferred directly to the computer via an analogue to digital converter. Any change in transmittance could be converted itno absorbance by equations (2.1),(2.2) as shown in Figure 2.2.

Absorbance $$\Delta OD = \log \frac{I_o}{I_o - I_t} \qquad (2.1)$$

since V=RI, so

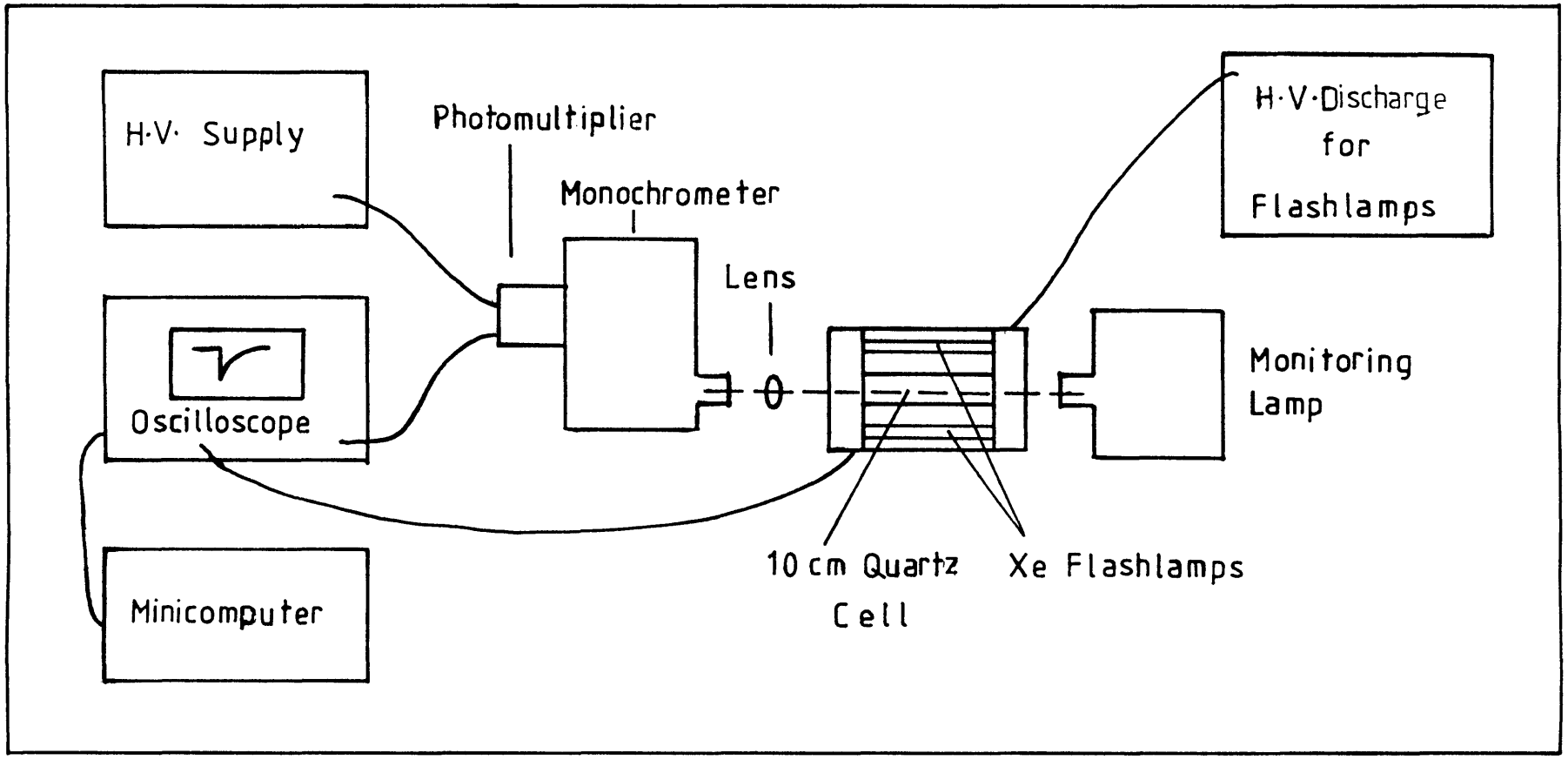


Fig. 2.1 Microsecond Flash Photolysis Apparatus

$$\Delta OD = \log \frac{V\infty}{V\infty - \delta V} \qquad (2.2)$$

The computer analysed the transmittance change in terms of first and second order kinetics by using linear least squares method as below:

For first order reaction:

$$x = \ln \Delta OD \text{ and } y = \text{time} \qquad (2.3)$$

for second order:

$$x = \frac{1}{\Delta OD} \qquad (2.4)$$

The rate constant can be calculated using least-squares linear regression with the following equations"

$$K = \frac{\Sigma[(x_i - \bar{x})(y_i - \bar{y})]}{\Sigma (y_i - \bar{y})^2} \qquad (2.5)$$

$$\text{and correlation coefficient} = \frac{\Sigma[(x_i - \bar{x})(y_i - \bar{y})]}{\Sigma[(x_i - \bar{x})^2 (y_i - \bar{y})^2]} \qquad (2.6)$$

Correlation coefficients were usually better than 0.99.

2.1.3 Laser Flash Photolysis

A pulsed laser reduced the time by a factor of 1000 and provided a monochromatic and coherent light sources. The Ruby laser consisted of Al_2O_3, containing about 0.05% by weight of Chromium ions as Cr_2O_3. Chromium ions give ruby its pink colour. The excitation of Cr^{3+} ions by flash is shown in Figure 2.3. Nanosecond flash photolysis experiments were made at pH 7.5 in a

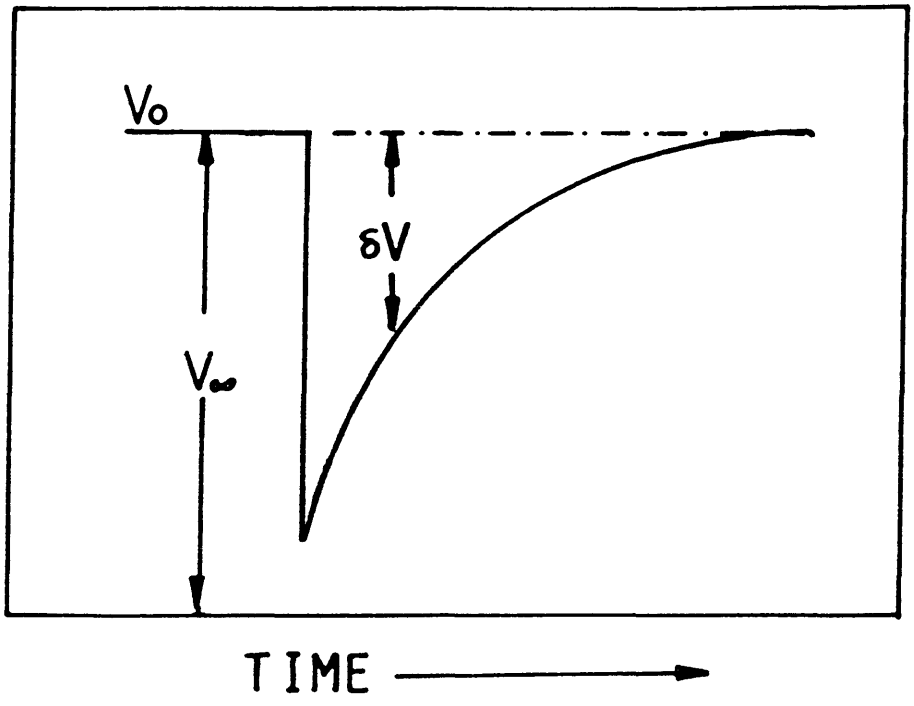


Fig. 2.2 Analysis of transients.

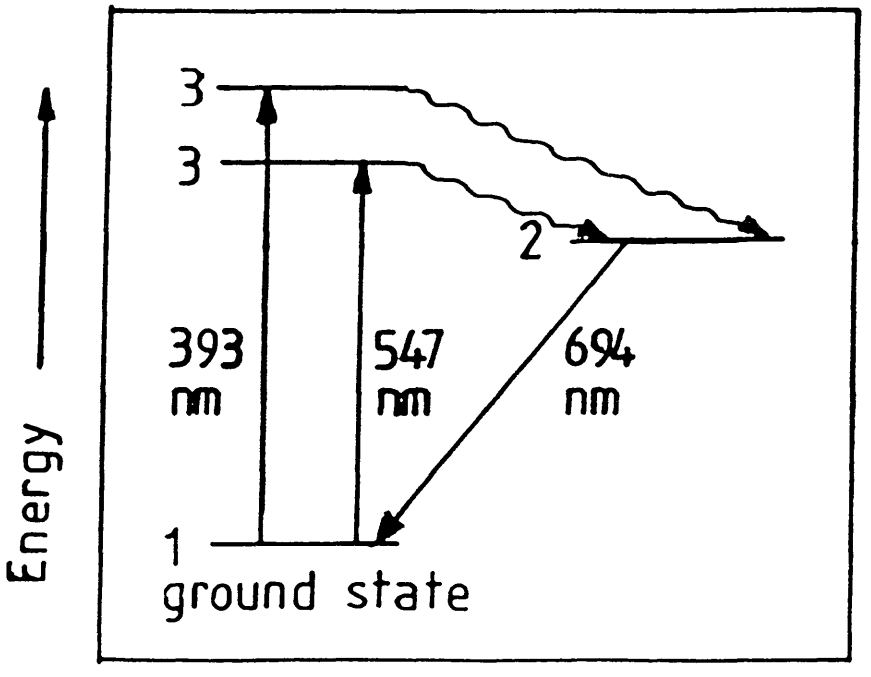


Fig. 2.3 The Cr^{3+} energy levels in the ruby laser (3-level laser).

1cm quartz cell using a Spectrum Laser Systems ruby laser with max output of 650mJ.

Data analysis was carried out on a BBC microcomputer, which was interfaced to the flash-photolysis system.

2.1.4 Dynamic Light Scattering

The size of colloidal CdS particles was determined by dynamic laser light scattering which is schematically illustrated in Fig. 2.4. A spectra physics model 168.2-W argon laser operating at 488nm was combined with a ganiometer to measure the amplitude of scattered light, using a Malvern K7025 correlator and an EMI 9863 photomultiplier tube in a Malvern RR 109 housing system. Samples were filtered through Millipore 0.22 μm filters. The average of CdS particles was 17nm. The size of particles depend on the method of preparation of colloids.

2.1.5 Absorption Spectroscopy

Energy absorbed in the IR region causes changes in vibrational energy accompanied by changes in rotation energy. Absorption in the visible and UV-regions changes the electron energy of atoms or molecules, accompanied by change in vibrational and rotational energy. The change in electronic energy involve the outer-electrons. With high-energy radiation, X-rays, the inner-electrons will be raised to an excited state. The energy levels of diatomic molecules are shown in Fig. 2.5.

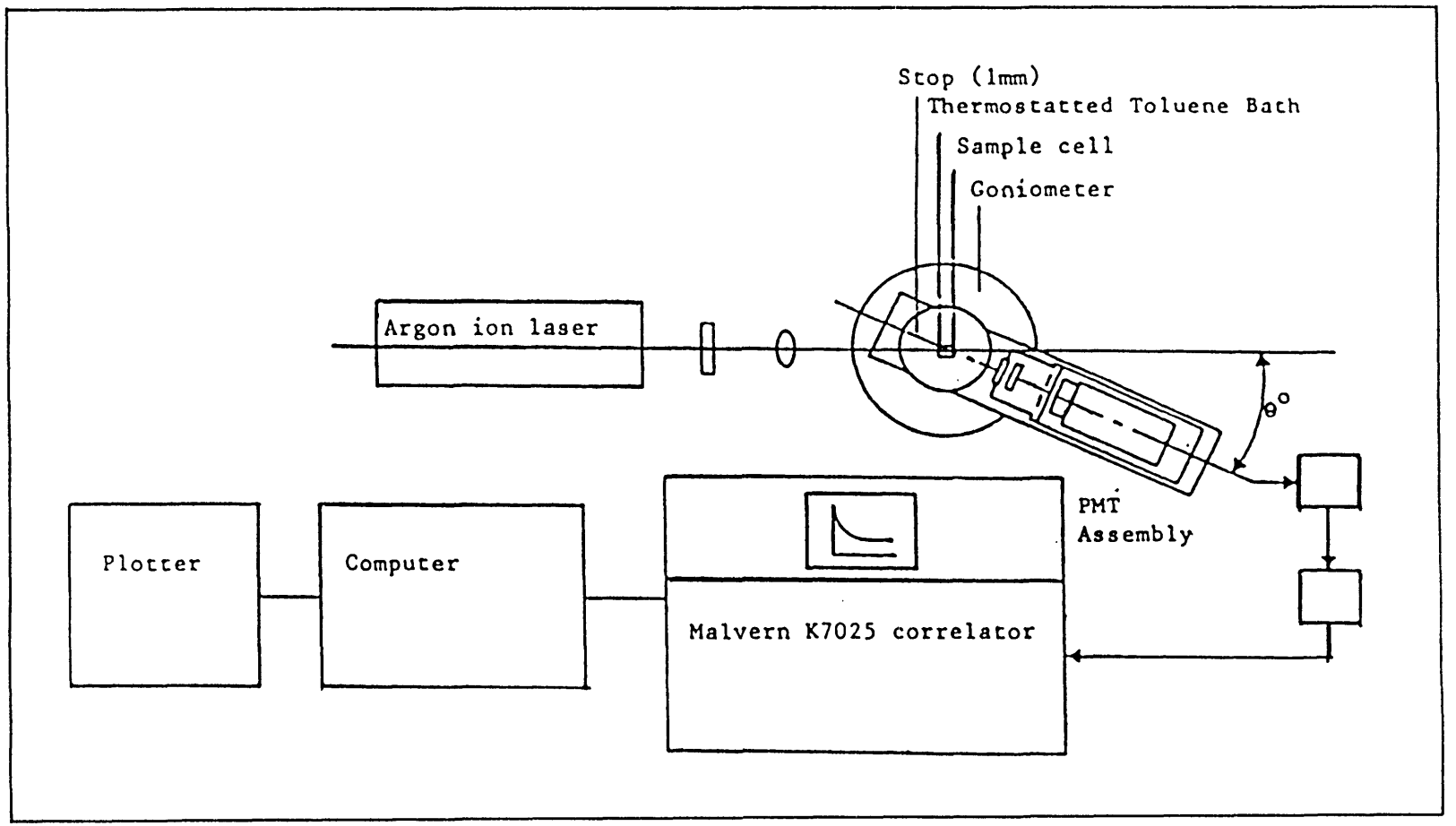


Fig. 2.4 Schematic diagram of Dynamic Light Scattering (DLS).

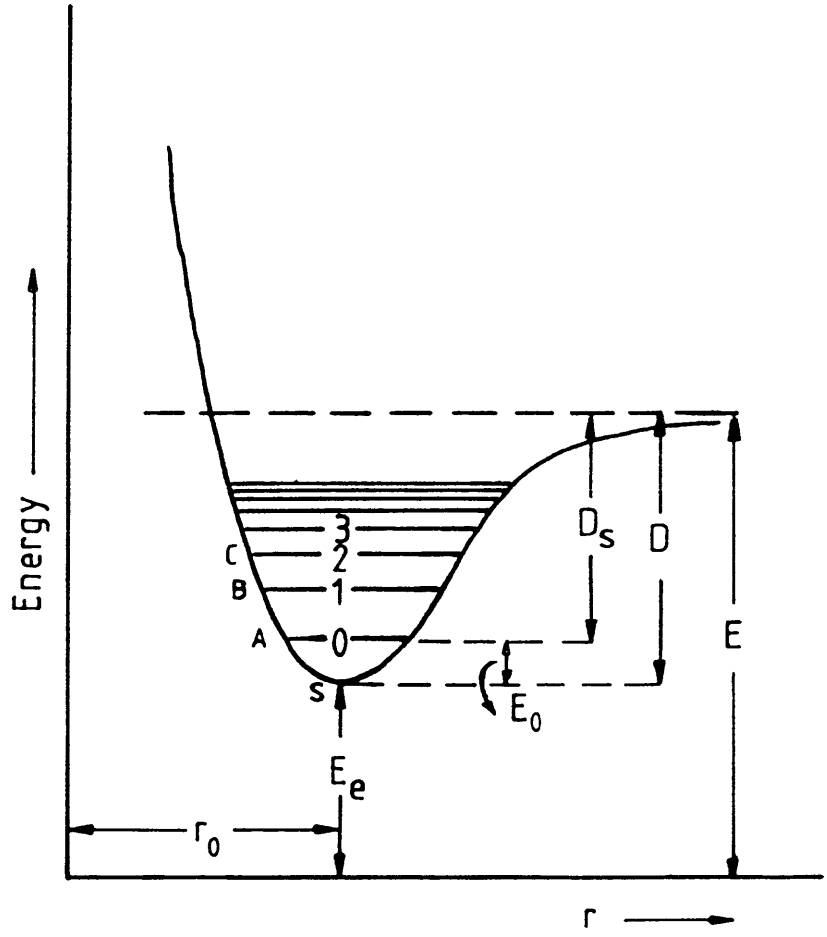


Fig. 2.5 Energy levels of diatomic molecule.

Absorption spectroscopy was used for analytical studies in the UV-Vis region. It is a powerful tool in the observation and study of low concentration and transient species, as in flash photolysis. Absorption spectroscopy consists of four major components as shown in Fig. 2.6.

Steady state absorption spectra were recorded by a double-beam Perkin-Elmer 554 and a Perkin-Elmer 402 for 1cm and 10cm quartz cells respectively at room temperature.

2.1.6 Emission Spectroscopy

The emission technique is about 1000 times more sensitive than absorption spectrophotometry. Fluorescence spectroscopy can detect a concentration as low as one part in 10^{10}. The reason for this high sensitivity is that luminescence measurement involves the detection of emitted photons. In contrast, conventional absorption spectrophotometry involves a determination of the difference between two measurements of light intensity, one derived from a cell containing solvent only and the other from a cell containing solute and solvent. The basic components of a luminescence instrument are shown in Fig. 2.7.

Luminescence intensity allows measurement of the change in concentration with time of the emitting species, while the wavelength distribution of the luminescence provides information on the nature and energy of the emitting species. The intensity

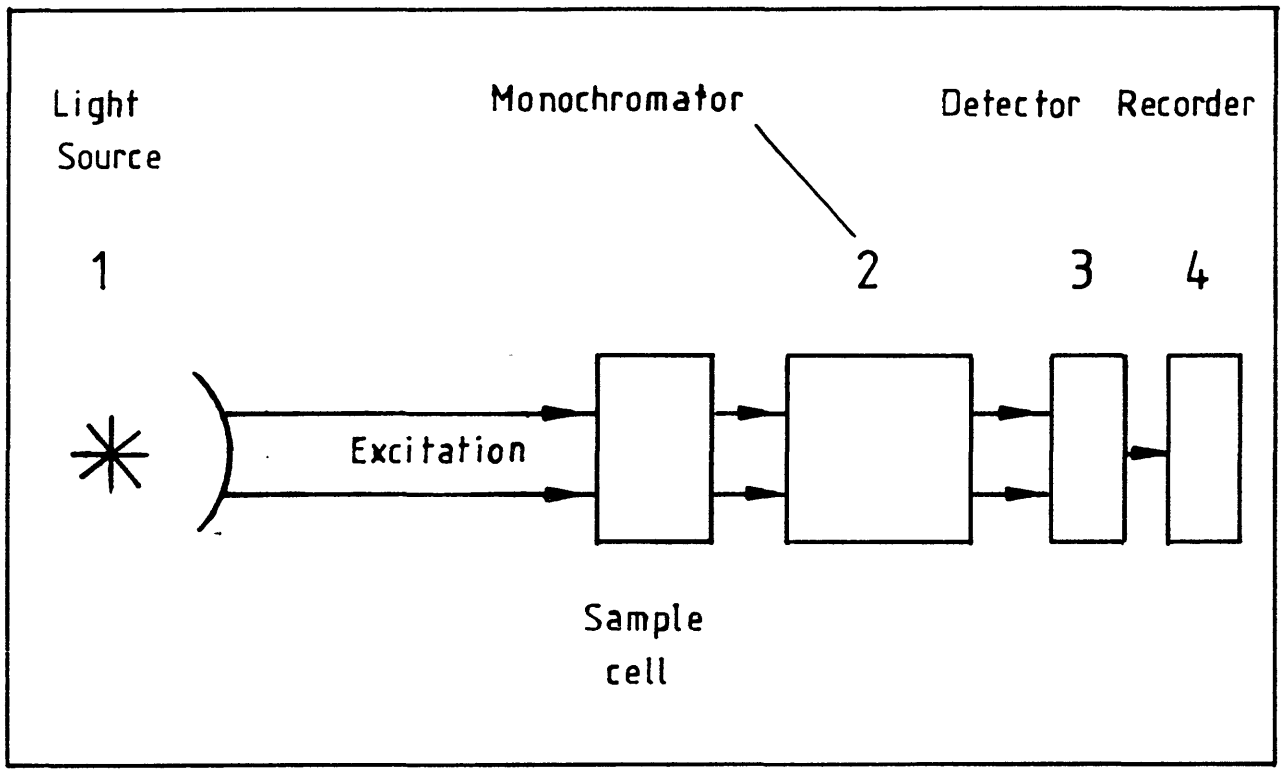


Fig. 2.6 Schematic diagram of absorption spectroscopy.

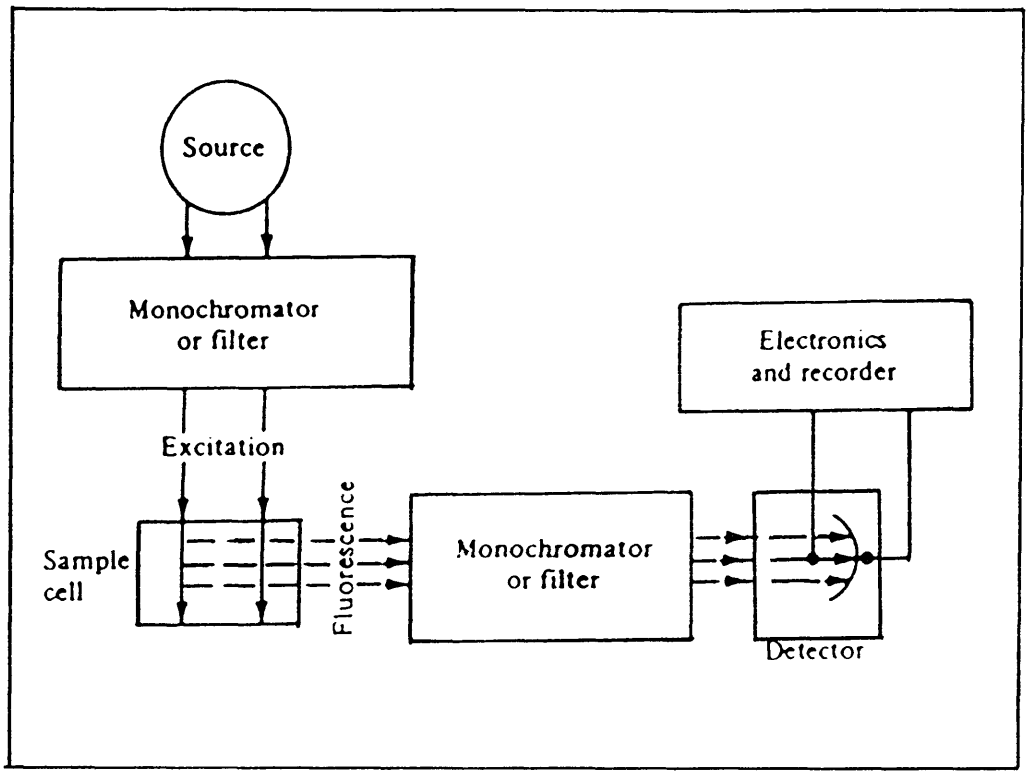


Fig. 2.7 Schematic diagram of luminescence spectroscopy.

of luminescence can be calculated by using Beer's law (equation 2.7).

$$I_L = S\eta_L I_o (1-e^{-\varepsilon cl}) \qquad (2.7)$$

In which S is the cross-sectional area of the sample under exciting radiation and η_L is the quantum efficiency of the luminescence. Equation 2.7 simplifies for fluorescence (if $\varepsilon cl < 0.05$) and phosphorescence (if $\varepsilon cl < 0.01$) as below

$$I_L = S\ \eta_L I_o\ \varepsilon cl \qquad (2.8)$$

$$I_L = KI_o c \qquad (2.9)$$

From equation (2.9) it becomes apparent that luminescence of a sample is directly proportional to the intensity of incident radiation, Io, and the concentration of luminescent species, c.

The emission/excitation spectra were measured on a Parkin Elmer MP4 and LS5 spectrofluorimeter, interfaced to the recorder. The photoemission (PE) spectrometer consists of two diffraction grating monochromators with continuously variable band pass selection from 0.2 to 20nm. The excitation monochromator selected wavelengths from 150 watt Xenon source lamp and illuminated the sample with monochromatic light in the range of 200-800nm. The emission monochromator emitted light at 90° angle to the incident light and permitted lective measurement of its intensity in the range of 200-800nm. All experiments were performed in a 1cm quartz cell.

2.1.7 Electron Microscope

Observation of colloidal particles such as CdS and ZnS, which are in the range of nm is impossible with an optical microscope. The resolution power of this apparatus is limited by the wavelength λ of the light used for illumination. The resolution limit δ (smallest distance to separate two objects) is given by

$$\delta = \lambda/2n\sin\theta \qquad (2.10)$$

where θ is half the angle subtended at the object (angular aperture), n is the refractive index of the medium object and objective lense and $n\sin\theta$ is the numerical aperture of the objective lense for a given immersion medium.

There are two techniques for overcoming the limitation of optical microscopy in the study of colloidal systems:

(i) Transmission and scanning electron microscopy

(ii) Dark-field microscopy

For measurement of colloidal semiconductors particles only the first technique was selected by the author during the experimental work. It is illustrated briefly below.

2.1.7.1 Transmission Electron Microscopy (TEM)

Determination of colloidal particle size was performed using a JEOL 200CX electron microscope with resolution of $1.4A^{o}$. A small amount of the sample was deposited dropwise on plastic or carbon film supported on a fine copper grid, any surplus wiped off with filter paper and dried in open air. The electron beams

were directed on the sample and scattered beams made the final image which could be made visible on a fluorescent screen. The amount of scattering depended on the thickness and atomic number of the sample's atoms.

2.1.7.2 Scanning Electron Microscopy (SEM)

In this technique only electron beams with medium energy scan across the sample in a series of parallel tracks. Interaction of electron beams with sample produces various signals, such as X-rays, cathodoluminescence, back-scattered electrons and secondary electron emission which can be detected on a fluorescent screen. The magnification in a SEM is less than in TEM but several hundred times greater than that in an optical microscope. The significant advantage of this technique is the great depth of focus which is very important in the study of colloids and surface science.

Determination of size of particles was carried out using a JEOL 35CF electron microscope. Samples before being subjected to energetic electron-beams should be either a conductor or have a thin layer of gold or graphite deposited on them by EM Scope evaporation apparatus. The main reason for this process is to control and earth the energetic beams.

2.1.8 The RRDE Apparatus

The Rotating Ring Disc Electrode (RRDE) consists of the various components as described in turn:

2.1.8.1 Electrodes

The RRDE consists of a platinum disc, an insulating gap of teflon, a platinum ring and a teflon mantle. The electrode surface was first polished with 25μm aluminium oxide in a glycerol slurry followed with diamond lapping compounds of 6μm and 3μm. The final polish was carried out by hand using 1μm and 0.3μm aluminia (Banner Scientific) in pure water on cotton wool. Usually only the final polish was repeated before each experiment. The schematic of a rotating ring-disc electrode is shown in Fig. 2.8.

The reference electrode employed was a home made saturated calomel electrode (SCE) for aqueous solution. The counter electrode was a platinum gauze.

2.1.8.2 Electronics

In all experiments a three electrode configuration was used (Fig. 2.9). The cell current flows between the working and the counter electrodes, while the potential of the working electrode is measured with respect to the reference electrode using a high impedance measuring device.

The basic unit used for the control and measurement electronics was the operational amplifier (op.amp.) Fig. 2.10. The properties of an ideal op.amp are

i. Zero current at the inputs

ii. $V_{in}^- = V_{in}^+$, provided there is a closed feedback loop

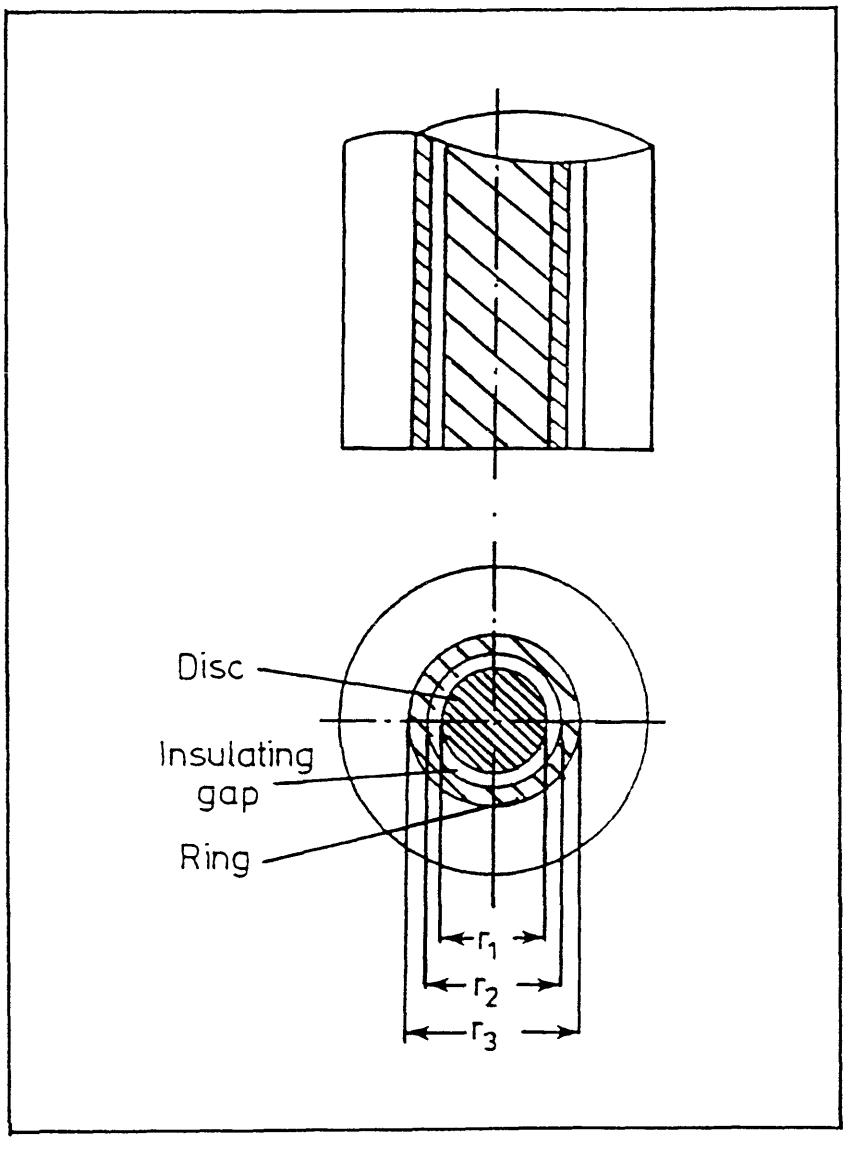


Fig. 2.8 Cross section of a RRDE.

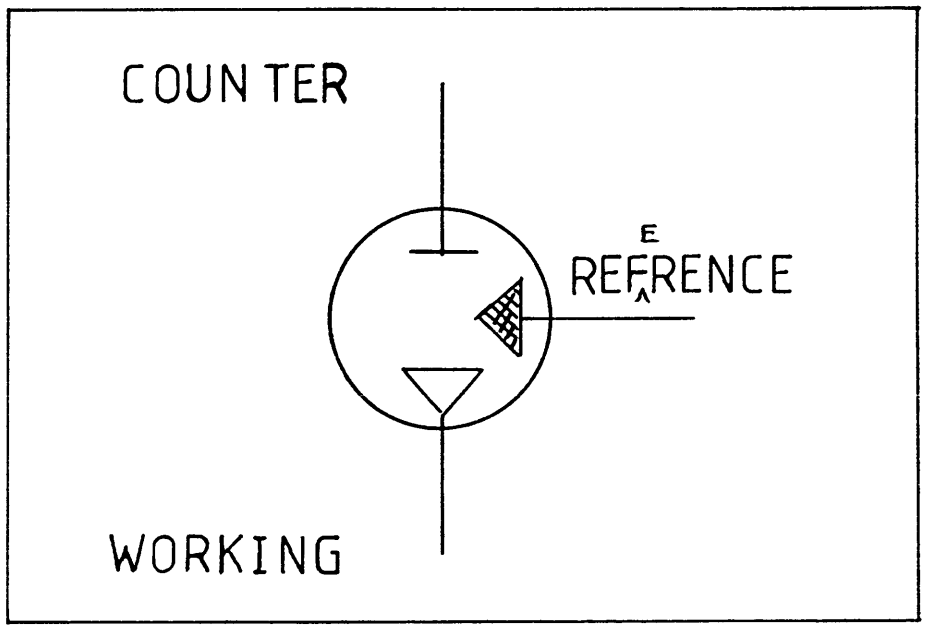


Fig. 2.9 The three electrode system.

by using 20kΩ resistance between the V_{in}^{+} and V_{out}

The circuitry was constructed on a modular basis comprising the following modules.

(I) Voltage Follower

In this case $V_1 = V_2$ (Fig. 2.11)

This provides a means of drawing zero current at the input, V_1, and giving a low impedance output of the same voltage.

(II) Voltage Inverter

For this module $V_1 = - V_2$ (Fig. 2.12)

(III) Summing Inverting Amplifier

This unit is used to add voltages and then multiply the sum by a factor -x, where x-1, 10 or 25 (Fig. 2.13).

$$(V_1 - V_3) + (V_2 - V_3) = \frac{V_3 - V_o}{x} \qquad (2.11)$$

and

$$d(V_1 + V_2) = - \frac{dV_o}{x} \qquad (2.12)$$

(IV) Potentiostat

Figure 2.14 shows schematic diagram of a potentiostat. This module allows the control of either one or two working electrodes, and employes three op-amps. Op-amp 1 holds the reference electrode at the chosen potential and forces current

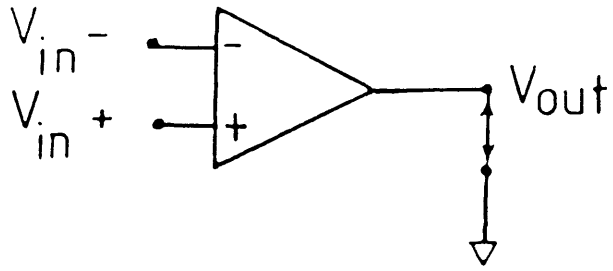


Fig. 2.10 An Op-amp.

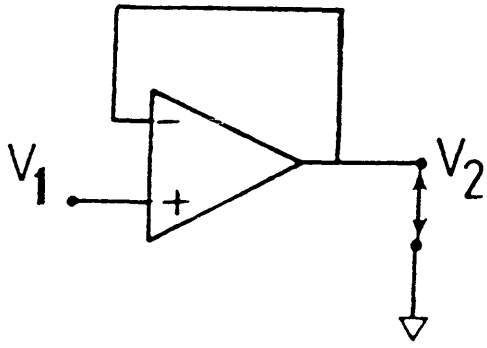


Fig. 2.11 Voltage follower.

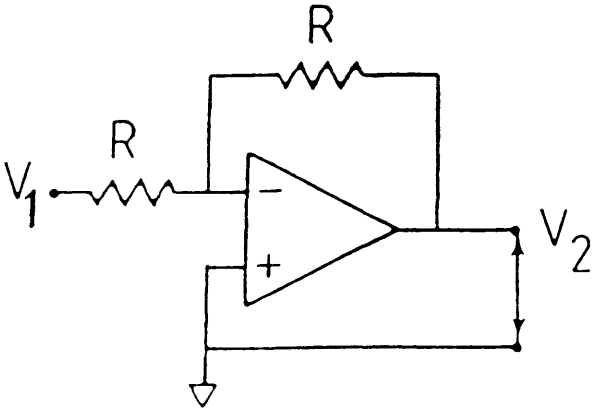


Fig. 2.12 Voltage inverter.

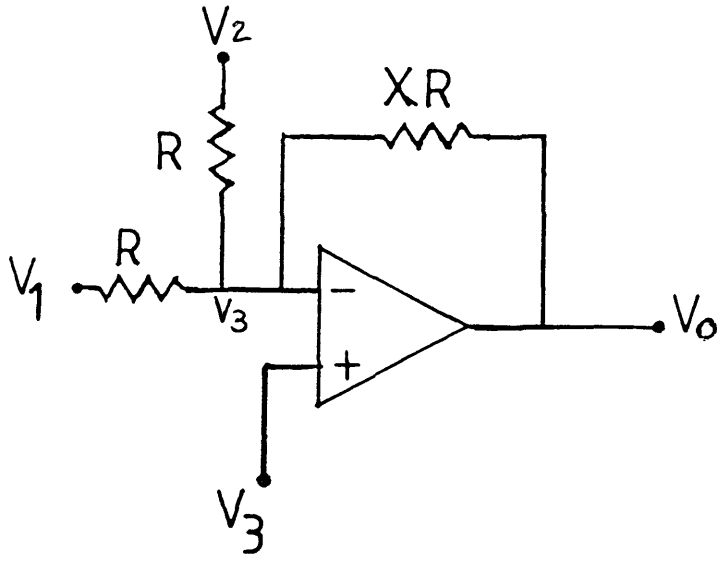


Fig. 2.13 Summing inverter amplifier.

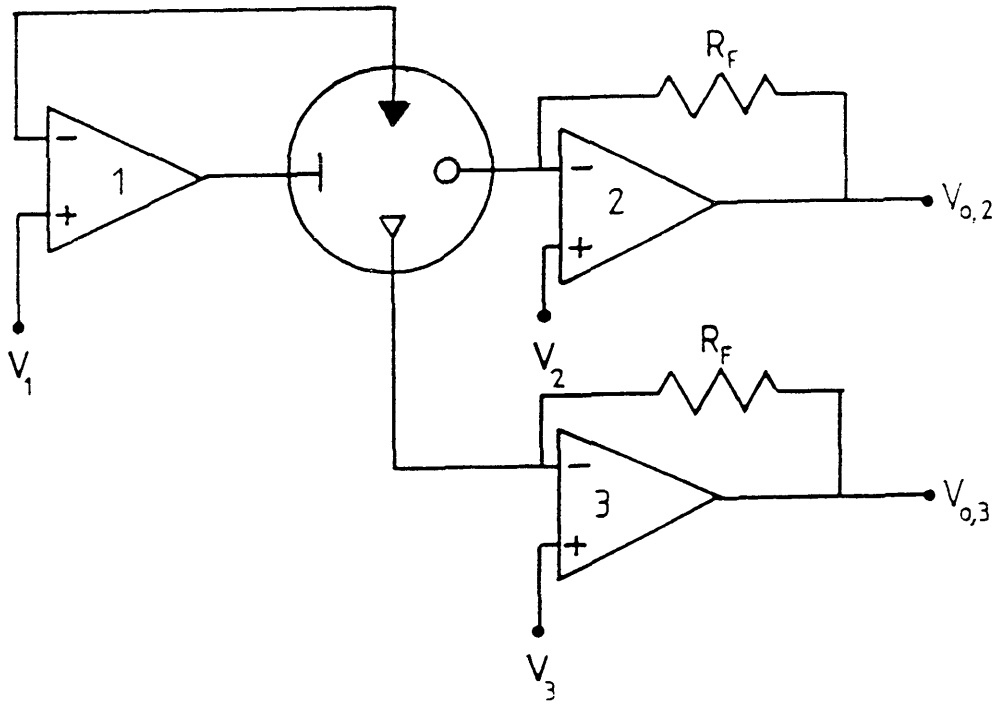


Fig. 2.14 A potentiostat.

through the counter electrode. Op-amps 2 and 3 are used to control the ring and disc electrode respectively. The output voltage of either disc or ring electrodes is found from

$$V_{out} = IR_F - V_{in}+$$

The current passed (by both Ring and Disc) is given by the differences between $V_{in}+$ and V_o, provided the value of R_F is known. R_F generally may be varied from 1kΩ to 1MΩ, to extend the range of currents that may be measured.

(V) Triangular Wave Generator

The TWG produces a triangular ramped voltage which consists of a wave generator (Fig. 2.15a) and a power supply (Fig. 2.15b). The power supply converts ±15V to ±8V and ±5V and allows the potential limits to be set independently up to ±5V. The range of sweep rates could be varied from 1mV/s to 2V/s. The setting of potential is also possible manually.

(VI) Voltage Source

This provides two variable sources which could be set to any value between ±5V for one source and ±1V for the other (Fig. 2.16).

2.1.8.3 Rotation System

The light source, electrodes and electrochemical cell were

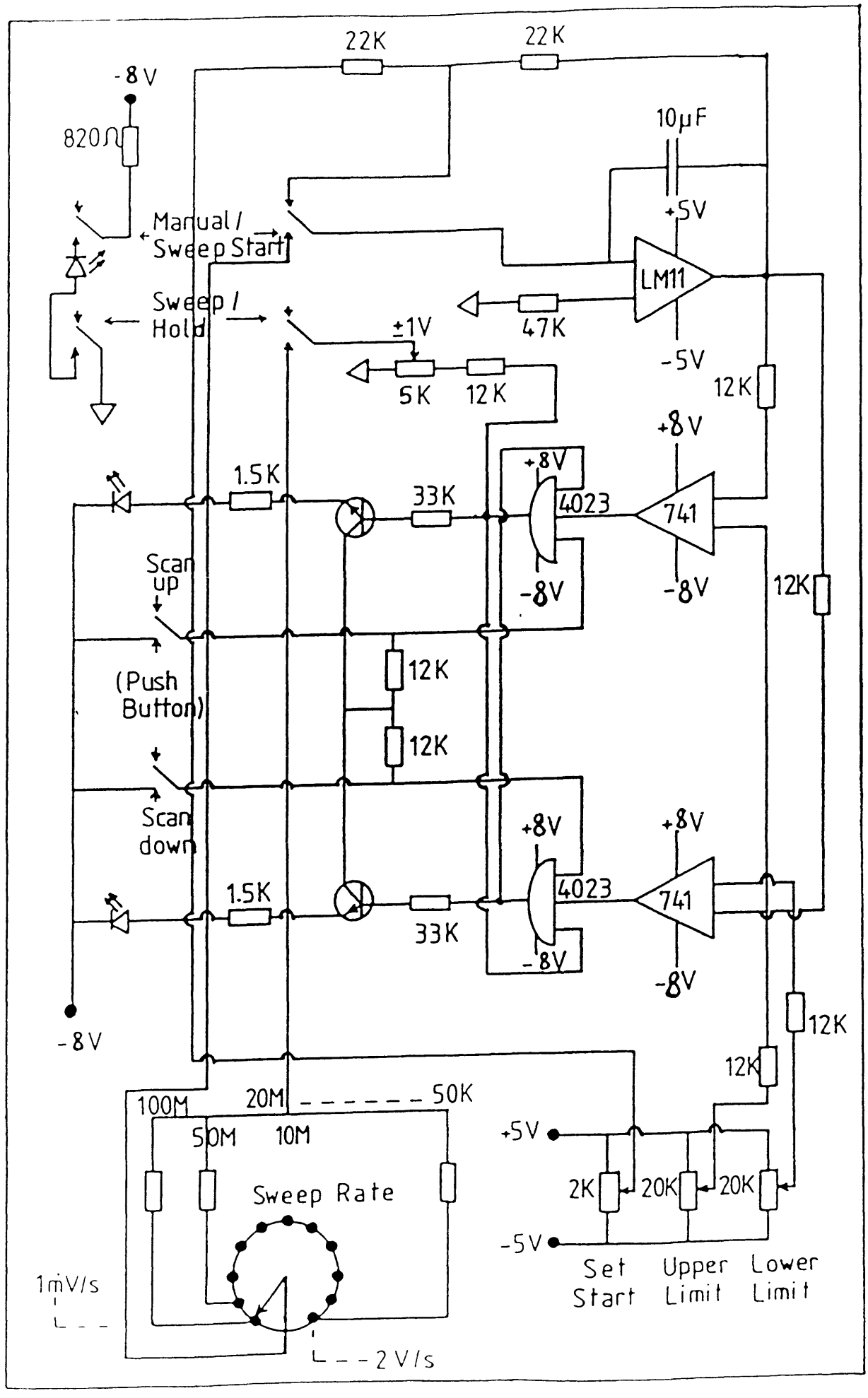


Fig. 2.15a A Triangular Wave Generator.

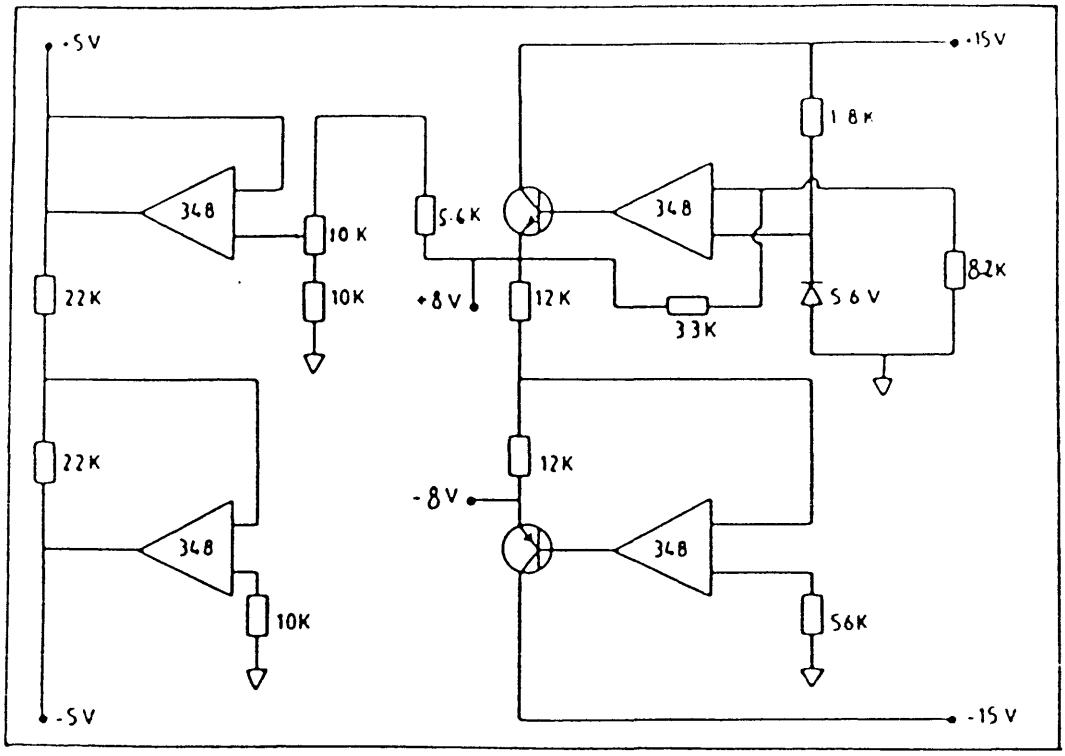


Fig. 2.15b A Power supply for Triangular Wave Generator.

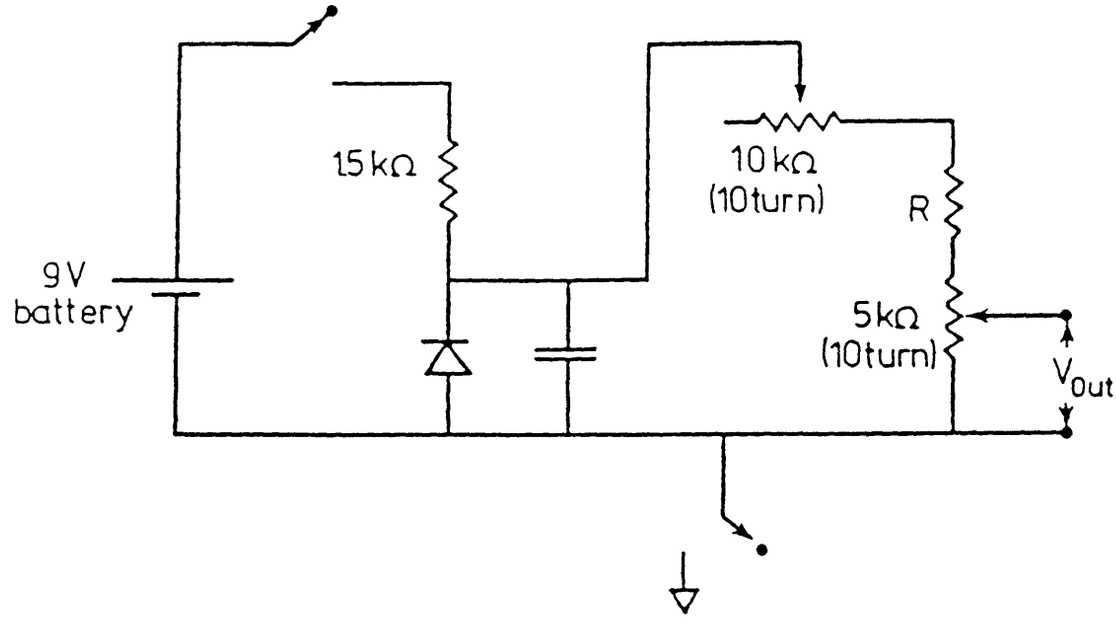


Fig. 2.16 Voltage Source.

R = 0, V_{out} = ± 5 V (maximum).

R = 22 kΩ, V_{out} = ± 1 V (maximum)

all mounted on a bearing block. The block supported on two vertical stainless steel rods attached to a heavy base to ensure stability. The motor was a printed armature d.c. servo motor with (Printed Motors Ltd). Rotention way controlled by an (Oxford Electrodes) motor controller with digital readout of the rotation speed to ±0.01HZ up to a maximum of 50HZ.

2.1.8.4 The Electrochemical Cell

The electrochemical cell was built of double-wall glass vessel with a quartz flat (Heraeus Silica and Metals Ltd). The double-wall allows circulation of water around the cell for temperature control. A side-arm was used to hold a fitted compartment containing the counter electrode to prevent any undesirable counter electrodes products from reaching the working electrode. The cell had a lid of teflon fitted with holes for the working electrode, Reference elctrode and for the nitrogen delivery teflon tube. Figure 2.17 shows the diagram of an electrochemical cell.

2.1.9 Light Source

The light source in RRD experiments was an AL/223, 250W, 24V quartz-iodine projector lamp with a filament temperature of 3350K. The lamp was powered by a Farnell 30/10s stabilised power supply. The light was focused onto the electrode using a front-silvared mirror as shown in Figure 2.18.

Ealing-IRI 25mm interference filters (10nm band width) were used to provide monochromatic light and Ealing neutral density

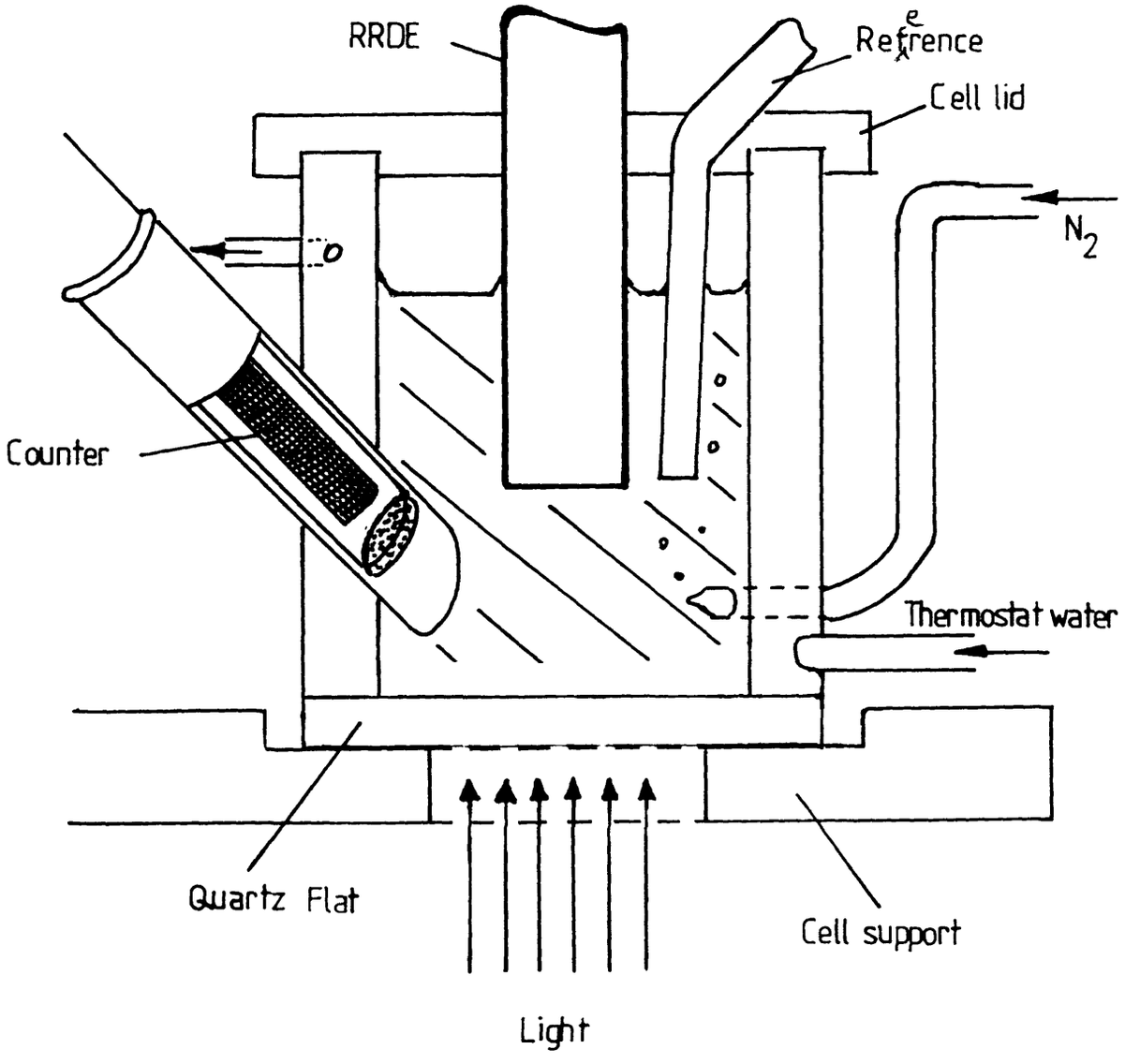


Fig. 2.17 Schematic diagram of the electrochemical cell.

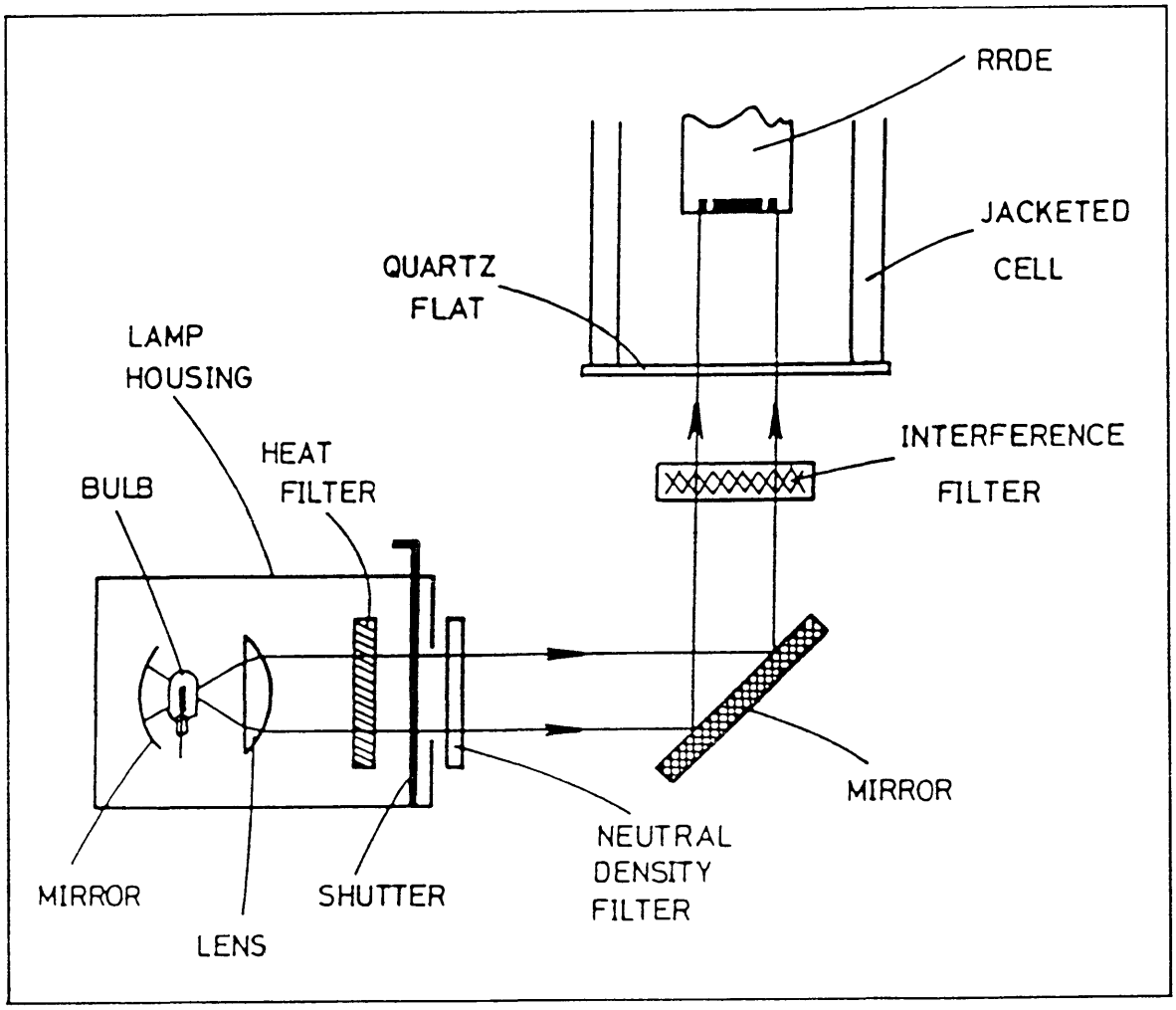


Fig. 2.18 A light source

filters were used to vary the irradiance.

2.2 Sample Preparation

2.2.1 **Colloidal CdS** was prepared by passing H_2S gas into a solution of $Cd(NO_3)_2$ (5×10^{-3} mol dm^{-3}) with (10^{-2} mol dm^{-3}) sodium hexametaphosphate (SHMP) as a supporting agent. The method of preparation was as described by Gratzel and coworkers[52], except that solutions were purged for about half an hour with N_2 to prevent occlusion of O_2 before bubbling with H_2S. Colloids were also made from Cd^{2+} and Na_2S with and without SHMP. In some colloidal CdS the cationic supporting agent cetyltrimethylammonium bromide (CTAB) was used instead of SHMP (Chapter 3).

2.2.2 **Platinized CdS** was used in Chapter 4. This method[138] involved the preparation of a pt-citrate complex by refluxing for 30min and 60min, a solution containing 30mg of Chloroplatinic acid [H_2ptCl_6, $6H_2O$ (BDH)], 30ml of a 1% sodium citrate solution [1gram citric acid (powder) and 80ml double-distilled water (DDW), then NaOH to adjust to pH 7-8, finally made up to 100ml], and 120ml of DDW. Final pH was 6.6. 50ml of pt-citrate + 1 gram CdS powder were stirred and then 5.8 gram of NaCl added. Pt/semiconductor precipitated. It was filtered and repeatedly washed with DDW before being dried in air.

2.2.3 CdS Thin Film Preparation (Chapter 6)

2.2.3.1 By Polymers

(i) 1% PVA was prepared in boiled DDW. 0.4gram $(Cd(NO_3)_2$ was dissolved in 1% PVA. A few drops were placed onto glass slide and water allowed to evaporate. 0.1 mol dm^{-3} Na_2S solution was prepared separately and the glass slides were dipped into this solution. A thin yellow film of CdS was observed on the surface of the glass slides. They were washed and left to dry in an autoclave at about 80^oC.

(ii) The above process was carried out with 1% polyvinylpyridine (PVP) and polyacrylamide (PAA). When the PAA was dissolved in boiled ethanol, the solution precipitated upon adding $Cd(NO_3)_2$.

2.2.3.2 **Dialysis Membrane**

Transparent dialysis membranes is produced by Fision Co. from cotton lint, one of the purest naturally-occuring cellulose sources. Normal molecular weight is reported by investigators[140] to be 12000 to 14000. The thickness of the membrane is 0.32mm and the average pore radius is $24A^o$. The membrane was washed in boiling DDW for about one hour followed by washing with normal temperature DDW to remove the glycerine. It was left to dry and then soaked for 24 hours in a Cd^{2+} ($5x10^{-2}$ mol dm^{-3}) solution at room temperature. After washing with DDW and drying it was dipped either into (10^{-3} mol dm^{-3}) Na_2S or purged with H_2S for a few minutes. Simultaneously the yellow colour appeared indicating immobilized CdS particles in the dialysis membrane. Finally the CdS membrane film was washed and dried.

2.2.4 Colloidal ZnS

This colloid was prepared in the same manner as CdS/SHMP. In the case of doped ZnS, purging with H_2S to yield ZnS was carried out after dissolving the dopant ions such as Eu^{3+}, Tb^{3+} in a solution containing (5×10^{-3} mol dm^{-3}) Zn^{2+}.

2.3 Materials

All the chemicals, suppliers and degree of purifications used by the author are listed in the following table 2.1.

Materials	Supplier	Purification	Materials	Supplier	Purification
$Cd(NO_3)_2, H_2O$	BDH	Analar	H_2S	BOC	
$CdCl_2, \frac{2}{3} H_2O$	Aldrich		O_2	BOC	
$Cd Br_2, 4H_2O$	BDH	98%	N_2	BOC	white dot
$Cd I_2$	Hopkin & William		Air	BOC	
$CdSO_4$	BDH		Water	-	double distilled
CdO	Aldrich		$H_2 Pt Cl_6$	BDH	
KCl	BDH		sodium hexameta-phosphate	BDH	
KBr	BDH				
KI	BDH		Methyle Viologen	BDH	Analar
$K_3Fe(CN)_6$	BDH		Methyle orange	Fision	99%
$K_4 Fe (CN_6).3H_2O$	BDH		EDTA	BDH	98%
$K_2 S_2 O_8$	BDH		Cysteine	Sigma	
$Na_2 S_2 O_3$	BDH		polyvinylalcohol	BDH	98%
			polyvinylpyridine	Aldrich	
$Zn Cl_2$	BDH		polyacrylamid	BDH	
$Zn (NO_3)_2, 6H_2O$	BDH		CTAB	BDH	
$MnCl_2, 4H_2O$	BDH		Visking tube	Fision plc	
$EuCl_3, XH_2O$			Citric acid	"	
$Eu (NO_3)_3.5H_2O$					
$TbCl_3, XH_2O$	Aldrich				
Na_2S	BDH	Analar			

CHAPTER 3

Time resolved photoredox reactions of collodial CdS

Introduction

Over the past few years CdS colloids have received considerable interest as microheterogeneous electrodes for solar energy conversion [52,73] or photocatalysis [145,146]. Colloidal semiconductors can be assumed to be dispersed microelectrodes in solution for the study of the kinetics of photoinduced electron transfer reactions.

The purpose of this Chapter is to describe the photophysical and photochemical behaviour of colloidal CdS and to study interfacial electron transfer at the surface of colloidal semiconductors. A relation between the kinetic data and particle size will be established.

3.1 Photoabsorption in CdS

When the semiconductor-electrolyte junction is illuminated with light, photons of energy greater than the semiconductor band gap (E_{gap})are absorbed and produce electron-hole pairs in the semiconductors. While photons with energy less than band gap are transmitted. The absorption coefficient, α, in a semiconductor varies with wavelength and near the band edge exhibits the following form [102,121,144]:

$$\alpha = A\,(h\nu - E_g)^{n/2}/h\nu \qquad \text{if } h\nu > E_g \qquad (3.1)$$

$$\alpha = 0 \qquad \text{if } h\nu < E_g \qquad (3.2)$$

in which A is a constant, and n depends on whether the transition is direct (n=1) or indirect (n=4) as shown in figure 3.1.

A typical absorption spectrum of CdS sols with sodium hexametaphosphate as a stabilizer is shown in figure 3.2.

The similar results were obtained by Grätzel, Henglein, Thomas and co-workers using different surfactants.

The onset of CdS colloid absorption at λ = 510 nm correlates with the band gap energy (2.42 eV) and the spectrum of single crystals.[142] Comparison of this spectrum with an ideal (theoretical) plot of absorption coefficient against wavelength as shown in Fig. 3.2, results that the absorption at the band edge does not rise as sharply. It is possible to interpret this as being due to the small size of the particles (less than 20 nm), so that light can pass through several particles before becoming completely absorbed. This is an important aspect of colloidal semiconductors in the study of the nature of luminescence and interfacial electron transfer kinetics.

Illumination of colloidal CdS produces electron-hole pairs which may reduce or oxidise suitable electron acceptors or electron donors respectively.

In the presence of oxygen as an electron acceptor photodecomposition of colloidal CdS is observed. These processes can be shown as below

$$CdS \xrightarrow{h\nu} CdS\ (e^-, h^+) \qquad \text{absorption} \qquad (3.3)$$

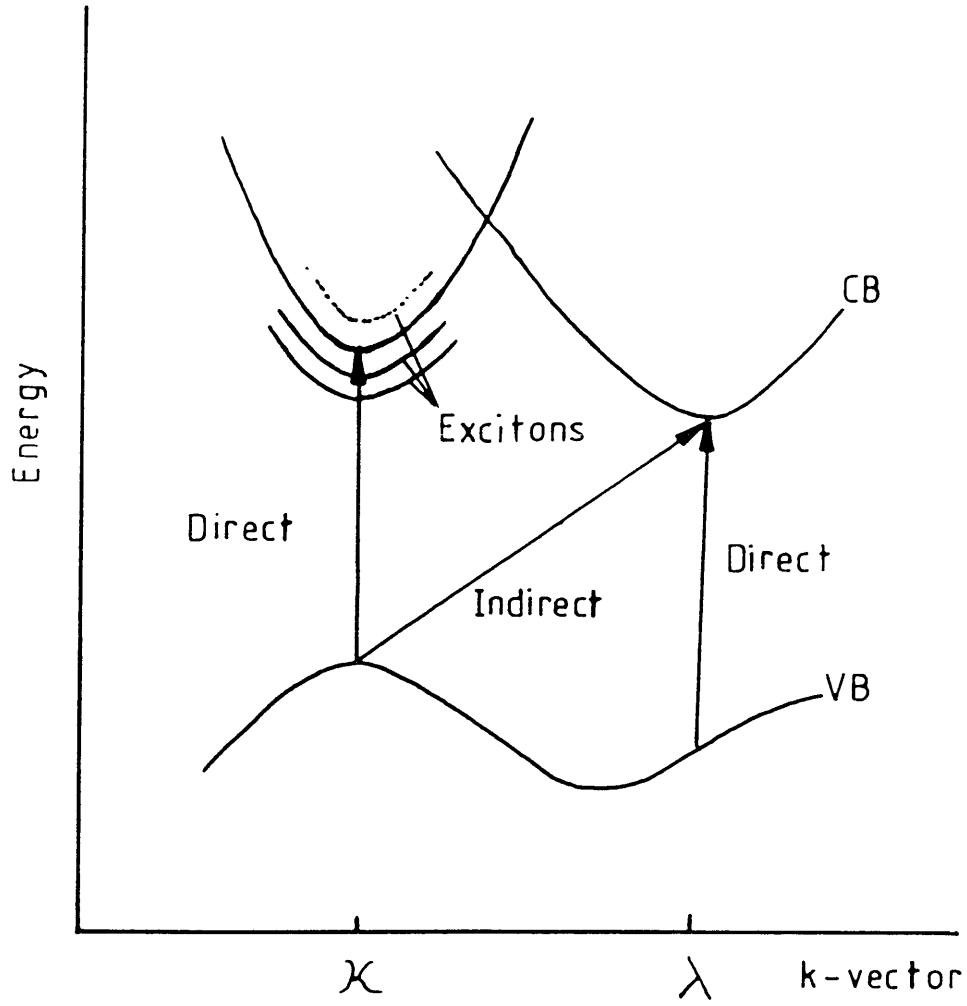


Fig. 3.1 The electronic transitions upon the absorption of a photon by the semiconductor.

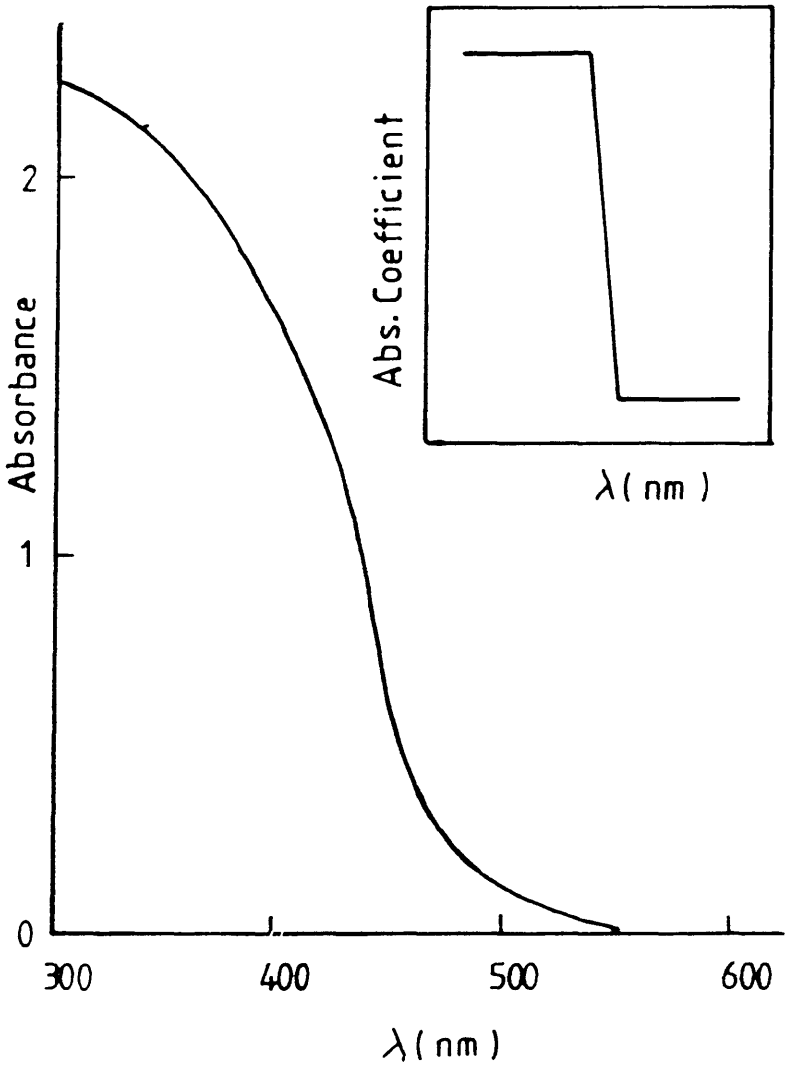


Fig. 3.2 Absorption spectrum of colloidal CdS (5×10^{-4} M), SHMP (10^{-3} M) at pH=7.5; Insert : theoretical wavelength dependence of the absorption coefficient.

$$e^- + h^+ \xrightarrow{h\nu} h\nu + \text{heat} \qquad \text{luminescence} \qquad (3.4)$$

$$e^- + O_2 \longrightarrow O_2^- \qquad \text{(superoxide) oxidation} \qquad (3.5)$$

$$2h^+ + CdS \longrightarrow Cd^{2+} + S \qquad \text{photodecomposition} \qquad (3.6)$$

Bard and Gerisher [147,148] reported that the standard redox potential for equation (3.6) is 0.32V VS. NHE which is sufficiently negative with respect to the value band edge in CdS at 1.74V vs. NHE so that oxidation of CdS by VB holes is thermodynamically favourable.

Photodecomposition of CdS can be prevented by using a suitable hole scavenger such as sulfide anions [56].

$$h^+ + S^{2-} \longrightarrow S^{\cdot-} \qquad (3.7)$$

$$S^{\cdot-} + O_2 \longrightarrow O_2^- + S \qquad (3.8)$$

Thomas and co-worker [143] reported that photodecomposition of colloidal CdS could be prevented by using sodium dodecyl sulfite (SDS) $H_3C(CH_2)_{11}SO_3^-Na^+$, as a stabilizer. Stability in the CdS/SDS colloid was achieved because oxygen was not reduced by the CB electrons and decomposition by holes was prevented by rapid recombination of holes with these CB electrons.

3.2 Photoluminescence of CdS

Absorption of light by colloidal CdS creates electron-hole pairs in the semiconductor and a substantial proportion of these

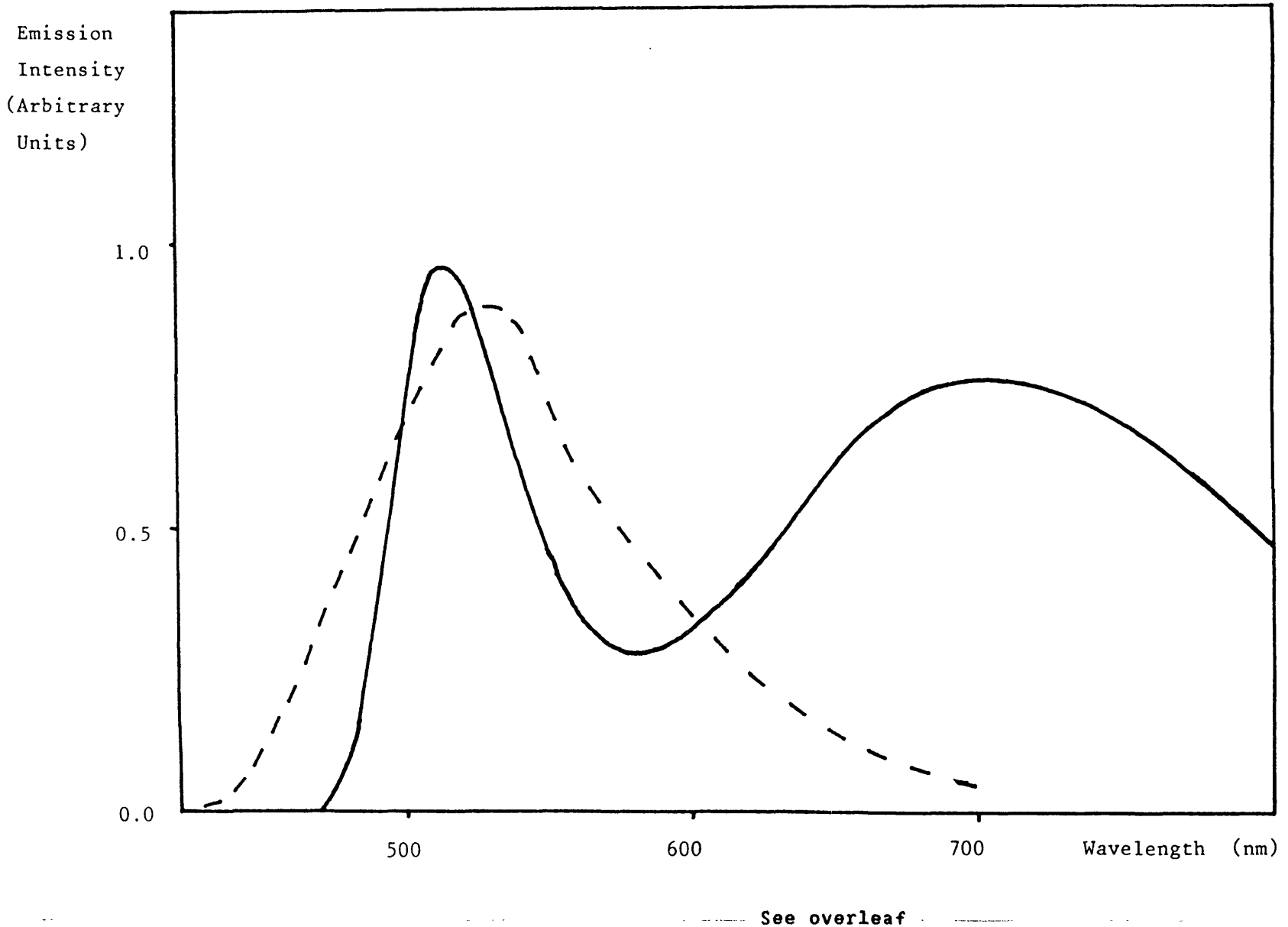
species recombine to give heat and a weak luminescence (hv in equation 3.4).

The direct recombination between an electron-hole pair (from CB to VB) which emits band gap light is a fast process. Previous workers have shown that the recombination process occurs on the nanosecond timescale[52,61]. In the case of colloidal CdS it is found to have a 300 picosecond lifetime[52]. A fraction of the photogenerated minority carriers (hole) can also react with electrons in intraband gap states e_t as below:

$$e_{CB}^- + V \longrightarrow e_t^- \qquad (3.9)$$

$$h^+ + e_t^- \longrightarrow V(+hv') \qquad (3.10)$$

where V is a vacant trap, $\bar{e}_t$ is a full trap and hv' is luminescence. Gratzel and Ramsden have used this mechanism to explain the observation of red (700 nm) luminescence from colloidal CdS[53]. We also observed such luminescence in colloidal CdS when photobleaching occurred on the microsecond timescale. It is found that the luminescence spectra were quite different for colloids prepared from H_2S and Cd^{2+} depending on whether they were stabilized with a cationic (hexadecyletrimethylammonium bromide, CTAB) or aniomic (Sodium hexametaphosphate SHMP) surfactant. THe H_2S colloids had two emission bands at 510 and 700 nm, as observed by Gratzel and Ramsden[53]. Whereas the material with excess S^{2-} showed only a band-edge emission at 530 nm (see fig. 3.3). These results show how the properties of this type of colloid depend critically on the method of preparation, which may account for different



See overleaf

Fig. 3.3 Luminescence emission from CdS colloids (a) prepared from H_2S(———) and (b) prepared from Na_2S(------); CdS 5×10^{-3} M, SHMP 10^{-2} M.

results being obtained in different laboratories.

In direct recombination the probability of electron-hole recombination is given by[149]:

$$- \frac{dn(t)}{dt} = a_r\, n(t)\, p(t) - a_r n_i^2 \qquad (3.11)$$

in which a_r is a proportionality constant for recombination, n(t) and p(t) as the number of electrons and holes remaining at time t respectively and $a_r n_i^2$ is the rate of thermal generation of electron-hole pairs. Since the electrons and holes annihilate each other in pairs, the instantaneous concentrations of excess carriers produced by a short pulse $\Delta n(t)$ and $\Delta p(t)$ are equal. Therefore

$$- \frac{d\Delta n(t)}{dt} = a_r\, [(n_o + \Delta n(t))(p_o + \Delta p(t))] - a_r n_i^2 \qquad (3.12)$$

$$= a_r \Delta n(t)(n_o + p_o) - \Delta n^2(t)$$

where $\Delta n_o = \Delta p_o$ are the initial excess electron and hole concentration at t = o and $n_o p_o = n_i^2$. If the $\Delta n^2(t)$ term is so small that

$$- \frac{d\Delta n(t)}{dt} = a_r (n_o + p_o)\, \Delta n(t) \qquad (3.13)$$

equation (3.13) may be rewritten as [144]

$$- \frac{d\Delta n(t)}{dt} = \frac{\Delta n(t)}{\tau} \qquad (3.14)$$

Where $\tau = \dfrac{1}{a_r\,(n_o + p_o)}$ is the excess carrier lifetime

At t = 0 $\Delta n\,(t) = \Delta n(0)$; hence[150]

$$\Delta n(t) = \Delta n(0)\, \exp\,(^{-t}/\tau) \qquad (3.15)$$

Trapping centres may be assumed as defect or impurity levels within the bandgap of the semiconductor. If a conduction band electron is trapped at a centre, then subsequently recombines with the VB hole before thermal re-excitation to the CB, the light emitted will be of lower energy than that due to band gap recombination. The nature of such an emission is dependent on the energy of the trapping centres. Localised energy levels within the band gap are important not only for luminescence, but also for conduction.

3.2.1 The quenching effect

The quenching of luminescence of CdS colloids can be explained as adsorption of ions or molecules on the surface of colloidal particles. Studies of fluorescence quenching by dissolved substances were expected to give some information about the scavenging of electrons or holes at the surface of the colloids.

The quenching of the fluorescence of semiconductor colloids by colloidal metals [60], by colloidal semiconductors and other solutes [58] was studied. It has been reported that charged solutes are generally stronger quenchers of the fluorescence than uncharged ones [56]. When the quencher is not adsorbed on the surface of the particles, its reduction potential should be less negative than the potential of the lower edge of the conduction band of the semiconductor for electron scavenging to occur.

3.2.1.1. Fe^{3+} Ions

As shown in figure 3.4, addition of a very low concentration of Fe^{3+}, 10^{-6} mol dm^{-3}, to 5×10^{-4} mol dm^{-3} CdS colloids, quenched about 20% of the blue luminescence. When the concentration of metal ions was increased to 5×10^{-5} mol dm^{-3}, the luminescence quenching rose up to 60% and 30% for blue and red emission respectively. The quenching effect of the ferric cation can be written as

$$Fe^{3+} + e^{-} \longrightarrow Fe^{2+} \qquad (3.16)$$

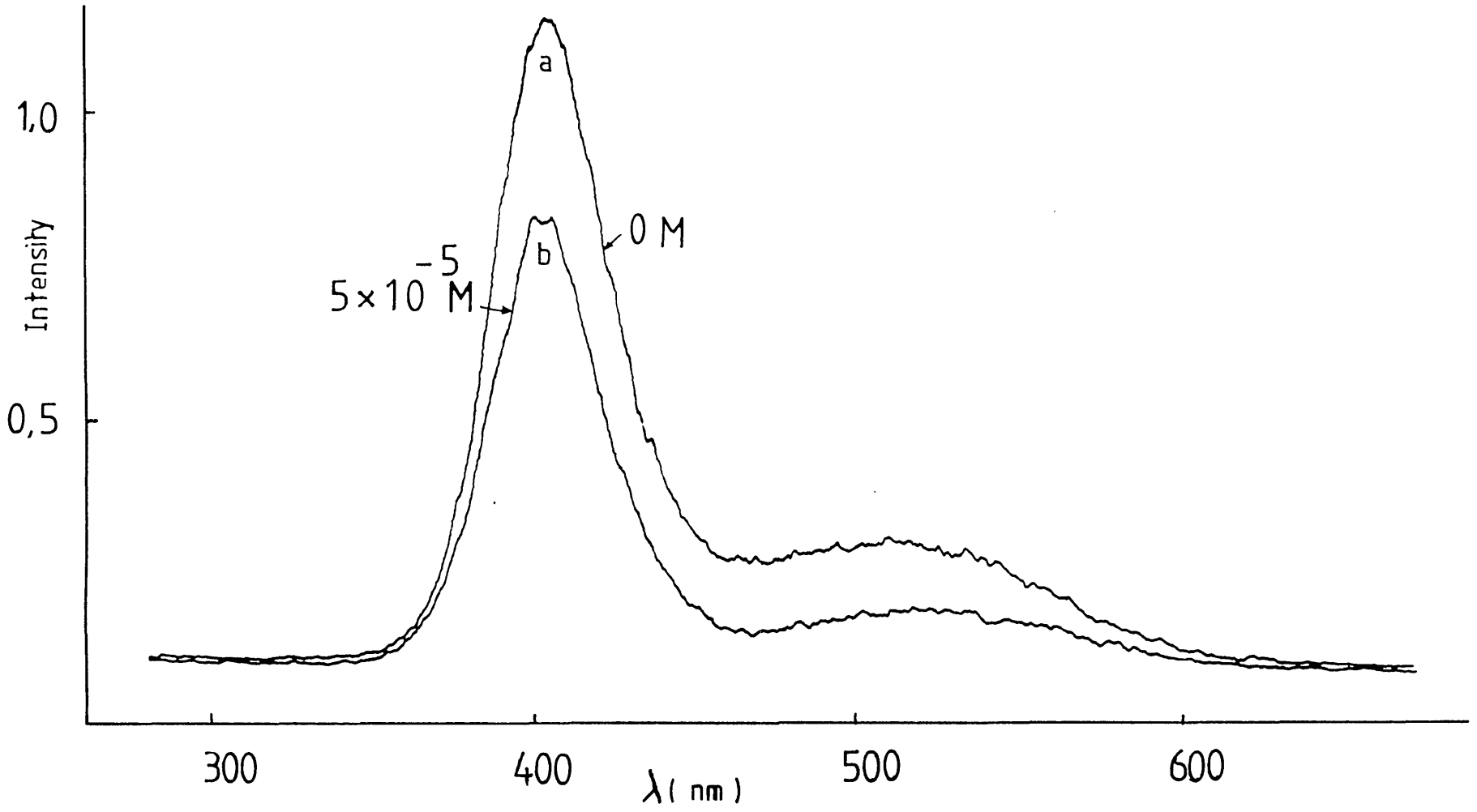
Fe^{3+} is more soluble and may be adsorbed more strongly than O_2 on the surface of CdS particles. The Ferrous cation produced by electron scavenging may be reoxidised by scavenging positive holes to regenerate ferric cation.

$$Fe^{2+} + h^{+} \longrightarrow Fe^{3+} \qquad (3.17)$$

According to the proposed mechanism for reduction and oxidation of metal ions, a small number of metal ions should be deposited on the surface of colloidal particles when illuminated in stationary condition. The magnitude of the quenching effect depends on the amount of this deposited metal.

3.2.1.2 Pt Colloids

Figure 3.5 shows the effect of platinum on the fluorescence of CdS sols. When 1.5×10^{-5} $moldm^{-3}$ of platinum citrate was added to 5×10^{-4} $moldm^{-3}$ of aerated colloidal CdS, about 50% of the blue luminescence and nearly all of the red luminescence were



See overleaf

Fig. 3.4 Luminescence quenching of CdS(5×10^{-4} M)/SHMP(10^{3} M) by Fe^{3+} (5×10^{-5} M).

(a) CdS alone

(b) CdS plus Fe^{3+}.

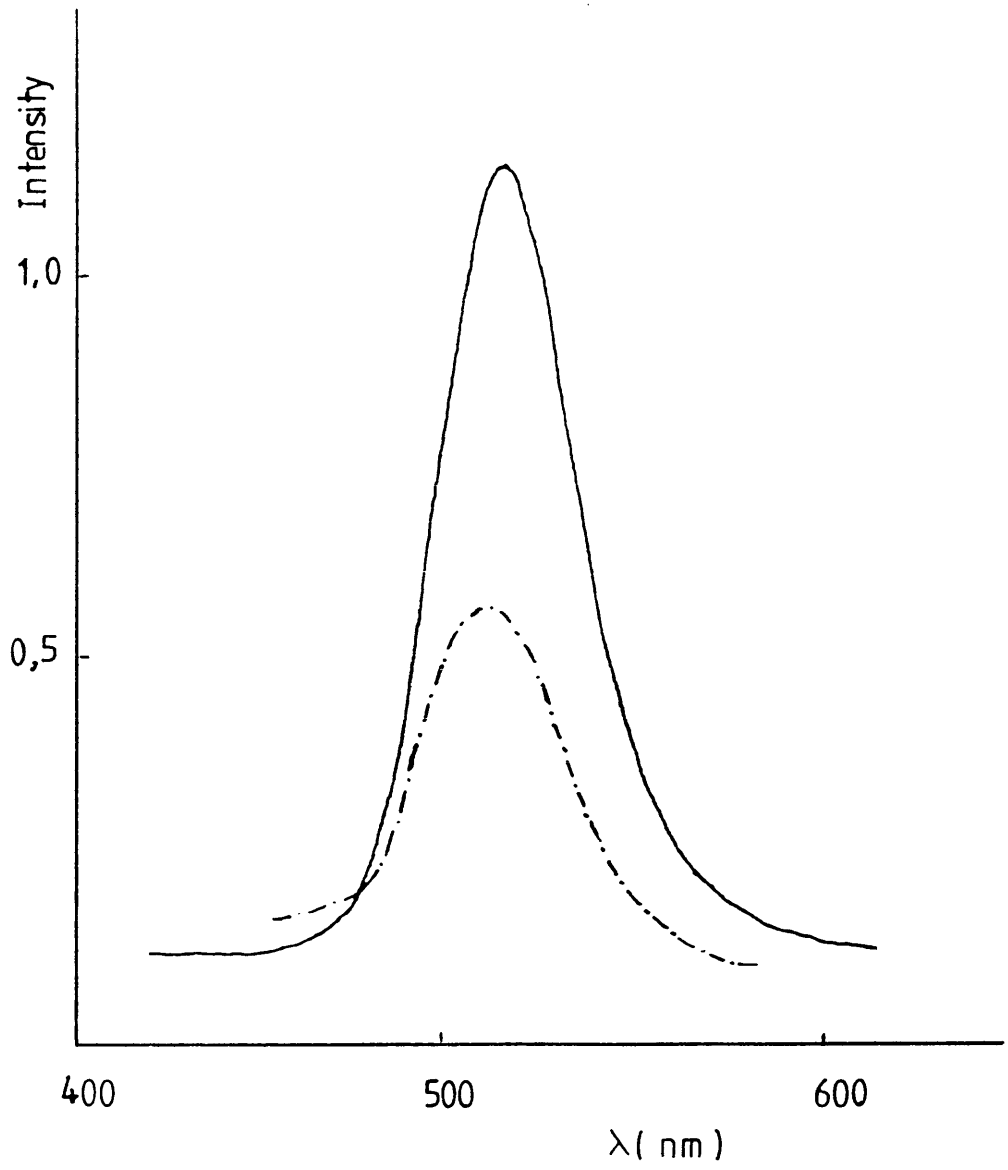


Fig. 3.5 Luminescence quenching of CdS(5×10^{-4} M)/SHMP (10^{-3} M) by Pt(1×5.10^{-5} M) colloids.

quenched. This quenching effect was observed immediately after the addition of colloidal pt showing the rapid interaction between the two types of particle. This result can be accomplished through the adsorption of Pt on the surface of CdS particles. This modification of a CdS particle's surface by platinum creates a heterogeneous surface which potentially can offer different sites for oxidation and reduction. Photogenerated electron-hole pairs in the presence of platinum particles lead to a degradation of colloidal CdS and H_2 evolution [56,187]. These reactions may be written as:

$$CdS \xrightarrow{hv} CdS(e^- h^+) \qquad (3.18)$$

$$2H^+ + 2\ e^- \longrightarrow H_2 \qquad \text{(Hydrogen evolution)} \qquad (3.19)$$

$$S^{2-} + 2h^+ \longrightarrow S \qquad \text{(Photodegradation)} \qquad (3.20)$$

The holes on the surface of CdS colloid easily oxidised anions such as S^{2-}, leading to a radical anion such as S^-. Further oxidation of S^- by hole scavenging produces the sulphur atom, S , which could act as a trap for electron.

Therefore by adding platinum the rates of quenching and of semiconductor degradation both increased and the capture of an electron by a Pt particle is accompanied by the consumption of proton and H_2 evolution.

3.2.2 Sonicating Effect

The effect of sonication on photoluminscence of platinised

CdS colloids is shown in figure 3.6. It is clear that sonicating pt/CdS sol increased its luminescence up to 45% . However, sonication only increased luminescence of unplatinised CdS sols by a small amount. This effect may be explained by the desorption of platinum particles from cadmium sulphide surfaces allowing the recombination of photogenerated electron-hole pairs, and hence luminescence to increase.

3.2.3 Doping Effect

It has been shown that[56] the fluorescence of colloidal CdS doped with less than 1% Cu^{2+} or Ag^{+} is much stronger than that of undoped ones. We have observed the same effect in CdS doped with Cu^{2+} and ZnS doped with Tb^{3+}.

3.3 Photobleaching of CdS

Photobleaching of colloidal CdS sols was observed when samples of CdS were subjected to a 10μs photoflash ($\lambda > 300$ nm). There was a small blue shift (3.0 nm) in the absorption edge. As shown in Figure 3.7, this resulted in a sharp decrease in absorbance in the region of 450 - 500 nm. As far as we know this transient has not been reported before, although Thomas and co-workers have described short-lived photobleaching at 475 nm for CdS particles in Nafion film[151]. In their case the sample was illuminated at low temperature (77K) and the absorption recovered completely in > 1 μs. This recovery matched the luminescence decay at 575 nm and was attributed to direct electron-hole

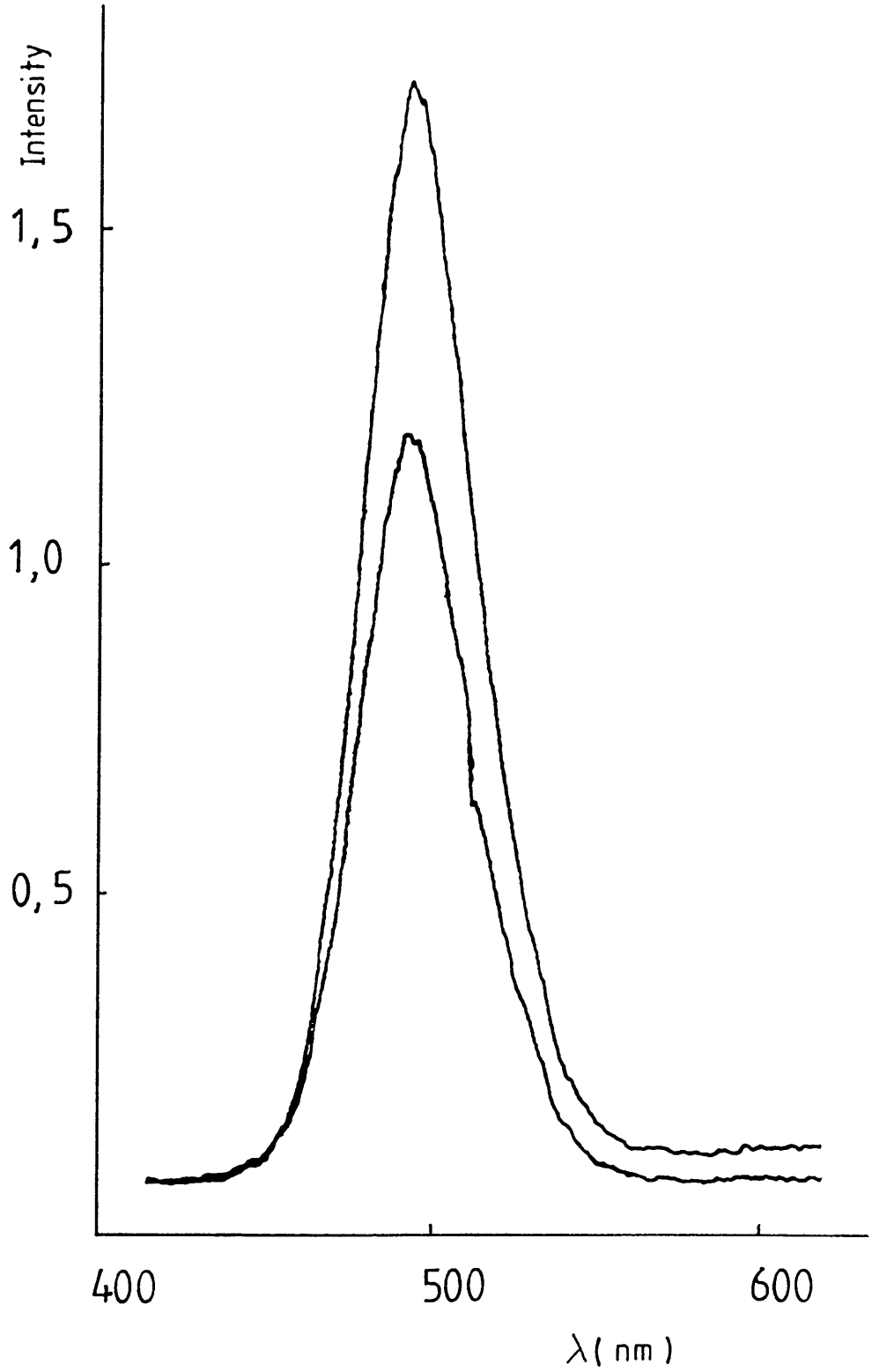
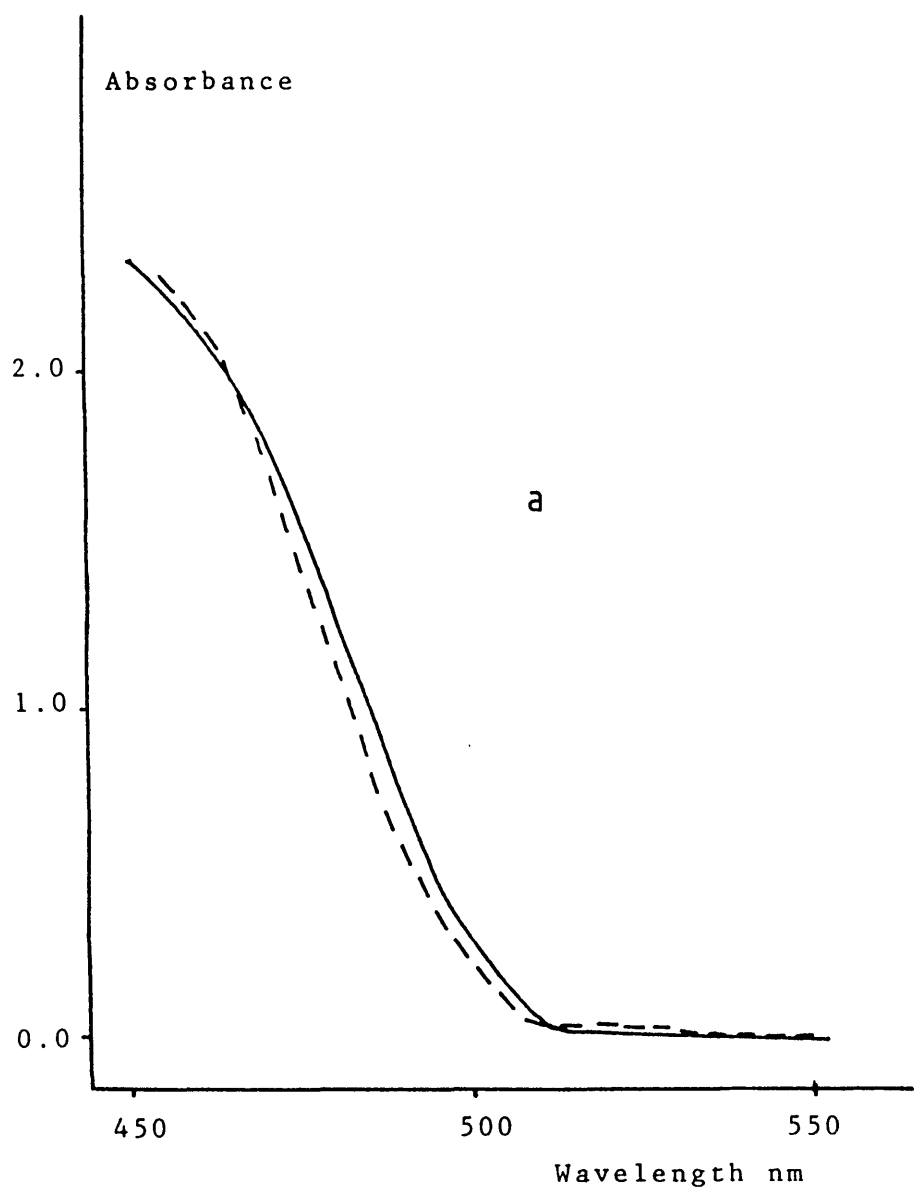
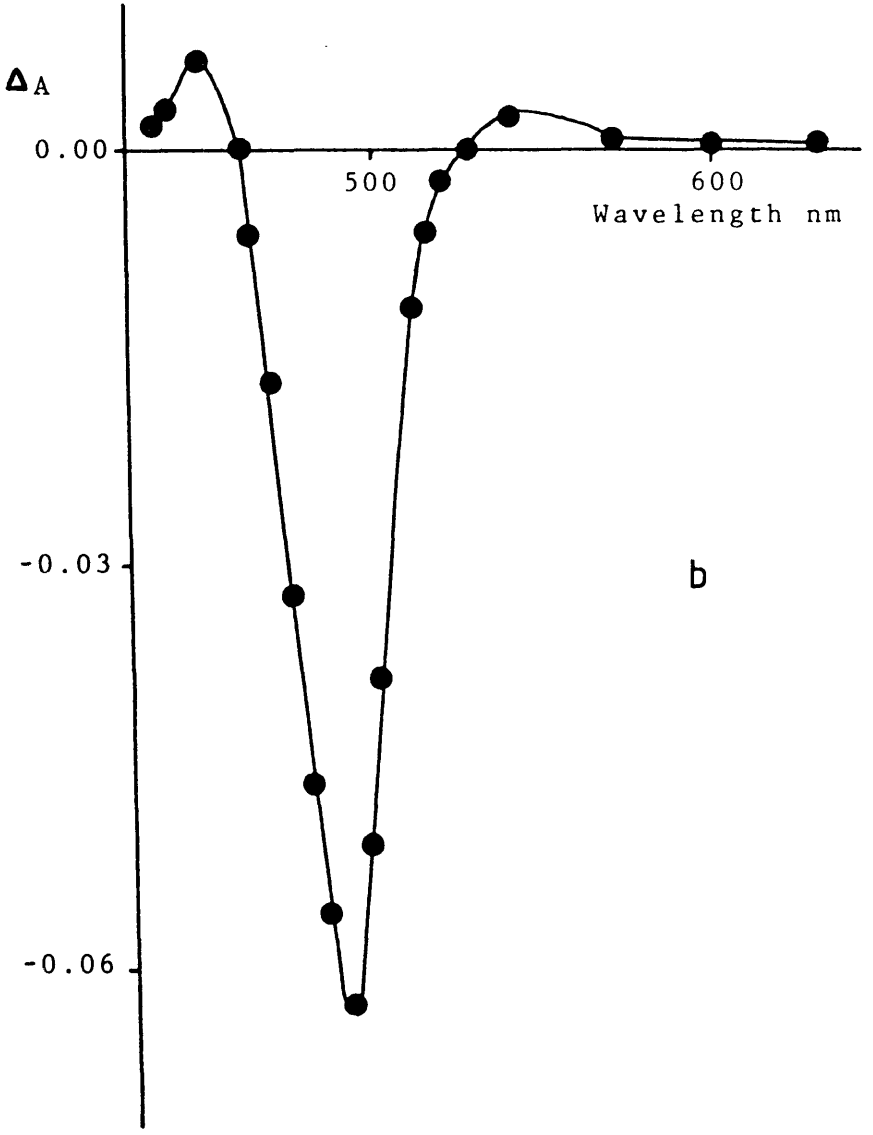


Fig. 3.6 Sonicating effect on the luminescence of CdS colloids.





(See overleaf)

Fig. 3.7 (a) Ground state absorption spectrum (———) and derived transient spectrum 10 ms after photoflash(------).

(b) Transient difference spectrum 10 ms after photoflash for N_2 purged CdS(5.10^{-4} M)/ SHMP 10^{-3} M and pH 7.5.

recombination. However, the results reported here deal with a process which occurs on the millisecond timescale at room temperature. It was also found that the magnitude of the transient signal was proportional to the square root of the flash intensity (fig 3.8) which suggests that the transient does not reflect the direct decay of photogenerated charge carriers. The majority of generated electron-hole pairs will directly recombine electron-hole pairs (eh) during the photoflash, so that the rate of photoabsorption (I_A) is balanced by the rate of recombination ($k_R[h][e]$):

$$I_A = k_R[h][e] \qquad (3.21)$$

The number of electrons and holes generated by the intense flash will greatly exceed their dark concentration. As a result their concentration during the flash will depend on the square root of the flash intensity:

$$[h] = [e] = (I_A/k_R)^{1/2} \qquad (3.22)$$

Any minor decay route present after 10 μs flash leading to a transient will depend on the steady-state concentration of electrons and holes in the flash and so on the square root of the flash intensity. In N_2- purged solutions the half-life for recovery of photobleaching was ca. 50ms. This transient absorption experiment was performed in order to gain further insight into the nature of electron-hole recombination of excited colloidal CdS sols.

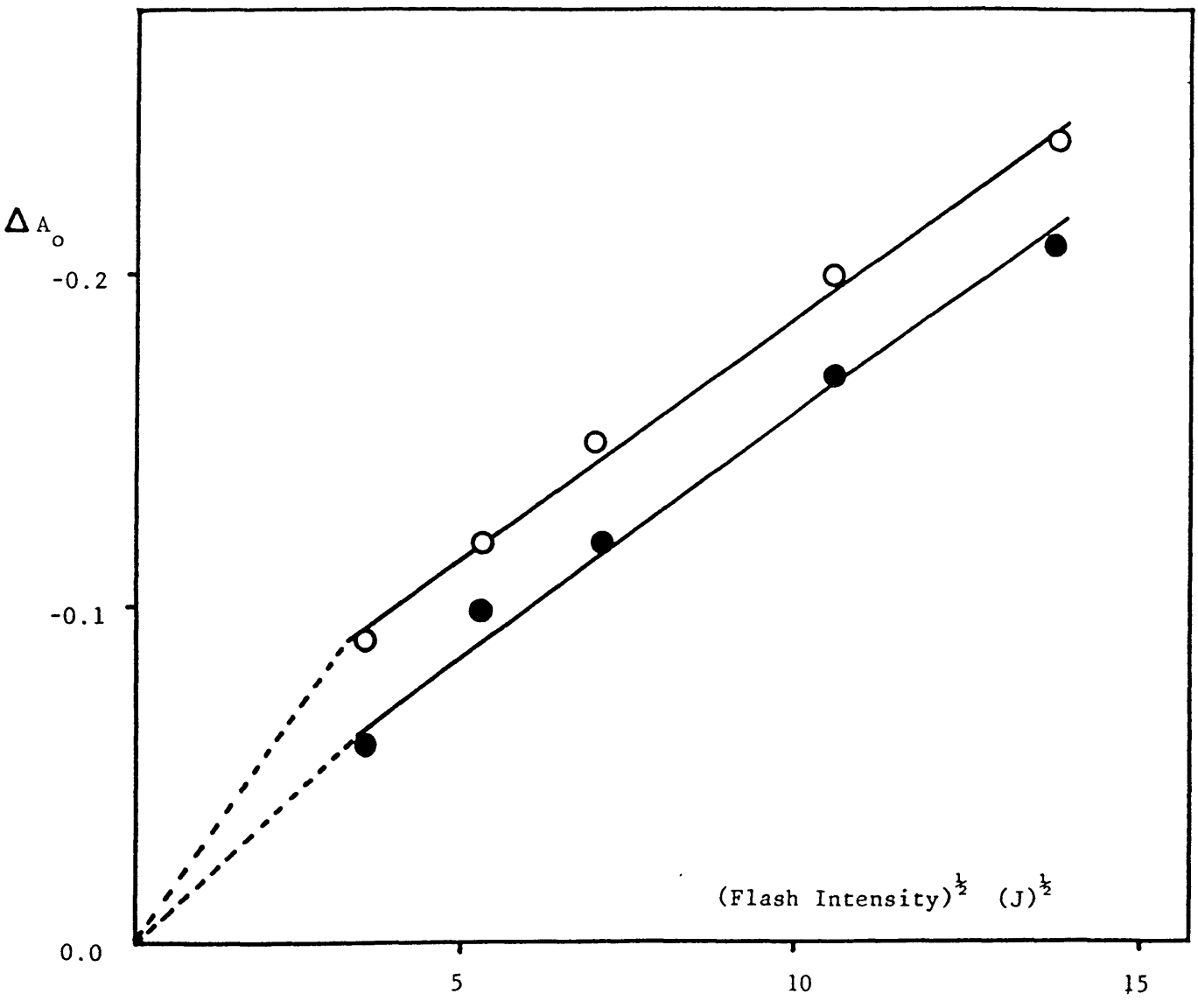
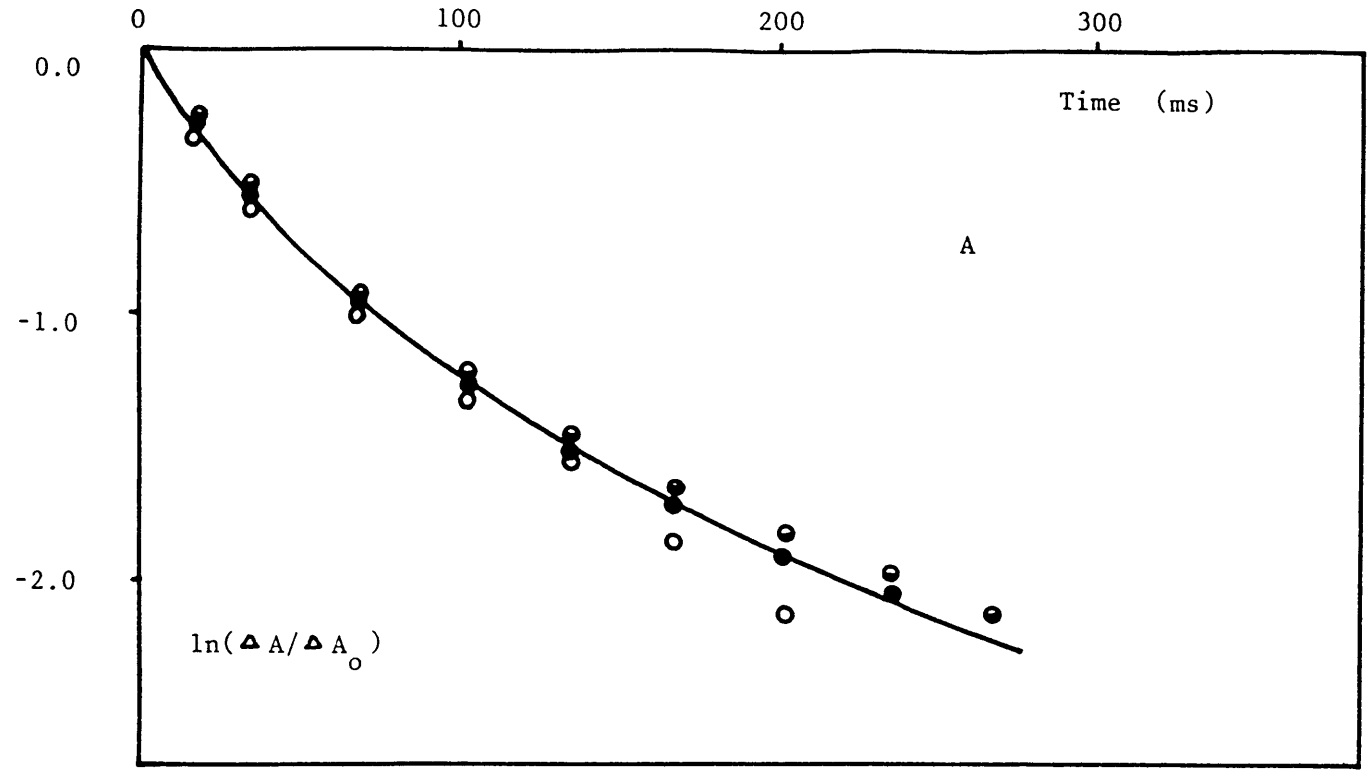


Fig. 3.8 Variation in initial absorption (ΔA_o) with flash intensity for CdS (5.10^{-4} M ; SHMP 10^{-3} M and pH 7) (a) alone (—●—) and (b) with 5.10^{-2} M cysteine (—○—).

3.4 The Kinetics of Electron Transfer Reactions

Considerable attention has been paid to the study of dispersed kinetics in heterogeneous systems.[44-47, 52-55, 82-84, 151-155] In the homogeneous system, the data can often be analysed by first- and second-order kinetics. In inhomogeneous systems such as semiconductor electrodes and colloidal particles, by contrast, reactions often do not obey simple first- or second-order kinetics. For instance, typical data for the recovery of the absorption of CdS colloids after a 10μs photoflash are shown in Fig. 3.9. These refer to a range of initial absorbance changes (ΔA_o) and are normalised to fit on a common curve by dividing by (ΔA_o). The data are shown as log ($\Delta A/\Delta A_o$). Such a normalising procedure will not work for systems where the kinetics are higher than first order. A simple first-order reaction would give a straight line, as in a classical homogeneous system whereas the semilogarithmic plots in Fig. 3.9 are not linear. The normalising procedure implies that the kinetics are first-order for any other of reaction, a change in A_o would alter the initial half-life and the curves would not be superimpossible. For example, if the reaction were second order the first half life would decrease by a factor of two when ΔA_o doubled. Similar non-exponential behaviour has been observed for electron transfer from TiO_2 to methyl viologen (Mv^{2+})[76] and seems to be common for colloidal semiconductors[61, 63, 84, 137, 151-155]. It may be resolved by postulating a distribution of first-order rate constants for a heterogeneous collection of particles. In collaboration with Bartlett and Wilde we have



See overleaf

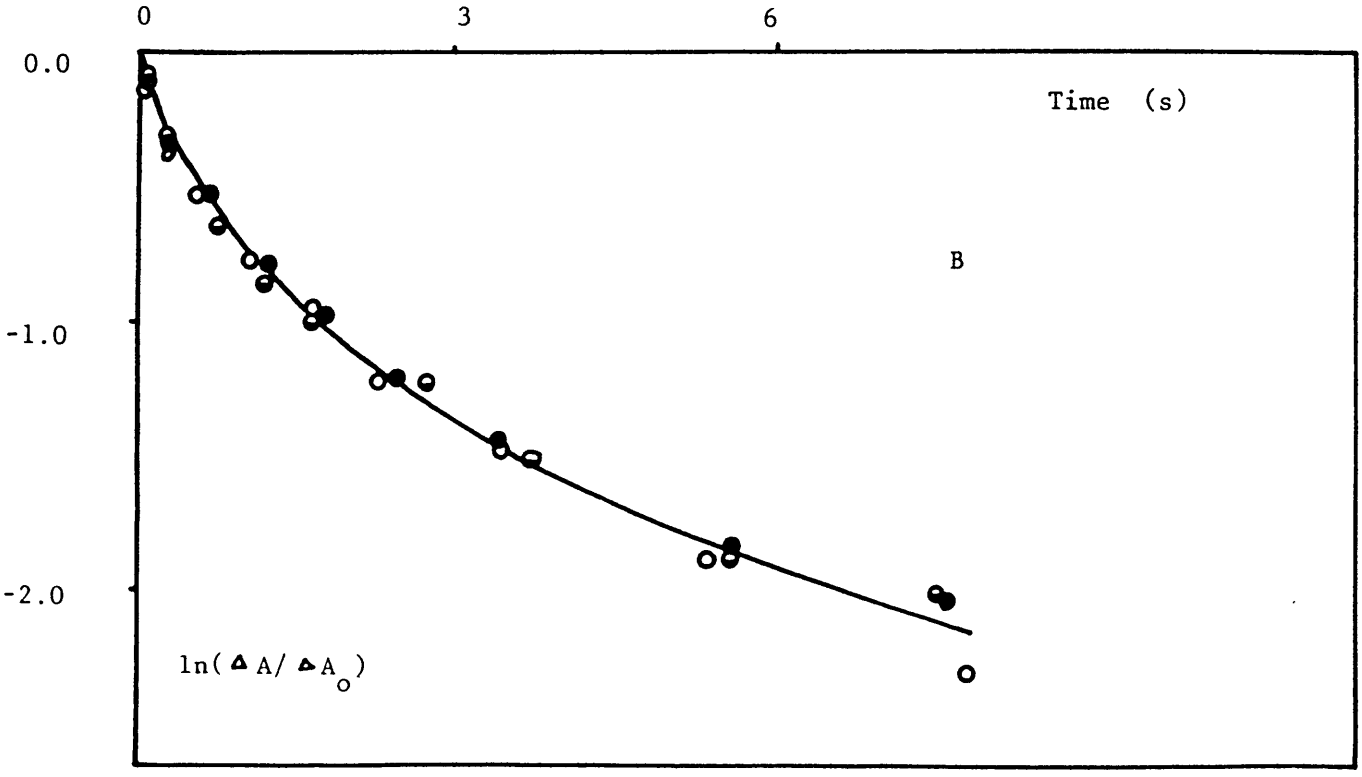


Fig. 3.9 Recovery of absorption at 485nm for CdS, (A) for CdS alone: (ΔA_o) was -0.09 (○), -0.13 (●), -0.19 (◒) and (B) for CdS plus cysteine (10^{-2} M) (ΔA_o): was -0.08 (○), -0.13 (●), -0.17 (◒). The curve was calculated from equation (3.31) with $\gamma=2\varrho=2\times0.7$ for (A) and $\gamma = 2\times\varrho = 2\times0.8$ for (B).

developed a general model for dispersed kinetics in heterogeneous systems[44].

In this method it is assumed that the first order rate constant is dispersed according to a normal distribution, $\exp(-x^2)$:-

$$k = \bar{k} \exp(\gamma x) \tag{3.23}$$

where $\bar{k}$ is the average rate constant and γ describes the spread of the Gaussian distribution. The rate law for first order reactions is

$$\frac{c}{c_o} = \exp(-kt) \tag{3.24}$$

Here we defined a dimensionless time, τ, related to the mean rate constant, $\bar{k}$, as

$$\tau = \bar{k}t \tag{3.25}$$

Substitution of equations (2.23) and (3.25) into (3.24) gives

$$\frac{c}{c_o} = \exp[-\tau \exp(\gamma x)] \tag{3.26}$$

Now intergrating equation (3.26) across the normal distribution, $\exp(-x^2)$, we find that the decay of the concentration, c, of species from their initial concentration, c_o, is given by:

$$\frac{c}{co} = \frac{\int_{-\infty}^{\infty} \exp(-x^2) \exp[-\tau \exp(\gamma x)]dx}{\int_{-\infty}^{+\infty} \exp(-x^2)dx} \tag{3.27}$$

where

$$\int_{-\infty}^{+\infty} \exp(-x^2)\, dx = \pi^{1/2}$$

when there is no dispersion, $\gamma = 0$ and equation (3.27) reduces to the simple first order exponential decay such as equation

$$\frac{C}{C_o} = \exp(-\tau) \qquad (3.28)$$

It is possible that the dispersion in the first order rate constant is caused by the dispersion in the radii of the particles. It has been shown that the rate of photochemical reaction in colloidal semiconductor particles is proportional to the surface area of the particles[76]. Hence if we write for the radial distribution

$$\ln(r) = \ln(\bar{r}) + \varrho x \qquad (3.29)$$

then the distribution of rate constants will be given by

$$\ln k_x = \ln \bar{k}_x + 2\varrho x \qquad (3.30)$$

This equation has the same form as equation (3.23). Hence the same results will obtain with

$$\gamma = 2\varrho$$

In systems such as flash photolysis of colloidal semiconductors, electron transfer reactions are initiated by the light absorption. In this case there is an additional complication of equation (3.27). Since the larger particles will absorb more light during the photoflash and produce more

electrons at t = o, the absorption of light will be a function of the volume of particles. Hence equation (3.27) will be modified in favour of the larger particles by $(r/\bar{r})^3$ so that

$$\frac{c}{co} = \frac{\int_{-\infty}^{+\infty} \exp(-z^2) \exp[-\tau\exp(\gamma z)]dz}{\int_{-\infty}^{+\infty} \exp(-z^2)\, dz} \qquad (3.31)$$

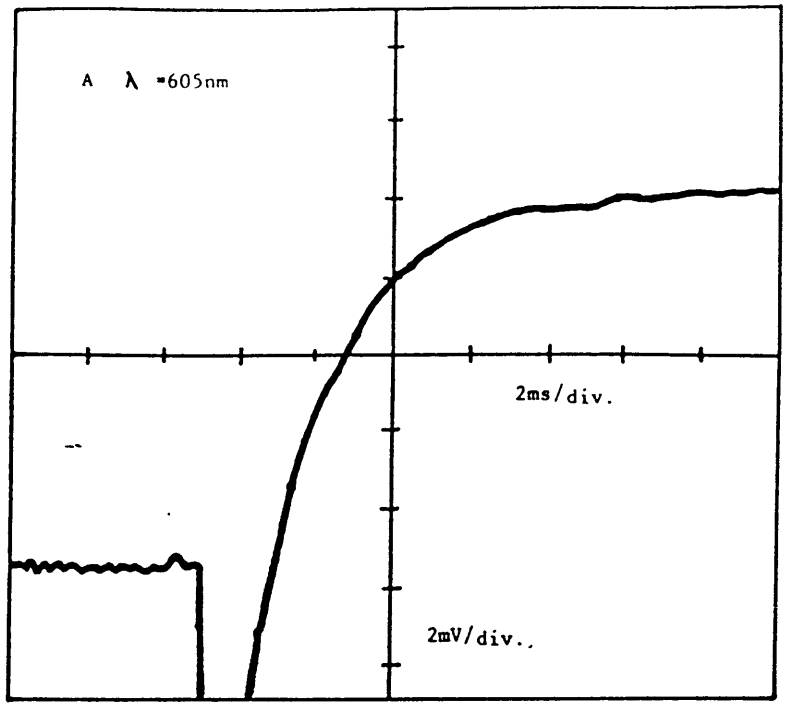
where the factor x is replaced by z using the equations (3.32) to (3.34):

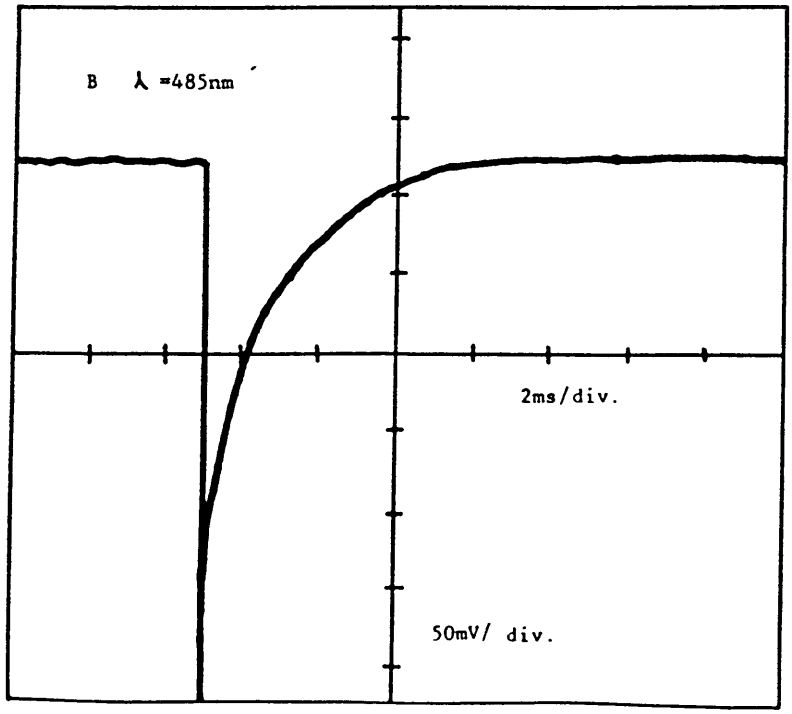
$$z = x - 3\varrho/2 \qquad (3.32)$$

$$\tau = \bar{k}_z t \qquad (3.33)$$

and $\gamma = 2\varrho$ with $\bar{k}_z = \bar{k}_x \exp(3\varrho^2)$ (3.34)

Equation (3.31) represents the distribution of more and faster electrons as the large particles immediately after the flash. Under this condition $\bar{k}_z$, the average rate constant for large particles, will be larger than $\bar{k}_x$, the average rate constant for a particle of average size. As mentioned above, in our studies on colloidal CdS with flash photolysis, we have found that the flash causes a transient change in the optical absorbances of the CdS. We attribute this change to the separation of photogenerated electrons and holes and their trapping by surface states. Typical data for transients are plotted in Fig. 3.10a. The data have been normalised on to a common curve by dividing (ΔA, by the initial absorbance change (ΔA_o), as above. Equation (3.31) was solved numerically with $\gamma = 2\varrho = 1.4$ to fit the common curve. The fit is reasonable and as





See overleaf

Fig. 3.10 Oscilloscope traces for formation of MV^{+} at 605nm (A) and recovery of absorbance at 485nm (B) for a colloid containing CdS (5.10^{-3} M), cys (10^{-2} M) and MV^{2+} (5.10^{-6} M)

mentioned before, the good agreement suggests that the process is first order with a dispersion of rate constants. By the time the reaction reaches the third half life there is some deviation from the theoretical curve in Fig. 3.10a but this is likely to result from baseline errors in the absorption measurements.

Another method can be used to determine the distribution of radii directly by dynamic laser light scattering[156, 157]. In this technique the logarithm of the autocorrelation function is plotted against the delay time. The slope of this plot is proportional to the diffusion coefficient $D(cm^2s^{-1})$. Typical data for CdS particles are shown in Fig. 3.11. A straight line would be obtained for perfectly monodisperse collection of particles. If the distribution of particle radii is given by equation (3.23) then since the diffusion coefficient[158] is proportional to r^{-1}, the distribution of diffusion coefficients will be

$$\ln D = \ln\overline{D} - \varrho x \qquad (3.35)$$

The curve in Fig. 3.11 was analysed using equation (3.31) with $\gamma=-\varrho$ and the best fit was found with $\varrho = 0.7$. This is in excellent agreement with the kinetics data and confirms that the non-exponential behaviour can be attributed to a dispersion in the radii of the particles. Interestingly the kinetic data are more sensitive to the variation in radius than the light-scattering measurements, since the rate constants depend on r^2. We may conclude firstly that the dispersion in the kinetic data is largely explained by the dispersion in the radii of the colloidal semiconductor (CdS) and secondly that the Gaussian

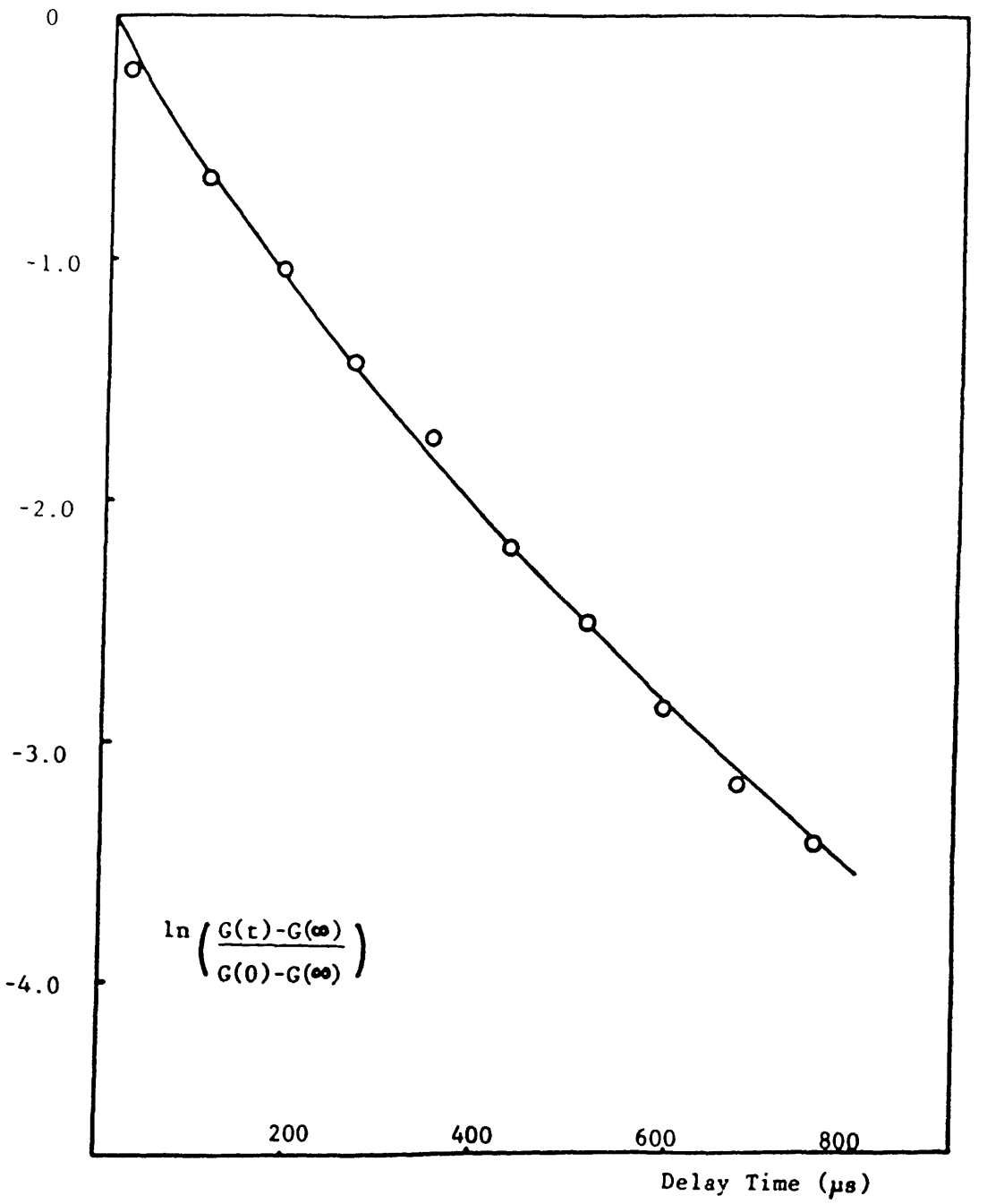


Fig. 3.11 Decay of the autocorrelation function of G(t) from Dynamic laser light scattering for CdS. The curve was calculated from equation (3.35) with $\rho = \gamma = 0.7$.

model is sufficient to analyse both the kinetics and the light scattering data.

Cysteine has previously been used as an electron donor for the reduction of water by sensitising CdS.[159, 160] When CdS colloids containing 10^{-2}mol dm^{-3} cysteine were flashed there was a strong decrease in the rate of recovery of absorbance and the process now occurred over a period of 10 seconds. However, as shown in Fig. (3.10b) the shapes of the curves were identical to those found for CdS alone. Applications of the same analysis gave the values of $\bar{k}_z$ and γ shown in Table 3.1. This shows that γ has remained essentially unchanged although $\bar{k}_z$ is much smaller.

TABLE 3.1 Decay constants ($\bar{k}_z$) for recovery at 485nm

Reaction conditions[a]	$\bar{k}_z/s^{-1}$	γ
CdS alone	15[b], 13[c], 14[d]	1.4
CdS/10^{-2}moldm^{-3} cysteine	0.6[e], 0.8[f], 0.6[g]	1.6
CdS/10^{-2}moldm^{-3} cysteine/10^{-6}moldm^{-3}MV^{2+}	350	1.4
CdS/10^{-2}moldm^{-3} cysteine/10^{-3}moldm^{-3}O_2	250	1.6

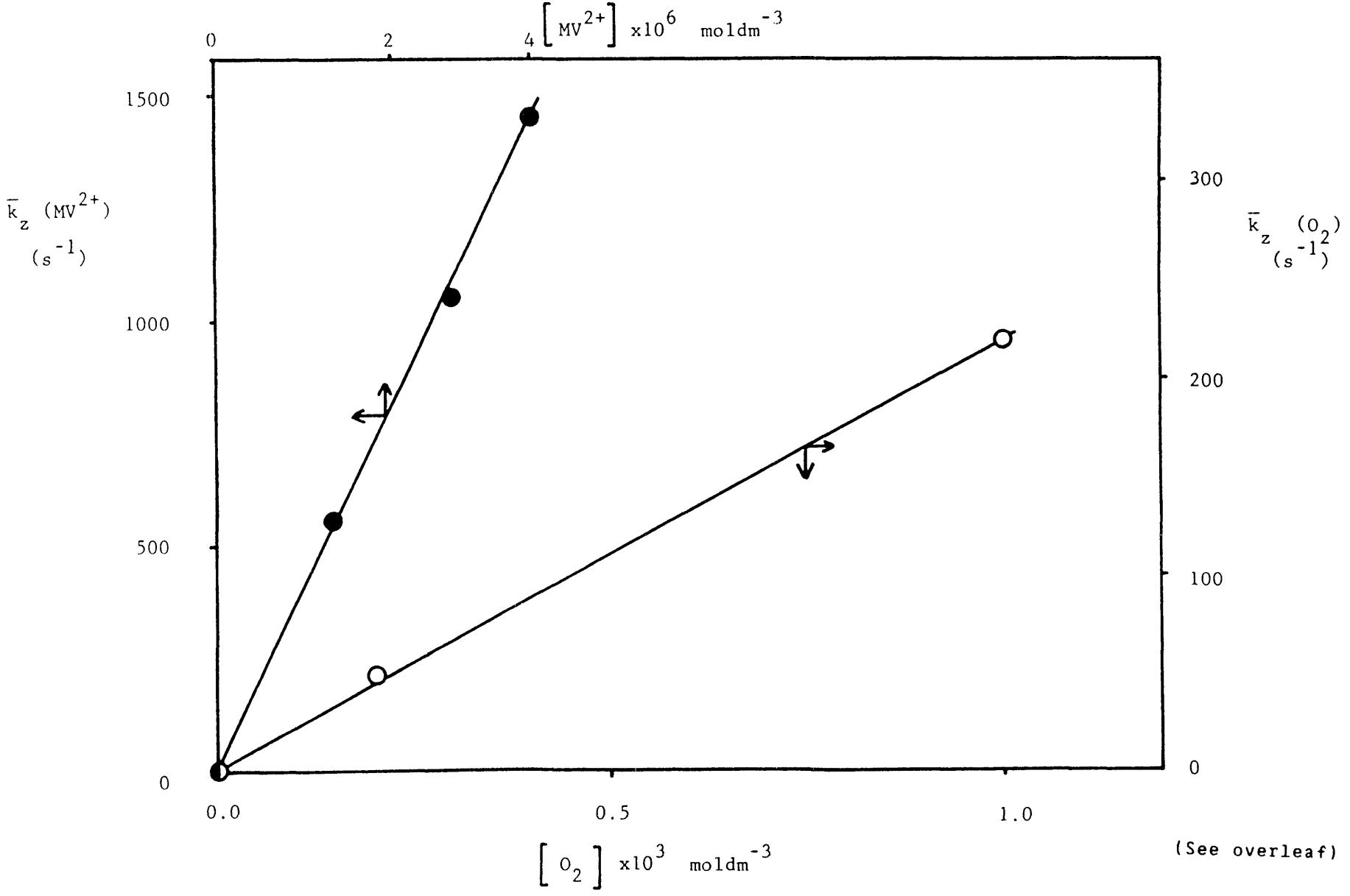
[a] Conditions as Fig. 3.7 unless specified

ΔA_o = [b] -0.08 [c] -0.16 [d] -0.23 [e] -0.08 [f] -0.14 [g] -0.17

3.5 Photoreduction of MV^{2+} and O_2

As described above, when colloidal CdS was flashed in the presence of 10^{-2}moldm^{-3} cysteine, the recovery occurred over a long time (low reaction process). By adding even a low concentration of the electron acceptor MV^{2+}(10^{-6}mol dm^{-3}) to the solution of CdS colloids containing 10^{-2} mol dm^{-3} cysteine, there was a marked acceleration in the rate of recovery (fast reaction process). As shown in Table 3.1 there was again no significant change in γ. The same result was obtained when O_2 was present as an electron acceptor in the solution of CdS and cysteine. Fig. 3.12 shows that $\bar{k}_z$ was linearly related to the concentration of O_2 or MV^{2+}. For samples containing cysteine (10^{-2}mol dm^{-3}) and MV^{2+} [(1-5)x10^{-6}mol dm^{-3}], the recovery at 485nm was accompanied by an increase in absorbance at 605nm due to formation of the cationic radical $MV^{+\cdot}$ (as shown in Fig. 3.10).

The correlation between the absorbance transient and electron transfer from the CdS particle to MV^{2+} forming MV^{+} shows that the absorbance change must be caused by electrons trapped on the particles. By comparing the absorbance change at 485 and 605nm when cysteine and MV^{2+} were present, the change in extinction coefficient for CdS at 485nm was found to be $-(7\pm1)\times10^{3}$dm^{3}mol^{-1}cm^{-1}. Both processes had the same rate constant , $\bar{k}_z$, and from Fig. 3.12 the bimolecular rate constant for electron transfer from the trapping sites in CdS to MV^{2+} was calculated to be 3.6 x 10^{8}dm^{3}mol^{-1}. The decay of the trapped electrons is impeded by cysteine which reacts with photogenerated holes but is accelerated by electron acceptors such as O_2 and



(See overleaf)

Fig. 3.12 Variation in rate constants for recovery at 485nm with O_2 (—○—) and MV^{2+} (—●—); concentrations and conditions as for Figure 3.7 plus 10^{-2} M cysteine.

MV^{2+}.

When no cysteine was present in the colloidal CdS solution, O_2 accelerated the recovery of absorbance (fast reaction process) at 485nm. However no photobleaching could be detected when only CdS and MV^{2+} were present. Instead MV^{+} was generated within the photoflash (10μs) for all concentrations of MV^{2+} ($>10^{-6}$moldm^{-3}) MV^{2+} is known to adsorb on CdS particles[61, 151] and can intercept direct electron-hole recombination. Clearly then, MV^{2+} was removing photogenerated electrons before they could be trapped in CdS, so that no photobleaching was observed. Apparently 10^{-2}mol dm^{-3} cysteine can inhibit the reaction of MV^{2+} with electrons at least for low MV^{2+} concentrations, since the absorbance transient and bimolecular electron transfer to MV^{2+} are both observed. This may result from preferential adsorption of cysteine on the surface of CdS.

To provide a full mechanism for our observations further experiments are required. We have chosen the following scheme which is consistent with our observations:

$$CdS + h\nu \longrightarrow CdS\ (e^-, h^+) \qquad (3.36)$$

$$e^-_{CB} + h^+ \longrightarrow \text{heat } (+ h\nu) \qquad (3.37)$$

$$h^+ + e_t \longrightarrow V\ (+ h\nu') \qquad (3.38)$$

$$e^-_{CB} + V \longrightarrow \bar{e}_t \qquad (3.39)$$

$$e^-_{CB} + (MV^{2+} \text{ or } O_2) \longrightarrow MV^{+} \text{ or } O_2^- \qquad (3.40)$$

$$cysSH + (V \text{ or } h^+) \longrightarrow 1/2\ (cysSScys) + H^+ \qquad (3.41)$$

where cysSH is cysteine, cysSScys is cystine, e^-_t is full trap electron, V is a vacant trap, h^+ is a hole in the valence and e^-_{CB} is a conduction band electron.

Reactions (3.36) to (3.38) will occur during the photoflash and result in a net increase in the concentration of conduction band electrons. Their subsequent reaction with vacant traps V (equation 3.39) is apparently a slow process and gives rise to decay curves on the millisecond timescale. Cysteine can react with V and possibly with h^+ to block the decay of conduction-band electrons. When O_2 or MV^{2+} are also present in the solution the rate of recovery increases as expected if the transient is due to e^-_{CB}, and the formation of MV^+ was observed. From these reactions the bimolecular rate constants for electron transfer to MV^{2+} and O_2 were found to be 3.6×10^8 and 2.2×10^5 $dm^3mol^{-1}s^{-1}$, respectively. The photochemical formation of superoxide (O^-_2) sensitised by CdS was first reported by Harbour and Hair.[161] Our experimental results show that interfacial electron transfer from CdS to O_2 is a slow process compared with electron transfer to MV^{2+}. Slow electron transfer to O_2 is encouraging since this would be an unfavourable side reaction in water photolysis. Fast electron transfer to MV^{2+} may result from electrostatic attraction between MV^{2+} and the negative CdS particles.

The number of electrons trapped during the photoflash can be estimated from Fig. 3.7. With a change in extinction coefficient of -7000 $dm^3mol^{-1}cm^{-1}$ at 485nm, the absorption change will correspond to an e^-_{CB} concentration of 10^{-6} mol dm^{-3} in a 10cm cell. This is equivalent to 800 e^-_{CB} per particle where each particle contains about 400,000 CdS. Similar numbers of

conduction band electrons have also been observed by rotating disc photoelectrochemistry of CdS colloids.[47]

3.6 Conclusion

This work presented the photophysical and photochemical behaviour of colloidal CdS particles. The colloidal semiconductors exhibit a lively photochemistry and are most useful for kinetic studies at the semiconductor/solution interface. The complex kinetic behaviour of electron transfer reactions in colloidal semiconductors are explained by the "Gaussian model". This model provides an explanation of the kinetics of heterogeneous systems where normalising a set of transient data causes them to fall on a common curved semilogarithmic plot. It is shown that the kinetics of heterogeneous systems such as colloidal semiconductor are not simple first- or second-order but result from a distribution of first-order rate constants. The dispersion in the kinetic transient in turn arises from a distribution of particle sizes. These types of transient, which are described in this work, should be a valuable probe for studying electron transfer reactions at the surface of colloidal particles. The studies of interfacial reactions in micro-heterogeneous systems add a new aspect to the field of photoelectrochemistry. The main goal of these efforts is evidently to understand the behaviour of colloidal semiconductor (CdS) in solar energy conversion and storage.

CHAPTER 4

Time-resolved surface effects in CdS colloids

The data presented in this chapter concern some aspects of surface effects in CdS colloids using time-resolved techniques. Photoreduction of methyl viologen, MV^{2+}, and its dimer desorption from the surface of particles into solution is discussed. The yield of reduced methyl viologen affected by variation of pH, adsorption of cysteine and pt, and photoflash intensity.

Introduction

Time-resolved photoexcitation techniques such as flash photolysis have been used to investigate photoinduced processes at the surface of colloidal CdS. In the past five or six years a new area of photochemistry has been established to study the behaviour of colloids, particularly colloidal semiconductors. Since the colloids are optically transparent, photochemical reactions can be studied by fast reaction techniques. Consequently the parameters which control charge transfer through the surface can be followed in real time and intermediates of reactions can be observed and characterised directly.

In the third chapter transient absorption change in the spectrum of colloidal CdS was discussed and assigned to electrons trapped on the particles after a short flash[45]. In the following section we discuss the photoreduction of methyl

viologen (MV^{2+}) and the desorption of dimer, $(MV^{+})_2$, from the CdS surface.

4.1 Desorption of dimer, $(MV^{+})_2$ from CdS surface

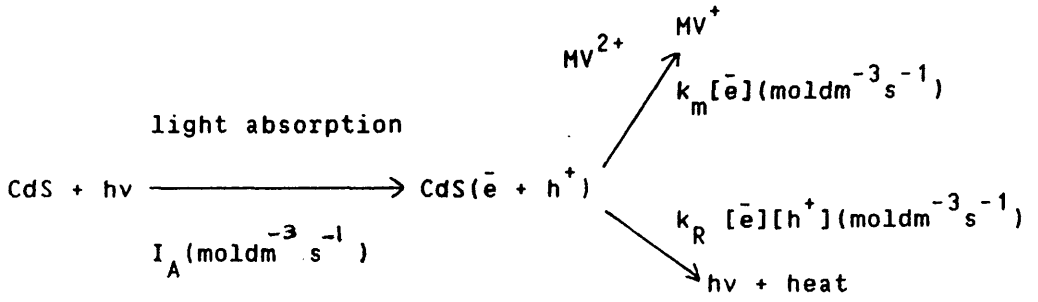
As we know the conduction band edge of CdS is around -0.6V vs. Normal Hydrogen Electrode potential (NHE)[162]. The redox potential of the MV^{2+}/MV^{+} couple is -0.446V vs. NHE and lies under the conduction band of CdS particle. Therefore, MV^{2+} can be reduced by electron transfer from the conduction band of CdS as below.

$$MV^{2+} + \bar{e}_{CB} \longrightarrow MV^{+}$$

It is also clear that any species undergoing the electron transfer reaction, such as MV^{2+}, must be adsorbed on the surface of the semiconductor particle, in order to react efficiently with the photoinduced electron-hole pairs. This means that the surfaces of semiconductor particles play an important role in this interfacial electron transfer process.

When CdS colloids (5×10^{-4}moldm^{-3} stabilised with 10^{-3}moldm^{-3} sodium hexametaphosphate) containing MV^{2+} (10^{-7}-10^{-2}moldm^{-3}) are subjected to a 10μs photoflash of visible light (λ > 400nm) reduced methylviologen (MV^{+}) is produced during the flash and is readily observed by its broad absorption spectrum between 450 and 800nm. This process has also been studied by other workers and these have shown that MV^{2+} is adsorbed on CdS particles and is then able to inhibit the recombination of photogenerated electrons and holes by intercepting electrons[61, 151]. Our

observation can be explained by Scheme I.



SCHEME 1

where k_M and k_R are rate constants for the photoreduction of MV^{2+} and recombination respectively. As mentioned in Chapter 3, the lifetime of carrier transition to the surface of CdS is much less than the recombination lifetime ($\sim 10^{-14}$:10^{-9}sec). Therefore photogenerated carriers in a small CdS particle will reach the surface before being destroyed by recombination process.

As a result, MV^+ is formed on the picosecond timescale and leads to a decrease or quenching of the long wavelength emission (hv') from the particles, since it reduces the amount of recombination occurring.

This is supported by Fig. 4.1 which shows that above a critical value the yield of MV^+ increases linearly with flash intensity. Similar results were obtained with TiO_2 colloids when the supporting polymer is an electron donor, such as polyvinylalcohol which can intercept charge recombination[163], and also in the photoreduction of MV^{2+} by colloidal CdS.[164]

In Scheme I this will occur when k_M is much larger than $k_R[h^+]$. It is interesting to compare this result with the

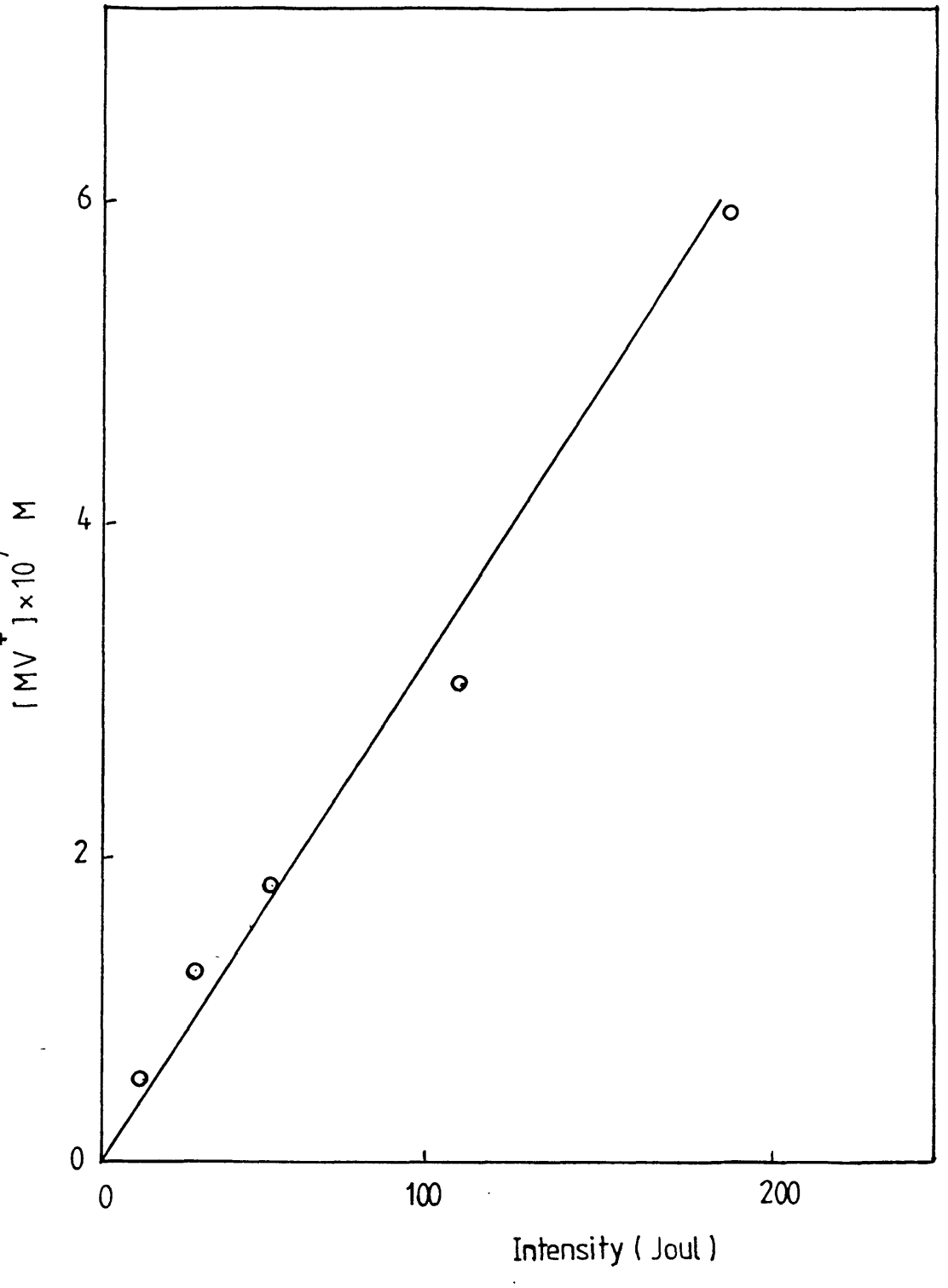


Fig. 4.1 Photoreduction of MV^{2+} (10^{-6} M) by CdS(5.10^{-4} M), SHMP(10^{-3} M) as a function of flash intensity.

dependence of the photobleaching of CdS on the flash intensity. In Chapter 3 it was shown that the transient bleaching resulted from a minor reaction pathway compared to charge recombination and that the concentration of electrons and hence the amount of the bleaching increased with the square root of the flash intensity.[45]

The transient absorption spectrum of photoreduced MV^+ is shown in Fig. 4.2 immediately after the photoflash and again 3ms later. During this short time, the spectrum shifts to a longer wavelength. The kinetic traces, in Fig. 4.3 show the spectral shift more clearly for 480nm and 600nm.

There could be at least two explanations for our observations:

i) Homogeneous dimer equilibrium;

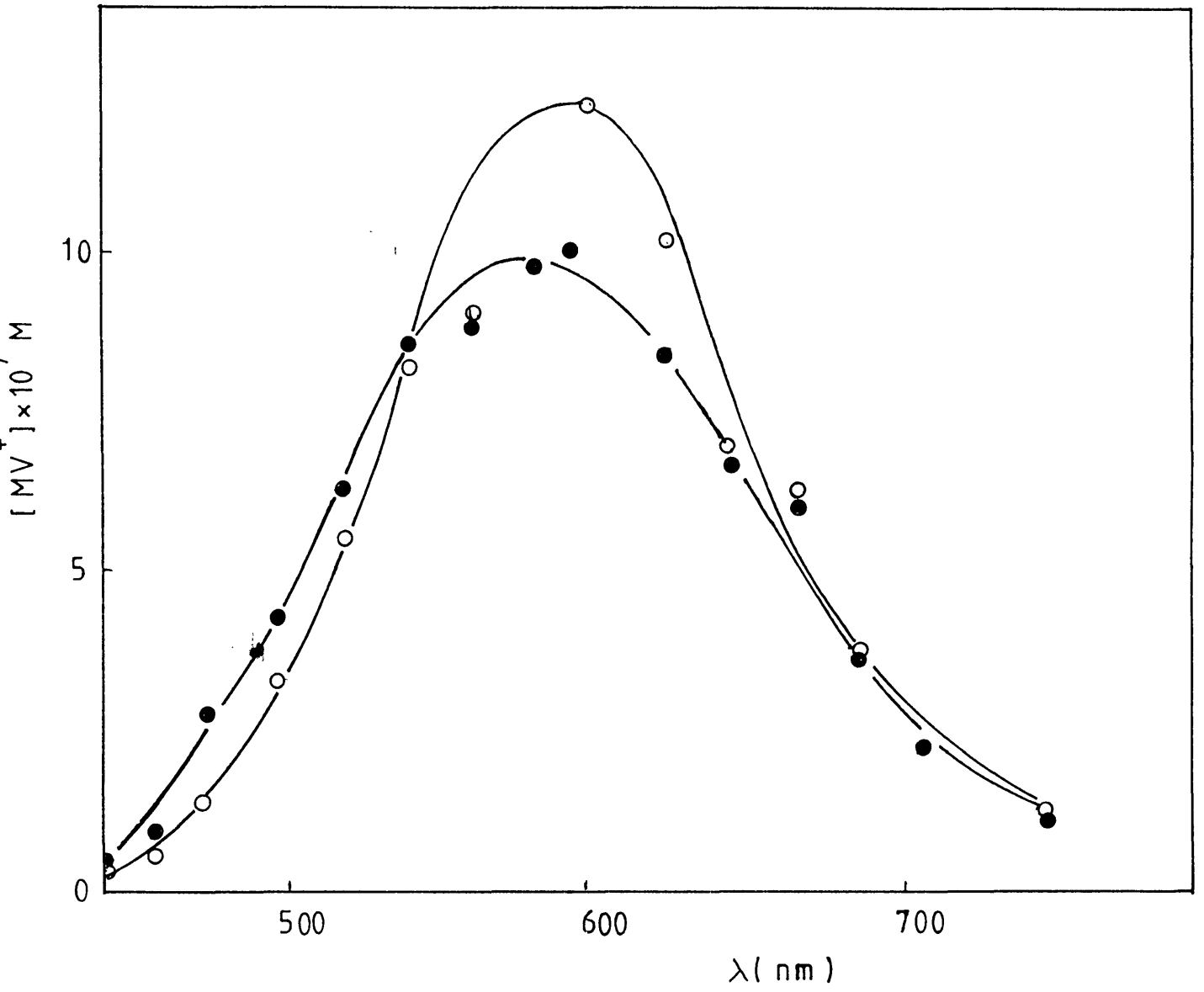
ii) desorption of dimer from the surface of colloidal CdS particles.

(i) In the first explanation it is possible that the high local concentration of photoreduced MV^+ leads to the formation of dimers. Kosower[165] has shown that the equilibrium constant for the dimerisation in homogeneous solution is:

$$2MV^+ \underset{}{\overset{K}{\rightleftharpoons}} (MV^+)_2 \qquad (4.1)$$

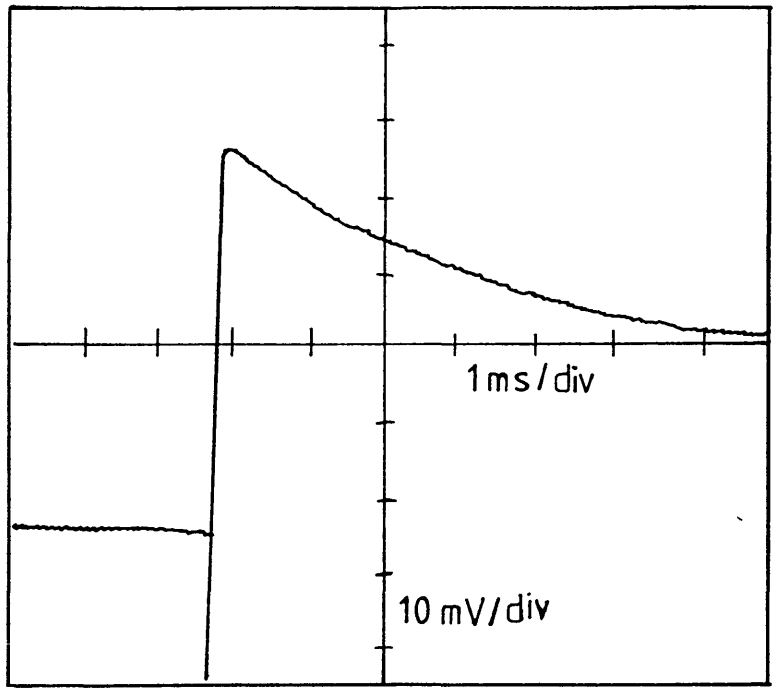
$$K = 2.6\times10^{-3} mol^{-1}$$

and the spectrum shows a similar shift, when dimers are present, to that shown in Fig. 4.2. In contrast research using time-resolved high resolution Raman Spectroscopy has found no evidence

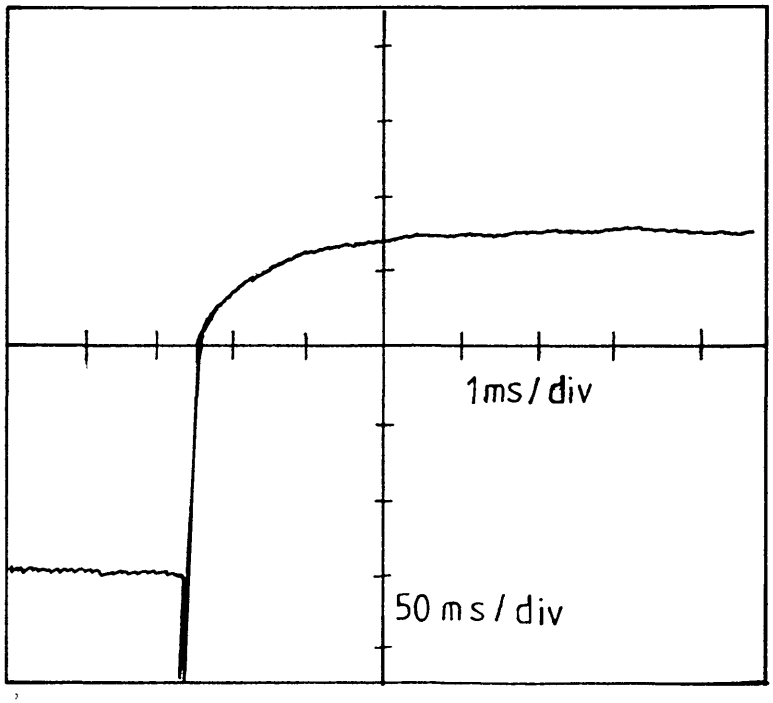


See overleaf

Fig. 4.2 Transient absorption spectrum of photoreduced MV^{2+} (4×10^{-3} M) by CdS (10^{-3} M) immediately after photoflash (○) and again 3 ms later (●).



A) 485 nm



B) 600 nm

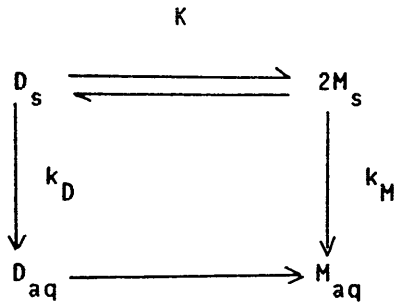
See overleaf

Fig. 4.3 Oscilloscope traces of (B) absorbance of photoreduced MV^{2+} at 605 nm and (A) recovery of absorbance at 485 nm for a colloid containing CdS(5.10^{-4} M) and MV^{+2} (4.10^{-3} M).

for specific adsorption of MV^+ on CdS.[166]

By using the mass transport model the particle size is calculated and found to be around 1000nm (Appendix 3), whereas the size of particles is measured as around 17nm by high resolution transmission electron microscopy. This model and some other calculations (Appendix 4), show that no dimers are formed in the solution to dissociate to the monomers.

(ii) In the second explanation of desorption surface kinetics we can write:



(4.2)

where k_M and k_D are the rate constants for desorption of monomer, MV^+, and dimer, $(MV^+)_2$ from the CdS particle, respectively. It is assumed that at $t = \infty$ no dimer exist in the bulk.

We have supposed that the dimers and monomers immediately after the photoflash are on the surface of CdS particles. Therefore we can write:

$$d_s = Km_s^2 \qquad (4.3)$$

where d_s and m_s are the concentrations of dimers and monomers respectively on the surface and K is the equilibrium constant.

The kinetics of the desorption reactions give:

$$\frac{d(2d_s + m_s)}{dt} = -2k_D\, d_s - k_M\, m_s \qquad (4.4)$$

These balance between the surface of area A and the bulk solution of volume V gives

$$2\,A\,d_s + A\,m_s + Vm = Vm_\infty \qquad (4.5)$$

in which m is the concentration of monomer at time t and m_∞ is the concentration of monomer at the end.

By changing the variables to

$$u = \frac{m}{m_\infty}, \quad v = \frac{A}{V}\,\frac{m_s}{m_\infty} \quad \text{and} \quad w = \frac{2d_s}{m_\infty}\,\frac{A}{V}$$

equation (4.5) becomes

$$u + v + w = 1 \qquad (4.6)$$

using equation (4.3) gives:

$$w = \frac{2Km_\infty V}{A}\,v^2 \qquad (4.7)$$

or $w = \gamma\, v^2$

where $\gamma = \frac{2Km_\infty V}{A}$

Multiplying equation (4.4) by $\frac{A}{Vm_\infty}$ gives:

$$\frac{d(w + v)}{d\tau} = -Kw - v \qquad (4.8)$$

where $\tau = k_M t$ and $K = \frac{k_D}{k_M}$

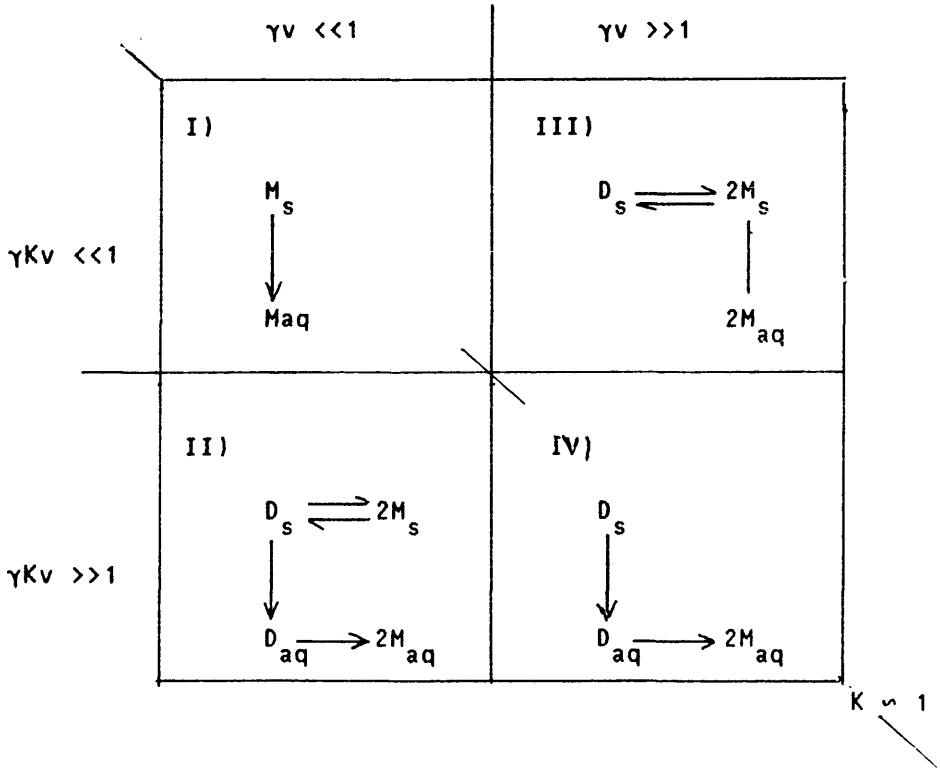
By substitution of $w = \gamma v^2$ in equation (4.8) we have

$$(2\gamma v + 1)\frac{dv}{dt} = -(\gamma K v + 1)v \qquad (4.9)$$

or

$$\frac{(2\gamma v + 1)}{v(1 + \gamma K v)}\frac{dv}{d\tau} = -1 \qquad (4.10)$$

The desorption reactions are assumed to be first-order, then using equation (4.10) we can have four cases as below:



CASE I

If $\gamma v << 1$ and $\gamma K v << 1$, then we have (by substitution) $d_s << m_s$ and $k_M = k_{desorption}$. In this case equation (4.10) becomes:

becomes:

$$\frac{\partial v}{\partial \tau} = -v \qquad (4.11)$$

or $$v = v_o e^{-\tau}$$

This means that the reaction is first order for v with t. Substitution of equation (4.11) by $v = (w/\gamma)^{1/2}$ and d_s from Appendix 5 gives

$$\ln \frac{(OD_o - OD_\infty)}{(OD - OD_\infty)} = 2k_M t \qquad (4.12)$$

As shown in Fig. 4.4, the experimental data for different concentrations of MV^{2+} are a good fit to equation (4.12). In this case only desorption of monomer from the CdS surface occurs.

CASE II

If $\gamma v << 1$ and $\gamma K v >> 1$, then we have

$$\frac{\partial v}{\partial \tau} = -\gamma K v^2 \qquad (4.13)$$

and $$\frac{1}{v} = \frac{1}{vo} + \gamma K \tau$$

or

$$\left(\frac{\gamma}{w}\right)^{1/2} = \left(\frac{\gamma}{w}\right)^{1/2}_{o} + \gamma K \tau$$

By substitution of parameters and using Appendix 5 we obtain

$$\frac{1}{(OD - OD_\infty)^{1/2}} - \frac{1}{(OD_o - OD_\infty)^{1/2}} = \frac{A}{vm_\infty (Ke_{eff})^{1/2}} k_D t \qquad (4.14)$$

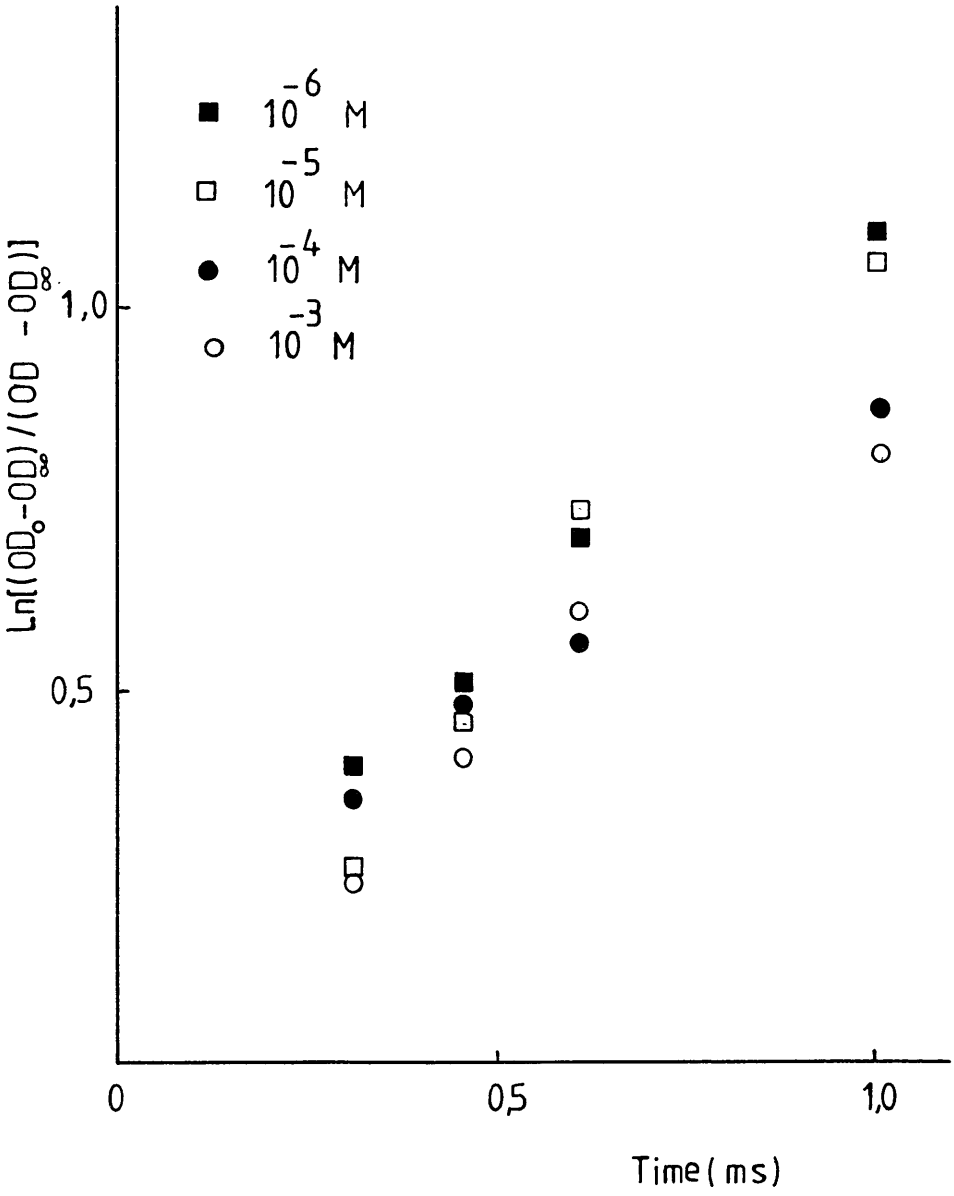


Fig. 4.4 Desorption of dimers, $(MV^{+})_2$, from CdS surface, where the solution contains CdS (5×10^{-4} M) and MV^{2+} (4×10^{-3} M).
CASE I & CASE IV.

Fig. 4.5 shows the plot of the left side of equation (4.14) against t, which is not a straight line. Since $\gamma v << 1$, then $K >> 1$. Therefore, desorption of the dimer from the surface should be very much higher than that of the monomer, i.e. $k_D >>> k_M$. This case is not possible, because the diffusion coefficient for dimer is less than monomer one.

CASE III

If $\gamma v >> 1$ and $\gamma K v << 1$, then we have

$$\frac{\partial v}{\partial \tau} = -\frac{1}{2\gamma} \qquad (4.15)$$

Integration of eq. (4.15) gives

$$v = v_o - \frac{1}{2\gamma}\,\tau$$

Substitution of v, w and d_s from Appendix 5 gives

$$(w)^{1/2} = (w_o)^{1/2} - \frac{1}{2(\gamma)^{1/2}}$$

or

$$(d_s)^{1/2} = (ds_o)^{1/2} - \frac{k_M}{4(K)^{1/2}}\,t$$

or

$$(OD_o - OD_\infty)^{1/2} - (OD - OD_\infty)^{1/2} = \frac{k_M}{4}\,\frac{e_{eff}}{K}^{1/2}\,t \qquad (4.16)$$

Fig. 4.6 shows the plot of the left side of eq.(4.16) against t, which is very scattered. This means that the experimental data cannot be fitted to equation (4.16) and therefore Case III does

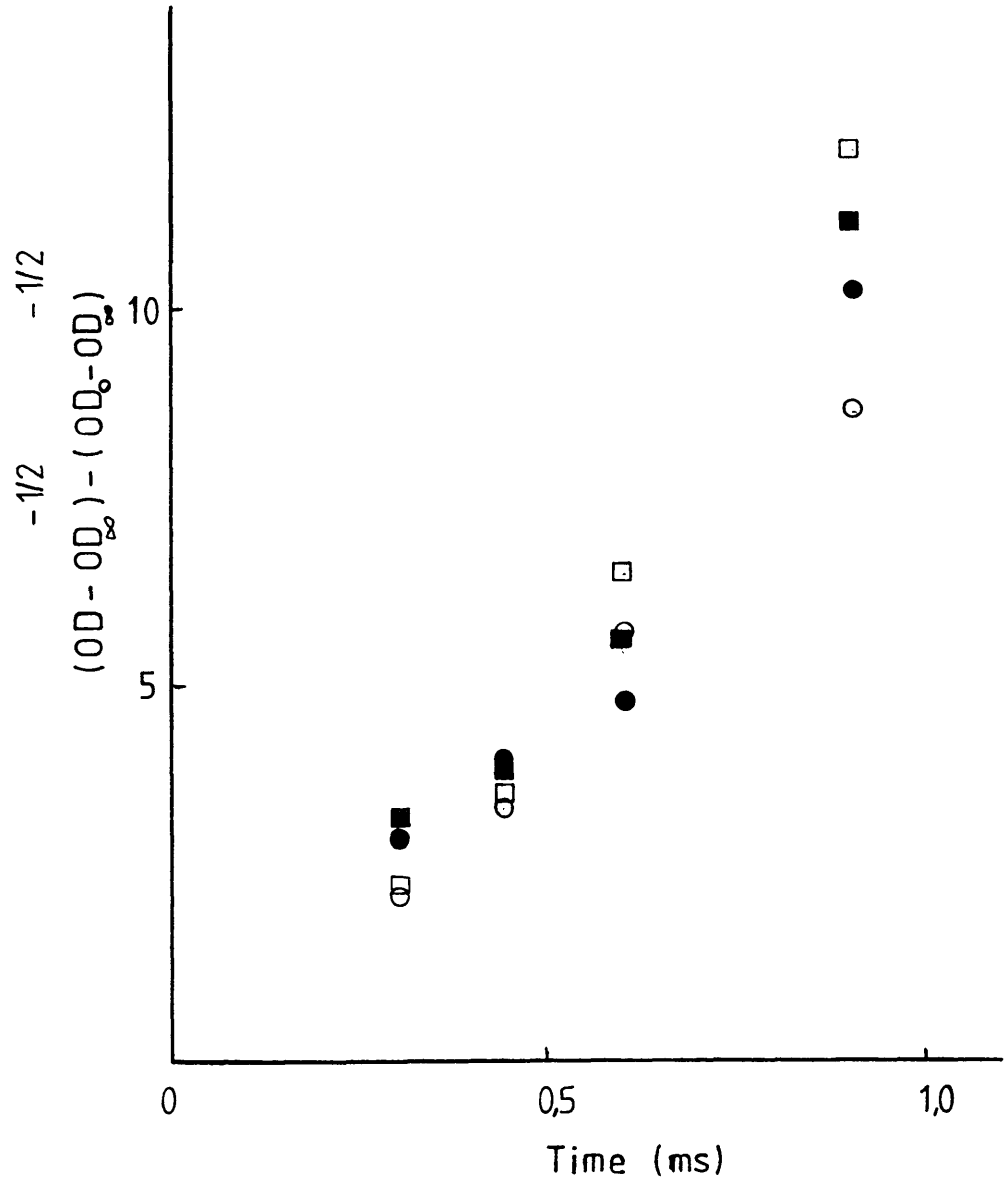


Fig. 4.5 Desorption of dimers, $(MV^+)_2$, from CdS surface, concentrations and conditions as for Fig. 4.4. CASE II.

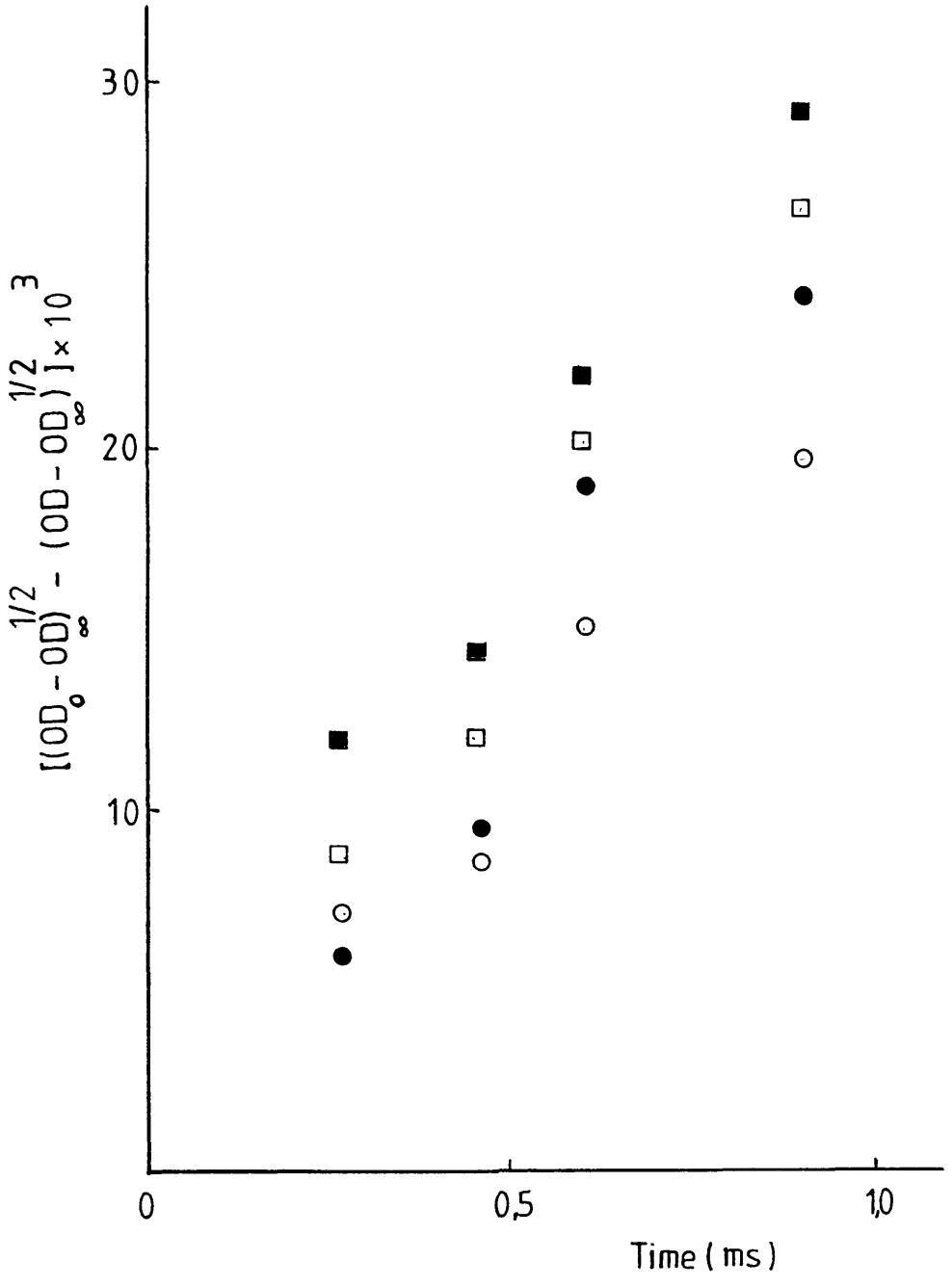


Fig. 4.6 Desorption of dimers, $(MV^+)_2$, from CdS surface, concentrations and conditions as for Fig. 4.4. CASE III.

not explain the situation observed in the experiments.

CASE IV

This case is the same as case I, except that $d_s >> m_s$ so that desorption of dimer from the CdS surface occurs, i.e. $k_D = k_{desorption}$

Of the above four cases, only case I and IV were first-order and thus consistent with our experimental data. To determine whether case I (monomer desorption) or case IV (dimer dispersion) is the correct one for our results, we go back to Fig. 4.2. In the monomer case, we expect the absorption curve after 3ms to be broader, and flattened with respect to that for the monomer adsorbed at the CdS surface immediately after flash. For case IV, the dimer desorbs from the surface, the absorption curve should be shifted with respect to the surface monomer (at t=o)[82,165]. Therefore, Fig. 4.2 reveals that the desorption of dimer rather than monomer, from the particle surface is more probably the case of the change in the absorption spectrum.

4.2 Cysteine effect on the yield of MV^+

In the third chapter we described the rate of reduction of methyl-viologen (MV^{2+}) to MV^+ from photoexcited CdS colloids in the presence of cysteine as an electron donor.[45] Where only 10^{-2}moldm^{-3} cysteine was present in the solution containing CdS and MV^{2+} [$(1-5)\times10^{-6}$moldm^{-3}], the yield of MV^+ was much smaller

than for CdS and MV^{2+} alone. The photoreduced MV^{+} was formed by a bimolecular process with a rate constant of 3.6×10^{8} $dm^{3}mol^{-1}$ s^{-1}. In the absence of cysteine the reaction appears within the photoflash for methyl viologen concentrations as low as $10^{-6}moldm^{-3}$ and the reaction involves direct electron transfer from the conduction band of CdS to adsorbed MV^{2+}.

The dramatic effect of cysteine on the yield of MV^{+} for a range of cysteine and MV^{2+} concentrations is shown in Fig. 4.7. Cysteine concentrations as low as $2 \times 10^{-4}moldm^{-3}$ decrease the yield of MV^{+} by up to a factor of 30. This effect and the shape of figure 4.7 suggest that cysteine effectively coats the surface of CdS particles, dislodges MV^{2+} from the surface and prevents the methyl viologen from accepting electrons and hence decreasing charges recombination. Instead the reduced methyl viologen is produced in a slower reaction with electrons trapped on the particles, so that it is now formed after the photoflash as shown in Fig. 4.8.

4.3 pH effect on the yield of (MV^{+})

It is well known that the reduction potential of an electron on oxide particles is controlled by the pH of the solution and this in turn controls the rate of electron transfer, for example from TiO_2 to methyl-viologen.[76] Due to the changing surface charge this is not generally the case for non-oxide semiconductors, such as CdS, since they are less susceptible to the surface protection. As shown in Fig. 4.9.a, the yield of

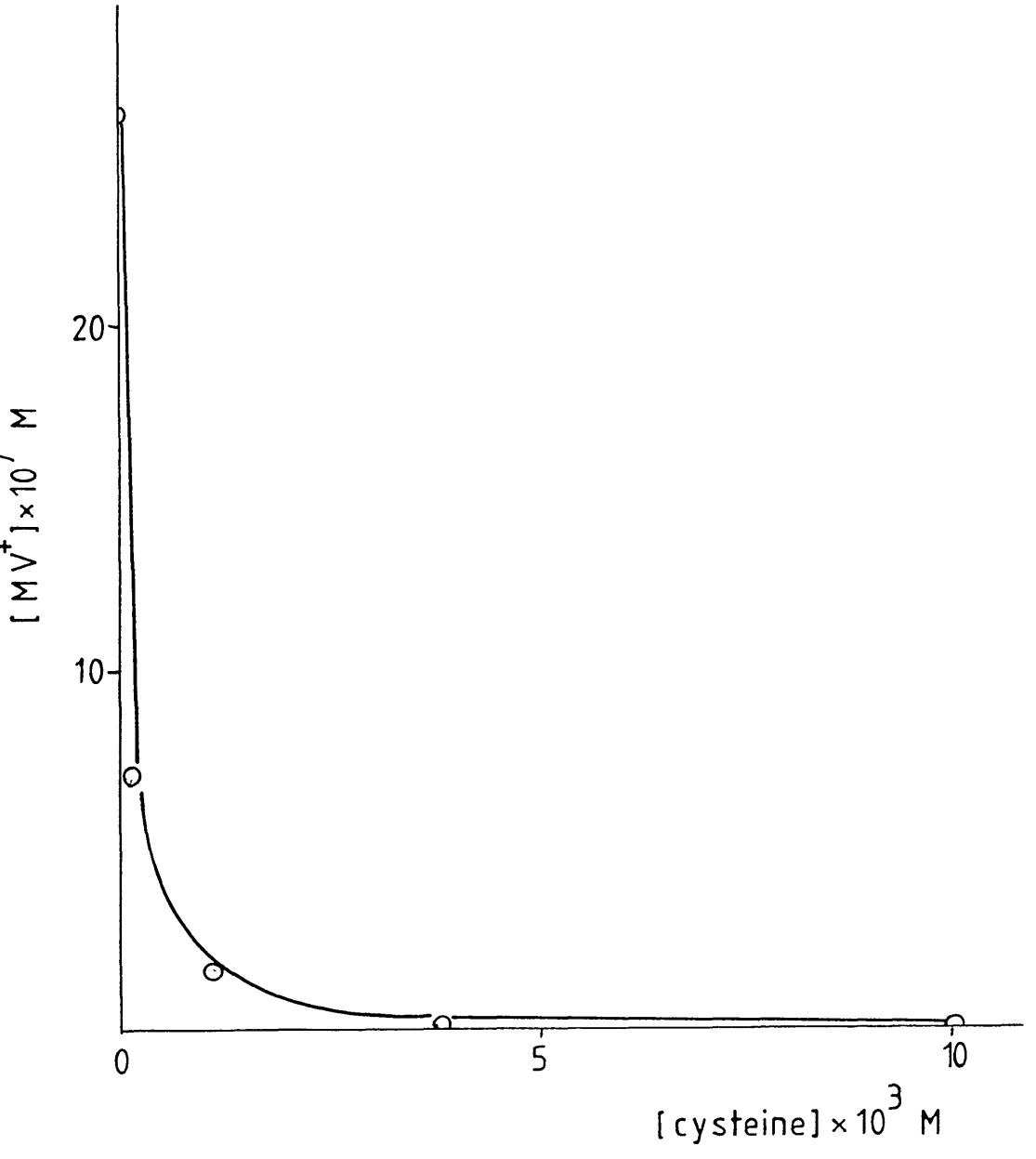


Fig. 4.7 Cysteine effect on the yield of photoreduced MV^{2+} for a colloid containing CdS(5×10^{-4} M) and MV^{2+}(10^{-2} M).

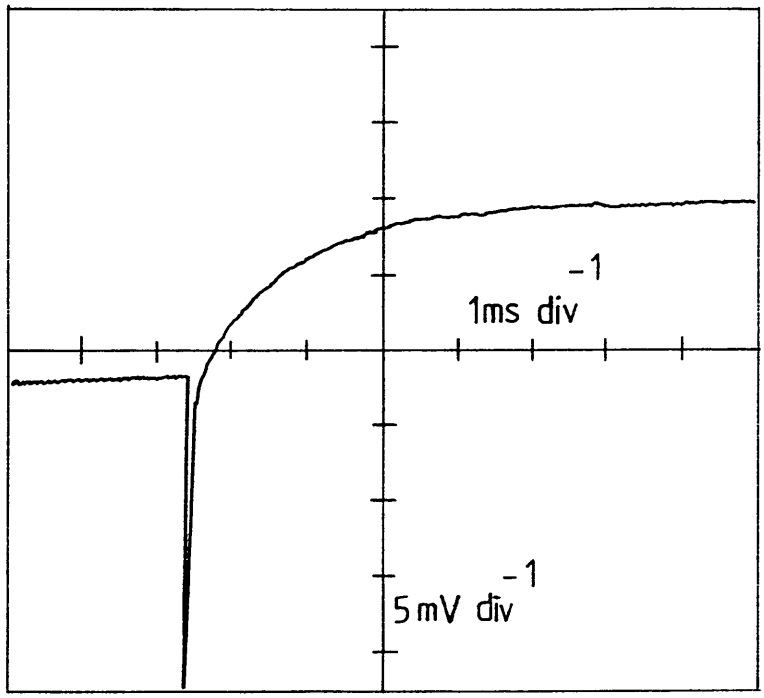


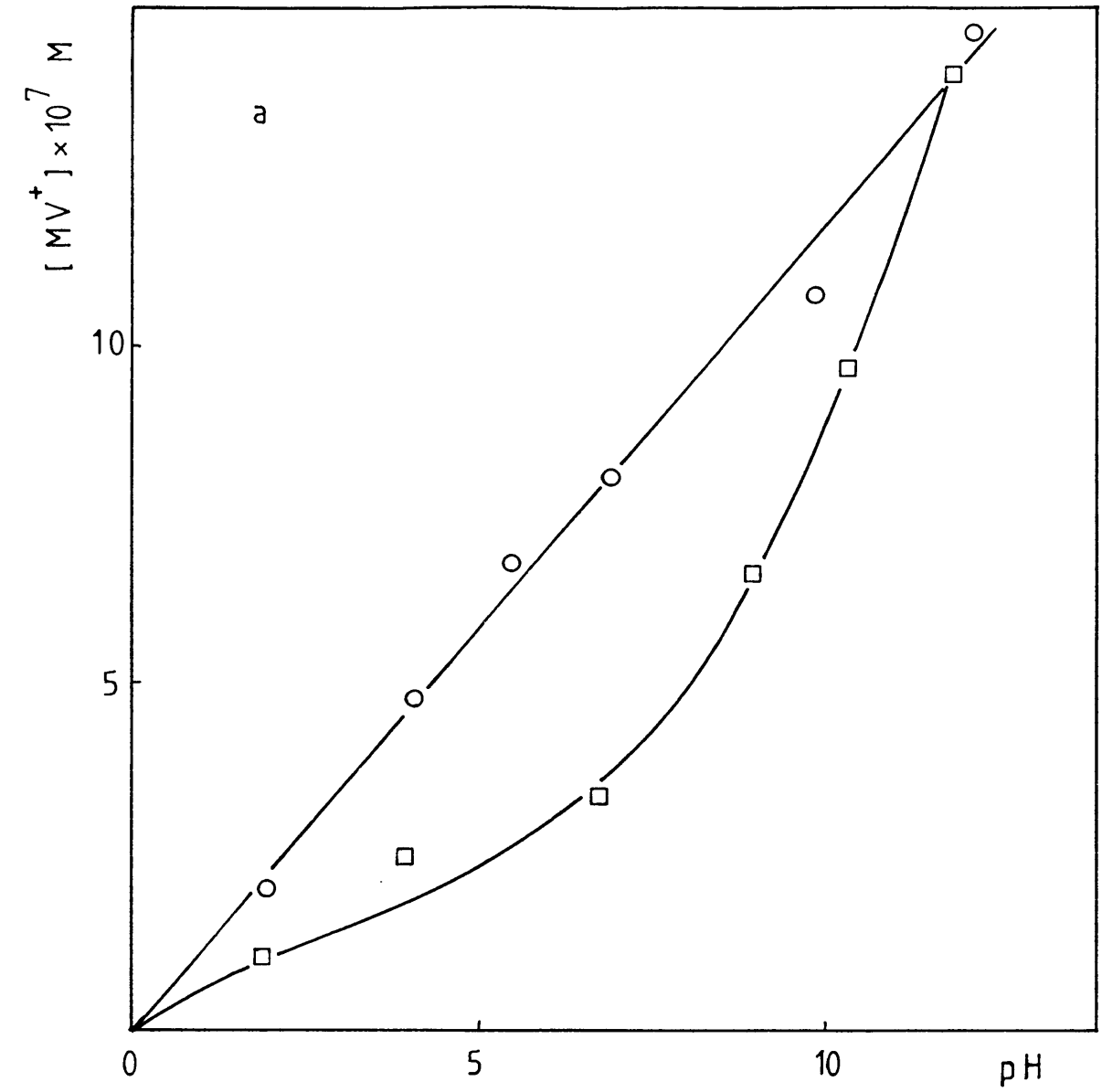
Fig. 4.8 Oscilloscope trace of photoreduced MV^{2+} after adding cysteine(10^{-2} M).

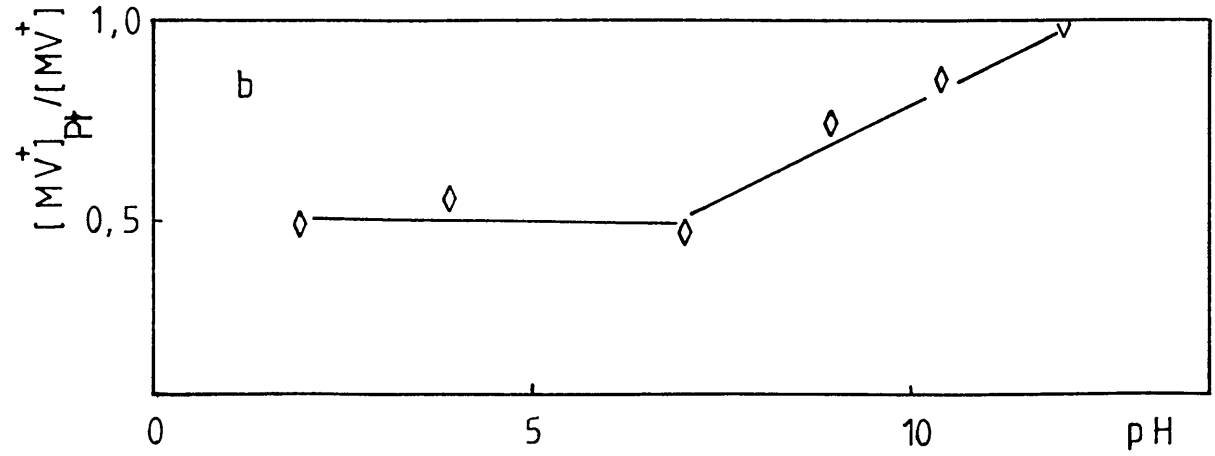
radical cation MV^+ increases approximately linearly with pH after the photoflash. Since the yield of viologen depends on competition between electron transfer to MV^{2+} and charge recombination, either charge recombination is slower at higher pH or the rate of electron transfer to methyl-viologen (MV^{2+}) increases with pH. The latter case seems the more probable explanation. In our solutions, the surface is coated with sodium hexametaphosphate as a stabilizer and this may reflect the concentration of protons in the solution. Alternatively, the pH effect on CdS particles may arise from a coating of cadmium oxide on the particles, which could similarly respond to pH changes by the adsorption of either cations, H^+ or anions, OH^-.

4.4 Pt effect on the yield of MV^+

The effect of Pt on the yield of methyl viologen radical cations (MV^+) at different pH is shown in Figs. 4.9.a and .b. In these experiments the platinised CdS particles were formed by mixing Pt and CdS colloids.

When Pt is present in solution the kinetics suggest that at pH 3-10 the Pt is attached to the CdS particles catalysing the reduction of protons to gaseous hydrogen. Thus the yield of MV^+ is smaller immediately after the photo flash. If the particles were not attached to the CdS, then the viologen concentration would be expected to be identical to that in the absence of Pt, immediately after the flash. When the Pt is bound to the particles, photogenerated electrons have three decay routes - charge recombination, reduction of MV^{2+} or reduction of water at

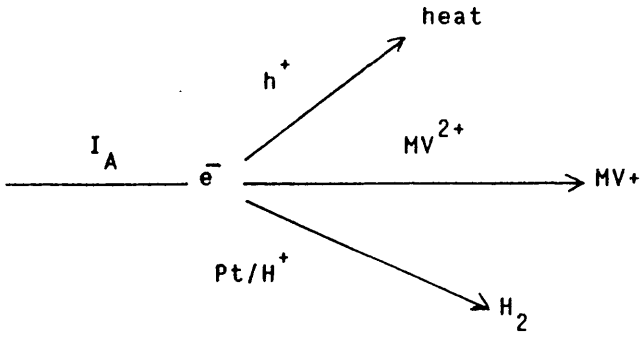




See overleaf

Fig. 4.9 pH-effect on the yield of photoreduced MV^{2+}:
(○) CdS(5×10^{-4} M) and MV^{2+}(10^{-2} M),
(□) 4% Pt/CdS(5×10^{-4} M) and MV^{2+}(10^{-2} M).

Pt islands - as shown in Scheme II.



SCHEME II

In the above scheme II there is either free carrier recombination (heat, hv') or electron transfer (MV^+, H_2). The relative yields of H_2 and MV^+ for a given Pt, as a catalyst and MV^{2+} concentration will depend on the overvoltage for the two processes, since this is expected to determine the rate constant for electron transfer in line with the Tafel equation.[82] The redox potential of MV^{2+} is fixed at -0.448 mV (against NHE) and is independent of pH,[52] whereas the redox potential for H_2 formation shifts by 59 mV per pH unit[52] according to the Nernst equation:

$$E'_o\ (H^+/H_2) = 0 - 0.059\ pH\ mV \qquad (4.17)$$

At pH 7.5 the standard potentials of the two reactions are the same and Fig. 4.9.b shows that below this pH the yield of MV^+ is significantly reduced. When the pH is increased above 7.5 the relative yield of MV^+ gradually increases until pH 12 when the yield is the same in the presence and absence of Pt.

Grätzel and Ramsden measured the effect of Pt on the yield of MV^+ at pH5 and observed that at 8% Pt loading, one third of

the conduction band electrons react with Pt.[52] In all of our experiments with MV^{2+} and Pt, the formation of MV^{+} was observed during the photoflash and its concentration did not significantly increase or decrease within 10μs of the flash. This suggests that MV^{+} does not readily transfer electrons to Pt bound to the CdS, even though the reaction is thermodynamically favourable below pH 7.5. Nor is MV^{2+} reduced by the low concentrations of H_2 formed on the Pt islands during the flash, a process would be thermodynamically favourable above pH 7.5. It is possible that these processes occur during the photoflash before MV^{+} or H_2 can leave the environment of the particles.

4.5 The effect of flash intensity on the yield of MV^{+}

We have shown (Chapter 3) that the magnitude of the transient signal in the absorption spectrum of CdS subjected to a photoflash is proportional to the square root of the flash intensity. In this section the effect of flash intensity on the yield of MV^{+} is studied in two ways as below:

4.5.1 At various pH

The effect of flash intensity on the yield of MV^{+} in solution containing CdS and 4%Pt colloids at different pH is shown in Fig. 4.10. At any pH the yield of reduced methyl viologen, MV^{+}, could be increased by increasing the flash intensity. When the CdS/Pt sols in the presence of MV^{2+} were flashed continually for about 20 times at pH = 12 and then

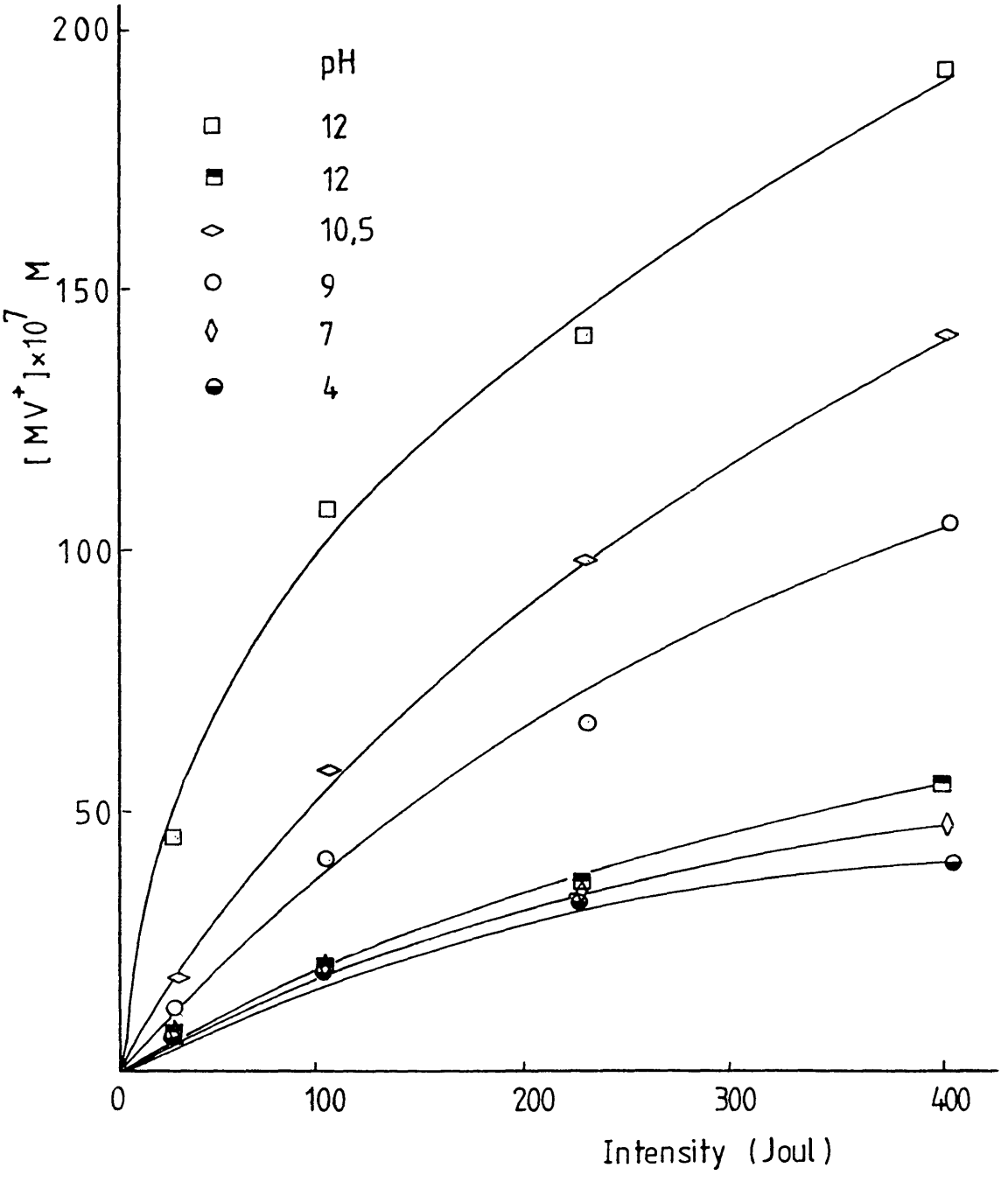


Fig. 4.10 The effect of flash intensity on the yield of MV^{+} for a colloid containing CdS(5×10^{-4} M) and MV^{2+}(10^{-2} M).

subjected to different flash intensity, the yield of MV^+ was reduced by a factor of 5. This effect may possibly be explained by decomposition of CdS particles in every photoflash.

4.5.2 Photodegradation of CdS

The quantum yield of degradation in the absence of any additives in aerated CdS sol has been reported as 0.04 CdS molecules per photon.[186] They also found that, in the presence of MV^{2+} at a concentration of 10^{-4}moldm^{-3}, the rate of degradation increased by a factor of 6. These effects can be understood in terms of the following mechanism:

$$e^- + MV^{2+} \longrightarrow MV^+ \qquad (4.18)$$

$$MV^+ + O_2 \longrightarrow MV^{2+} + \bar{O}_2 \qquad (4.19)$$

It has been shown[56] that oxygen itself does not efficiently pick up electrons directly from CdS particles. Hence, MV^{2+} facilitates the removal of electrons, and the remaining positive holes efficiently oxidise sulfide anions to sulfur:

$$h^+ + S^{2-} \longrightarrow S^- \qquad (4.20)$$

$$S^- + O_2 \longrightarrow S + O_2^- \qquad (4.21)$$

The superoxide radical anions mainly form H_2O_2.[186] The rate of degradation of aerated CdS sols was analogously increased by addition of Pt sols.

In our experiment, when deaerated CdS sols were illuminated

in the presence of 10^{-2}moldm^{-3} of MV^{2+} and different per cent of Pt sols photodegradation of CdS was observed, as shown in Fig. 4.11. Adsorbed Pt colloids caused a retardation of the degradation of CdS in the presence of MV^{2+}. The proposed mechanism of photodegradation of CdS in the presence of Pt is shown as:

$$H^+ + e^- + Pt \longrightarrow Pt\text{-}H \qquad (4.22)$$

together with equations (4.20) and (4.21), and in the presence of both pt and MV^{2+}, retardation of degradation, is shown as:

$$Pt\text{-}H + h^+ \longrightarrow Pt + H^+ \qquad (4.23)$$

The effect of flash intensity on degradation of CdS is also shown in Fig. 4.11. By increasing flash intensity from 10kV to 20 kV the rate of degradation approximately doubled. This process may possibly be first-order, but due to insufficient results, we cannot prove it.

4.6 Conclusion

The studies presented here serve to illustrate the important features of surface effects in the colloidal semiconductor, CdS, by using time-resolved techniques:

When MV^{2+} is photoreduced at the surface of colloidal CdS, desorption of the dimer cationic methyl viologen radical, $(MV^+)_2$, from the surface of the particle into the bulk of solution causes a shift in the absorption spectrum after the photoflash.

The presence of a low concentration of cysteine in the

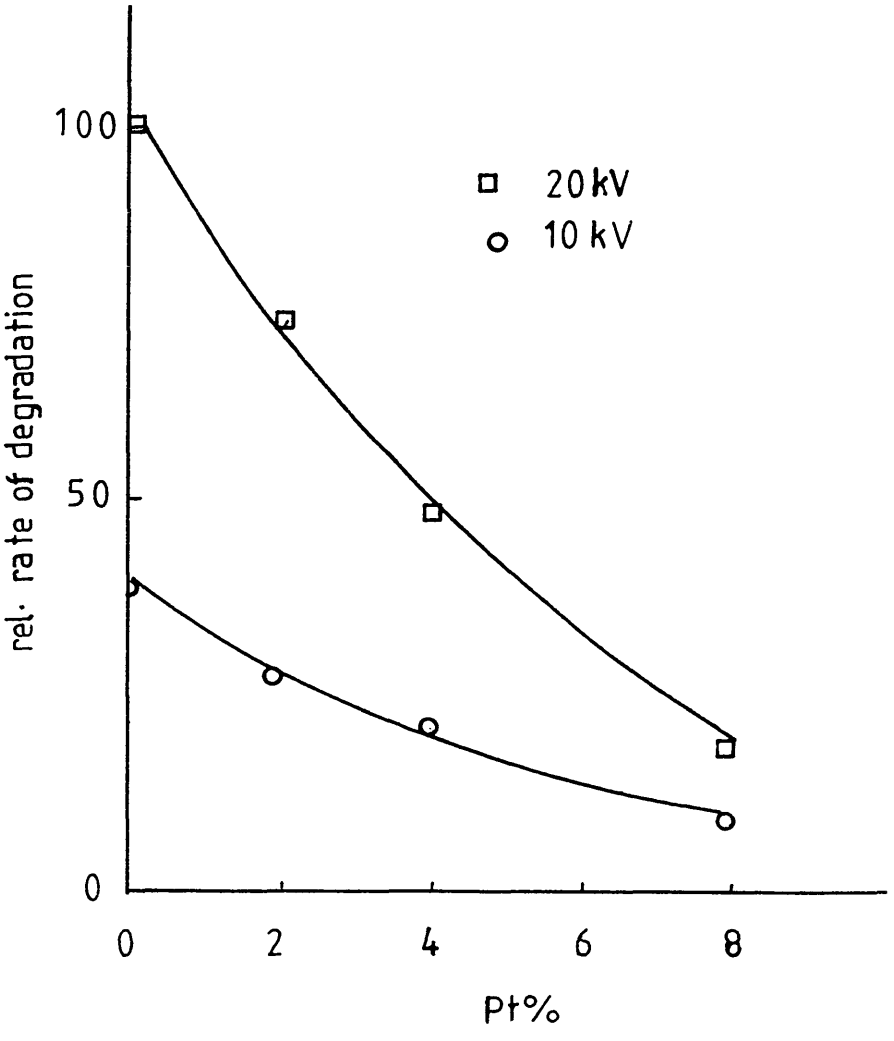


Fig. 4.11 The effect of platinum on the yield of photodegradation of colloidal CdS (5×10^{-4} M)/SHMP(10^{-3} M).

solution containing CdS and MV^{2+} prevents the adsorption of MV^{2+} on CdS particles and reduces the yield of MV^{+} by a factor of 30.

The yield of MV^{+}, in the absence of any additives, increases with pH (pH 2-12). This effect may be explained by the increasing of the potential of conduction band's electron on the particle with pH.

The yield of MV^{+} in the presence of adsorbed pt is reduced at pH < 7.5. However, above pH 7.5 it is the same as that obtained in the absence of Pt. This is because the reduction potential of H^{+} above pH 7.5 is more negative than that of MV^{2+} and the reduction of MV^{2+} by any H_2 which was formed on the Pt "islands" during the photoflash is thermodynamically favourable.

Thus the study of surface effects in the photo-electrochemistry of semiconductors provides valuable information in the search for an efficient method of solar energy conversion.

CHAPTER 5

Photochemistry of Colloidal ZnS

In the last two chapters (3,4), the kinetics, photophysical and photochemical behaviour of colloidal CdS have been described. It was shown that the photoreduction of adsorbed molecules, photodegradiation of the colloid, photobleaching of the absorption of the colloid and the quenching of its luminescence can be explained in terms of the formation of electron-hole pairs by bandgap photoexcitation of CdS and subsequent reactions of these charge carriers. In this chapter we likewise consider absorption, luminescence, photodegradiation and the kinetics of interfacial reactions at ZnS particles.

INTRODUCTION

Zinc sulfide is a n-type (II-XI) semiconductor with a much larger energy band gap (3.64 eV) than that in CdS (2.42 eV). Tributsch and Bennett[170] have found that the upper edge of the valence band in ZnS is located at about 2.3V which is 0.8V more positive than that of CdS. Similarly, the lower edge of the conduction band is loacated at -1.4V which is more negative than in CdS. Therefore electrons in ZnS should have more reducing power and positive holes stronger oxidising power than in CdS.

The photochemistry of ZnS particles in aqueous suspension was studied more than fifty years ago.[171, 172] It not only

photolyses but also catalyses the photo-decomposition of water.[60,173,181] From the viewpoint of solar energy utilization, the photo-(electro)chemical behaviour of colloidal ZnS has been intensively studied during the last few years.[173,181] However, the solar production of hydrogen by photolysis of water using ZnS has drawn little attention, because ZnS is photodegradable in water.[171] But in the presence of an electron donor, such as tetrahydrofuran, methanol or ethanol it has been found that ZnS is very efficient in the photocatalytic cleavage of water.[182]

ZnS exists in two crystal forms: Blende (cubic) and Wurtzite (hexagonal). Its valence band consists largely of s and p orbitals from sulfur and the conduction band is mainly due to s states of Zinc metal.[183] ZnS possesses high specific resistance and therefore it is difficult to study by electrochemical methods. The direct observation of photochemical reactions in ZnS complements electrochemical investigations. In the following section some aspects of the photophysical and photochemical behaviour of colloidal ZnS are considered.

5.1 Photophysical Properties

5.1.1 Absorption Spectrum

The absorption spectrum of $5x10^{-3}$moldm^{-3} undoped colloidal ZnS with $5x10^{-3}$ moldm^{-3} of sodium hexametaphosphate as a stabiliser at pH$\sim$7.5 is shown in Fig. 5.1. The onset of the light absorption was observed at 336nm, which is very close to

the band gap energy of the macrocrystalline ZnS. Therefore colloidal ZnS is transparent in the visible region and this allows one to study the surface photoeffects in more detail. As shown in Fig. 5.1. at wavelengths shorter than 336nm (corresponding to photon energies greater than the band gap), the absorption rises steeply. This means that the absorption spectrum of colloidal ZnS particles is typical of that for a crystalline semiconductor. When the concentration of colloidal ZnS was lowered from $5x10^{-3}moldm^{-3}$ to $10^{-3}moldm^{-3}$ a shoulder appeared around 300nm and the onset of absorption shifted from 336nm to 320nm. This means that dilution of the stoick solution by a factor of 5 produce smaller colloidal semiconductors particles. It was also found that the stability of the diluted solution is much greater than that of the stock solution. Therefore dilution prevents the coagulation of colloidal particles and precipitation in a short time. There is a fair similarity between our results and those reported by Henglein and coworkers[177] for the absorption spectrum of undoped ZnS colloids.

5.1.2 The Fluorescence of ZnS

The fluorescence spectrum of undoped colloidal ZnS is shown in Fig. 5.2. The colloidal ZnS fluorescences upon excitation with light of wavelength below 320nm.[58] As shwon in Fig. 5.2 the broad fluorescence spectrum of ZnS starts at 335nm (the onset of the absorption spectrum). ZnS has a larger quantum yield of fluorescence than CdS. It is reported that the quantum yield for

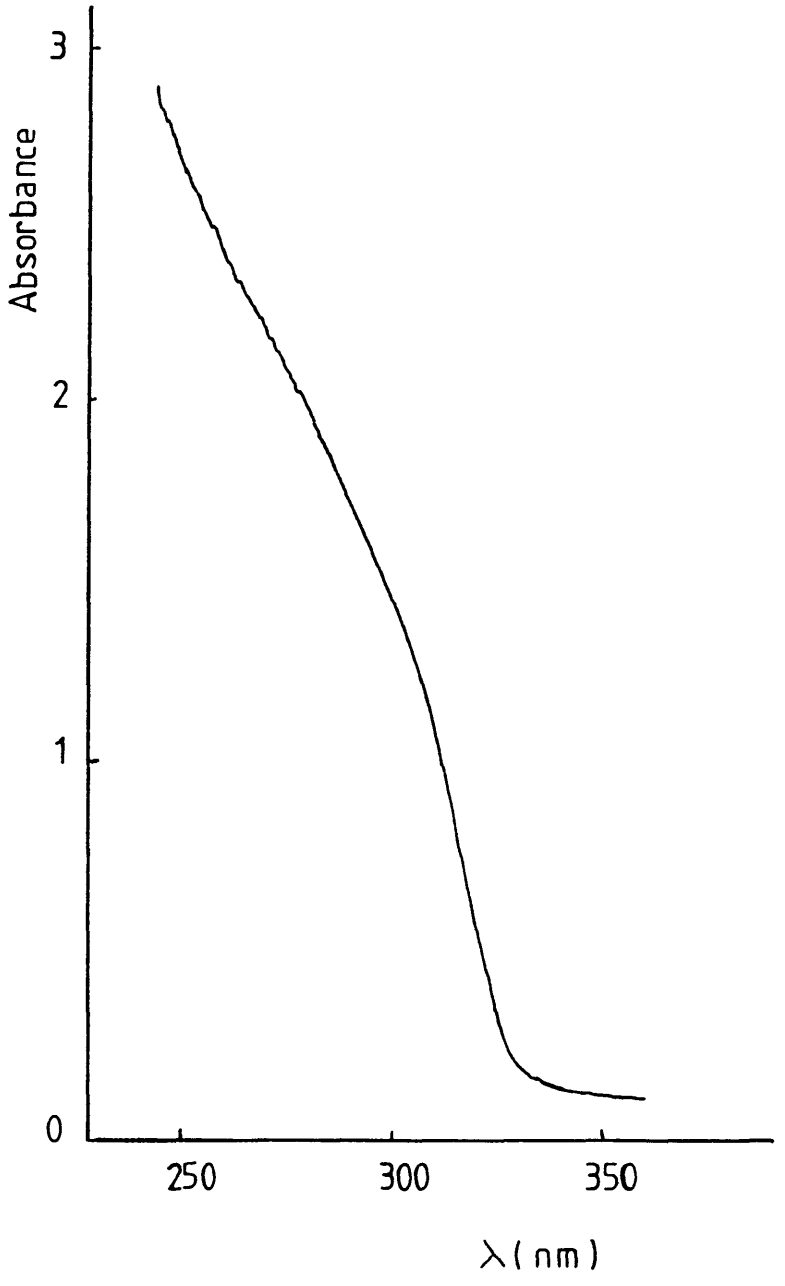


Fig. 5.1 Absorption spectrum of undoped ZnS ($5x10^{-3}$M).

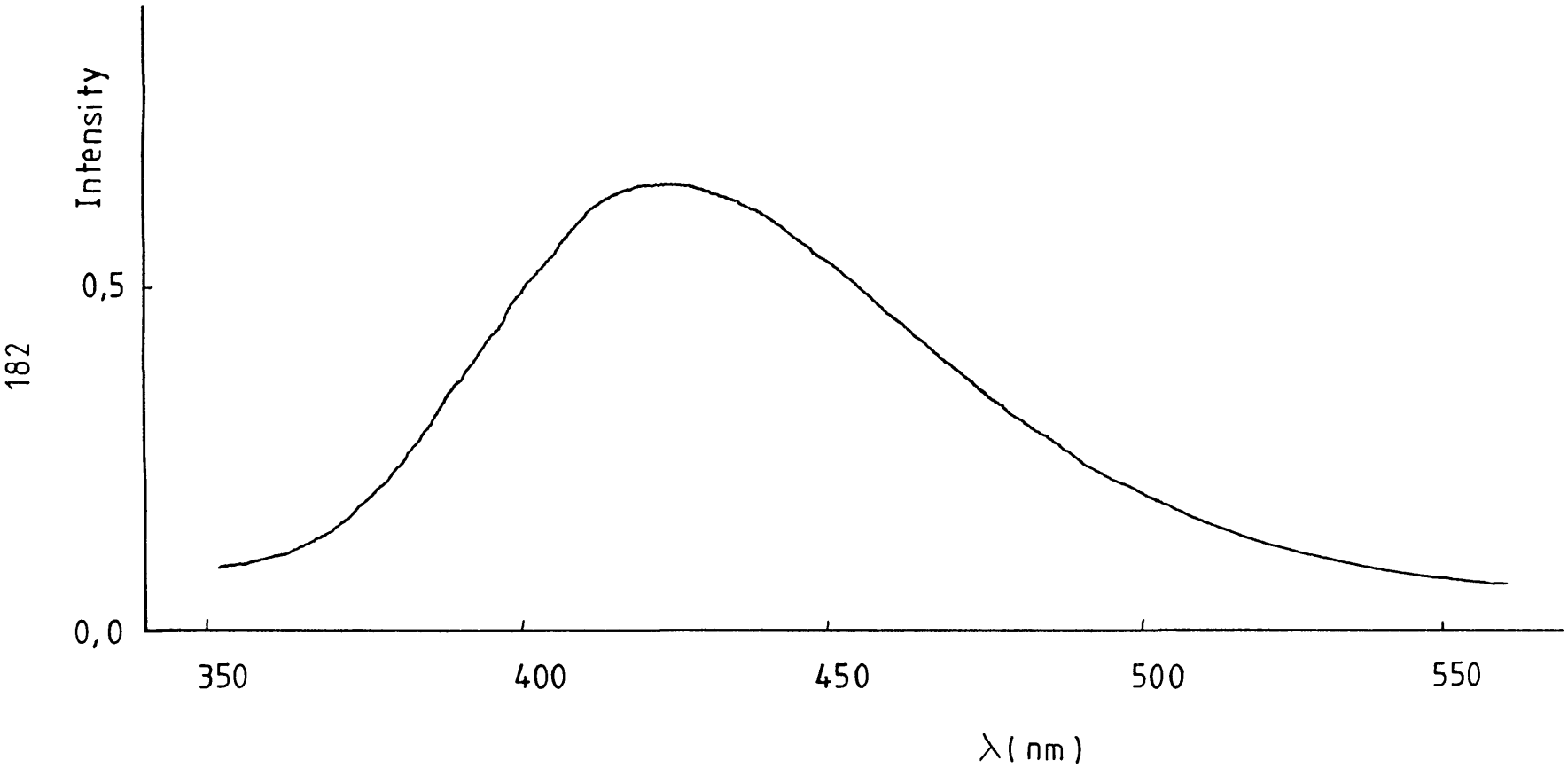


Fig. 5.2 Fluorescence spectrum of undoped ZnS(5×10^{-3} M).

ZnS is 13%, while that for CdS is only 2%.[60] Because of the high emission efficiency of the ZnS crystal, luminescence studies of both doped and undoped colloidal ZnS are more convenient than for CdS or TiO_2.

5.1.2.1 Quenching Effect

Quenching of the fluorescence of colloidal ZnS is observed in the presence of an electron acceptor such as methyl viologen. This effect is shown in Fig. 5.3. Addition of even low concentrations of MV^{2+} has a dramatic effect on the quenching of fluorescence. For example, addition of $8x10^{-6}moldm^{-3}$ methylviologen as one third of the photoluminescence of ZnS. Increasing the concentration of MV^{2+} increased the quenching effect. As shown in Fig. 5.4, 95% of the fluorescence was quenched by $8x10^{-5}moldm^{-3}$ MV^{2+}. This means that metyhyl viologen is strongly adsorbed at the surface of ZnS particles and removes excited conduction band electrons from the surface of the semiconductor particles. Hence the yield of electron-hole recombination which is responsible for the fluorescence, is decreased by increasing the concentration of electron acceptor in solution. The remaining holes on the valence band may decompose the ZnS particles. The mechanism for quenching and degradation is:

$$ZnS \xrightarrow{h\nu} ZnS(\bar{e}, h^+) \qquad (5.1)$$

$$\bar{e} + MV^{2+} \longrightarrow MV^+ \qquad \text{Quenching} \qquad (5.2)$$

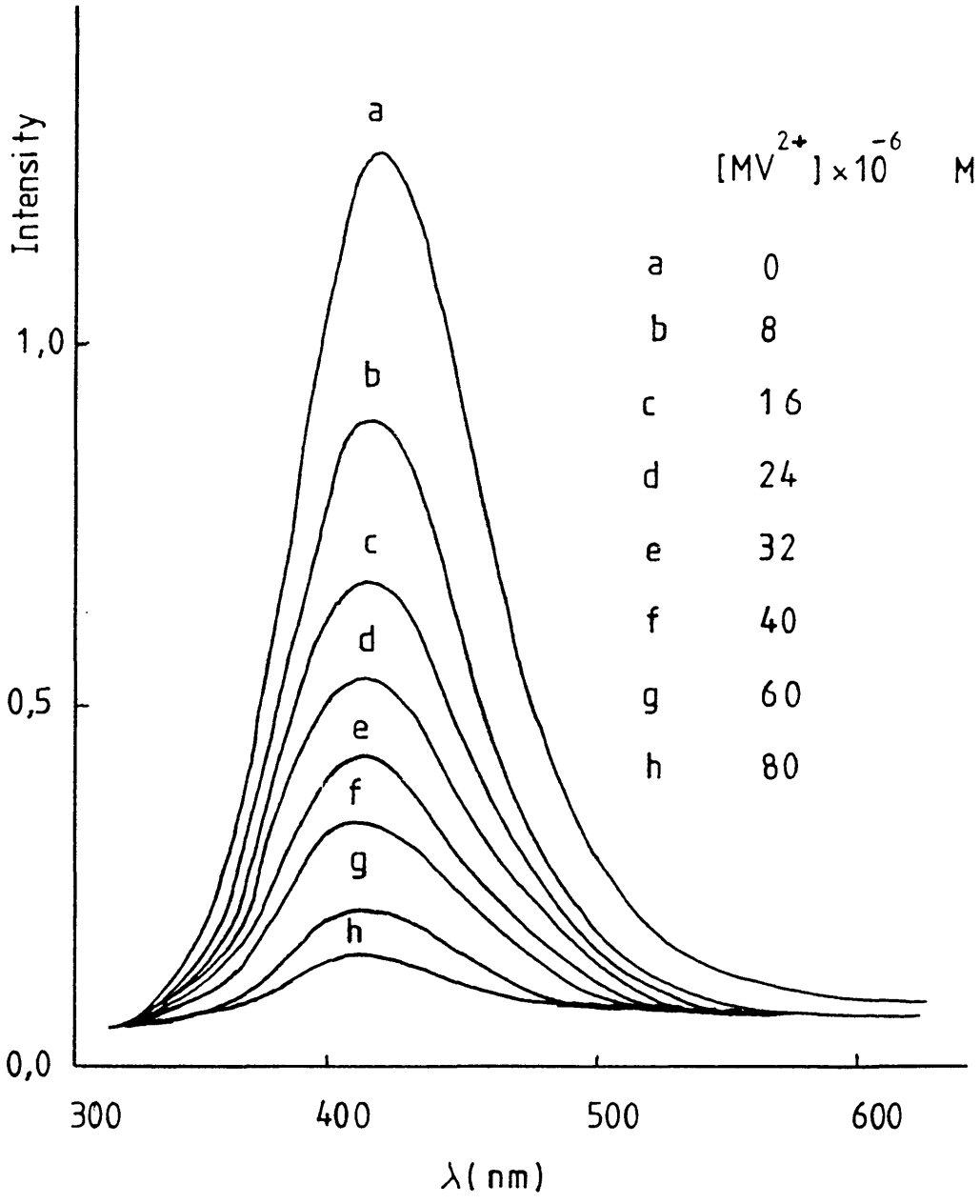


Fig. 5.3 Fluorescence quenching of undoped ZnS(5×10^{-3} M) using MV^{2+}.

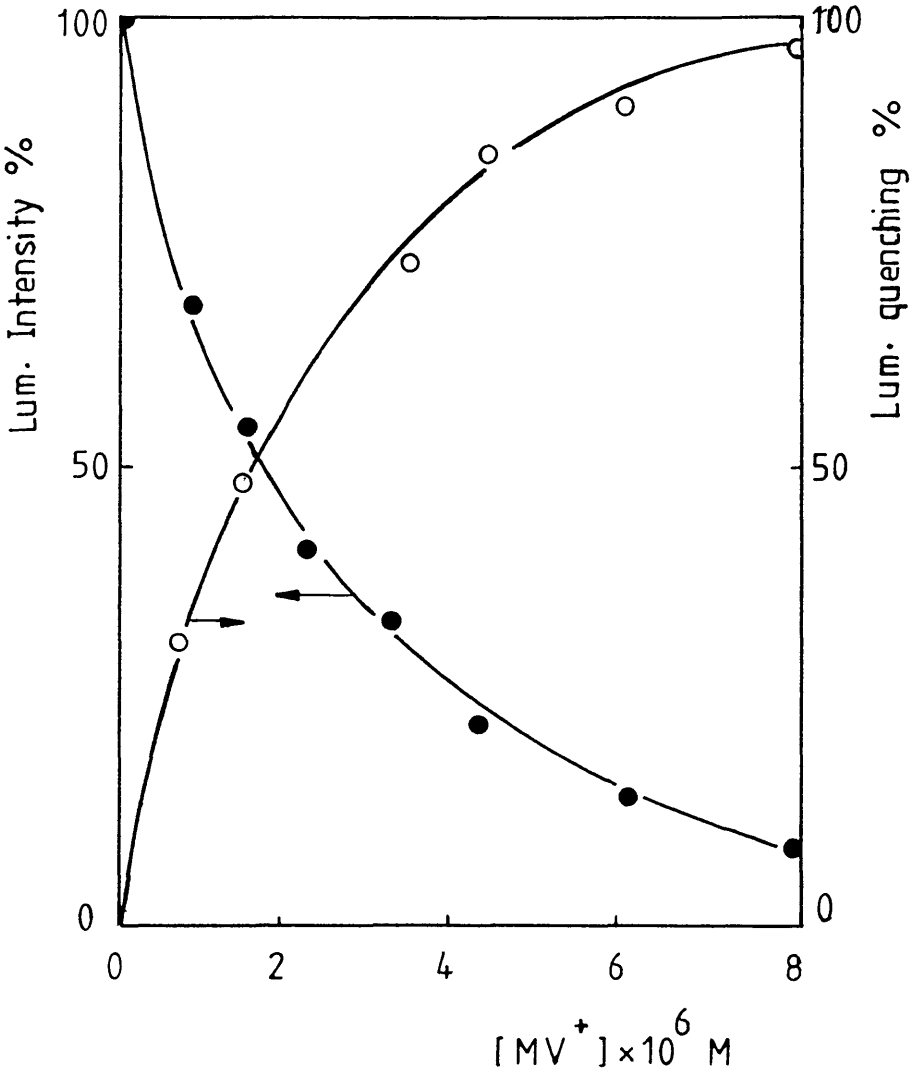


Fig. 5.4 The effect of MV^{2+} on the fluorescence intensity of undoped ZnS(5×10^{-3} M).

$$\bar{e} + h^{+} \longrightarrow h\nu' \qquad \text{Luminescence} \qquad (5.3)$$

$$2h^{+} + S^{2-} \longrightarrow S \qquad \text{Degradation} \qquad (5.4)$$

Fig. 5.3 shows that the time of illumination has an effect on the quenching. For example, after 2min illumination, the quenching increased by about 4%. This may be explained either as adsorption of more quenchers on the surface of colloidal semiconductor particles during the illumination, or as photodecomposition of the colloid. Photodegradation of ZnS could be decreased by adding hole scavengers such as Na_2S or methanol.

5.1.2.2 The Kinetics of Quenching at the Interface

The kinetics for the reaction of excited electrons in the conduction band with molecules of methyl viologen (MV^{2+}) adsorbed on a colloidal ZnS surface coated with sodium hexametaphosphate (SHMP) as a stabiliser are described by the poisson equation as illustrated in Fig. 5.5. The equation is:

$$\ln \frac{I_o}{I} = \frac{[MV^{2+}]}{[\bar{N}]} \qquad (5.4)$$

where I_o and I are the absence and presence of methylviologen respectively and $\bar{N}$ is the number of reaction sites on the surface of colloids. The figure also shows a Stern-Volmer plot of the fluorescence of ZnS as a function of the concentration of MV^{2+}, according to the standard relationship:

$$\frac{I_o}{I} = 1 + \frac{kq\ [MV^{2+}]}{k_o} \qquad (5.5)$$

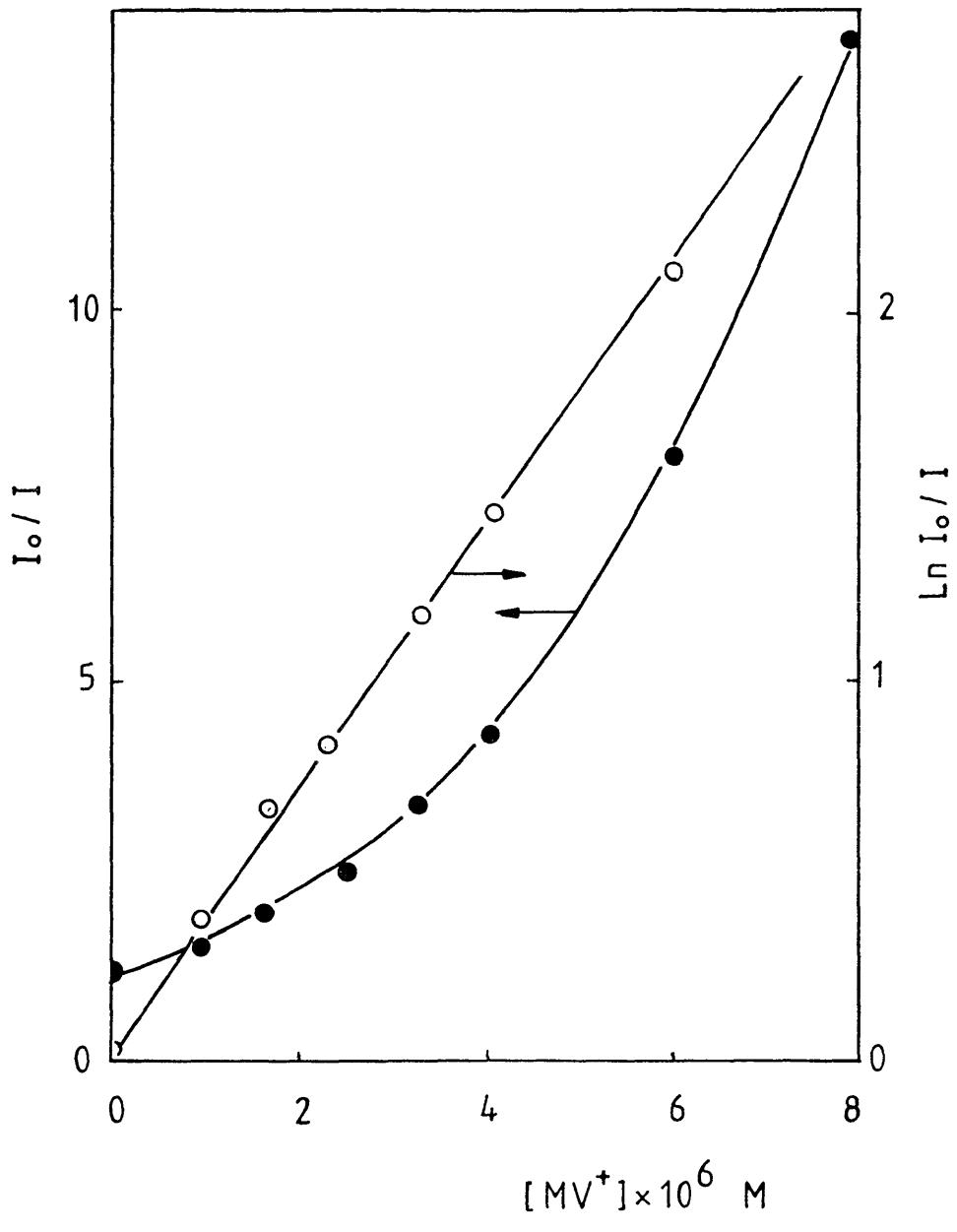


Fig. 5.5 Stern-Volmer plot (●) and Poisson plot (○) of undoped ZnS(5×10^{-3} M) fluorescence quenching by MV^{2+}.

where Kq is the quenching rate constant for the reaction between MV^{2+} and excited electrons in ZnS and k_o is the recombination rate constant. Fig. 5.5 shows that a steady-state Stern-Volmer plot of fluorescence quenching is curved, but a semilogarithmic plot is linear, indicating that the data are explained by Poisson kinectics. Analysis of the data by equation (5.4) provides information on the reaction sites, $\bar{N}$. From the slope of the straight line, the site concentration is calculated to be about $3x10^{-5}$mol.

5.2 Photophysical Properties of Doped ZnS

5.2.1 Absorption Spectrum

The doped colloidal ZnS particles were prepared from $5x10^{-3}moldm^{-3}$ zinc chloride with $10^{-2}moldm^{-3}$ phosphate stabiliser and different concentrations of doped materials. They were prepared at room temperature and solutions were flushed with nitrogen both before and after purging with H_2S. The absorption spectrum of Mn^{2+}-doped ZnS is shown in Fig. 5.6. The absorption spectra of ZnS colloids doped with Tb^{3+}, Eu^{3+}, Mn^{2+}/Tb^{3+} and Mn^{2+}/Eu^{3+} were all observed to be similar to that of Mn^{2+} doped ZnS (Fig. 5.6). The onset of absorption of all of these spectra was found to be between 325 and 335nm, similar to the undoped ZnS.

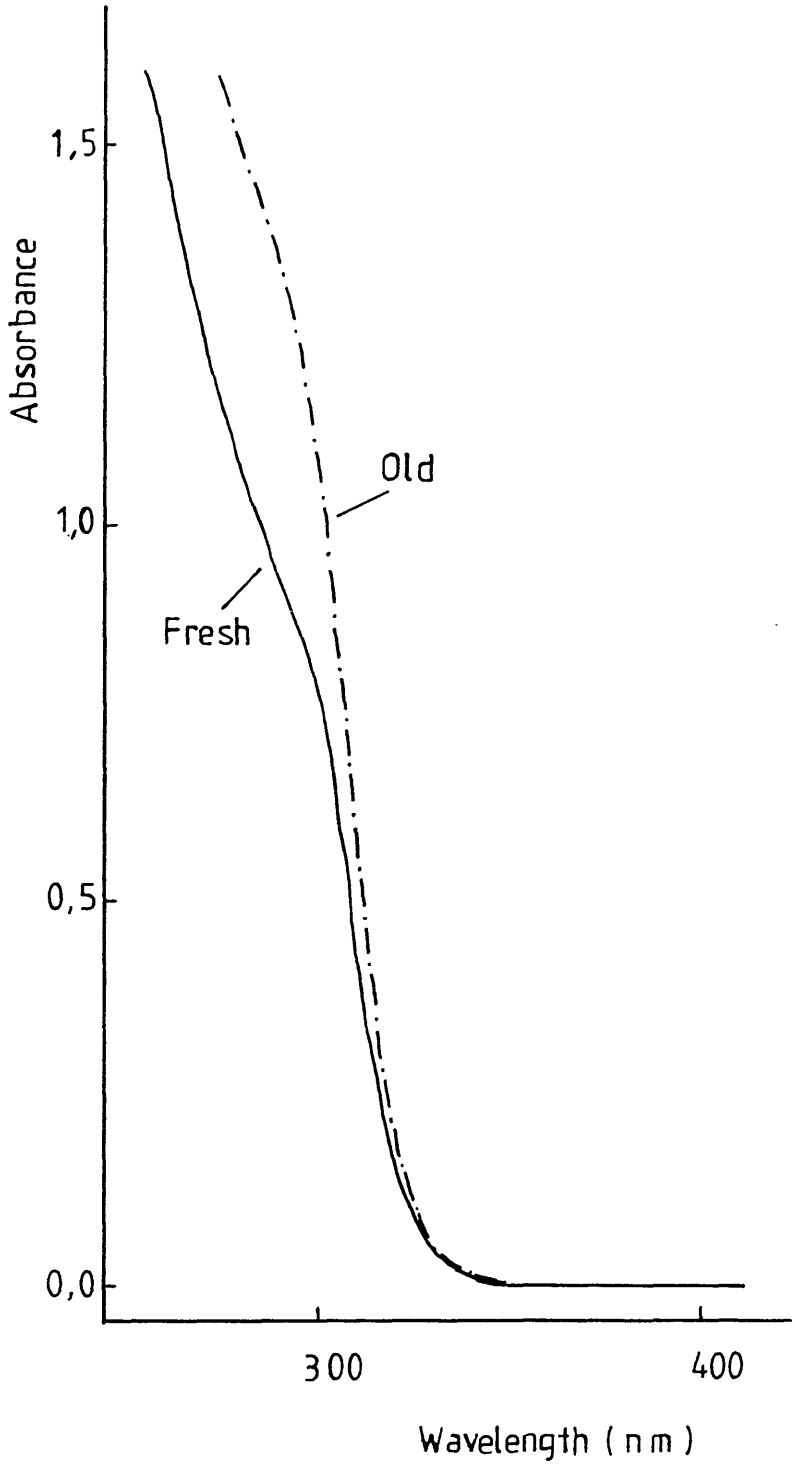


Fig. 5.6 Absorption spectrum of ZnS (5×10^{-3} M) doped with 10% Mn^{2+}.

5.2.2 Fluorescence Spectrum

The luminescence of colloidal ZnS and Mn^{2+}-doped ZnS was first reported by Bard and Becker.[174] They obtained a maximum luminescence efficiency of 0.08 for a 5% Mn^{2+}-doped ZnS dispersion. When the colloidal dispersion was prepared under oxygen free conditions, they obtained a weak blue and strong orange luminescence around 430nm and 580nm respectively. In our method, when 10% Mn^{2+}-doped ZnS colloids were prepared at room temperature and flushed with nitrogen, strong blue and weak red emissions, centered at 430nm and 670nm respectively, were observed. As shown in Fig. 5.7. the intensity of the blue emission is about 20 times that of the red luminescence. There is a great difference in both the emission centers and the intensities of the red and orange luminescence observed in the two methods. This difference may arise from the different methods of preparation and the quantity of Mn^{2+} and sulfide ions added during the preparation.

The blue luminescence of Mn^{2+}-doped ZnS colloids lies in the spectral region associated with luminescence from self-activated centers which is attributed to various kinds of lattice defects.[184,185] The orange emission in Bard's experiment arises from incorporation of Mn^{2+} in the crystal lattice. Its intensity depends on the amounts of Mn^{2+} doping and excess sulfide ions. The appearance of the Mn^{2+} emission required the absence of excess sulfide ions and the presence of dissolved oxygen in solution.[174] In our experiment the disappearance of orange luminescence may be attributed to the presence of excess

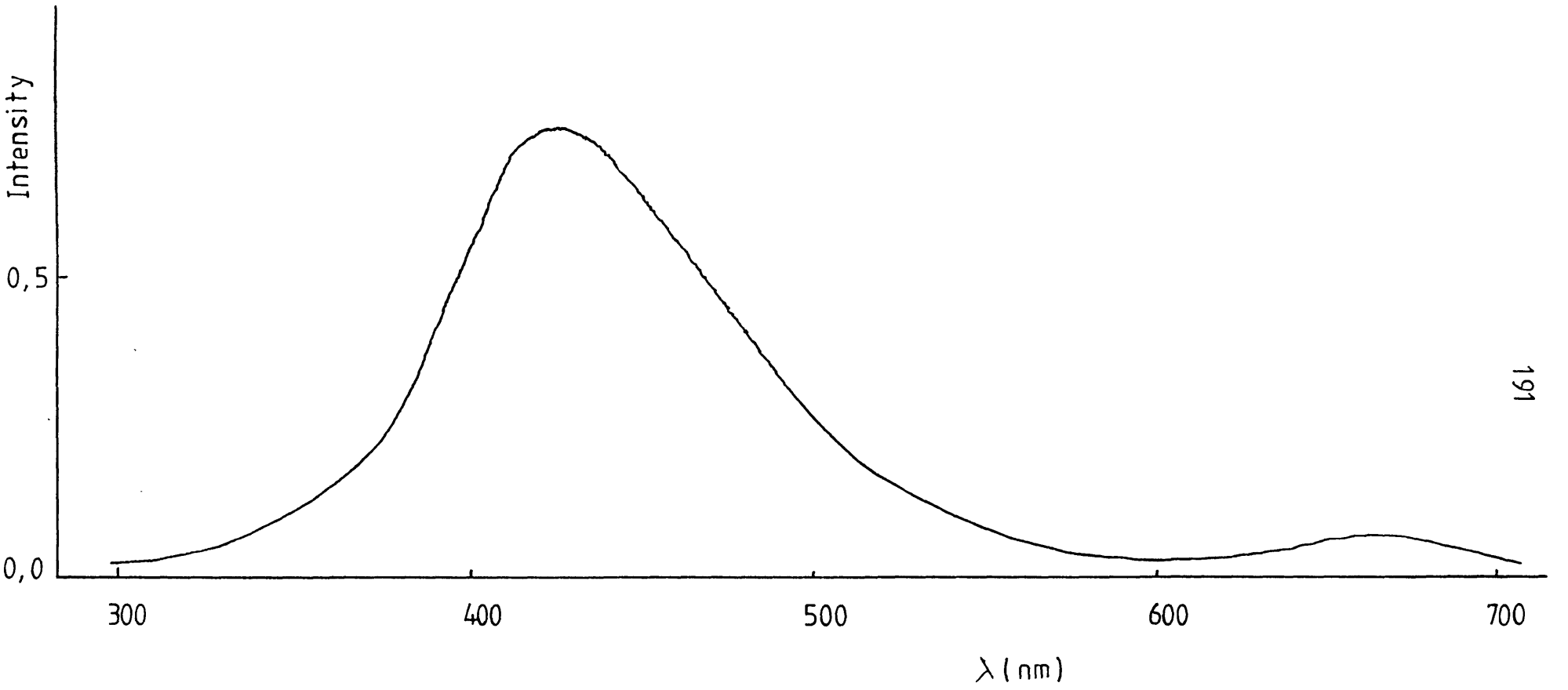


Fig. 5.7 Fluorescence spectrum of ZnS (5×10^{-3} M) doped with 1% Mn^{2+}.

sulfide ions and the absence of dissolved oxygen. The weak red luminescence in our experiment may possibly be due to scattered light.

The blue luminescence of zinc sulfide colloids doped with Mn^{2+}/Tb^{3+}, Mn^{2+}/Eu^{3+}, Eu^{3+} or Tb^{3+} are very similar to that of the Mn^{2+} doped ZnS. For 1% doping of the above-mentioned colloids, the Tb^{3+}-doped one had the most intense blue emission. If the doping in this colloid was increased to 3%, the blue luminescence increased by a factor of 15%.

When the colloidal ZnS was doped with 1% Tb^{3+} + 1% Mn^{2+} there was a decrease of about 30% in the blue luminescence compared to the 1% Tb^{3+}-doped ZnS. Our experimental results are explained as follows.

Uchida has observed that self activated luminescence (SAL) appears strongly in ZnS phosphors with excess zinc but disappears in phosphors having excess sulfur.[189] He therefore suggested that the self activated luminescence (SAL) center is associated with sulfur vacancies which are located below the conduction band. Sulfur vacancies in ZnS generate localised donor sites which can attract and trap electrons. Emissions occurs when a trapped electron recombines with a hole in the valence band or in some acceptor level. (Fig. 5.8).

T_b^{3+} ions present in the bulk of ZnS will act as sulfur vacancies and increasing their concentration increases the sulfur vacancies so more electrons will be trapped in localised donor sites. It has been argued that the Mn^{2+}-doped site can attend holes and act as a hole trapping site.[189,190] Therefore, the number of trapped electrons and holes when both Tb^{3+} and Mn^{2+} are

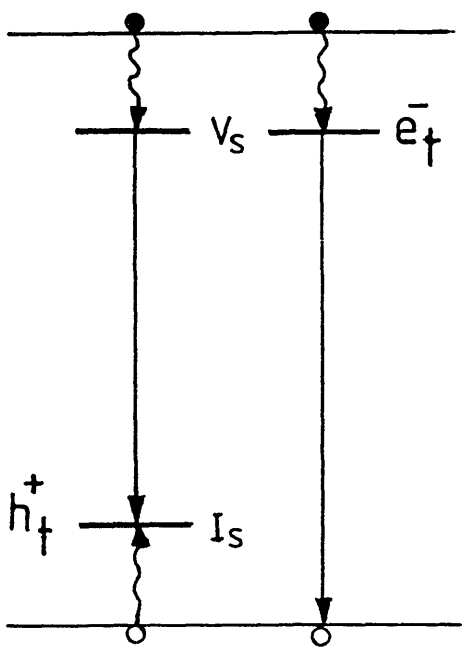


Fig. 5.8 Luminescence mechanism for colloidal ZnS emission.

V_S: sulfur vacancy

I_S: sulfur Interinsity

e^-_t: electron traped level

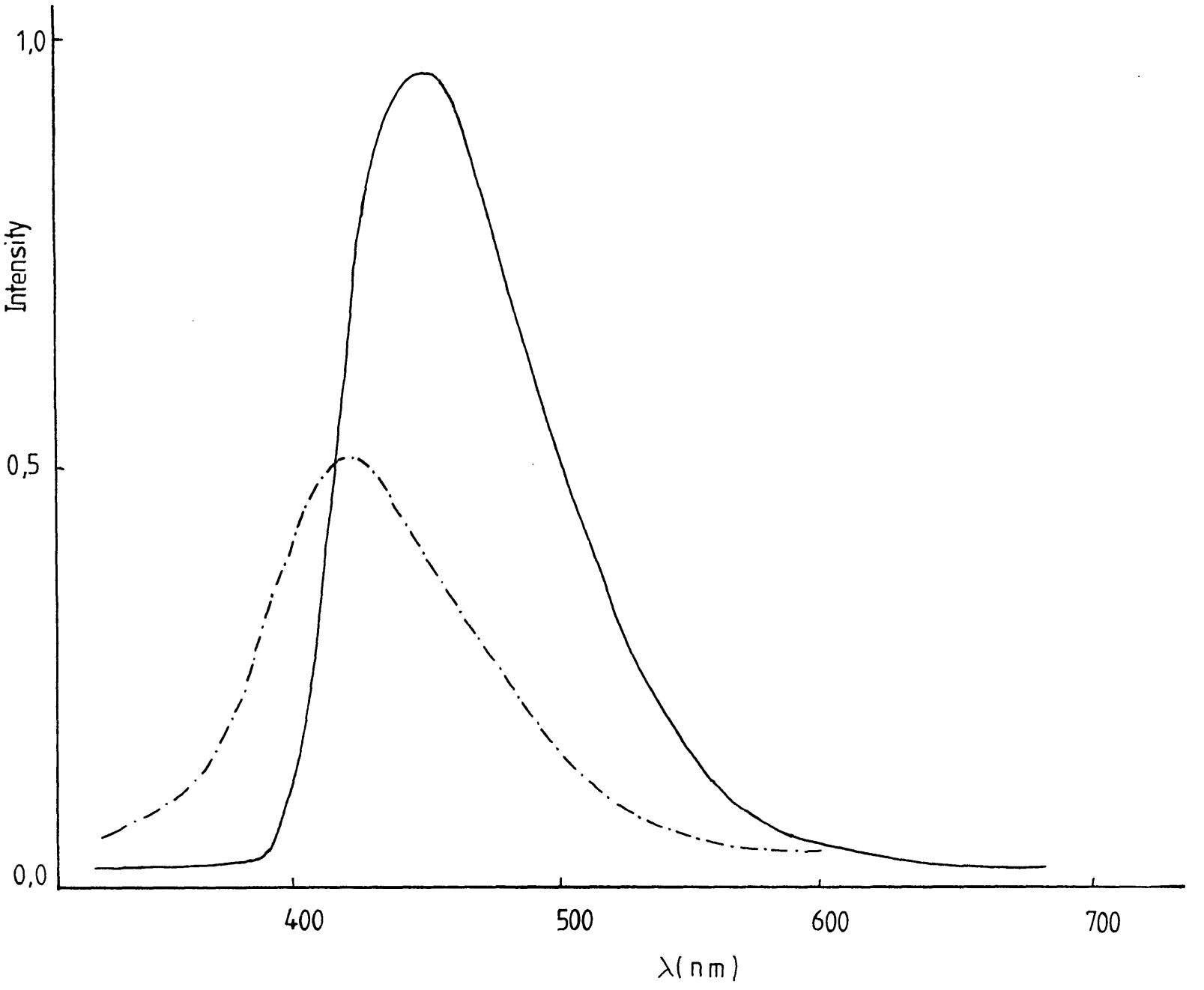
h^+_t: hole traped level.

present may be increased and consequently the direct $\bar{e}h^{+}$ pair recombination decreased.

5.2.3 Aging Effect

The solubility of ZnS in water is so low ($7x10^{-2}$ gram/cm^3) that, if a dilute solution of Zn^{2+} is mixed with a S^{2-} solution of high concentration, Zn^{2+} will exist entirely in the form of solid ZnS in the equilibrium condition. Small ZnS particles are less stable than larger ones and tend to dissolve rapidly.[202] The dissolved ions, in order to achieve higher thermodynamic stability, tend to transfer from smaller to larger particles as a function of time. This effect is the "aging effect" or Ostwald ripening.

It has been reported that the absorption and emission spectra of undoped and doped ZnS particles changed upon aging for about one day.[175, 177] We have obtained similar results for solutions of colloidal ZnS doped with Mn^{2+}, Eu^{3+}, Tb^{3+}, Mn^{2+}/Eu^{3+} or Mn^{2+}/Tb^{3+}, after aging for 80 days. As shown in Fig. 5.9 the luminescence intensity of ZnS doped with Mn^{2+}/Tb^{3+} is doubled after 80 days and shifted about 25nm towards red luminescence. The emission intensity of Zn/Tb^{3+}-doped ZnS was nearly the same. This indicates that, with aging the size of the particle was slightly increased. The smooth curve in the aged solution shows that the distribution of the particles during this period becomes more uniform. This uniformity may be attributed to the settling of particles with time.



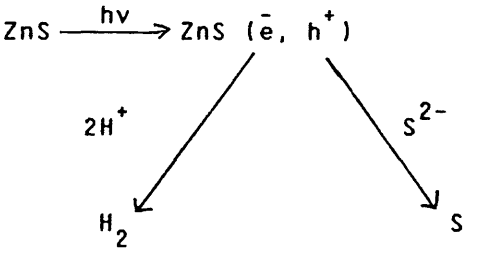
See overleaf

Fig. 5.9 Aging effect on the emission spectrum of ZnS doped with 2% Tb^{3+}/10% Mn^{2+}.

5.2.4 Photodegradation

Colloidal ZnS photochemically unstable. The effect of irradation time on the fluorescence of fresh 2% Tb^{3+}-doped ZnS is shown in Fig. 5.10.

The photodecomposition of ZnS crystals and powders in the presence and absence of various additives has been recently studied.[177] In the absence of oxygen no degradation was observed for CdS but a very slow degradation was observed for both doped and undoped ZnS colloids. In the latter case one may write the following mechanism for degradation:



The conduction band in ZnS colloids possesses a more negative potential than in CdS, which facilitates H_2 formation, and the valence band has a more positive potential, which may oxidise the sulfide. H_2 production has not been tested by us, but Kirsch has recently reported H_2 formation by near UV illumination of ZnS powder.[173]

Photodegradation is a process that competes with electron hole recombination. In the presence of an electron scavenger, a significant rate of degradation can be achieved. This is because removal of electrons from the conduction band gives the positive holes a greater chance to oxidise sulfide ions, thus promoting the degradation.

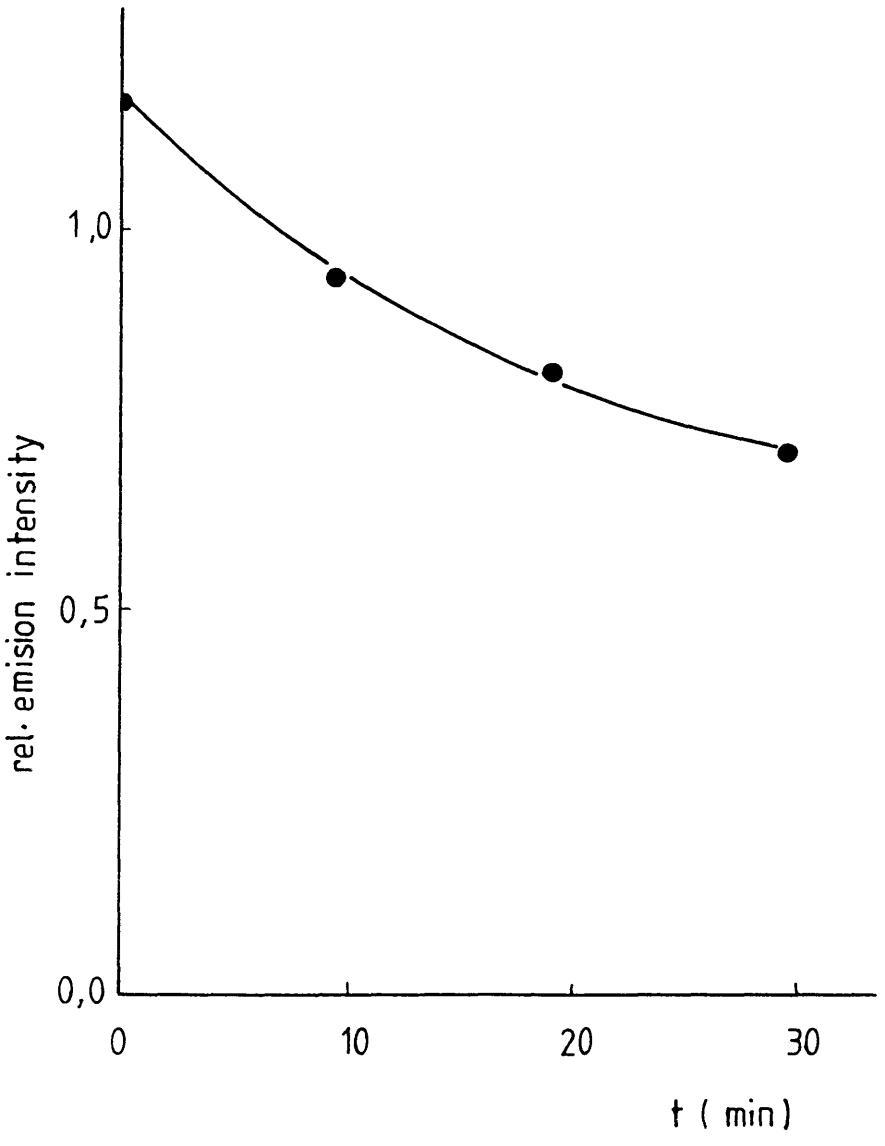


Fig. 5.10 Irradiation effect on the fluorescence intensity of 2% Tb^{3+}-doped ZnS($5x10^{-3}$ M).

Recently Reber and Meier have been reported that sulfide and sulfite ions in solution are hole scavengers which stabilise the ZnS surface very efficiently against anodic photodegradation.[191] They have produced sixteen litres of hydrogen with 1.0g of ZnS in 35h without any observable deactivation of the photocatalyst.

5.3. Kinetics Study

The photoinduced charge transfer reaction at the interface of undoped colloidal ZnS was studied by time-resolved microsecond flash photolysis. When the solution containing colloidal ZnS ($5x10^{-3}moldm^{-3}$) and KBr ($3x10^{-3}moldm^{-3}$) was deaerated and then subjected to a microsecond flash, a transient absorption was observed on the timescale of several hundred milliseconds. When the same concentration of KBr was flashed in the colloidal CdS solution, the transient was on the sub-millisecond timescale. These transients revealed that the photoreaction of ZnS with KBr was slower than that of CdS colloids. Such a striking difference in the process of two colloidal semiconductors could be due to the difference in band gap energies.

In the introduction, we have shown that the electrons and holes in the conduction and valence bands of ZnS possess more reducing and oxidising power respectievly than that of CdS. By this explanation, we may be able to suggest that the slow reaction of KBr with ZnS arises from photo-oxidation of bromide to bromine by the positive holes of ZnS colloids.

5.4. Conclusion

Absorption spectra of doped and undoped ZnS colloids have been shown to be similar with an onset at around 330nm, indicating that the absorption spectra of ZnS colloids are typical of those for a crystalline semiconductors.

The study of the fluorescence of ZnS doped with Mn^{2+}, Eu^{3+}, Tb^{3+}, Mn^{2+}/Eu^{3+} or Mn^{2+}/Tb^{3+} indicated that Mn^{2+}/Tb^{3+} may have more electron and positive hole traps than the others. The study of trapped charge carriers in the particle is very important as they can influence the photocatalytic activity and photodecomposition of the semiconductor.

In the kinetics study of a wide band gap semiconductor (such as ZnS) with respect to a narrow band gap one (such as CdS), we have demonstrated the photo-oxidation of bromide to bromine on the surface of ZnS colloids.

CHAPTER 6

Photophysical and Photochemical Properties of CdS Immobilised Within Dialysis Membrane

Introduction

The aim of this chapter is to draw attention to the photophysical and photochemical aspects of cadmium sulfide immobilised in a dialysis membrane (DM). The study of absorption spectra of CdS incorporated into membranes and polymers showed that small semiconductor particles were formed. The techniques of both steady-state and pulsed methods have been successfully used to investigate some reactions at the semiconductor-liquid interface. Photoreduction of MV^{2+}, photo-oxidation of methyl orange and luminescence quenching by MV^{2+} were studied by trapping CdS particles in the membrane.

Studies using colloidal CdS have been discussed in previous chapters. Colloidal semiconductors possess the potential for solar energy conversion and therefore have been studied by a growing number of laboratories worldwide.[44-90,192-198]

Ideally, colloidal semiconductor particles should be small, uniform and stable. The smaller the particle the greater is the chance of charge carriers escaping to the surface of particle before recombination occurs. Very small colloidal semiconductor particles, which are named Q-particles, are a subject currently under intense investigation.[193,196,199-215] The size of

particle has a dramatic effect on the semiconductor properties of these colloids.

When the size of semiconductor particle decreases, the band gap is blue shifted. The smallest diameter for colloidal CdS reported is about 5nm and even less.[199,201-202,206] It is difficult for such a small particle to be stable in solution for a long time and coagulation occurs. Furthermore CdS and more generally, the non-oxide n-type semiconductors are unstable and under illumination photoanodic decomposition occurs. Stabilisation of small semiconductor particles with respect to photodecomposition involved the use of either organised surfactant assemblies such as micelles, reversed micelles and vesicles[67-70,143,193,196-197,222-224] or solid matrices such as Clay, cellulose, Nafion or a polyurethane membrane.[151,216-221]

It has been shown that <u>in situ</u> generation of small CdS particles in such systems enhanced their stability and produced semiconductor particles of a more uniform size.[151] The polymer immobilised semiconductor has several advantages:

i) They are very simple to remove from solution for analysis of the reaction solution and regeneration of the semiconductor particles.

ii) The polymer matrix may play a role in ion-exchange properties, concentrating some solution reactants and rejecting others.[220]

iii) The membrane system offers the potential for charge transfer with separation of the reduced and oxidised products.

iv) Stability to flocculation and/or precipitation.

v) Usefulness in flow systems.

vi) Very simple preparation.

vii) Fabrication to multicomponent systems is possible.

In an effort to obtain a better understanding of these systems, CdS particles were synthesised within several polymers and dialysis membrane. The photophysical and photochemical behaviour of these systems are discussed in the following sections.

6.1 CdS in Polymer

The thin film of embedded CdS was prepared using different polymers as mentioned in chapter 2. Thin films of CdS with various stabilisers such as polyvinyl alcohol (PVA), polyacrylamide (PAA) and poly (2-vinyl)pyridine (PVP) were successfully prepared on the glass slide and their photophysical behaviour studied. The best results were obtained using 1% PAA.

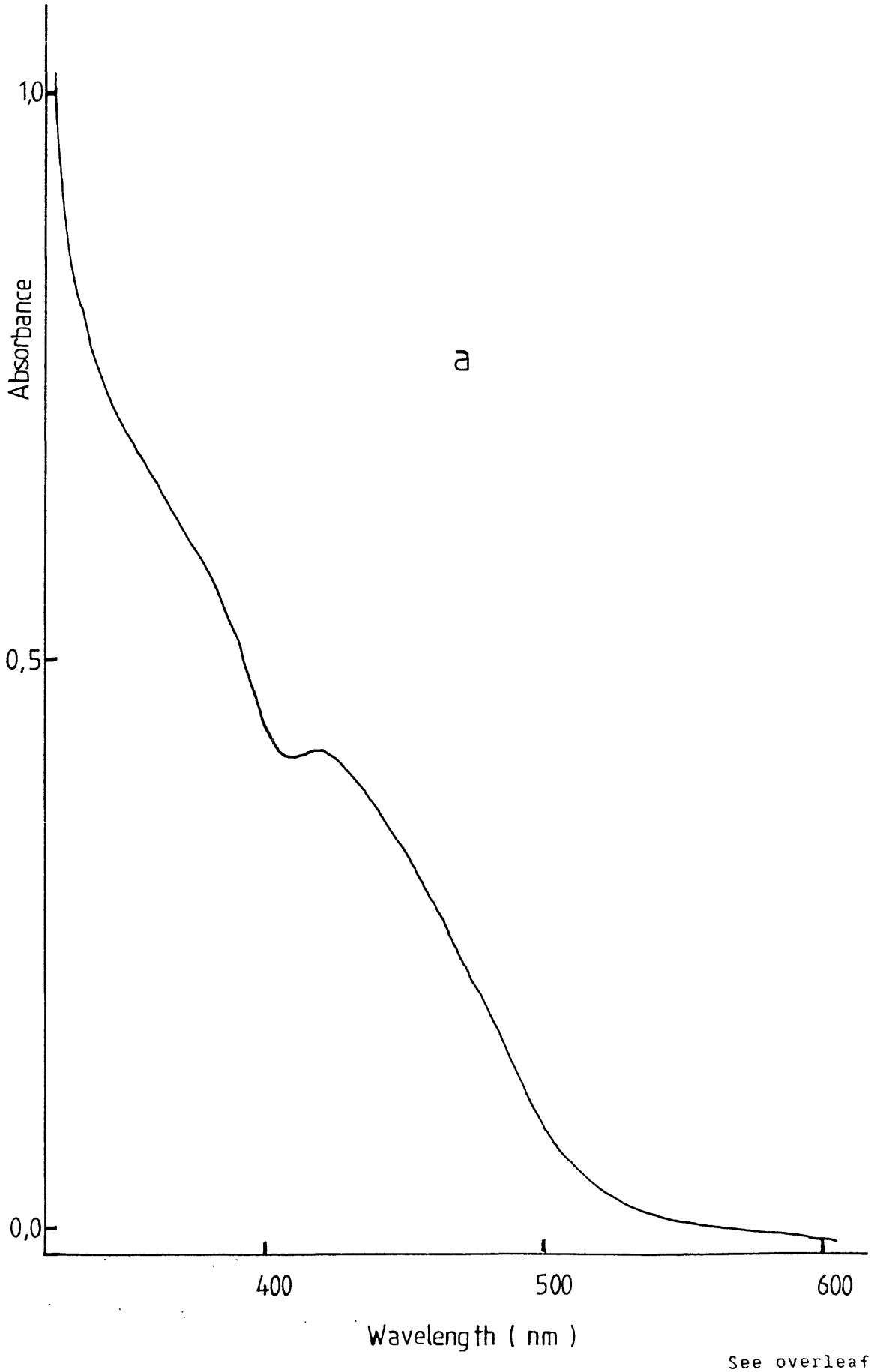
Fig. 6.1a shows the absorption spectrum of *in situ* generated CdS in 1% PAA polymer. The onset of the absorption spectrum started at 515nm, which is similar to the onset of colloidal CdS absorptions, as mentioned in the last two chapters. There is also a weak maximum at about 420nm. We can attribute this maximum to excitation of electrons from the valance band to exciton states (the natural excited states of the lattice, where the charge carriers do not move independently of each other). At shorter wavelengths (Fig. 6.1a) the absorbance increases and a very weak shoulder at the blue edge of the band gap appears

around 370nm. Development of this shoulder in agreement with Brus[203] and Henglein[206] corresponds to the exciton state.

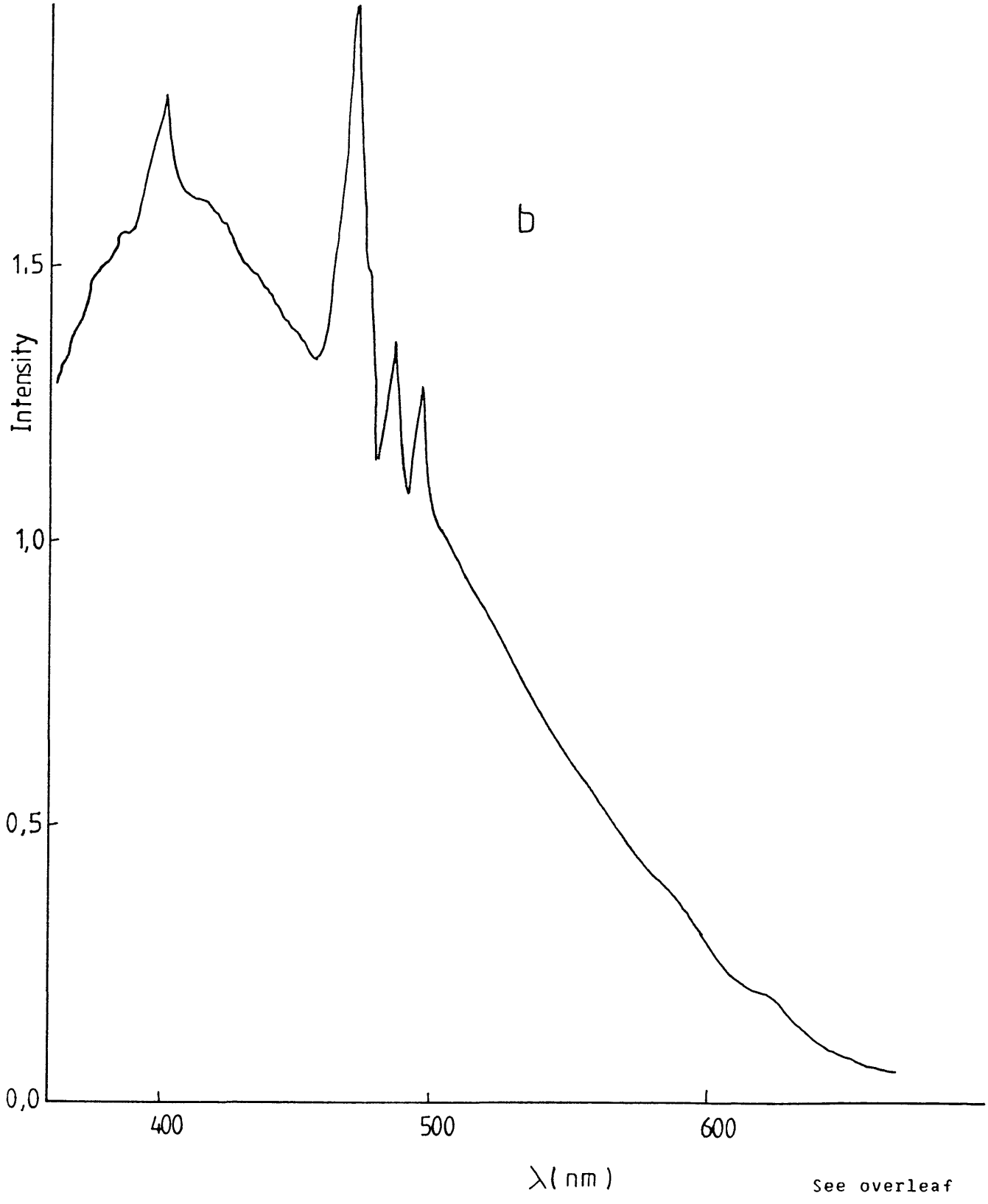
The fluorescence spectrum contains broad and sharp bands around 390m and 470nm respectively and two weak sharp bands at 490m and 500m. Lee and Meisel[229] reported that, due to some non-exchangeable impurities (the amount of impurity varies from batch to batch) in the prepared film, excitation of the polymer film in the UV region (λ_{ex} = 260, 300nm) resulted in the emission band at 390nm. We can also attribute the first maximum to the impurity present in the polymer. Other peaks can be attributed to the emission of the non-uniform surface of the polymer film (Fig. 6.1b). Although, shape of the fluorescence was not dependent on the wavelength of the exciting light, its position did depend on this wavelength.

6.2 CdS in Dialysis Membrane (DM)

Recently, immobilisation of CdS particles into special matrices has received considerable attention.[151,216-221] Some workers have produced CdS particles in thin films of different membranes in order to study the photochemical, photophysical and photocatalytic properties of such systems.[151,180,220,225] However, no mention has been made concerning the preparation of CdS incorporated into DM.



See overleaf



See overleaf

Fig. 6.1 (a) Absorption and

(b) emission spectra of CdS (5×10^{-2} M) incorporated into 1% PVA;

$\lambda_{ex} = 300$ nm.

6.3 Photophysical Properties

In this section special attention was focused on the absorption spectra of DM alone and incorporated with CdS colloid. Before proceeding with an account of the photophysical properties, it is pertinent to consider the nature of thin film dialysis membrane.

DM, as mentioned in the second chapter, is produced from cellulose ($C_6H_{12}O_5$), and contains water, glycerol as a humectant and small quantities of sulfur compound (0.1%). Both glycerol and sulfides may be removed by proper washing. The normal molecular weight is reported[140] to be 12000-14000. The average pore radius of the membrane is reported as 24A^o (thickness 0.32nm) which is the correct size to immobilise small particles of CdS colloids.

DM as well as Nafion[151] became slightly yellow after being stored in air at room temperature for a long time. The yellowish coloured compound may be due to degradation and/or an oxidation product of the polymer. It can be removed by boiling repeatedly in distilled water. The film of DM with incorporated CdS is bright yellow/orange (depending on the concentration of synthesised CdS) and transparent. Therefore it is a medium whose photophysical, chemical properties can easily be studied.

6.3.1 Absorption

Figure 6.2 shows the absorption spectrum of 8cm^2 of the dialysis membrane and CdS film measured in a 1cm quartz cell.

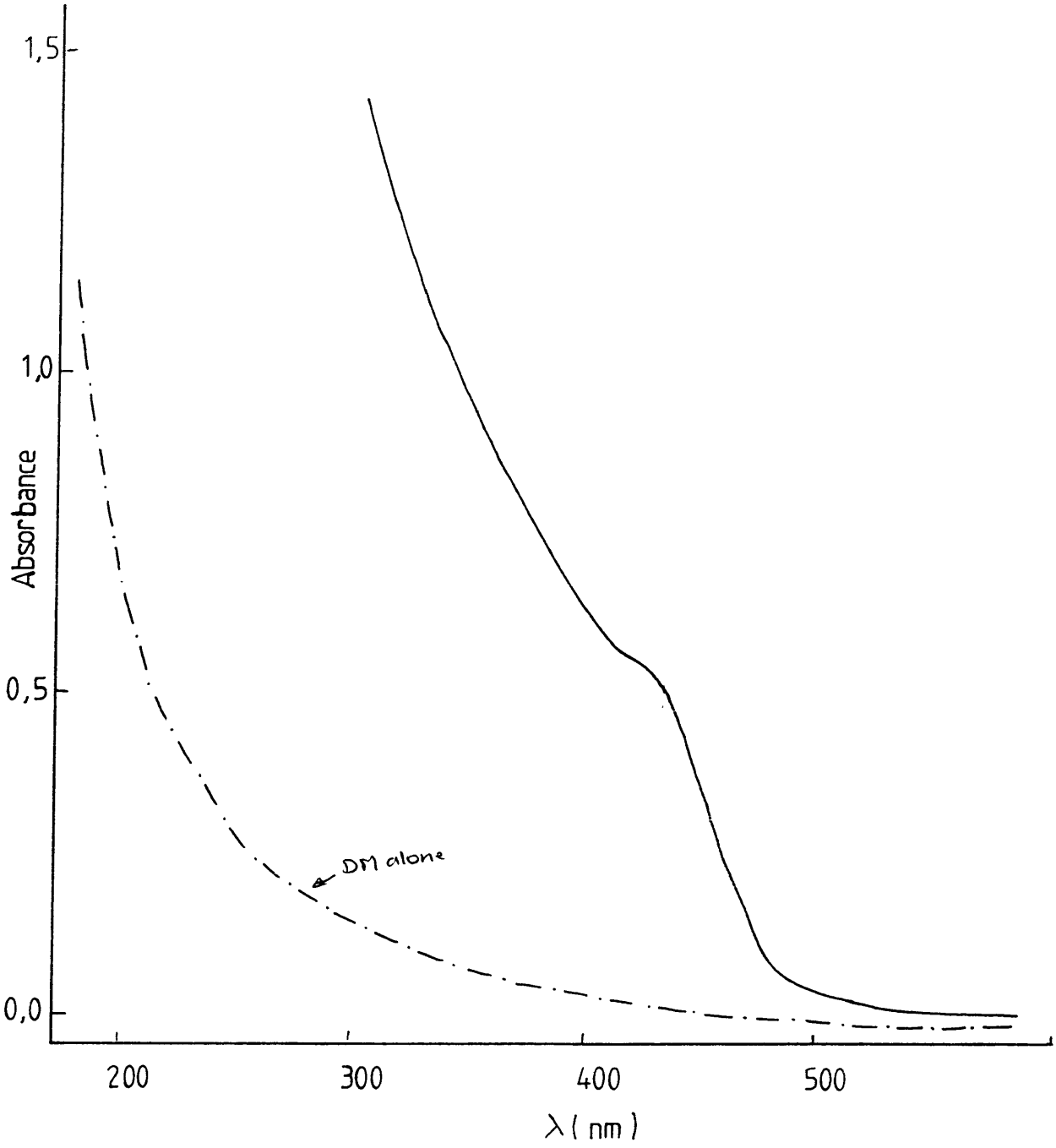


Fig. 6.2 Absorption spectrum of CdS (10^{-2} M) immobilised in the DM.

This figure indicates that the DM is transparent in the visible region but absorbs light of the UV region. This figure also shows the absorption spectrum of CdS (from 10^{-2}moldm^{-3} $Cd(NO_3)_2$) immobilised within DM. The absorption threshold of incorporated CdS is at about 480nm i.e. the onset of light absorption was shifted towards shorter wavelength. In other words, small colloidal particles are formed within the DM. If the Cd^{2+}-trapped film is permitted to soak in Na_2S (0.1moldm^{-3}) for a long time, the membrane becomes orange in colour and at still longer times translucent. Furthermore its absorbance becomes greatly enhanced at all wavelengths.

We have attempted to measure the size of the incorporated particles using high resolution transmission and scanning electron microscopies. But due to the low resistivity (and high thickness) of the membranes to high energetic electrons the film burnt and we could not determine the size of the particles. This may be the only disadvantage of the DM with respect to other membranes such as Nafion.

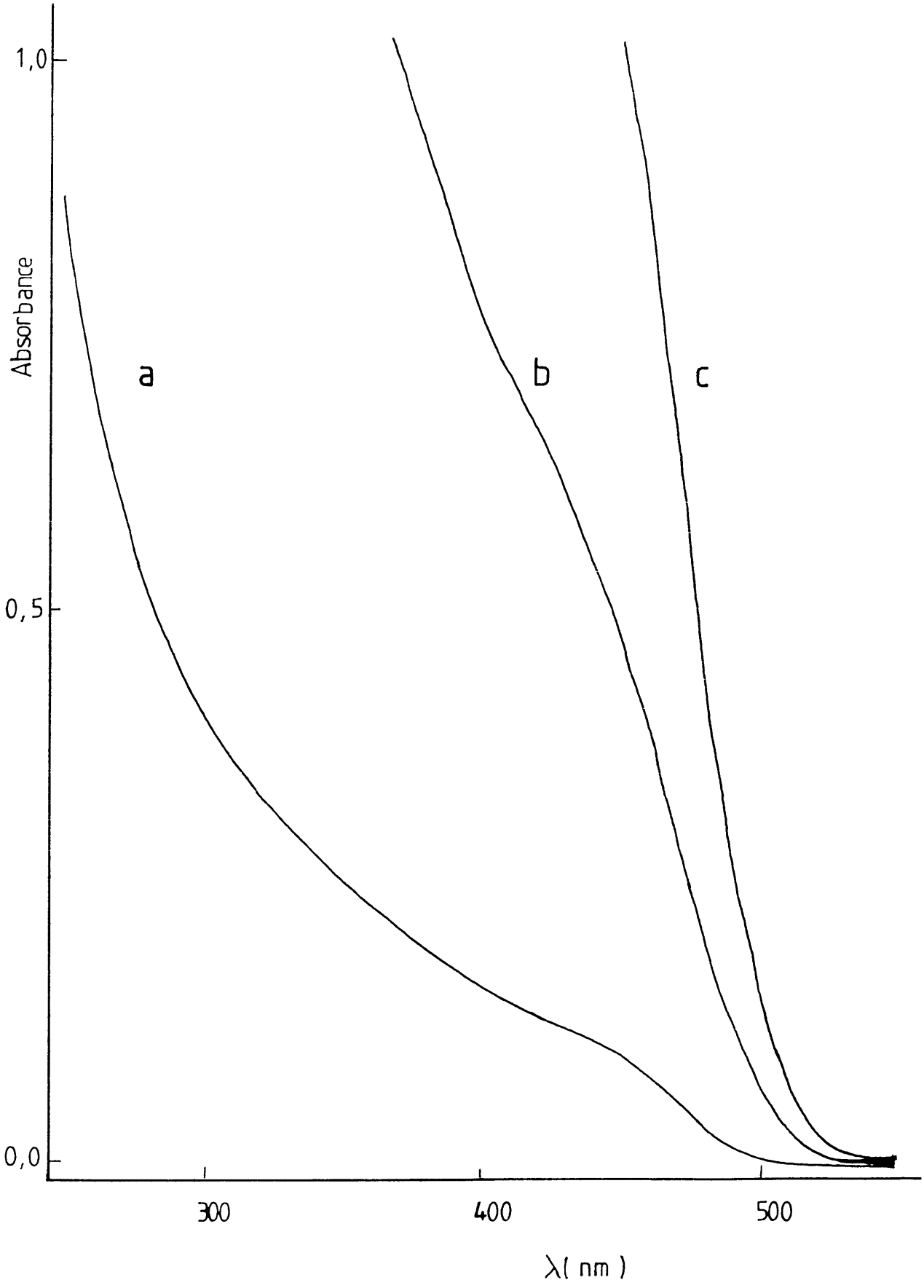
From the estaimations by Henglein and coworkers,[208] this value of the absorption edge (480nm) corresponds to an average particle diameter of less than 5nm. This estimated size for CdS particles is consistent with the membrane pore size. Therefore small CdS particles are trapped within the pores of the dial;ysis membrane. The absorption spectrum of CdS incorporated into the DM is affected by at least two factors. The concentration of CdS particles and the method of preparation.

6.3.1.1 The Concentration Effect

When the concentration of immobilised CdS was increased (by dipping DM into concentrated Cd^{2+} before using Na_2S) from 10^{-2} to $10^{-1}moldm^{-3}$ (Fig. 6.3.) the absorption threshold shifted from 480nm to 520nm. This shift towards longer wavelength indicates that larger particles are formed within the DM by increasing the concentration of CdS.

6.3.1.2 The Effect of Preparation

The thin film of CdS prepared from $10^{-2}moldm^{-3}$ Cd^{2+} cations and $5x10^{-2}moldm^{-3}$ of sodium Hexametaphosphate as a stabiliser either by adding Na_2S or by purging with H_2S gas. A striking difference was observed in the absorption spectrum of the two types of CdS in the DM. CdS which was prepared by purging with H_2S had an onset of absorption at 497nm while that of the film prepared by Na_2S was at 480nm. This difference was even larger when there was no supporting agent. This wavelength was also observed to depend on the salt of Cd^{2+} ions, as listed in Table 6.1.



See overleaf

Fig. 6.3 The concentration effect on the absorption onset of CdS film.

a) 10^{-2} M

b) $5x10^{-2}$ M

c) 0.1 M.

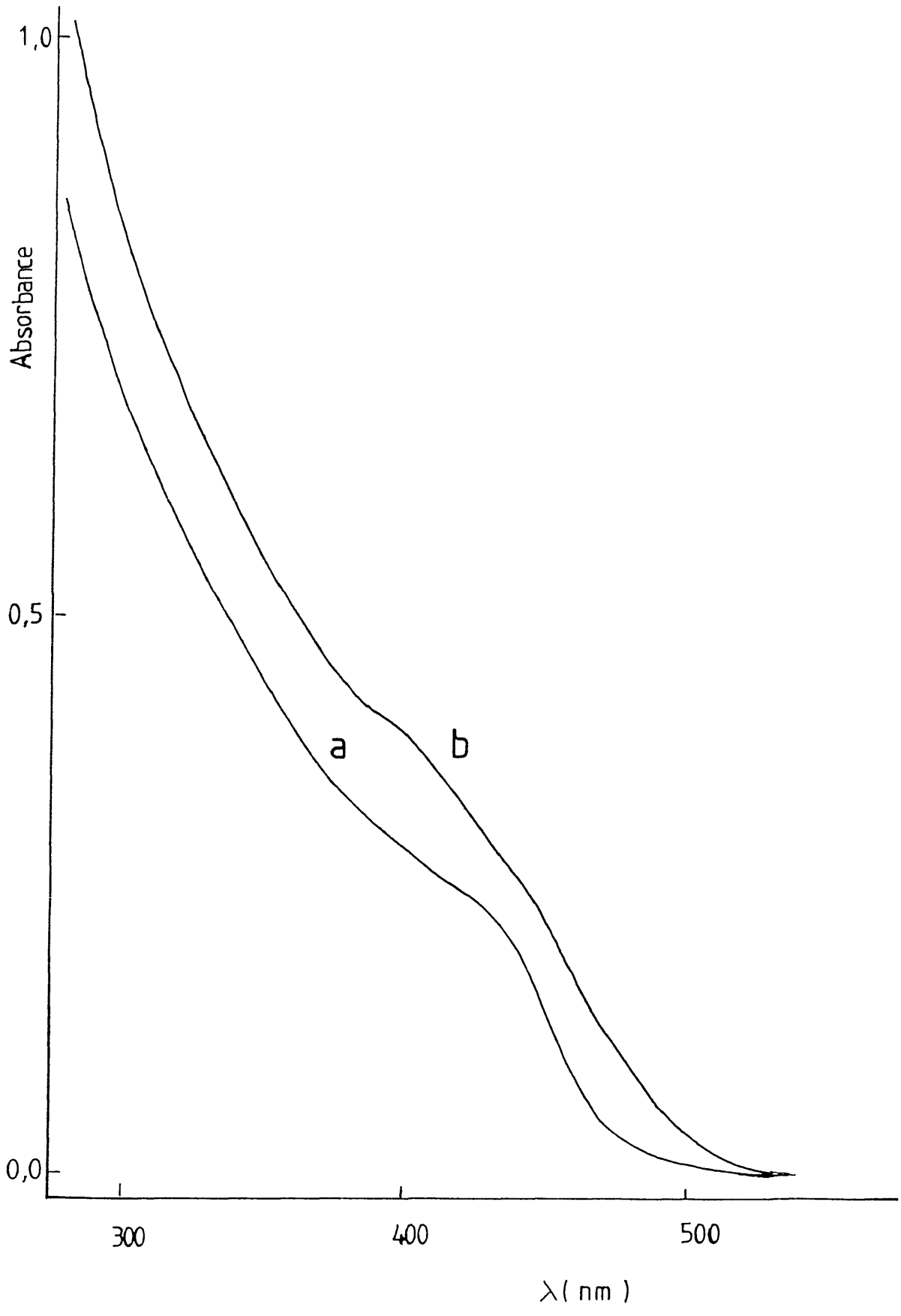
TABLE 6.1: The effect of Cd^{2+} ions and preparation method on λ_{th}

Cd^{2+}	Threshold wavelength (λ_{th}) in nm	
	Na_2S	H_2S
Chloride	476	504
Bromide	480	504
Iodide	502	520
Nitrate	480	497
Sulphate	510	537

Table 6.1 shows that the onset of absorption was affected by the method of preparation with the smaller CdS formed by Na_2S. The formation of large particles when purging with H_2S may arise from the rate of H_2S passing the surface of the membrane which is difficult to control. The difference in the spectrum of CdS (from cadmium chloride) prepared by the two methods is presented in Figure. 6.4.

The smooth curves of the absorption spectrum reveals that the CdS particles have a uniform size distribution in the DM membrane. In our studies by scanning electron microscopy (SEM) we observed the rough surface of the CdS film but not detect any of the CdS particles when the film was not burnt at the beginning of the study.

Bard and coworkers[221] have reported that the crystal structure affected the efficiency of hydrogen production. They



See overleaf

Fig. 6.4 The effect of preparation method on the absorption spectrum of CdS film(10^{-2} M):

a) CdCl(5×10^{-2} M), DM, Na_2S(0.1 M)

b) CdCl(5×10^{-2} M), DM, H_2S(gas)

have produced CdS-impregnated Nafion films by two different methods. By using SEM they observed a striking difference in the surface roughness of α- and β- CdS in Nafion with β being much rougher. They found that β- CdS (cubic) was much more active with respect to hydrogen photoreduction than α- CdS (hexagonal). The preparation of Nafion/β-CdS also had the advanatge of being very reproducible with respect to the rate of H_2 evolution. Large particles were observed by XRD for the cubic film, while the hexagonal film surface was flat and no particles were observed. The similar result was obtained when we used SEM with a cold stage to avoid the film burning. We could expect that, in agreement with Bard's results,[220-221] in our preparation method, cubic and hexagonal CdS particles wre synthesised within the DM when prepared by H_2S and Na_2S respectively.

The absorption spectrum shown in Figure 6.4 for CdS incorporated within dialysis membrane appears similar with that of colloidal CdS stabilised with sodium Hexametaphosphate when prepared by H_2S.

6.3.2 Emission

Figure 6.5 shows the emission spectrum of $5x10^{-2}moldm^{-3}$ CdS film at room temperature. The emission peak maximum occured at 520nm. This is virtually identical to the luminescence of colloidal CdS which had been prepared with Na_2S and stabilised with sodium Hexametaphosphate. Luminescence studies of CdS film, prepared either by H_2S or Na_2S, were carried out for different

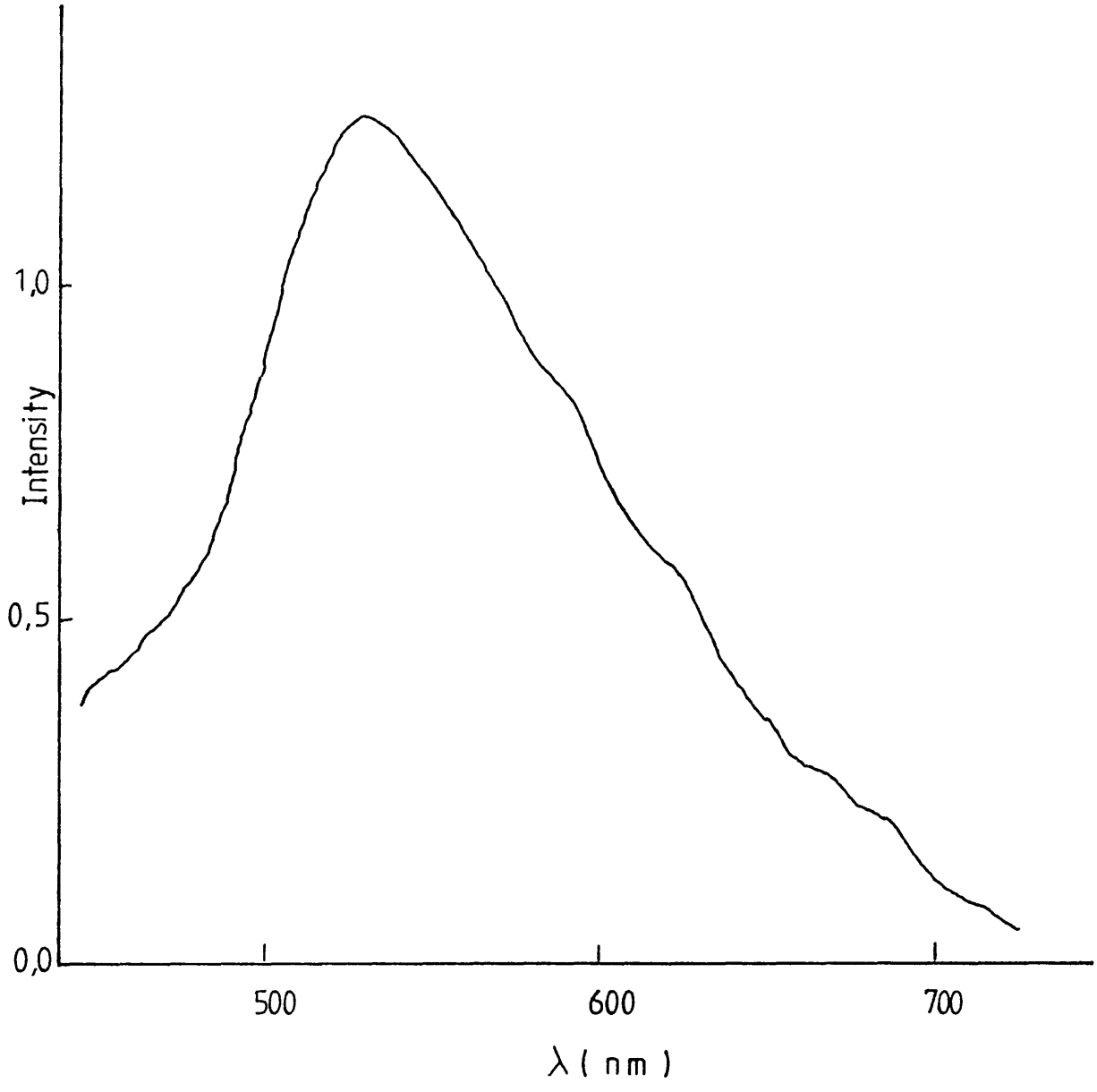


Fig. 6.5 Emission spectrum of CdS film (5×10^{-2} M).

λ_{ex} = 350nm Filter: 43 μm.

cadmium salts. The results are listed in Table 6.2.

TABLE 6.2: The emission spectra maxima of different CdS films when excited.

Cd^{2+}	λ_{em} (nm)	
	Na_2S	H_2S
Chloride	480	490
Bromide	480	510
Iodide	500	515
Nitrate	515	530
Sulphate	485	500

Table 6.2 shows that the emission peak maximum (λ_{em}) for the two types of CdS film are different. Comparison of data represented in Tables 6.1 and 6.2 indicates that the λ_{th} and λ_{em} in CdS film which is prepared with H_2S are higher than those for the film prepared with Na_2S. This effect may be due to the large number of defects incorporated in the lattice of CdS or upon the particles surface, especially in the CdS film prepared with H_2S.

When the preparation method changed and the DM was soaked in cadmium nitrate for about three months (Method II) the emission spectrum changed and a broad green and red luminescence were observed at 520 and 660nm respectively. The appearance of a red luminescence in Method II implies that long term soaking of the DM in Cd^{2+} solution may cause an excess of Cd^{2+} ions and hence

centres. This can be proved by quenching the red luminescence which is extremely sensitive to the presence of electron acceptors such as methyl viologen. Excess sulfide ions also quench the red peak due to filling of the sulfur vacancies, while excess cadmium ions increase the number of sulfur vacancies and hence increase the red luminescence.[53] Luminescence quenching will be discussed in greater detail in section 6.4.1.

6.3.2.1 Effect of Water

It has been shown that synthesis of CdS in solid matrices produces small uniform particles, enhanced in stability from coagulation. In order to keep them stable and uniform even after removal of the water, it is necessary to study the effect of water on the surface properties of small CdS particles.

Figure 6.6 shows that water has quite a significant effect on the emission spectrum of CdS film. We can expect that the interaction of water molecules with charge carriers at the surface of the CdS film would quench emission. When the CdS film was removed from the water and left to dry in the open air, the original spectrum was obtained. A similar effect was reported for CdS deposited in Porous Vycor Glass.[143] This work leads us to suggest that the process is reversible and water contact with synthesised CdS particles in the DM does not damage them. Furthermore, wet film decreases the scattering of emission which occurs in dry conditions for the green emission.

CdS film appears to be stable over many years in the absence

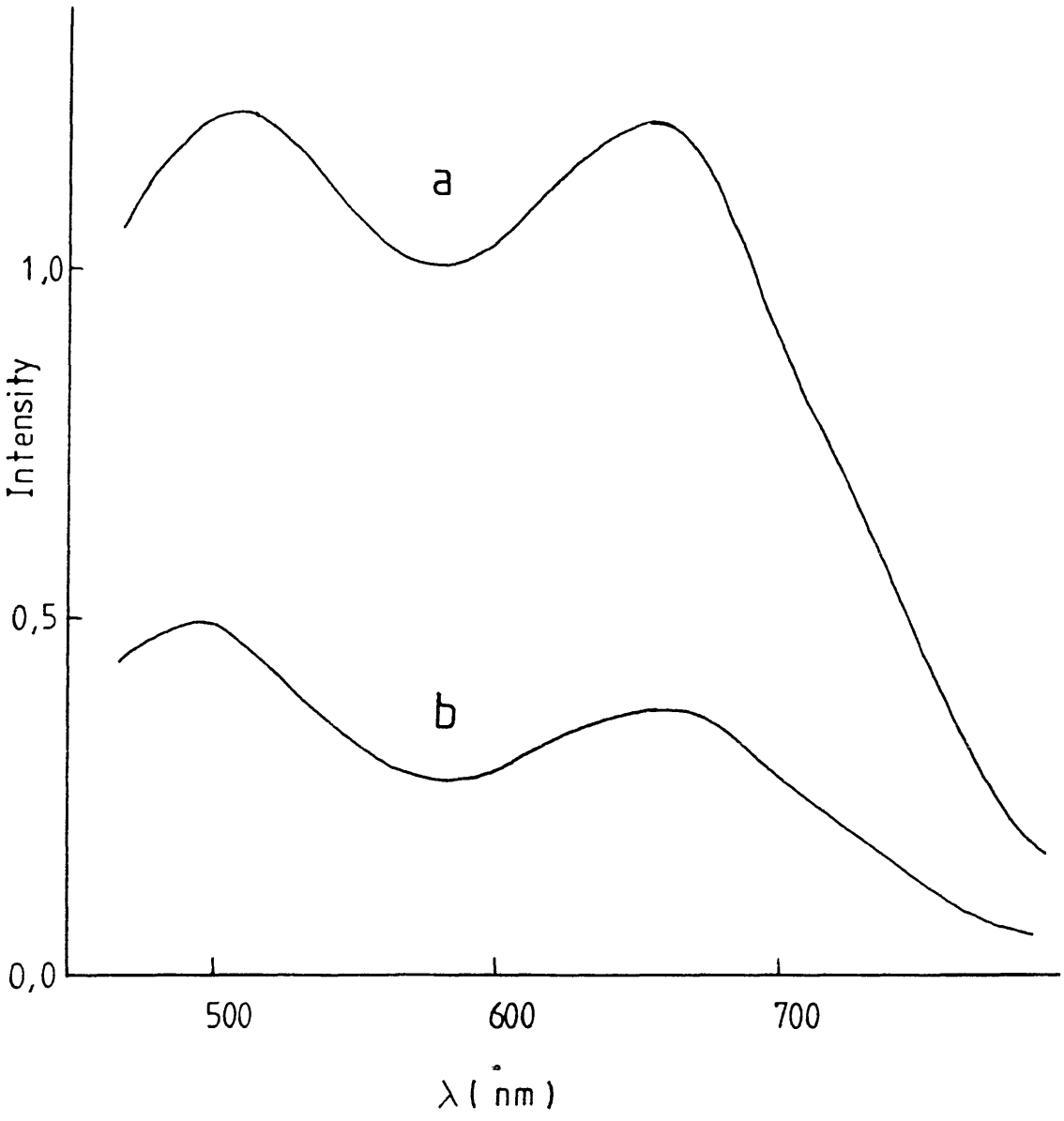


Fig. 6.6 Water effect (b) on the emission spectrum of dry (a) CdS film(10^{-2} M), λ_{ex} = 400nm Filter: 43μm.

of oxygen. When the film was kept in the open air over 12 months, a small fraction of oxidation occured on the CdS film. The effect of water on the absorption of the CdS film is shown in Figure 6.7. A small change in the absorption spectrum occurs below 480nm. However above 480nm the absorption increased and extended to longer wavelengths. In the presence of water, the clusters may migrate from membrane pores to the surface and grow continuously toward large particles over a long period. This behaviour is similar to what has been observed in colloidal solution.[202-203,209-211]

6.4 Photochemical Properties

This section deals with the photochemical behaviour of CdS film using flash photolysis and steady state techniques. Here we are concerned with photoanodic dissolution of CdS film and its stabilisation, photoreduction of methyl viologen and photo-oxidation of methyl orange by CdS film and the effect of some ellectron donor and acceptors on the yield of photo-oxidised methyl orange. Luminescence quenching as a photochemical reaction is discussed in the following section.

6.4.1. Luminescence Quenching

A luminescence quenching study was carried out by adding methyl viologen (8×10^{-5} moldm^{-3}) in a 1cm double-sided quartz cell containing ca. 8cm^2 CdS film (0.5moldm^{-3}) and water (3ml). In contrast to green luminescence (which was increased by 10%), the

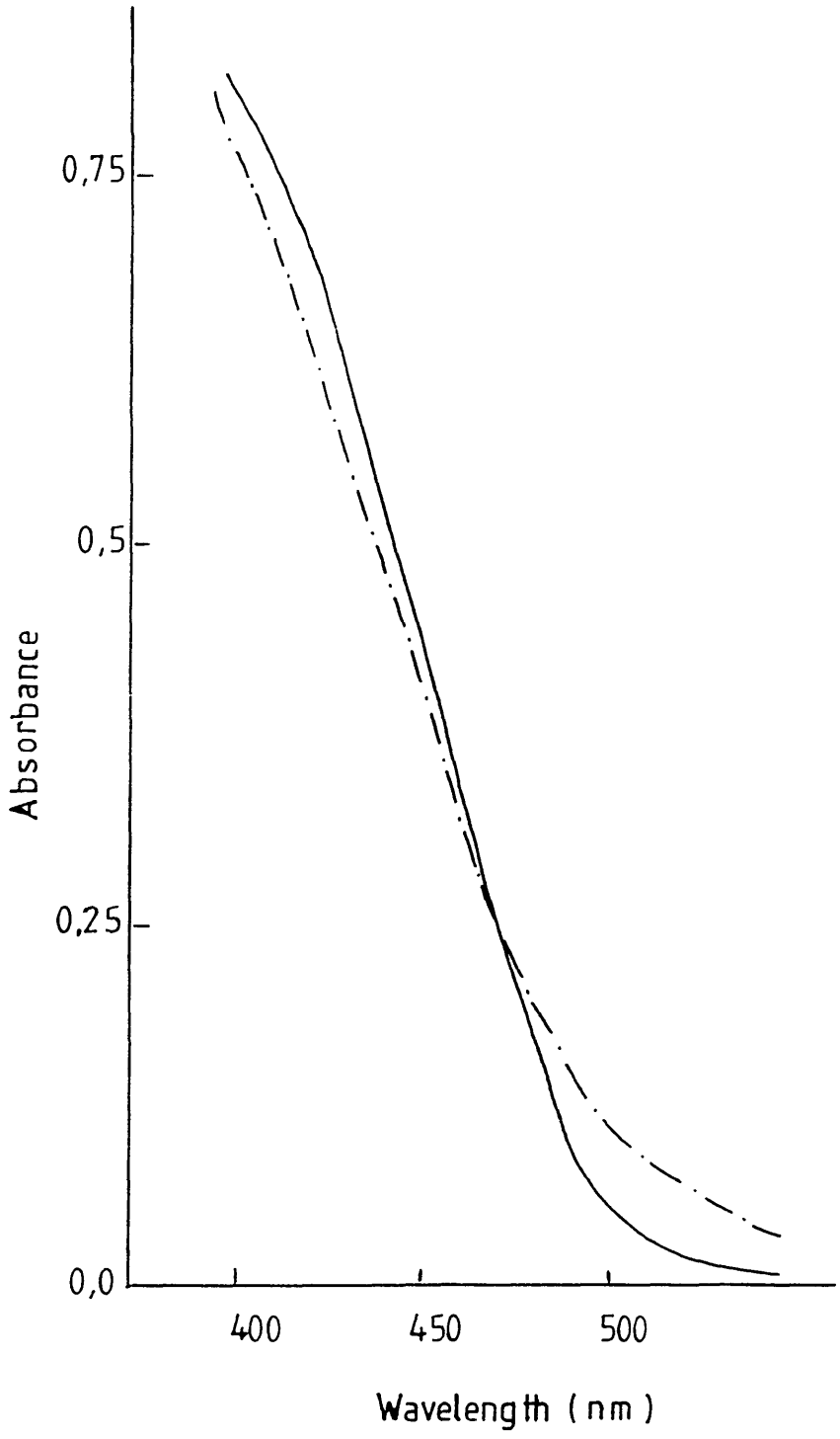


Fig. 6.7 Water effect (—·—) on the absorption spectrum of dry (——) CdS film(10^{-2} M).

red luminescence was quenched by about 50%. Increasing methyl viologen concentration fivefold ($4x10^{-4}$ moldm^{-3}) increased red luminescence quenching to over 90%.

It is reported that the quenching of the red luminescence of colloidal CdS by methyl viologen follows a poisson distribution:[54]

$$\frac{I}{I_o} = \exp(-Q) \qquad (6.1)$$

where I_o and I are the emission intensities in the absence and prescence of a concentration of quencher, $Q(MV^{2+})$ of molecules per particle.

Equation (6.1) shows that one molecule of MV^{2+} per particle is sufficient to completely quench the luminescence. Q is the quenching factor and is given by:

$$Q = N[MV^{2+}]/[CdS]$$

$$= \ln \frac{Io}{I} \qquad (6.2)$$

Where N is the number of CdS molecules per particle. By plotting the quenching data in accordance with equation (6.2), we can obtain a straightline. Its slope gives the number of CdS molecules per particle, N. Figure 6.8 shows such a plot. From the slope of this figure N=1100 ± 100. The average radius of CdS particles can be calculated from equation (6.3):

$$(r/cm) = \frac{(3M\ N\ )^{1/3}}{(4\pi\varrho\ N_A)} \qquad (6.3)$$

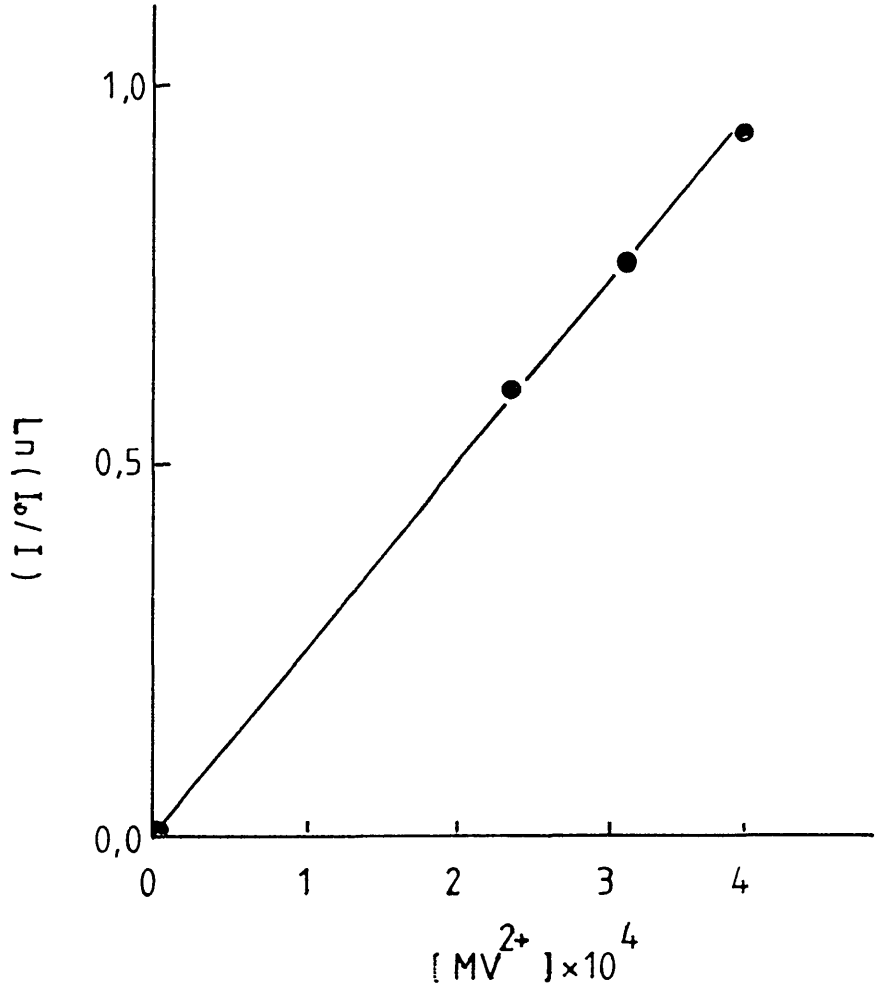


Fig. 6.8 Poisson plot of MV^{2+} quenching effect on the red emission of CdS film(10^{-2} M).

where M is the molecular weight in g, ϱ the density and N_A Arogadro's numbers. Equation (6.3) gives a diameter of 8.2nm for N=1100 This is about twice that of an elementary particle as estimated from the photophysical properties of CdS film in section 6.3.1. The difference can be explained in terms of aggregation of particles to form a cluster which are in electronic contact, so that one MV^{2+} per cluster suffices to quench its luminescence. This is not unusual, since the Bohr radius of the electron in CdS is given by:

$$r_e = \frac{h^2 \varepsilon_o \varepsilon}{e^2 \pi m^*} = 2.4 \text{ nm} \qquad (6.4)$$

For CdS ε = 8.9 and $m^* = 0.2m_e$

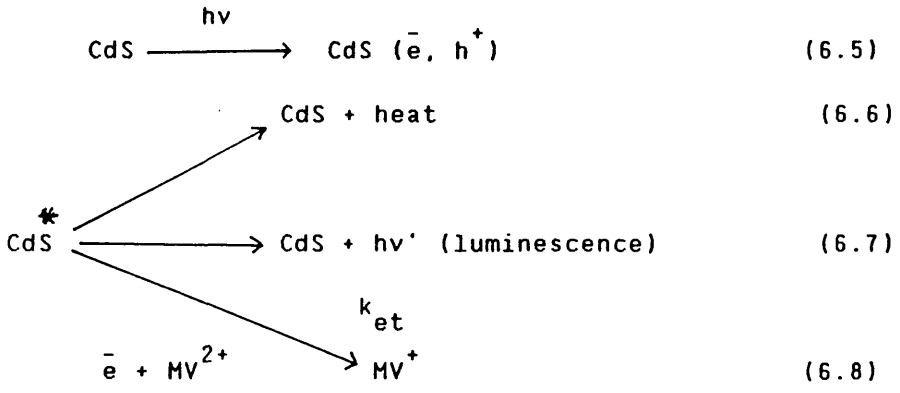
This value is comparable to the dimension of the elementary particle. However, it is surprising that one MV^{2+} ion is sufficient to quench luminescence from an aggregate consisting of two or more elementary particles. This explanation leads us to propose the possibility of an inter-particle electron and energy transfer.

6.4.2 Flash Photolysis Experiment

In order to gain further insight into the mechanism of electron transfer reactions of excited CdS film, a transient absorption experiment was performed using microsecond and nanosecond Flash photolysis techniques.

In the nanosecond technique a 1cm double-sided quartz cuvette containing $0.1 moldm^{-3}$ CdS film ($8cm^2$) and $4x10^{-3} moldm^{-3}$

methyl viologen as an "electron relay" was deaeranted and subjected to a 347nm pulse from a Ruby laser with a 20ns half width. Upon excitation by the laser pulse, transient absorption at 395 and 605nm relating to reduced methyl viologen (MV^+ were observed. In the absence of O_2 the mechanism of electron transfer is described by the following equations:



We have shown[45] that the electron transfer rate constant, k_{et}, in equation (6.8) in colloidal CdS solutions has a value of about $10^8 s^{-1}$ in agreement with data published by several authors.[48,49,194,228] However, Figure 6.9 reveals that the absorption transient in CdS immobilised within the DM extended over 8μs ($k_{et} = 10^5 s^{-1}$) for both 395 and 605nm wavelengths. Such a significant difference in k_{et} between immobilised and colloidal CdS solutions may be explained by bleaching of MV^+ by the positive holes.

It is reported[59] that during the high-energy pulse hydrated electrons, hydrogen ions and hydroxyl radicals are formed:

$$H_2O \longrightarrow e^-_{aq} + H^+ + OH^\cdot \qquad (6.9)$$

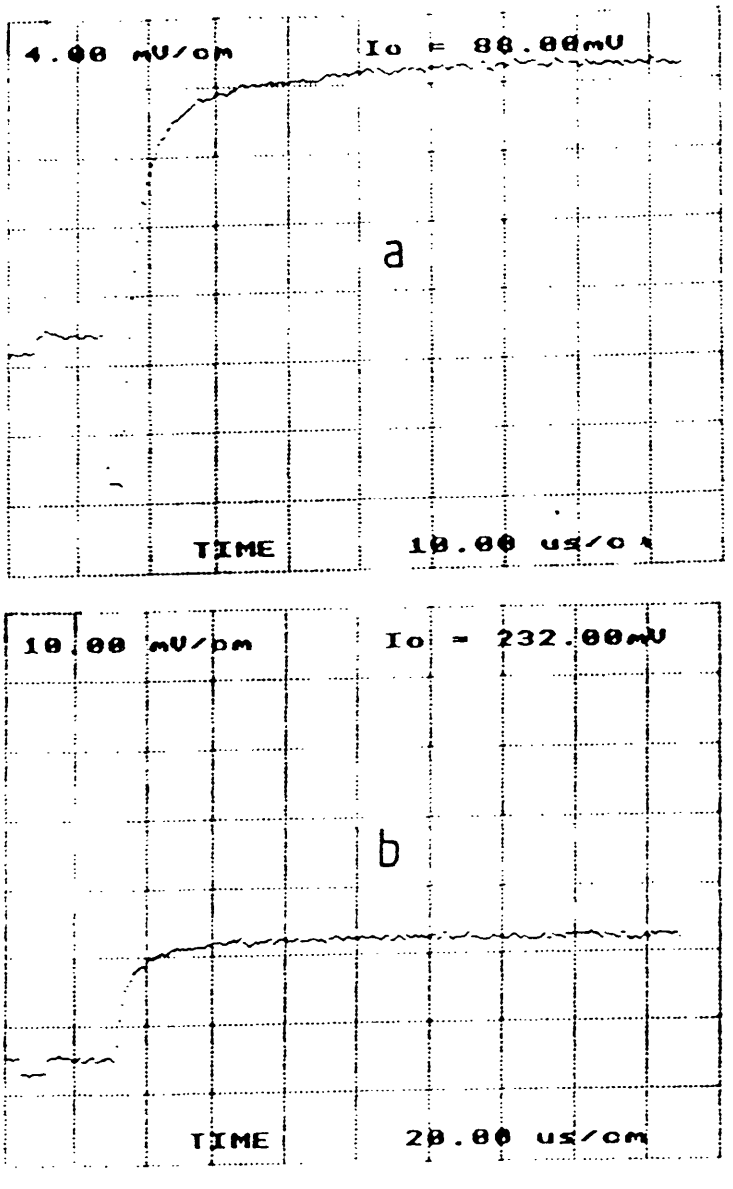


Fig. 6.9 Oscilloscope traces of MV^{+}, photoreduced from MV^{2+} (4×10^{-3} moldm^{-3}) by CdS film (10^{-2} M) at (a) 395 and (b) 605nm using nanosecond laser flash.

Photo-emitted electrons from CdS particles, which are hydrated in aqueous solution, may react with CdS particles and be stored by them. OH radicals attach on CdS (equ. 6.10), resulting in the injection of positive holes, which can re-oxidise the reduced methyl viologen in the absence of O_2:

$$OH^{\cdot} + CdS \longrightarrow CdS^{+} + OH^{-} \qquad (6.10)$$

$$CdS^{+} + MV^{+} \longrightarrow CdS + MV^{2+} \qquad (6.11)$$

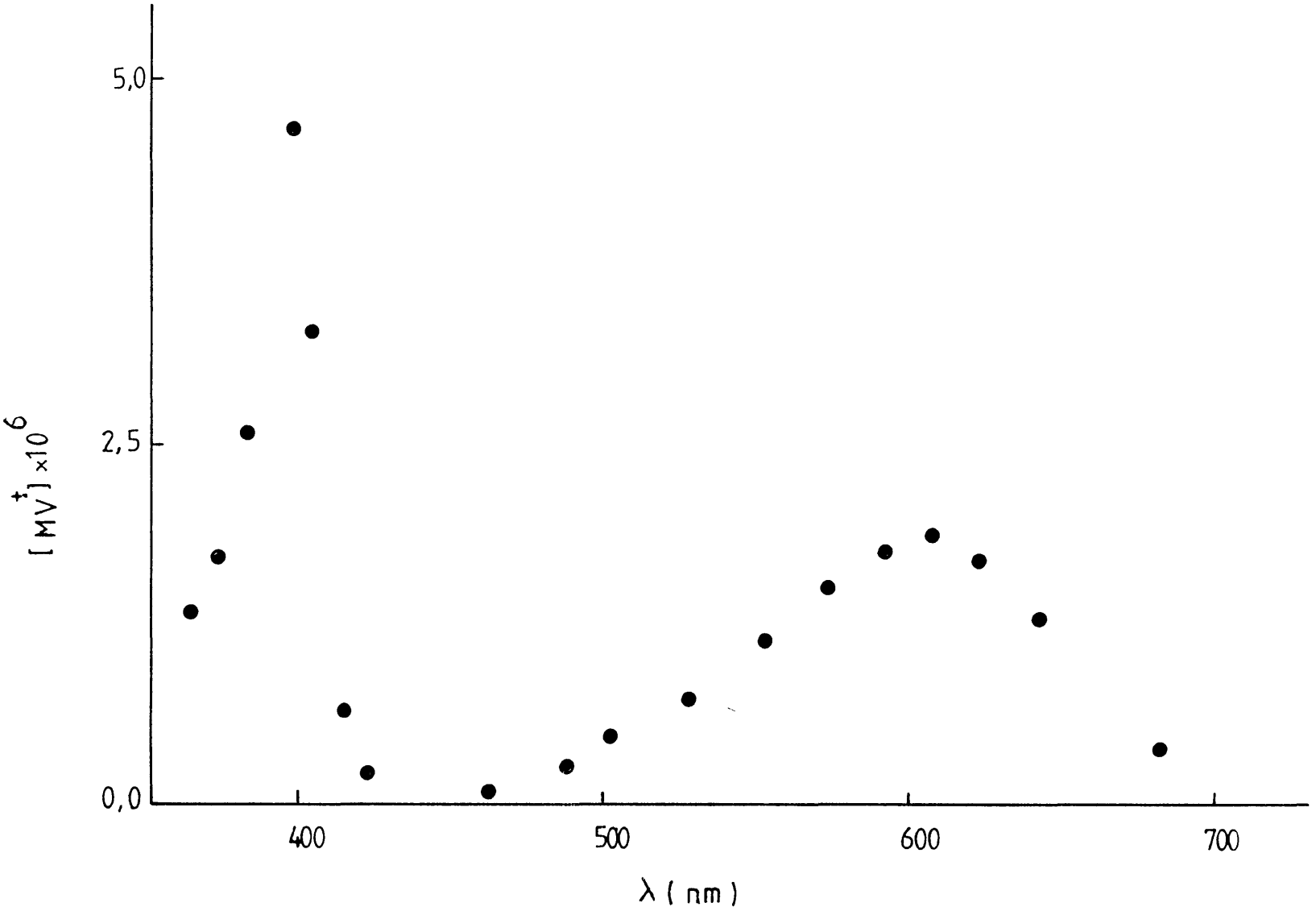
If O_2 were present, reoxidation of MV^{+} by localised holes is prevented as:

$$MV^{+} + O_2 \longrightarrow MV^{2+} + O_2^{-} \qquad (6.12)$$

This reaction is faster than that given by equation (6.11) and photoanodic dissolution occurs.

The fact that the absorption of the radical cation (MV^{+}) continued to increase after the laser flash indicates the existance of an excess of positive holes and a long-lived oxidising intermediate in the photolysis of CdS film. The amount of MV^{+} formed corresponded to the amount of consumed holes. The same effect as observed by Gratzel and Henglein in colloidal TiO_2 [81,84] supported by polyvinylpyridine and polyvinyl alcohol polymers respectively.

Figure 6.10 shows the optical absorption on the millisecond timescale of methyl viologen (4×10^{-3} moldm^{-3}) in a dearated solution containing CdS film using a microsecond flash. This is attributed to the long-lived oxidising intermediates, MV^{+}, from the photolysis of CdS film. The sharp and broad peak maximum at



Sea overleaf

Fig. 6.10 Absorption transient of MV^{+}, photoreduced from MV^{2+}(10^{-2}moldm^{-3}) by CdS film(10^{-2} M) using microsecond flash.

395 and 605nm apparently belong to methyl viologen reduced by excited electrons of the conduction band of CdS film. Absorption at 395nm is stronger than 605nm by a factor of three. Such a strong absorption at 395nm was not observed by us using colloidal CdS solution. The reason may be due to formation of large particles which scattered the flash light. In other words, Figure 6.10 indicates the absence of scattered light due to the formation of small particles in the dialysis membrane. The shape as well as the long-lived oxidising intermediates depends on the method of preparation of the CdS film.

One way to increase the availability of viologen for reduction is to increase the methyl viologen concentration. Figure 6.11 shows that the MV^{+} yield approaches a value of 3×10^{-6} $moldm^{-3}$ at 605nm as the methyl viologen concentration increases.

6.4.3 Steady-State Experiments

The continuoius illumination technique has been used to study the reduction of methyl viologen by conduction-band electrons. The photocorrosion effects, the stabilisation of CdS film and the photo-oxidation of methyl orange by valance band holes are also described.

6.4.3.1 Photoreduction of MV^{2+}

A deaerated solution of methyl viologen (1.5×10^{-4} $moldm^{-3}$) containing CdS film (0.1$moldm^{-3}$) was continuously irradiated with

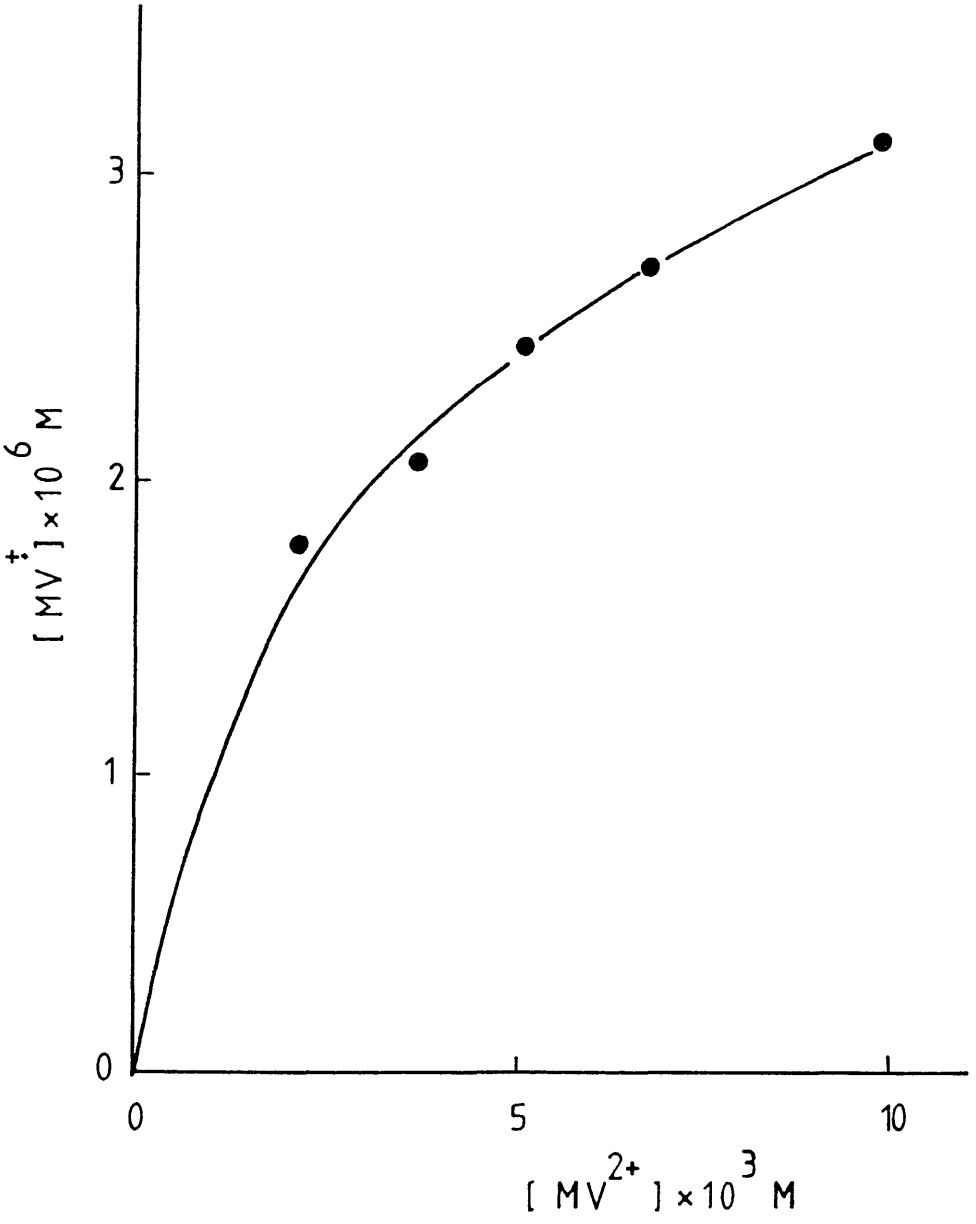


Fig. 6.11 The yield of MV^{+}, photoreduced from MV^{2+} by CdS film(10^{-2} M) immediately after microsecond flash as a function of methyl viologen concentration.

a 900W Xenon lamp in a steady state experiment. The spectral change observed by continuous iradiation is shown in Figure 6.12. The bluish color with absorption maximum at 605 and 395nm develops with white light irradiation due to the formation of the methyl viologen radical, (equation 6.8). After approximately 20 minutes irradiation the system appears to reach a photostationery state. When the sample is irradiated for a long time the yield of viologen radical cation diminishes. This effect, as described in the flash photolysis experiment, involves hole (h^+) oxidation of MV^+ (equation 6.11) followed by re-reduction of MV^{2+} (produced in equation 6.8) by conduction band electrons. Another approach to the hole reaction is the formation of hydroxyl radicals which are compatible with the oxidation of viologen radicals and are adsorbed to the surface of CdS film:

$$h^+ + H_2O \longrightarrow (OH^{\cdot})_{ads} + H^+ \qquad (6.13)$$

The adsorbed hydroxyl radicals can reoxidise the viologen radical according to equations (6.10) and (6.11). Figure 6.12 shows that prolonged irradiation produced a new absorption around 380nm which was absent prior to iradiation. Grätzel and coworkers observed the same effect by polymeric viologen with colloidal TiO_2 when the sample was irradiated for a long time and then aerated.[81] They also obtained an isobestic point at approximately 460nm as was obtained by us with CdS film. These similarities suggest that the new absorption at 380nm is due to the second reduction of viologen radical cation to the doubly reduced form $MV^{\bullet}$. This is likely to be due to addition of hydroxyl radicals to MV^+.[231] The slower growth of $MV^{\bullet}$

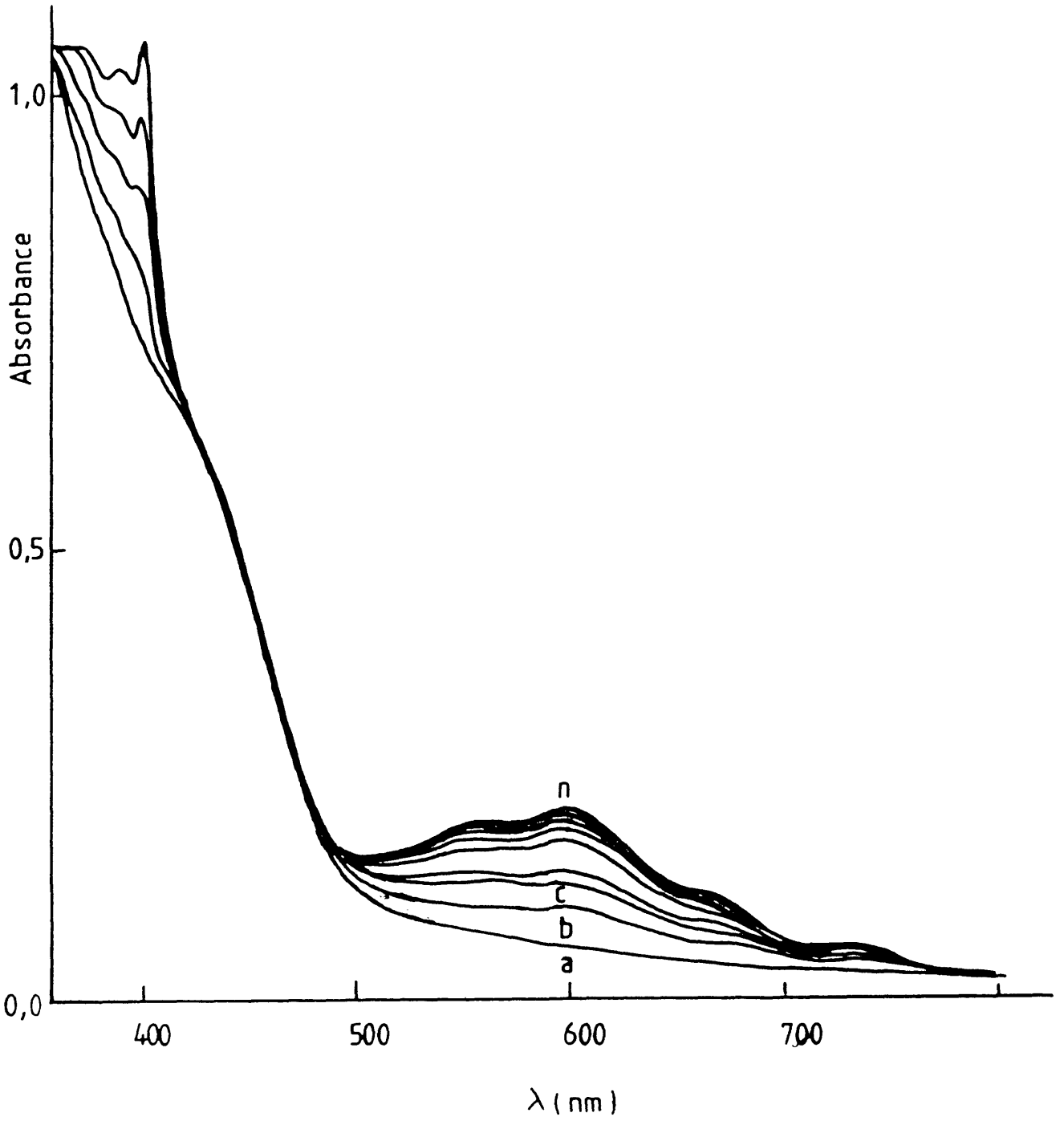


Fig. 6.12 Absorption of MV^{+}, photoreduced from MV^{2+} (1.5×10^{-4} M) by CdS film(10^{-2} M) as a function of time using steady-state techniques (900W Xenon lamp).

absorption indicates a considerably lower rate for this process. The second reduction proceeds only after virtual completion of the first reduction. Grätzel's results show that after reaching a maximum after 2 minutes the 380nm absorption of doubly-reduced viologen radical ($V^{\cdot}$) diminishes as irradiation is continued. They suggest that the viologen moiety decomposes while undergoing a photostationary cycle, i.e. hole-oxidation of $V^{\cdot}$ to V^{+} and subsequent re-reduction by conduction-band electrons to $V^{\cdot}$. In our experiment such photostationary cycle was not observed upon irradiation of up to 20 minutes. In our experiment we only observed the monomer (MV^{+}), while they observed monomer and dimer.[81] The absorption maxima for viologen radical cation monomer occurs at 605 and 395nm, while for dimers at around 540 and 360nm.[81,194]

When the concentration of methyl viologen was increased from $1.5x10^{-4}$ to $10^{-3}moldm^{-3}$ the same photostationery state occurred ten time more quickly (2 min). This leads us to conclude that an approximately inverse relationship exists between concentration of MV^{2+} and the irradiation time required to reach a stationary state. This conclusion is represented in Figure 6.13. Another important result from Figure 6.13 is that a quantum yield of close to 10% was obtained for electron transfer in the stationery state experiment. The high rate and yield of electron transfer in continuous irradiation may be explained by more precipitation of radical methyl viologen onto the CdS film and therefore formation of MV^{+} and $MV^{\cdot}$.

When the sample containing CdS film and methyl viologen

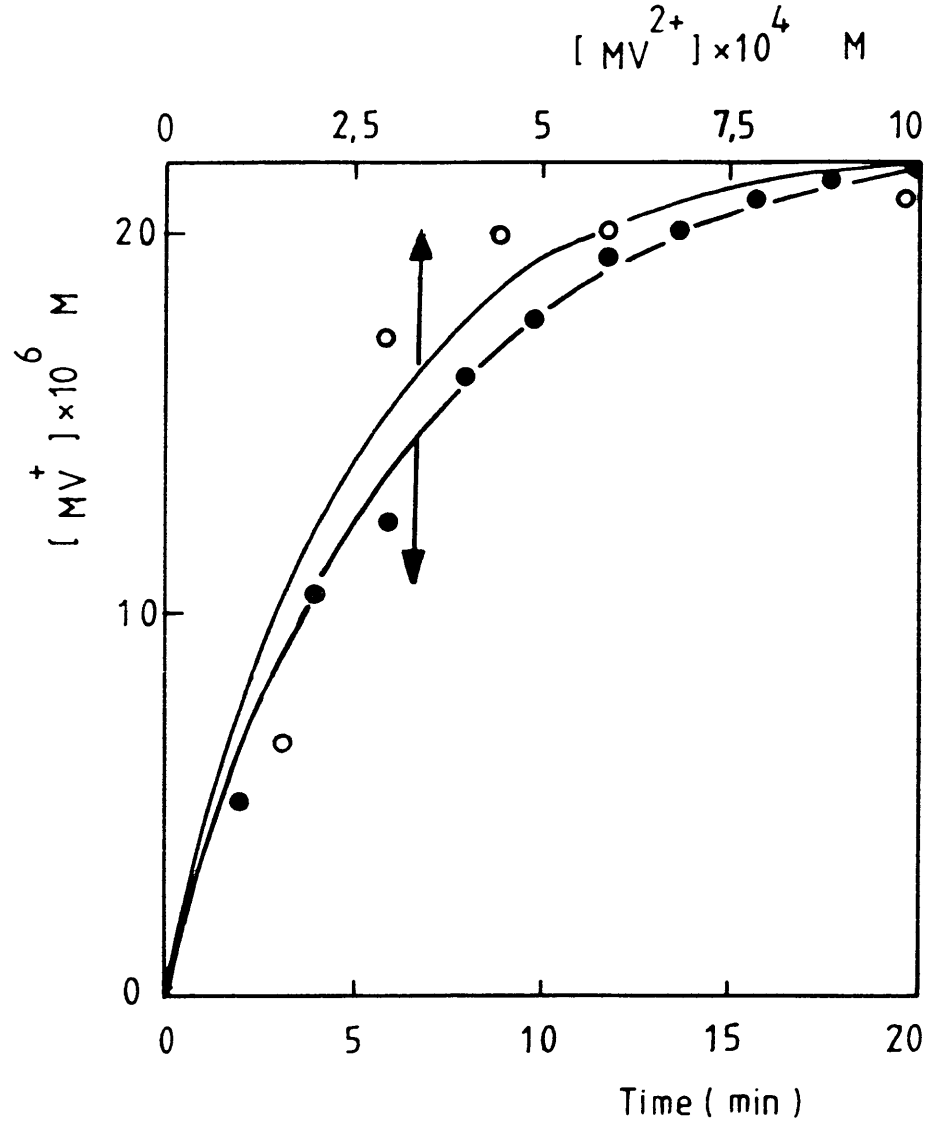


Fig. 6.13 The yield of MV^+, photoreduced from MV^{2+} using CdS film(10^{-2} M) as a function of time in SS techniques.

(○) t = 2 min

(●) $[MV^{2+}] = 1.5 \times 10^{-4}$ M

(10^{-3}moldm^{-3}) was deaerated and subjected to a monochromatic beam at 450nm and irradiated for 15 minutes, the same results (single and doubly-reduced methyl viologen) were obtained as with white light irradiation. In the former case the yield of MV^{+} was about 10% lower than the latter case. (Figure 6.14).

6.4.3.2 Photocorrosion of CdS Film

In chapter 4 we have discussed the photodegradation of colloidal CdS in the presence of oxygen. The photoanodic dissolution of metal sulfides and selenides is an obstacle to the use of these materials in photochemical and photoelectrical systems.[56,186,232] The same effect was observed for CdS synthesised in the DM. When the CdS film, in the absence of O_2, was irradiated continuously using a 900w xenon lamp for about 20 min, no corrosion effect was observed. Figure 6.15 shows that dissolution occurs at an appreciable rate only in the presence of oxygen.

It has been shown that the only oxidation product of CdS[56,177,232-233] and ZnS[177] is sulfate anions:

$$CdS + O_2 \xrightarrow{h\nu} Cd^{2+} + SO_4^{2-}$$

The corrosion effect is clearly observed in the CdS film and the yellow colour of film decreased as a function of irradiation time.

Certain electron acceptors such as Tl^{+} and MV^{2+} ions accelerate the dissolution of CdS.[56,186] Figure 6.16 shows

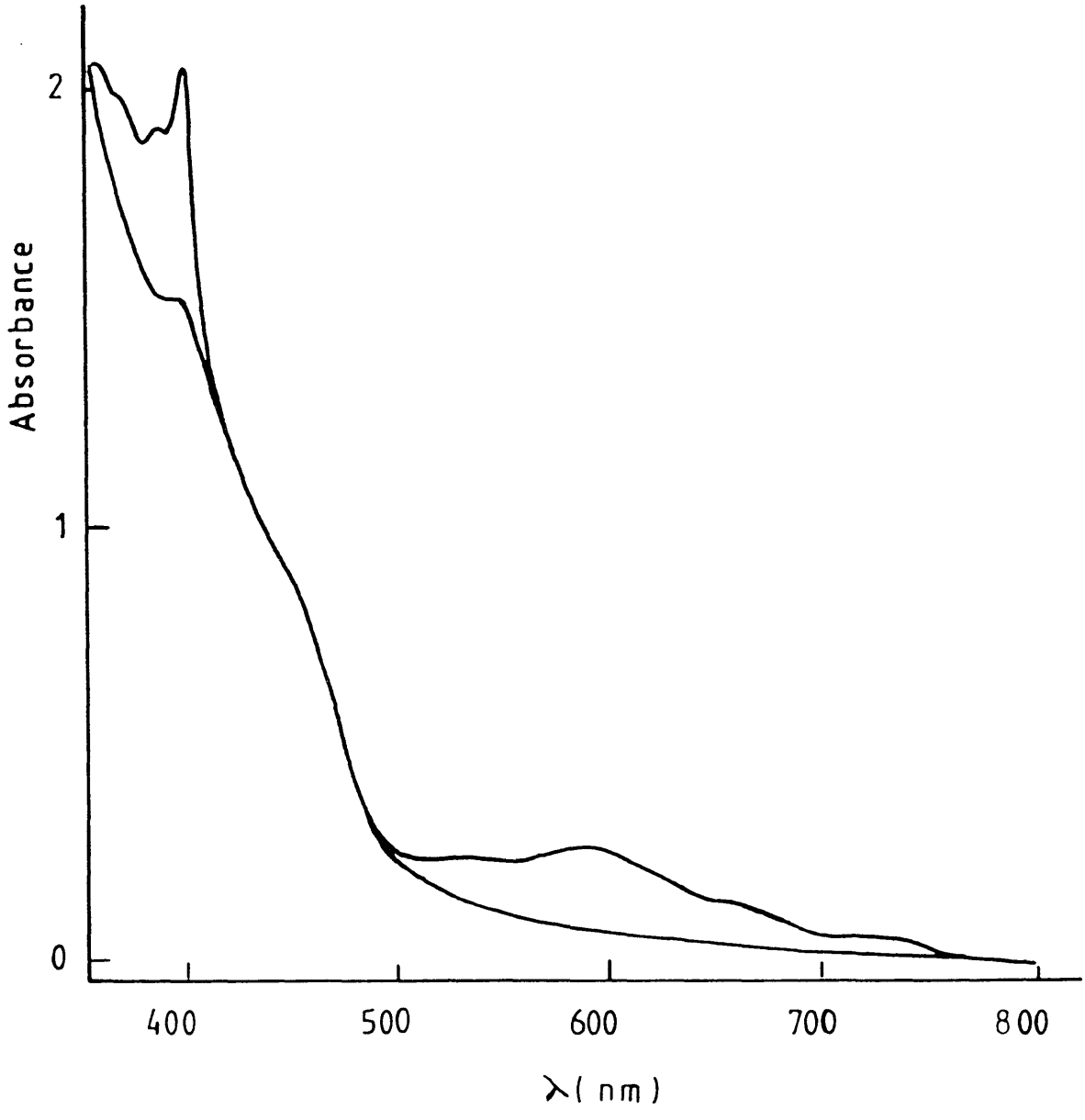


Fig. 6.14 Absorption spectrum of MV^{+}, photoreduced from MV^{2+} (10^{-3} M) by CdS film (10^{-2} M) using 450nm monochromatic irradiation.

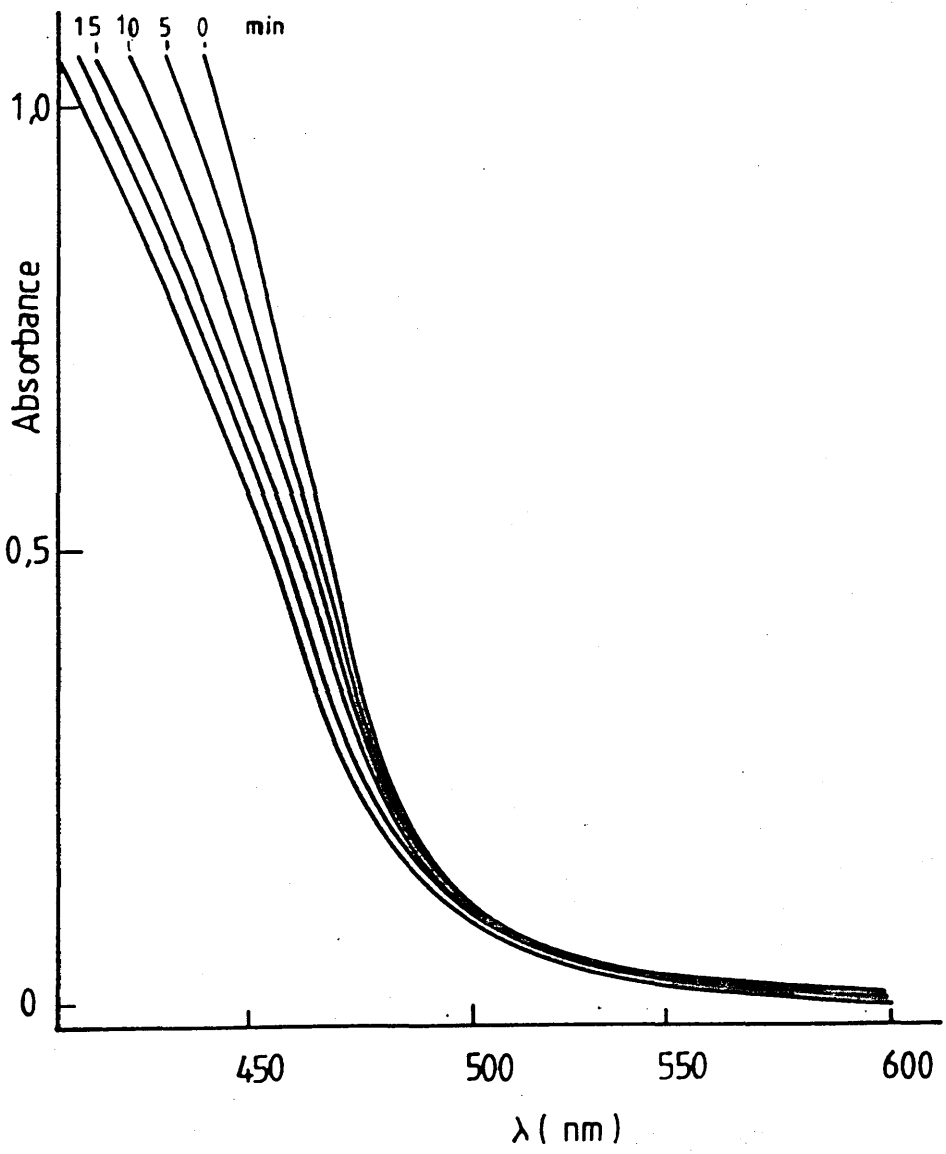


Fig. 6.15 Photodegradation of CdS film(10^{-2} M) in the presence of oxygen.

that in the presence of oxygen the reduced methyl viologen (MV^+) completely disappeared and this was the only time that the dissolution effect was observed in the steady state experiment.

The mechanism of photodegradation in the absence of MV^{2+} is described by equations (6.5)-(6.7) and (6.15)-(6.17):

$$e^- + O_2 \longrightarrow O_2^- \qquad (6.15)$$

$$h^+ + S^{2-} \longrightarrow S^- \qquad (6.16)$$

$$S^- + O_2 \longrightarrow SO_2^- \xrightarrow[\text{oxidation}]{\text{further}} SO_4^{2-} \qquad (6.17)$$

The initiation of photocorrosion occurs by excited conduction-band electrons being scavenged by dissolved oxygen [Equ. (6.15)]. However, O_2 as an initiator of photocorrosion cannot be substituted by other electron scavengers. For example, no dissolution was observed in a dearated solution of MV^{2+} containing CdS film (Figure 6.16). In the absence of oxygen rapid re-oxidation of MV^+ by the positive holes takes place [(Equ. (6.11)]. When O_2 is present, the re-oxidation reaction by positive holes is prevented by reaction (6.12) which is faster than the reaction (6.11). Since reaction (6.8) is faster than (6.15), then in the presence of MV^{2+} and O_2 the positive holes can more efficiently oxidise sulfide anions.

6.4.3.3 Quantisation Effect

Another point to be noted from Figure 6.15 is that the absorption spectrum of photodegraded CdS film shifts to shorter

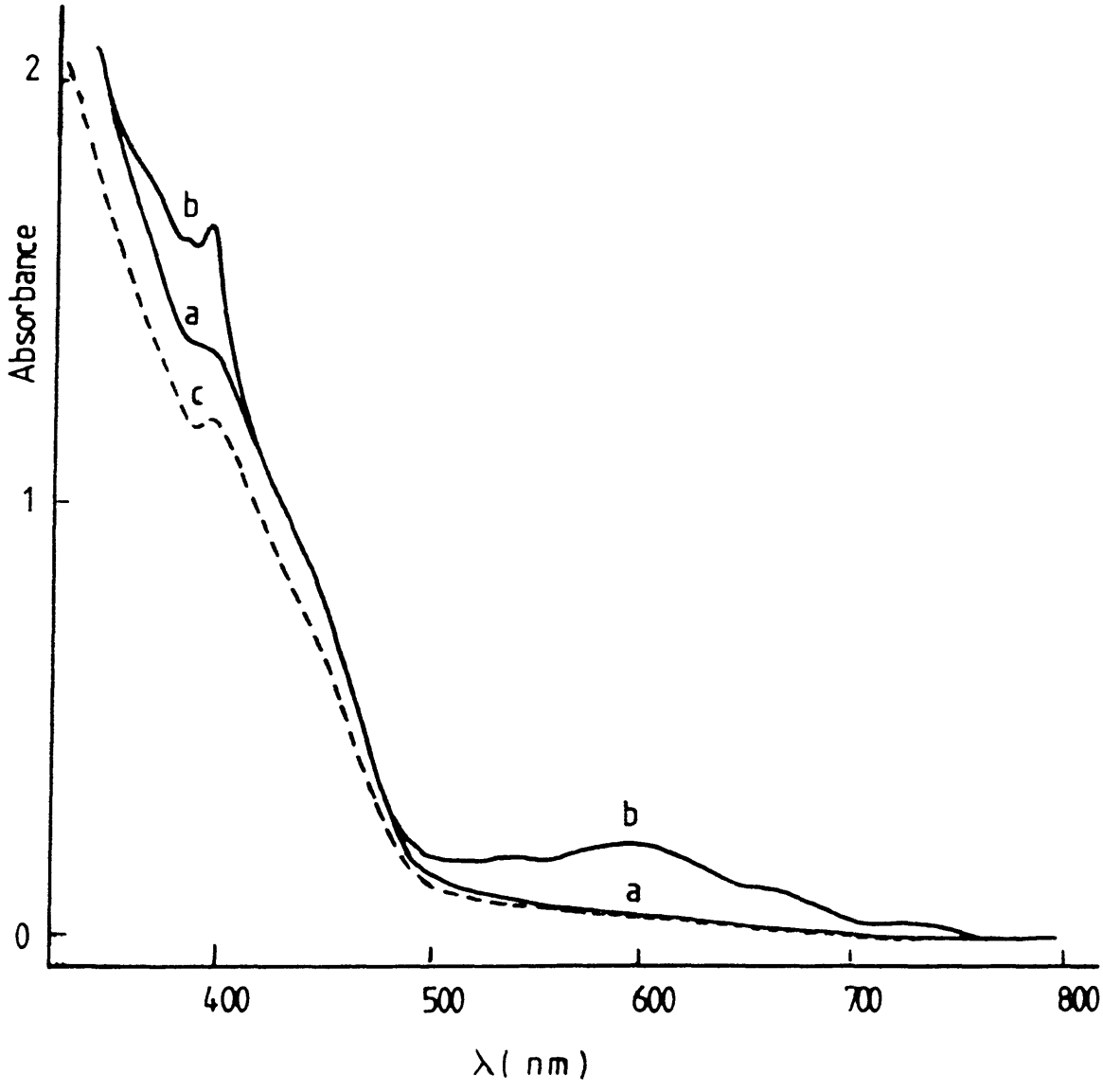


Fig. 6.16 The effect of O_2 on the yield of MV^+, photoreduced from MV^{2+} (10^{-3} M) by CdS film(10^{-2} M).

(a) deaerated solution before irradiation

(b) deaerated solution after 2 min irradiation

(c) aerated solution after 2 min irradiation.

wavelengths after irradiation with the intense light of a xenon lamp. The onset of absorption (before irradiation) was around 508nm, i.e. slightly below the onset of 515nm where macrocrystalline CdS absorbs. During photodegradation of CdS film, the particles become smaller and the onset was shifted to below 500nm. Henglein,[206] using a photodissolution experiment with a CdS solution, developed methods for the preparation of extremely small particles both in aqueous solution and in organic solvents in which a size quantisation effect was observed for the first time.

Q-semiconductor particles, such as cadmium arsenide,[236] cadmium phosphide,[235] cadmium selenide,[205] zinc selenide[205] and zinc sulfide[205] were made using the precipitation techniques. Q-materials are characterised with the prefix "Q" to show that their optical and catalytic properties differ from macrocrystalline materials. The Q indicates that the quantum mechanical effect is responsible for these changes. For example, Cd_3P_2 and Cd_3As_2 are black semiconductors with 0.5 anmd 0.1eV. band gaps respectively, which adsorb in the infrared. When the size of the Cd_3P_2 particles is decreaszed from 10 to 2nm, the band gap is shifted from above 0.1eV to about 3eV. The Q-Cd_3P_2 particles with 3eV band gap exhibit a white colour with a yellow tinge. The onset of absorption of this semiconductor shifted from infrared for normal particles to the visible region in the Q-state.

In Q-materials, the photo-induced electrons and positive holes should be on more negative and positive potentials

respectively than in the macrocrystalline materials. For example, Q-CdS particles catalyse the formation of hydroperoxide $(CH_3)_2C(OH)OOH$ when they are illuminated in aerated propan-2-ol solution, while larger particles are not efficient in this respect.[206]

The studies on the photocorrosion effect of CdS are important for the understanding of photo-electrochemical reactions. The observations of quantum mechanical size effects in extremely small particles have added a new dimension to the physics and chemistry of colloidal systems.

6.4.3.4 Stabilisation of CdS Film

When the solution containing CdS film and cysteine (8×10^{-5}moldm^{-3}) as an electron donor was dearated and then irradiated by the intense light of a xenon lamp, there was no significant effect on photocorrosion of the CdS film. Increasing the concentration of cysteine to 10^{-2}moldm^{-3} completely blocked the photocorrosion effect during continuous illumination. This effect may be explained by the coating of CdS film with cysteine as described with colloidal CdS solution in Chapter 4. We have shown that cysteine concentrations as low as 2×10^{-4}moldm^{-3} decrease the yield of electron transfer from the conduction band of CdS into MV^{2+} by a factor of 30. The same explanation can be proposed for stabilisation of CdS film i.e. the cysteine effectively coats the CdS film surface, dislodges O_2 and prevents the corrosion effect (Figure 6.17).

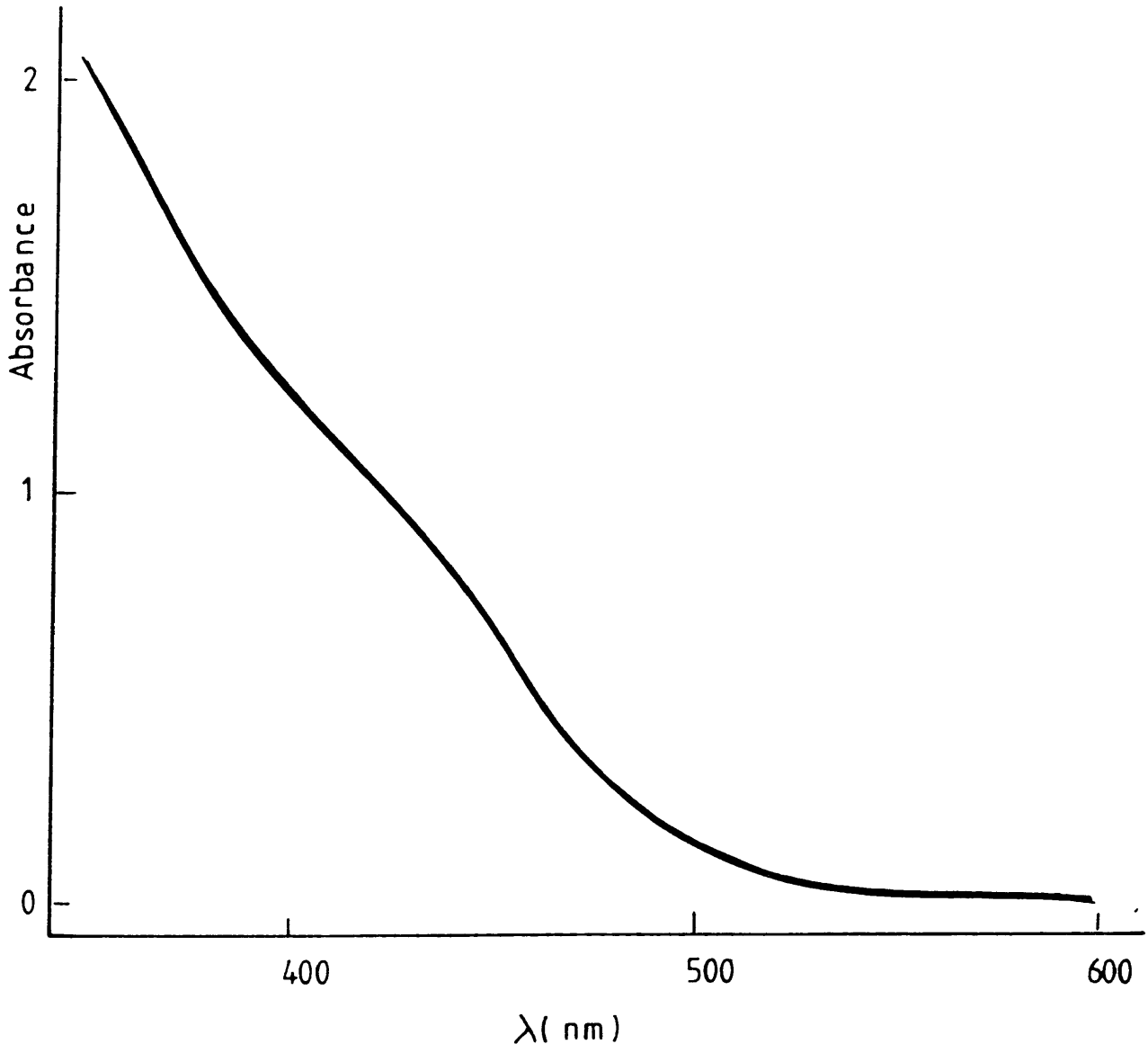


Fig. 6.17 Cysteine (10^{-2}moldm^{-3}) effect on the photocorrosion of CdS (0.1 M) film.
$t = 6$ min.

6.4.3.5 Photo-oxidation of Methyl Orange

The chemistry of methyl orange (4-[p-(dimethylaminophenylazobenzenensulphonic acid, sodium salt) with the formula:

$$MO: \quad (CH_3)_2NC_6H_4N = NC_6H_4SO_3^-$$

has recently been studied by our groups to probe reduction and oxidation reactions at the surface of TiO_2 and ZnO colloidal particles.[77-78,236] In continuation of this work, we began to investigate the photo-oxidation of methyl orange on CdS immobilised in the DM.

As shown in Figure 6.18, MO absorbs light in the visible region and the maximum occurs at 465nm, which is close to the absorption onset (around 480nm) of the immobilised CdS colloid. MO belongs to a class of coloured azocompounds which are one of the commenest classes of organic dyes.[237] It has been used as an indicator in the analysis of bromine,[238] and can be used as a probe for photochemical oxidation reactions of semiconductor/liquid interfaces.[78,236]

When the solution containing CdS film (10^{-3}moldm^{-3}) and methyl orange (5×10^{-5}moldm^{-3}) was purged with oxygen and then irradiated with an intense light of the xenon lamp, the absorption is destroyed (Figure 6.19). The photocorrosion of CdS particles in the presence of oxygen is well known. In order to determine whether the destruction is due to either CdS or methyl orange or both we used another CdS film as a reference to determine the absorption of methyl orange alone. The change of

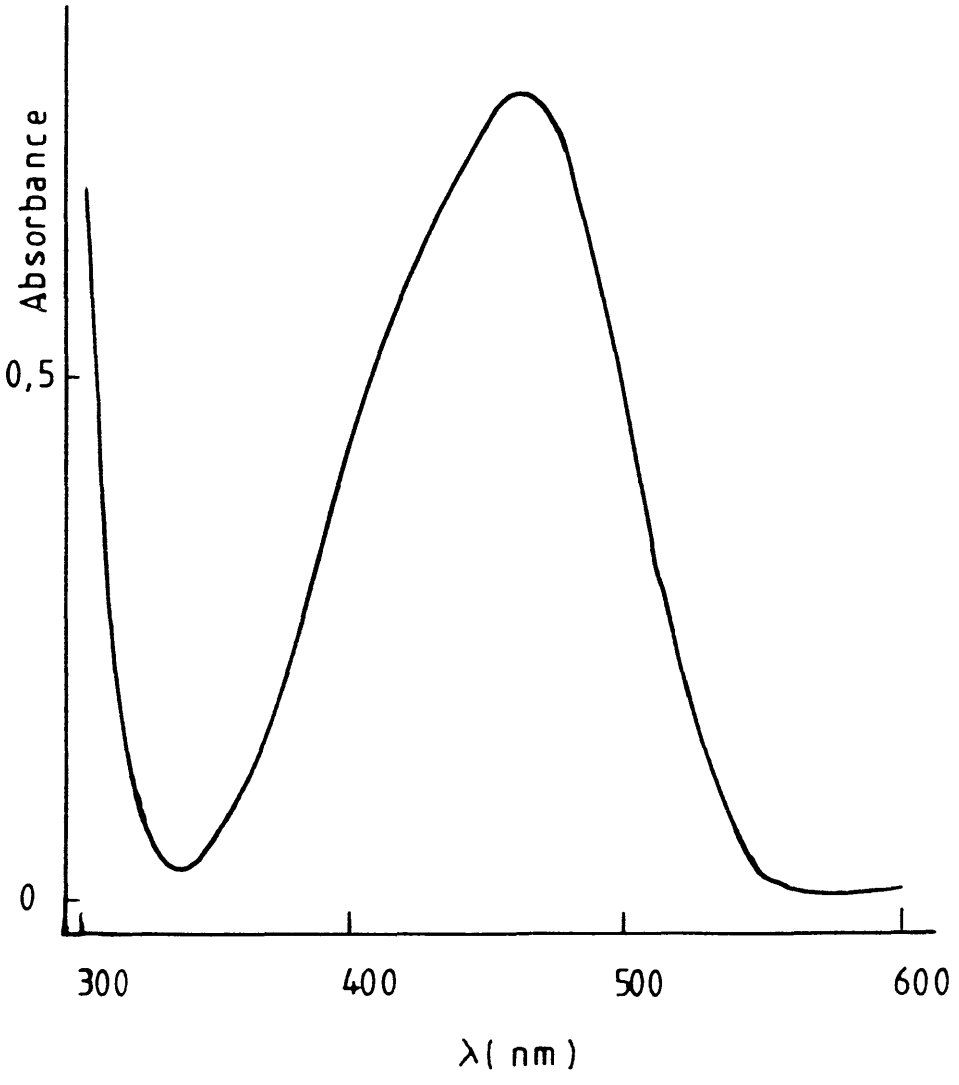


Fig. 6.18 Absorption spectrum of methyl orange (5×10^{-5} M).

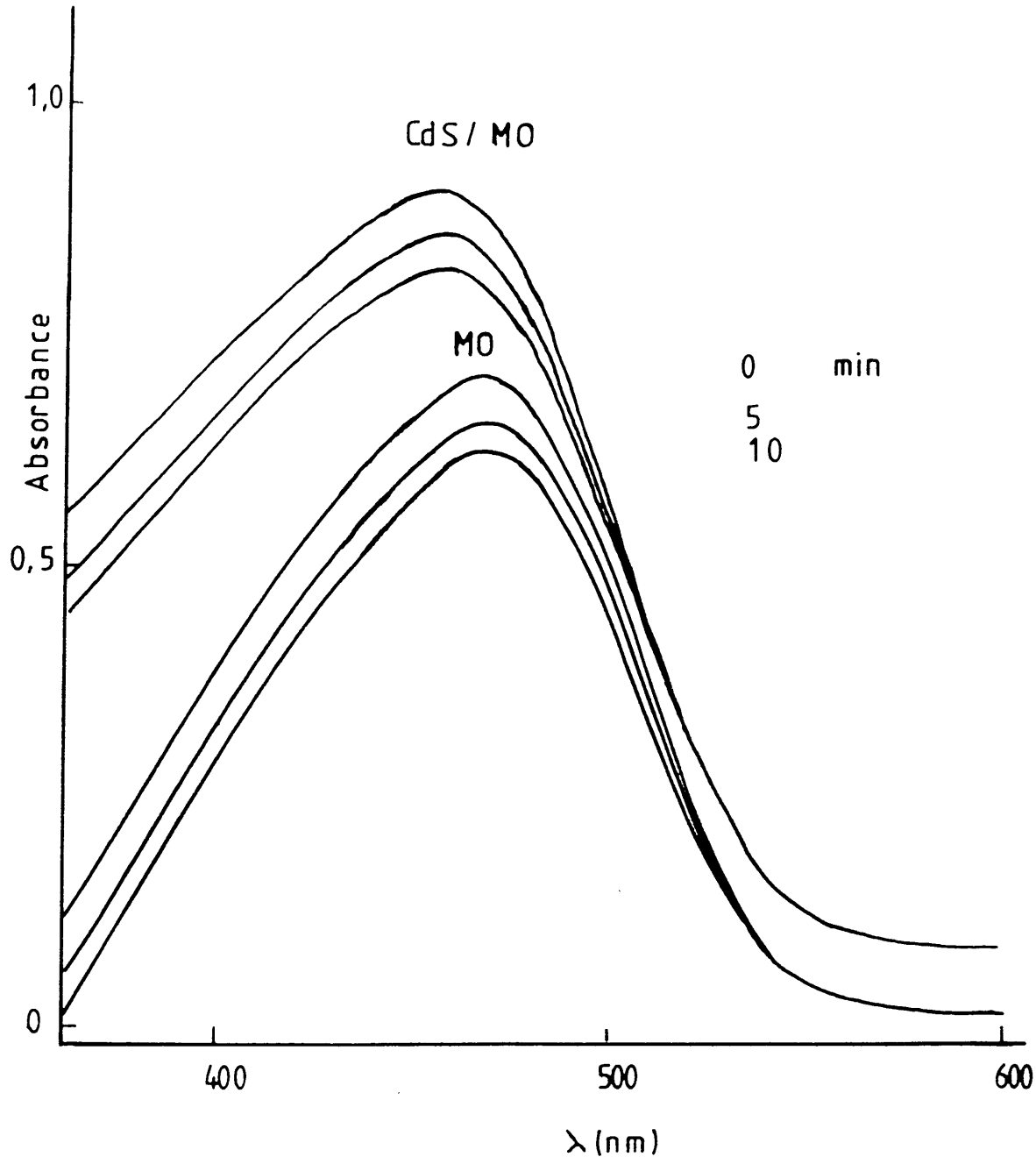


Fig. 6.19 Photo-oxidation of methyl orange (5×10^{-5} M) by CdS film(10^{-2} M):

Upper) without CdS film as a reference,

Lower) with CdS film as a reference.

the absorption spectrum is shown in (Figure 6.19). This figure clearly demonstrates that the spectral change can only be attributed to methyl orange. It is similar to that observed when methyl oranbge is photo-oxidised by colloidal TiO_2,[78] ZnO[236] or thermally oxidised by bromine.[238] Methyl orange is remarkably stable and is not bleached by visible or near U.V. light. The energy absorbed by methyl orange is rapidly lost by the fast photo-isomerisation reaction.[77-78.239] Apparently the bleaching of the dye in the presence of CdS film can only be attributed to photo-oxidation of the dye by photo-induced positive holes of the CdS valance band. The photoproducts of the reaction were identified[236] by NMR spectroscopy. It was found that the oxidation reaction occurred in a number of stages. The majority of the photo-oxidation belongs to the demethylation of methyl orange.

The kinetics of dye oxidation under conditions of constant oxygen concentration are shown in Figure 6.20. This figure indicates that the reaction is zero-order with respect to methyl orange. The same result has been reported for photooxidation of methyl orange by ZnO colloids.[236] Photolysis of methyl orange for up to 60min in the presence of ZnO gives a linear region and then the rate of reaction decreases. The initial linear region for ZnO is also shown in Figure 6.20. Photo-oxidation of methyl orange by ZnO colloid and CdS film was carried out at the same concentration and under the same conditions. Comparing our results (CdS) with the reported data (ZnO) shows that photo-oxidation of methyl orange with CdS film is more than three times faster than that with ZnO colloids. This difference may arise

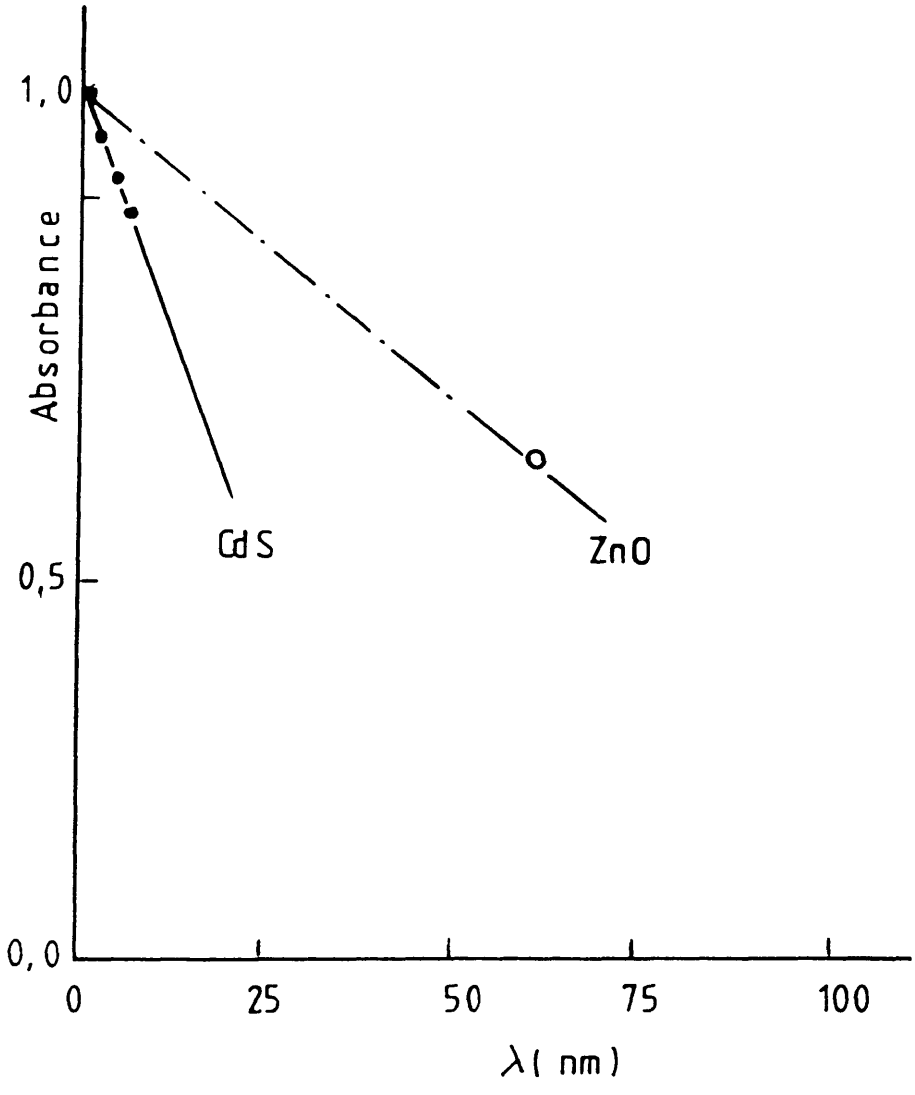


Fig. 6.20 Absorption change of photo-oxidised methyl orange (4×10^{-5} M) as a function of time:
CdS within film (10^{-3} M),
ZNO colloids (7.5×10^{-3} M).

from the narrower band gap of CdS film (2.42eV) compared to ZnO (3.12eV). We can conclude that, under the same conditions, the efficiency of methyl orange oxidation by CdS film is much higher than by ZnO colloids.

6.4.3.5.1 Cysteine (cys) Effect

In section 6.4.3.4 we have shown that 10^{-2}moldm^{-3} cys completely prevented photodegradation of CdS film. When the solution containing CdS film, $5x10^{-5}$moldm^{-3} methyl orange and $9x10^{-3}$moldm^{-3} cys was aerated and irradiated for about 10min, photo-oxidation of methyl orange decreased. In the same conditions the photo-oxidation process in the absence of cys was about 10 times faster. That means that cys, as a positive hole scavenger, not only stabilises the CdS film but also prevents the dye bleaching under continuous irradiation. This effect possibly may arise from the coating of the CdS film with cysteine which prevents the tight binding methyl orange to the CdS surface necessary for the photo-oxidation process to occur.

6.4.3.5.2 Methyl Viologen (MV^{2+}) Effect

Addition of methyl viologen to an aerated solution of CdS film and methyl orange increased the yield of photo-oxidation. Addition of only MV^{2+} ($6x10^{-4}$moldm^{-3}) to the above solution approximately doubled the yield of photo-oxidised methyl orange. Excited electrons in the conduction bands of CdS film can be

scavenged more rapidly by electron acceptors, such as MV^{2+} and then by oxygen therefore decrease electron-hole recombination. Hence excess positive holes at the surface of CdS film can in turn to scavenged by methyl orange and so increase the yield of the oxidised dye.

6.4.3.5.3 The Combined MV^{2+} and Cysteine Effect

In the last two sections we have studied the effect of cysteine and methyl viologen on the yield of photo-oxidised methyl orange MV^{2+} in the absence of cysteine doubled the yield of photo-oxidation. When cysteine (10^{-2}moldm^{-3}) was added to the aerated solution containing CdS film (10^{-3}moldm^{-3}), methyl orange ($5x10^{-5}$moldm^{-3}) and MV^{2+} ($6x10^{-4}$moldm^{-3}) and irradiated under steady state conditions, no photo-oxiidation was observed. That means the cysteine as stated in the previous sections, efficiently coated the surface of CdS film even in the presence of MV^{2+} and prevented any photo-oxidation from occurring.

6.4.3.5.4 Poly Phosphate Effect

The effect of sodium hexametaphosphate (SHMP) as a supporter, on the yield of methyl orange oxidation has been studied into two ways: (i) before, and (ii) after preparing the CdS film.

(i) Before Making CdS Film

In this method SHMP (10^{-3}moldm^{-3}) was added to the continuously stirred solution of cadmium nitrate ($5x10^{-2}$moldm^{-3}) and the DM. Then the DM was immersed in sodium sulfide (0.1moldm^{-3}). In this method we prepared supported CdS film. Then the aerated solution of methyl orange ($5x10^{-5}$moldm^{-3}) containing supported CdS film was irradiated for about 5 minutes. No significant photo-oxidation was observed.

(ii) After Making CdS Film

When the SHMP (10^{-3}moldm^{-3}) was added to the aerated solution of CdS film and methyl orange, then irradiated for about 5 minutes, photo-oxidation of methyl orange was observed.

We can conclude that the polyphosphate has little effect on the yield of photo-oxidation of methyl orange except when it supports CdS particles in the DM. This means that polyphosphate molecules were adsorbed onto CdS particles (in the former case) and these prevented significant attachment of methyl orange molecules to the CdS.

6.4.3.5.5 Polyphosphate and MV^{2+} Effect

When the polyphosphate effect was studied in the presence of methyl viologen ($6x10^{-4}$moldm^{-3}), not only did photo-oxidation of methyl orange occur but also photodegradation of CdS film was observed. This process has been studied in both cases of adding polyphosphate before and after preparing the CdS film. In the latter case, the yield of photo-oxidation of methyl orange and

photodegradation of CdS film was much higher than in the former case. These observations indicate the significant effect of SHMP in reducing both photo-oxidation and photodegradation processes. These effects are represented in Figures 6.21 and 6.22. In these figures, photo-oxidation is shown in part a, while both photo-oxidation and -degradation are depicted in part b. It seems that the yield of photo-degradation is higher than the photo-oxidation. This effect may be explained by absorption of MV^{2+}, as an electron acceptor, on the surface of CdS particles. Photogenerated electrons in the conduction band of CdS film can be removed by MV^{2+}, while excess positive holes on the CdS surface may partially oxidise methyl orange and partially oxidise sulfide anions of the CdS particles (photodegradation). Figure 6.21 shows that the latter case is dominant.

6.5 Conclusion

In this chapter a simple method of preparing and immobilising small colloidal CdS (diameter < 5nm) within inexpensive matrices such as dialysis membrane was developed. This system keeps the particles from coagulating and is very simple to remove from solution for analysis of the reaction products and regeneration of the uniform semiconductor particles. It is also useful in flow systems.

Formation of small CdS particles within the DM was determined using absorption spectroscopy and particle size and shape were estimated by electron microscopy. The dramatic effect of particle size on the photophysical and -chemical properties of

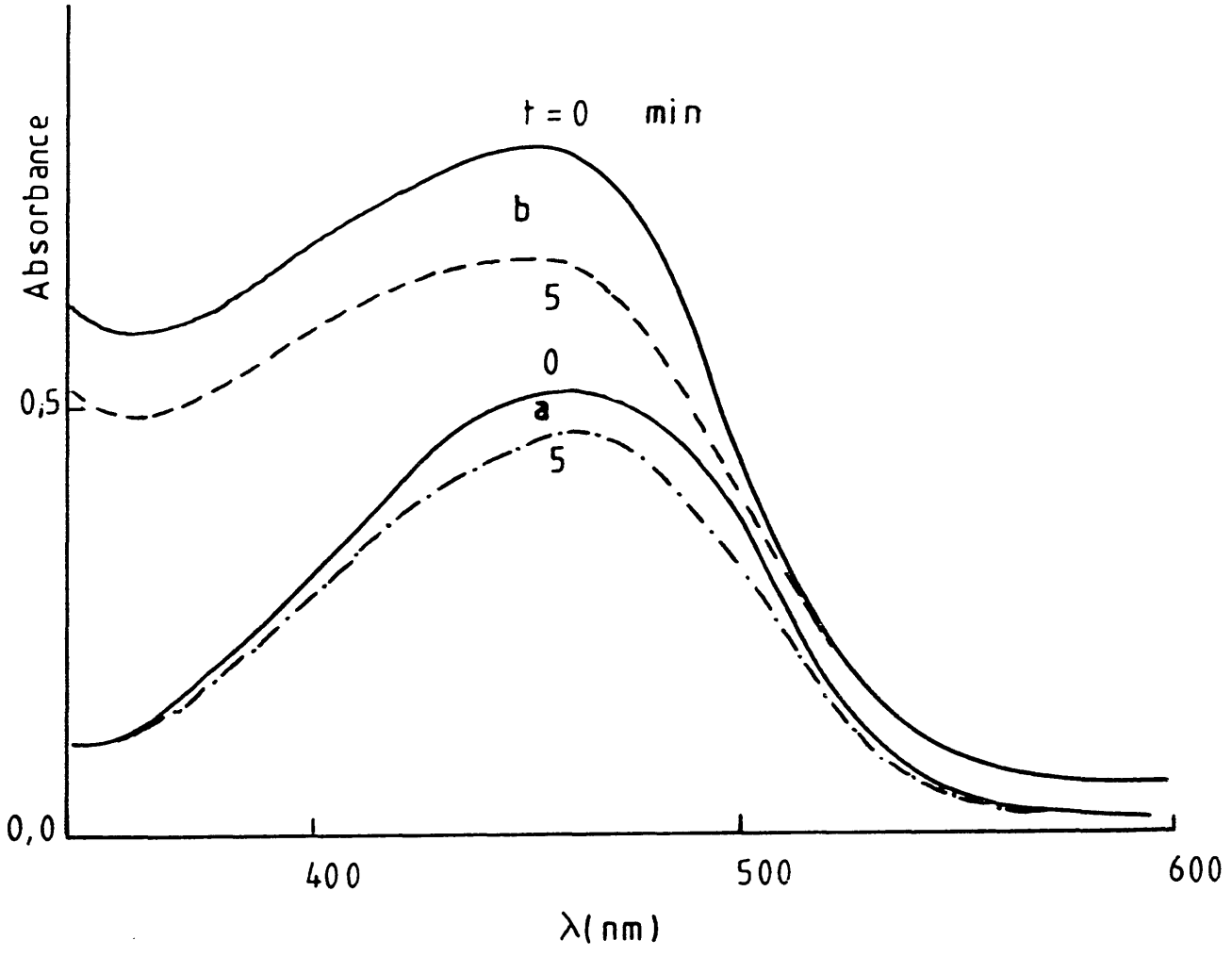


Fig. 6.21 Poly phosphate (SHMP = 10^{-2} M) effect on the photo-oxidation of methyl orange in the presence of CdS film (10^{-2} M) and MV^{2+} (6×10^{-4} M):

b) without CdS film as a reference

a) with CdS film as a reference.

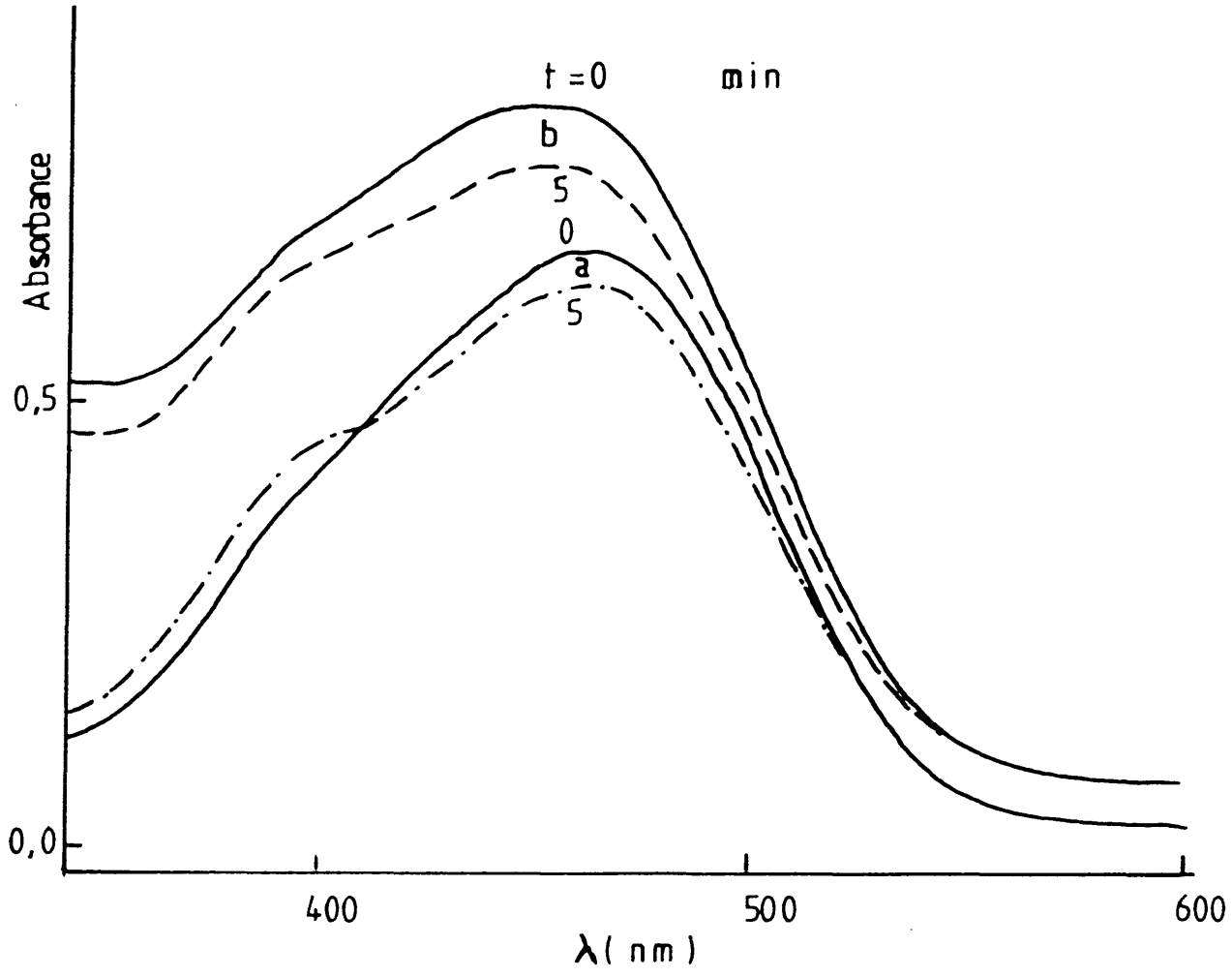


Fig. 6.22 Supported CdS effect on the photo-oxidation of MO(5×10^{-5} M), (conditions as Fig. 6.19).

colloidal semiconductors was discussed. The photo-physical and -chemical behaviour of this system was studied using Flash photolysis (FP) and steady state (SS) techniques. Using these techniques we optimised the CdS film with respect to the colloidal CdS soslution. The study of photophysical properties of CdS film, prepared by different methods and from different cadmium salts, revealed that the smaller CdS particles were formed using Na_2S instead of H_2S and that high absorption was obtained using cadmium sulfate ($CdSO_4$).

The photochemical properties of CdS film were studied using some electron-donors and -acceptors. Photoreduced methyl viologen (MV^+) and doubly-reduced methyl viologen ($MV^\bullet$), were observed in the SS technique. Methyl viologen efficiently quenched the red emission of CdS film. Photocorrosion of CdS film was studied in the presence of oxygen.

The photocorrosion effect was completely prevented using cysteine ($10^{-2}moldm^{-3}$) as an electron donor. Photo-oxidation of methyl orange was observed using CdS film in the presence of oxygen. The effects of an electron donor (cys), electron acceptor (MV^{2+}) and supporting agent (SHMP), either individually or in combination on the yield of photo-oxidised methyl orange were studied.

These results indicate that the method developed for immobilising CdS particles in the DM yields an excellent medium to study both photo-physical and -chemical properties of small, trapped CdS particles. It will be important in developing an understanding of the important photoreactions involved in solar energy conversion and storage.

CHAPTER 7

Modified Electrode

This chapter considers briefly polypyrole (PPy) modified electrodes and incorporation of CdS particles into PPy film.

Introduction

In the last decade, interest in the field of conducting polymers has dramatically increased.[241-290] Most electrodes which have been modified with these polymers have made use of the Polyvinyl system.[240] Unfortunately they are not sufficiently conductive to achieve a useful current density. Electronically conducting polymers, such as PPy, can significantly improve the stability of n-type semiconductors, such as CdS, against photoanodic dissolution in an electrolyte during photoelectrochemical reactions.[241-249, 271, 289-290] The mechanism of stabilisation involves the high conductivity and large capacitance (the number of oxidised molecules per monomer unit) of the polymer and the presence of electroactive redox species to efficiently trap the photogenerated holes before they react with the semiconductor to destroy it.

7.1 Chemical Modification of Electrodes

When an electrode, such as carbon or platinum, is dipped into a solution containing some species, its surface becomes

covered with a layer of species' molecules. The presence of such adsorbed species will often modify the electrochemical behaviour of the electrode. Figure 7.1 shows how electron transfer occurs at the modified electrode. The discovery of conducting polymers such as polysulfur nitride, $(SN)_n$,[250] and doped polyacetylene, $(CH)_n$,[251] has encouraged the search for other polymeric systems with greater conductivity and chemical stability.

Polypyrole (PPy), as a conducting polymer, has been studied for many years.[252-254] Since 1979, worldwide research has been carried out on the use of PPy film for different purposes and many papers, describing their preparation, physical and chemical properties and their behaviour as modified electrodes, have been published.[255-290] In the following section, we consider the different methods of preparation of modified electrodes.

7.2 Preparation Techniques

Modified electrodes can be prepared by several different techniques as below:

7.2.1 Chemisorption

Some species find the surface of the electrode more hospitable than the bulk solution and so at most a monolayer coat (about 10^{-2}molcm^{-2} or 6×10^{13} molecules cm^{-2}) attaches spontaneously to the surface. For example, organic species

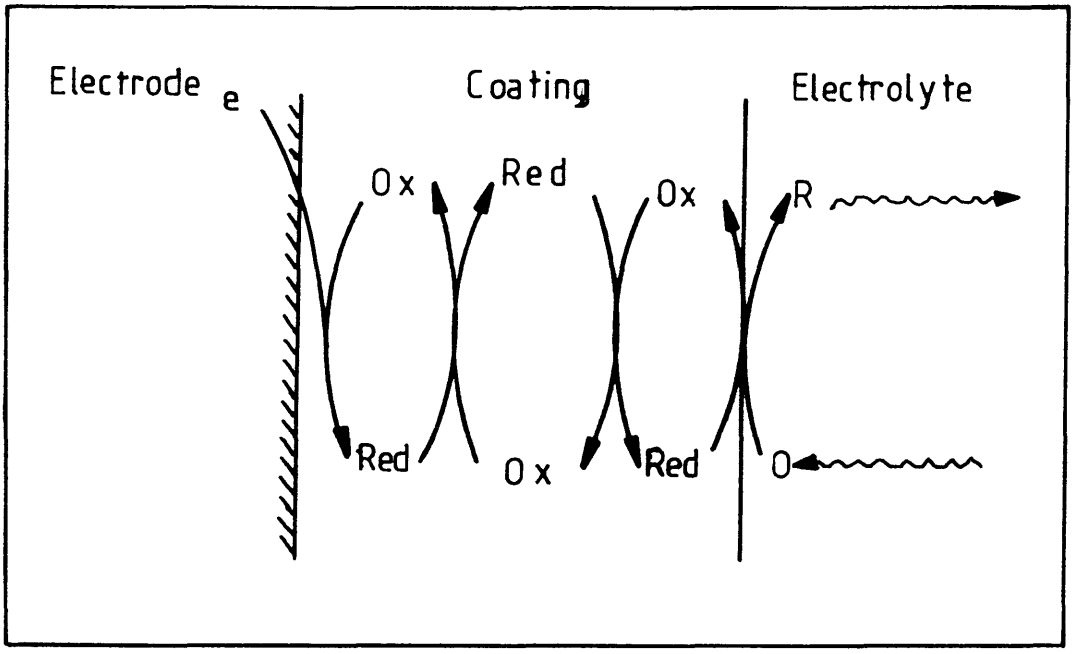


Fig. 7.1 Schematic diagram of mediated electron transfer at a chemically-modified electrode.

containing double bonds are often hydrophobic and strongly adsorb from aqueous solutions on carbon or platinum surfaces. This method has frequently been used for modification of electrodes by porphyrin[291] and polypyridine.[293]

7.2.2 Covalent Attachment

In this technique covalent bonds are formed between the electrode and the molecules (Figure 7.2). The electrode surface can be "silanised" by reaction with an organosilane and subsequently with another molecule of interest. In this case the silane is a means of immobilisation of the molecule at the surface. This method has been employed by many workers and is generally restricted to monolayer coats.

7.2.3 Polymer film

By dipping the electrode into a solution containing a dissolved polymer and leaving the solvent to evaporate , a thin film forms (ca. o.1 - 10 μm) on the surface of the electrode. The best method for producing more uniform film , which is also used in the production of semiconductor chips, is spin _ coating. In this method the rotation speed of electrode into solution is as low as 1 to 4 Hz and the applied potential on the electrode sweeps during the deposition of film on the surface.

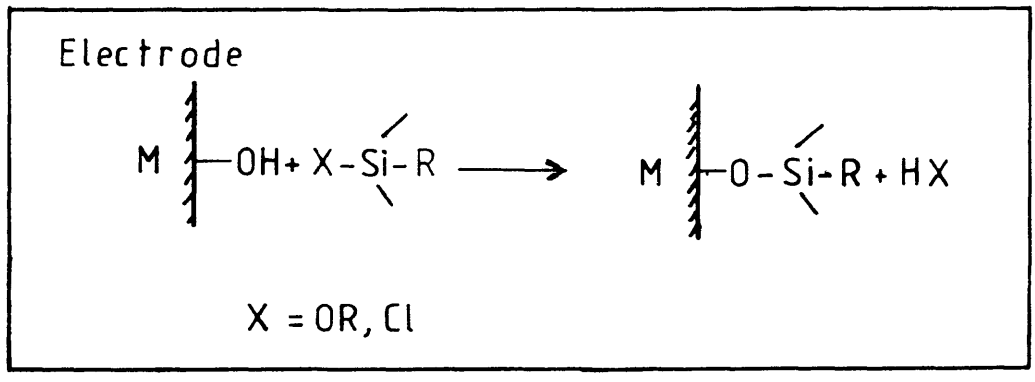


Fig. 7.2 Schematic diagram of an electrode modified by covalent attachment techniques [Ref.298].

7.3 Characterisation

After the modification of the electrode surface, one must prove that the desired polymer has been made and find out about the properties and nature of the layer. Since one may be dealing with a very small amount of material on the surface, rather sensitive analytical techniques are required. To learn about the composition and structure of the layers or chemical and physical properties, several different methods are available.

7.3.1 Electrochemical Method

Using electrochemical techniques even monolayer amounts of material can be analysed, since small currents can be measured quite readily and, by Faraday's law, 10^{-10} moles of material per cm^2 is equivalent to about 10^{-5} coulombs (n=1). Thus, the cyclic voltammetry of a monolayer of material, as shown in Fig. 7.3, will demonstrate a peak with an integrated area equivalent to that amount of material on the electrode surface. The position of the peak on this potential axis is a direct measure of the redox potential of the couple on the surface. For thicker layers (n=2,3...), the electrochemical response will show larger integrated areas, representing greater amounts of material on the electrode surface.

7.3.2 Spectroscopic Techniques

Electron spectroscopy, such as X-ray photoelectron and Auger electron spectroscopy, can be used for an analysis of the elements present in the surface layers. Direct optical spectroscopic measurements in the visible, IR and UV regions are also possible, either by absorption, when the films are on a transparent electrode substrate, or by reflectance for metal substrates.

7.3.3 Other Methods

Direct observation of the surface by optical or scanning

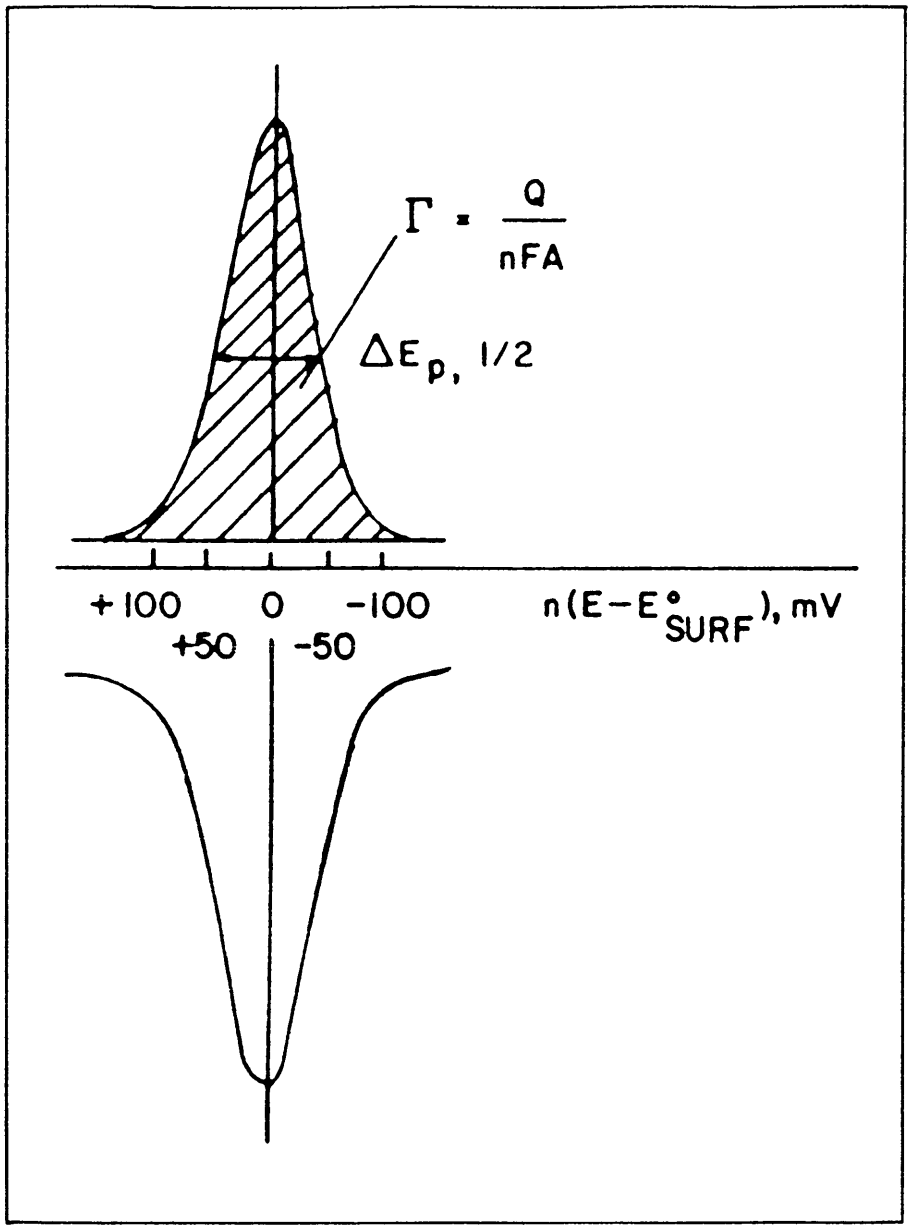


Fig. 7.3 The ideal cyclic voltammogram of a monolayer of material.

Γ: the amount of material on the electrode

Q: in coulombs

n: the number of electrons in the electrode reactions

F: Faraday constant

A: the electrode area. [Ref.298]

electron microscopy is often useful for multilayer films to provide information about the texture and porosity of the layers. An important measurement that is difficult to make is the determination of the thicknesses of the layers. Techniques for measuring hard, dry, films with thicknesses greater than 10nm have been developed for applications in semiconductor technology. But applying such techniques to the softer films on electrode surfaces cause problems because such films change dimension when they are immersed in the electrolyte solution. Therefore measurements of dry coat thickness can only be considered as rough estimates for the thickness as used under electrochemical conditions.

7.4 Applications

Recently conducting organic polymers have generated widespread interest as potential choice materials for a variety of applications. However, the utilisation of electrodes modified by such conducting polymers is described briefly below:-

7.4.1 Electrocatalysis

Many reactions such as the reduction of oxygen or the oxidisation of natural gas components to CO_2 (for use in fuel cells), do not occur readily at inexpensive electrode surfaces such as carbon.[298] For example, the rate of oxidation of ascorbic acid is dramatically improved at electrodes coated with cationic fixed site polypyrrole films, when compared to that of

naked glassy carbon electrodes.[283] Thus, it is necessary to catalyse these reactions by introducing suitable, stable layers to the electrode surface. The electrocatalytic properties of the surface modification of semiconductors was also examined using transition metals (pt, Rh, RuO_2) immobilised in polymer films such as polystyrene.[271]

7.4.2 Electronic Devices

Electrodes in electrochemical cells that change colour or emit light when excited electrically are of interest in the production of displays for electronic devices.[298] This type of modified electrode with polymer layers, which can change colour when they are oxidised or reduced, is called an electrochromic system. For example, modification of Au microelectrode arrays by oxidation of pyrrole and N-Methylpyrrole fabrices molecule-based electronic devices.[299] Since the reduced form of these polymers are insulating and the oxidised forms are electronically conducting, it is possible to prepare electronic devices that are analogous to diodes and transistors using adjacent microelectrodes connected with polymer.

7.4.3. Batteries

During the last decade, worldwide research has been carried out on the use of polymer films for reversible electrodes in secondary batteries.[286, 304-310] The main emphasis has been on polymeric batteries either with polyacetylene as the cathode

active material and Li as the anode.[304, 308] It has been found that the polyacetylene electrode has some stability problems. Polypyrrole films have been chosen as polymer films for this purpose, since when PPy is electrochemically oxidised, it changes from an insulator into a highly electronically conductive polymer. Therefore PPy cells[286] can be used as secondary batteries.

7.4.4 Photoelectrochemical Applications

The utilisation of polymeric materials in this field of solar energy conversion[275, 285] and protection of semiconductor photoannodes[241-249, 289-290] in photoelectrochemical cells is attracting much attention. Techniques for surface modification are useful in preventing photodegradation in semiconductor electrodes. For example, a silicon electrode upon immersion in an aqueous solution usually rapidly forms an insulating oxide layer that prevents useful operation of the cell. In aqueous solution, water plays a key role in the solvation of electrode lattice ions or supplies oxygen for forming passive oxide layers.[300-303] In principle, the absence of a liquid electrolyte may increase the stability of the photoelectrochemical cell for operation in an energy conversion scheme. When a layer of the electronically conductive polymer such as polypyrrole is deposited on the electrode surface, the semiconductor electrode shows much more stable behaviour. Modification of semiconductors can also improve the efficiency of

solar energy conversion to electricity and can be employed to incorporate catalysts on the electrode to promote desired reactions.[298]

In the following sections we describe our results with regard to the modification of a platinum electrode surface using CdS colloids immobilised within polypyrrole.

7.5 Experimentals

7.5.1 Electrodes

A platinum rotating ring disc electrode (RRDE) was selected as the working electrode whose surface was to be modified with polypyrrole. It was initially polished mechanically using a rotating polishing disc across which the electrode was swept by an arm. The polishing procedure was carried out as follows:-

(i) 25, 6 and 3μm diamond lapping compounds respectively,

(ii) Hand polishing using a slurry of 1 μm alumina in doubly distilled water with a cotton wool.

(iii) Final hand polishing using a 0.3μm alumina to a mirror finish.

The reference electrodes were home-made Ag/Ag^{+} or saturated colomel electrodes (SCE).

The counter electrode was platinum gauze.

Electronics and the rotation system have been described in the second chapter.

7.5.2 Cell Assembly

The cell was a glass vessel of capacity 125cm^3 with an outer jacket through which water was pumped for thermostatting purpose. All experiments were carried out at 25^oC. A side arm carried the counter electrode compartment which was separated by a glass frit to exclude the products of the counter electrode reaction from the working electrode. A teflon led covered the upper side of the cell and had holes for the working and reference electrodes and also a hole for a teflon tube leading nitrogen through the solution (Figure 2.17).

7.5.3 Purification

Deionised and doubly-distilled water (DDW) was prepared through a Millipore Milli-Q filter system.

Pyrole was distilled around 130^oC under an inert atmospher and colourless purified pyrole was stored in a refrigerator under argon.

7.6 Incorporation of CdS in Polypyrole Films

We have shown that conducting polymers such as polypyrrole (PPy) have been used to protect semiconductor photoanodes. Interestingly, this polymer (PPy) can be modified by inclusion of catalytic agents in order to improve the surface kinetics for the oxidation process that occurs at the semiconductor photoanode.[289]

Inclusion of metallic particles such as cadmium, cobalt, copper, lead, nickel, palladium, platinum, silver or zinc in conducting polymer films have been reported by several authors.[272, 311-313] As far as we know, no report has been published about immobilisation of CdS particles in PPy.

From this point of view we have studied the modification of a platinum electrode by immobilising CdS particles within a film of PPy on the surface. This system was expected to have some advantages as below:-

(i) modification of metal surface by semiconductor;

(ii) obtaining Shotteky barrier for solar energy conversion;

(iii)protecting semiconductor photoelectrode from corrosion;

(iv) catalysing photoelectrochemical reactions.

Preparation of such catalyst-containing films will be considered in the following section. The generally accepted structure of the polypyrrole chain is shown in Figure 7.4.

7.6.1 Coating Procedure

In order to prepare immobilised CdS within PPy film on the surface of a Pt-electrode, two different methods were employed as below:

(i) In the first method PPy film was prepared by electrochemical oxidation of pyrrole on a platinum electrode in a three-electrode electro-chemical cell, where the reference electrode was either a saturated calomel electrode (SCE) for aqueous solutions or a silver/silver ion (Ag/Ag^+) electrode for non-aqueous solutions and the counter electrode was

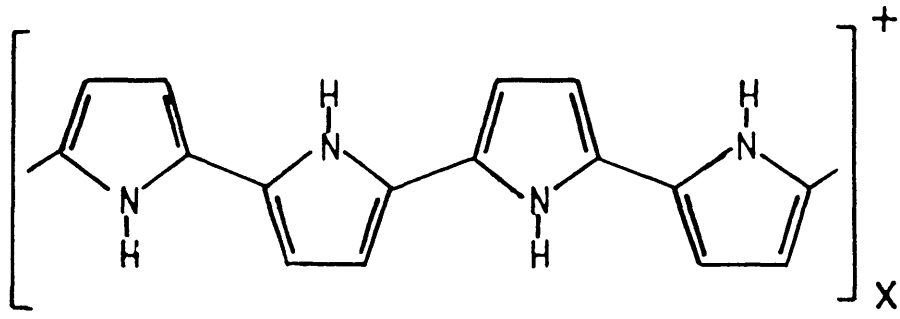


Fig. 7.4 The structure of polypyrrole.

platinum gauze. The electrolytic solution consisted of purified, deoxygenated acetonitrile containing 0.1mol dm^{-3} Tetrabutylammonium tetrafluoroborate [(TBTA):[CH_3 CH_2 CH_2 $CH_2)_4$ N (BF_4)] as a supporting electrolyte and $5x10^{-2}moldm^{-3}$ distilled pyrrole.

When the applied potential for oxidation of pyrrole was between 0.1 and 0.80V and the rotation speed of the working electrode was adjusted to 1Hz, we obtained an adherent shiny coat on the surface. Its colour changed from yellow to blue and then black by extending oxidation and thereby increasing the thickness of the film.

When the applied potential was increased up to 1.0V, a black PPy film was quickly formed, indicating a thick coat.

From our results in Chapter 6 where CdS particles were immobilised in DM, we expected to be able to immobilise them in PPy film also. In an attempt to immobilise CdS particles on the surface of an electrode modified by PPy, the former non-aqueous solution containing acetronitrile, TBAT and PPy was replaced by fresh colloidal CdS ($10^{-3}moldm^{-3}$) containing sodium nitrate ($0.1moldm^{-3}$) as a background electrolyte under an oxygen-free atmosphere. The modified electrode was immersed in this solution with a rotation speed of 1Hz. The experiments were carried out at room temperature.

In order to investigate whether the colloidal particles were incorporated into the film or not, the easiest way is to observe a thin yellow layer of CdS colloids within the PPy film. This was difficult to investigate because the PPy

film was either yellow (thin coat) or black (thick coat). Another way was to study the CV behaviour of the modified electrode.

(ii) In the second method, PPy ($5x10^{-2}moldm^{-3}$) was injected into a fresh solution containing CdS colloids ($10^{-3}moldm^{-3}$) and sodium nitrate ($0.1moldm^{-3}$), and the platinum plate ($1cm^{3}$) acting as a working electrode was immersed in the solution. The rotation speed was selected as 4Hz. The experiment was carried out at room temperature under nitrogen atmosphere to remove oxygen from the solution. By applying a potential in the range of 0.0-0.8V, electrodeposition of PPy from aqueous solution on the platinum plate was observed. The pH of solution was 7.5.

7.6.2 Results

In the first method, when the platinum electrode was coated by PPy film and then immersed in CdS solution, surprisingly we observed deactivation of the electrode modified by PPy film in every cycle of the CV technique.

Figure 7.5 shows the cyclic voltammetry of PPy in a fresh solution of CdS colloids under deoxygenated conditions. This figure shows that the activation of the modified electrode decreases in every cycle. This effect was greater with increasing rotation speed and with illumination of the solution and electrode by the Xenon lamp.

In the second method, to detect the presence of CdS

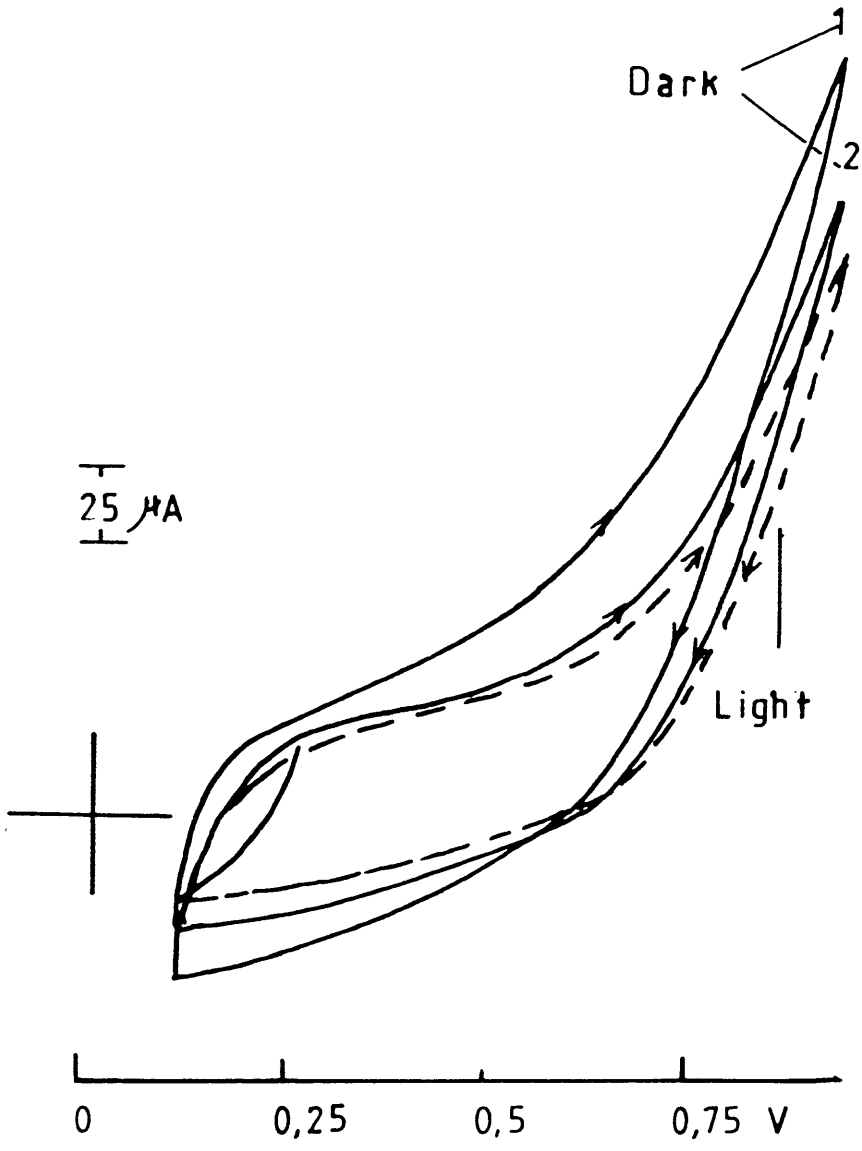


Fig. 7.5 Cyclic voltammogram of Pt-electrode modified by PPy.

particles on the surface of PPy film, we used scanning electron microscopy (SEM). Using SEM analysis revealed that no CdS particles existed on the surface of the electrode modified by PPy film. So it seems likely, CdS particles are not immobilised within PPy film. Cyclic voltammetry curves in the second method were similar to those of the first method, we can suggest that in the first method as well as the second method, no CdS particles were incorporated into the PPy film.

7.7 Conclusion

Photo-electrochemical studies of modified electrodes are leading to better understanding of charge transfer reactions through surface layers. The study of modified electrodes using immobilised n-type semiconductors within an electronically-conducting polymer remains field of high activity. Our results for photo-electrodeposition of CdS onto polypyrrole reveals that n-type semiconductors such as CdS cannot be doped onto Polyrrole. These results also leads us to suggest that the PPy films formed in our experiemnts were possibly free of pores.

Appendix 1

Sinclair Basic programme used to analyse the kinetic data in terms of first and second order reactions using a least squares fit.

```
    1 REM PRINT AT 0,0;IN 63: GO
TO 1
    2 REM IF12
    5 DEF FN T()=((65536*PEEK 236
74+256*PEEK 23673+PEEK 23672)/50
): REM TIME IN SECONDS
   20 OUT 63,5: CLEAR 60000: DIM
A(10): DIM B(5,450)
   30 LET R=60000: LET A=63
   35 REM GO SUB 9500
   36 PRINT AT 5,5;"BIAS = ";IN 6
3;"      ": PRINT AT 10,5;"This s
hould be 125. Press S when set"
  IF INKEY$="s" THEN GO TO 40
   37 GO TO 36
   40 LET bias=IN 63
   41 PRINT AT 0,0;"STOP(1) ANALY
SE(2) OR INPUT(3) ?
                    ": INPUT A(1)
   50 IF A(1)=1 THEN GO TO 5000
   60 IF A(1)=2 THEN GO TO 141
   72 PRINT AT 0,0;"Enter one wor
d name of data      ": INPUT a$
   79 CLS
   80 REM INPUT DATA
   81 PRINT AT 0,0;"TIME PER CM (
ms) ?                ": INPUT
A(5): PRINT AT 0,0;"Enter mV/cm
                    ": INPUT S
   82 IF IN A>(bias+5) THEN GO TO
 90
   83 IF IN A<(bias-5) THEN GO TO
 90
   84 GO TO 82
   90 PRINT AT 0,0;"Transfering D
ata"
   91 POKE 23674,0: POKE 23673,0:
 POKE 23672,0
   92 FOR N=0 TO 400
   95 POKE R+N,IN A
  116 NEXT N
  117 PRINT "TIME = ";FN T(): PAU
SE 200
  120 GO SUB 6000
  122 PRINT AT 0,0;"Set baseline
using u, d, r and lkeys.  Press
s when complete."
  123 LET x=25: LET y=5: GO SUB 6
000
  124 LET baseline=(y+20)*200/150
  140 GO TO 40
  141 REM CONVERSION OF I TO O.D.
  148 PRINT AT 0,0;"Use keys r, l
, u and d to move  start."
  149 PRINT "Press s when start s
elected."
  150 LET x=20: LET y=75: GO SUB
8000
  160 LET A(9)=2+
  161 PRINT AT 0,0;"Use keys r, l
, u and d to selectend. Press s
when  end selected.
                    "
  162 IF INKEY$="s" THEN GO TO 16
2
  163 LET x=230: LET y=75: GO SUB
 8000
```

```
 165 LET A(2)=2*A
 170 PRINT AT 0,0;"Io Value in m
V (usually 880mV) ?
                                  INPUT
 A(4)
 185 PRINT AT 0,0,"Calculating O
ptical Density etc."
 187 LET A(5)=A(5)/40000: REM CO
NVERTS MS PER CM INTO US PER POI
NT FOR 400 POINTS PER 10 CM
 200 FOR Q=A(9) TO A(2)
 201 PRINT AT 1,15;Q
 205 LET B(1,Q)=S*((PEEK (R+Q))-
baseline)/25.5
 220 LET T=(Q-1)*A(5)
 230 LET B(5,Q)=T
 240 LET X=A(4)-B(1,Q)
 250 LET X=A(4)/X
 260 LET X=.434294*LN (X)
 270 REM X= DELTA O.D.
 280 LET B(2,Q)=X
 290 LET B(3,Q)=LN (ABS (X))
 300 LET B(4,Q)=1/ABS (X)
 310 NEXT Q
 320 CLS : PRINT "FIRST(1) OR SE
COND(2) OR QUIT(3)OR REANALYSE(4
) ?": INPUT A(6)
 330 IF A(6)=4 THEN GO SUB 6000
 331 IF A(6)=4 THEN GO TO 121
 340 IF A(6)=2 THEN GO TO 1000
 350 IF A(6)=3 THEN GO TO 40
 355 PRINT AT 0,0;"Calculating F
irst Order Rate    Constant
                    "
 360 LET T=0
 370 LET X=0
 380 FOR S=A(9) TO A(2)
 381 PRINT AT 1,15;S
 390 LET T=T+B(5,S)
 400 LET X=X+B(3,S)
 410 NEXT S
 420 LET V=A(2)-A(9)+1
 430 LET T=T/V
 440 LET X=X/V
 450 LET F=0
 460 LET G=0
 470 LET H=0
 480 FOR Q=A(9) TO A(2)
 481 PRINT AT 1,15;"    "
 482 PRINT AT 1,15;Q
 490 LET Z=B(3,Q)-X
 500 LET Y=B(5,Q)-T
 510 LET G=G+Z*Z
 520 LET Z=Z*Y
 530 LET F=F+Z
 540 LET H=H+Y*Y
 550 NEXT Q
 560 LET F=ABS (F)
 570 PRINT AT 0,0;"FIRST ORDER R
ATE CONSTANT=";
 580 PRINT F/H;
 590 PRINT "SEC-1                "
 600 PRINT "CORRELATION COEFFICI
ENT=";
 610 PRINT F/SQR (G*H)
 620 PRINT
 630 PRINT "PLOT FIRST ORDER DAT
A? (Y=1 N=2)": INPUT A(6)
 640 IF A(6)=1 THEN  GO TO 2000
 650 IF A(6)=2 THEN GO TO 320
1000 REM SECOND ORDER ANALYSIS
1005 PRINT AT 0,0;"Calculating s
econd order rate    constant
                    "
```

```
1010 LET T=0
1020 LET X=0
1030 FOR S=A(9) TO A(2)
1031 PRINT AT 1,15;S
1040 LET T=T+B(5,S)
1050 LET X=X+B(4,S)
1060 NEXT S
1065 LET V=A(2)-A(9)+1
1070 LET T=T/V
1080 LET X=X/V
1090 LET F=0
1100 LET G=0
1110 LET H=0
1120 FOR Q=A(9) TO A(2)
1121 PRINT AT 1,15;"    "
1122 PRINT AT 1,15;Q
1130 LET Z=B(4,Q)-X
1140 LET Y=B(5,Q)-T
1150 LET G=G+Z*Z
1155 LET F=F+Y*Z
1160 LET H=H+Y*Y
1170 NEXT Q
1180 PRINT AT 0,0;"SECOND ORDER
RATE CONSTANT=";
1190 PRINT F/H;
1200 PRINT "M-15-1 (ASSUMING E=1
,L=1)"
1210 PRINT "CORRELATION COEFFICI
ENT=";
1220 PRINT F/SQR (G*H)
1230 PRINT "PLOT DATA ?(Y=1 N=2)
"; INPUT A(6)
1240 IF A(6)=1 THEN GO TO 2300
1250 IF A(6)=2 THEN GO TO 320
2000 REM PLOT FIRST ORDER DATA
2001 CLS
2005 PLOT 10,10: DRAW 230,0
2006 PLOT 10,10: DRAW 0,160
2080 PRINT AT 21,5;"TIME ";1000*
A(5);"ms/point"
2090 PRINT AT 0,0;"LN (DELTA O.D
.)"
2095 PRINT AT 2,10;a$
2100 FOR W=A(9) TO A(2)
2105 IF W/2>INT (W/2) THEN GO TO
 2195
2110 LET P=B(3,W)-B(3,A(9))
2120 LET P=150-(P*150/(B(3,A(2))
-B(3,A(9))))
2130 LET P=ABS (INT (P))
2190 PLOT ((W+1-A(9))*200/(A(2)-
A(9)))+10,P+10
2195 NEXT W
2200 PRINT AT 17,5;"k =";
2201 PRINT F/H;
2202 PRINT "S-1"
2220 PRINT AT 19,5;"CC=";
2221 PRINT F/SQR (G*H)
2222 PRINT AT 1,5;"COPY PLOT? (Y
=1 N=2)"; INPUT A(8)
2223 IF A(8)=1 THEN GO TO 2999
2224 IF A(8)=2 THEN GO TO 320
2300 REM PLOT SECOND ORDER DATA
2310 CLS
2315 PLOT 10,10: DRAW 230,0
2316 PLOT 10,10: DRAW 0,160
2390 PRINT AT 21,5;"TIME ";1000*
A(5),"ms/point"
2400 PRINT AT 0,0;"1/(DELTA O.D.
)"
```

```
2405 PRINT AT 2,4;a$
2410 FOR W=A(9) TO A(2)
2415 IF W/2>INT (W/2) THEN GO TO
 2490
2420 LET P=B(4,W)-B(4,A(9))
2430 LET P=P*150/(B(4,A(2))-B(4,
A(9)))
2440 LET P=ABS (INT (P))
2480 PLOT ((W+1-A(9))*200/(A(2)-
A(9)))+10,(P/1.2)+10
2490 NEXT W
2500 PRINT AT 2,2;"k2=";
2510 PRINT F/H;
2511 PRINT "M-1S-1"
2520 PRINT AT 4,2;"CC=";
2530 PRINT F/SQR (G*H)
2540 PRINT AT 1,5;"COPY PLOT ?(Y
=1 N=2)": INPUT A(8)
2550 IF A(8)=1 THEN GO TO 2999
2560 IF A(8)=2 THEN GO TO 320
2999 PRINT AT 1,5;"
          ": LPRINT : LPRINT : LPRI
NT : COPY : GO TO 320
5000 STOP
6000 REM Plot data
6001 CLS : PLOT 0,0: DRAW 255,0:
 PLOT 0,0: DRAW 0,170
6002 PRINT AT 2,1;"Voltage"
6003 PRINT AT 20,10;"Time"
6010 FOR N=1 TO 400
6020 IF N/2>INT (N/2) THEN GO TO
 6040
6030 PLOT N/2,((PEEK (R+N))-20)*
150/200
6040 NEXT N
6050 PRINT AT 0,0;"Copy Plot (Y=
1, N=2)": INPUT reply
6060 IF reply=2 THEN RETURN
6070 PRINT AT 0,0;a$;"
                    ": COPY : LPRIN
T : LPRINT : LPRINT
6075 LPRINT "mV/cm = ";S: LPRINT
   LPRINT "ms/cm = ";A(5)
6100 RETURN
8000 REM Move cursor
8020 PLOT x,y
8030 IF INKEY$="" THEN GO TO 803
0
8040 IF INKEY$="r" THEN GO TO 81
00
8050 IF INKEY$="l" THEN GO TO 82
00
8060 IF INKEY$="s" THEN RETURN
8065 IF INKEY$="u" THEN GO TO 91
00
8066 IF INKEY$="d" THEN GO TO 92
00
8070 GO TO 8030
8100 PLOT INVERSE 1;x,y: LET x=x
+1: GO TO 8020
8200 PLOT INVERSE 1;x,y: LET x=x
-1: GO TO 8020
9100 PLOT INVERSE 1;x,y: LET y=y
-1: GO TO 8020
9200 PLOT INVERSE 1;x,y: LET y=y
+1: GO TO 8020
9900 REM Test subroutine
9910 FOR n=0 TO 400
9920 POKE (R+n),130*EXP (-n*0.00
1)+30-2*RND
9930 NEXT n
9900 RETURN
```

Appendix 2

Sinclair Basic programme used to fit two exponentials to the kinetic data in chapter 3.

```
   1 REM Interfaced Dual Exponen
tial - IFDE
   2 LET c=0
  10 OUT 63,5: CLEAR 60000: DIM
B(5,450): DIM A(10): LET R=60000
: LET A=63
  11 REM  GO SUB 1000
  20 PRINT AT 0,0;"Stop (1), Ana
lyse (2), Input(3) or Reanalyse(
4) ?": PRINT "
                          ": INPUT A(
1)
  30 IF A(1)=1 THEN STOP
  40 IF A(1)=2 THEN GO TO 65
  45 IF A(1)=4 THEN GO TO 64
  50 IF A(1)=3 THEN GO SUB 200
  60 GO TO 20
  64 GO SUB 250
  65 GO SUB 400
  70 GO SUB 500
  75 GO SUB 550
  80 GO SUB 600
  90 GO SUB 700
 100 GO SUB 800
 105 PRINT AT 0,0;"Calculate Chi
square (y=1,n=2) ?": INPUT A(1)
 106 IF A(1)=2 THEN GO TO 20
 107 IF A(1)=1 THEN GO TO 110
 108 GO TO 105
 110 GO SUB 900
 120 GO TO 20
 150 STOP
 200 REM Input data
 205 CLS : PRINT AT 0,0;"Enter n
ame of data": INPUT a$: CLS
 210 IF IN A>150 THEN GO TO 220
 211 IF IN A<100 THEN GO TO 220
 212 GO TO 210
 220 FLASH 1: PRINT AT 0,0;"TRAN
SFERING ";a$: FLASH 0
 221 FOR N=0 TO 400
 230 POKE (R+N),IN A
 240 NEXT N
 250 REM Plot data
 251 CLS : PLOT 0,0: DRAW 255,0:
 PLOT 0,0: DRAW 0,170: PRINT AT
2,1;"Voltage": PRINT AT 20,10;"T
ime"
 260 FOR N=0 TO 400
 262 LET Y=(PEEK (R+N)-25)*175/2
05
 263 IF Y>175 THEN NEXT N
 264 IF Y<0 THEN NEXT N
 265 PLOT N/2,Y
 266 NEXT N
 270 PRINT AT 0,0;"Copy Plot (y=
1,n=2) ?": INPUT A(1)
 271 IF A(1)=2 THEN GO TO 300
 272 IF A(1)=1 THEN GO TO 274
 273 GO TO 270
 274 PRINT AT 0,0;a$;"
                          ": COPY : LP
RINT : LPRINT : LPRINT
 300 REM Set baseline
 301 PRINT AT 0,0;"Enter mV per
cm.
                          ": INPUT S
 302 PRINT AT 0,0;"Set baseline
with U,D,L and R   keys": PRINT
"Press S when complete."
 303 LET X=25: LET Y=15: GO SUB
2000
 304 LET BASELINE=(Y*205/175)+25
 305 RETURN
```

```
 400 REM Conversion of voltages
to LN ABS(delta OD)
 401 PRINT AT 0,0;"Set START (t=
0) with U,D,L and R keys      ":
 PRINT AT 1,0;"Press S when comp
lete."
 402 LET X=20: LET Y=75: GO SUB
2000
 403 LET T0=2*X
 404 PRINT AT 0,0;"Set END (t=oo
) with U,D,L and R keys": PRINT
"Press S when complete."
 405 IF INKEY$="s" THEN GO TO 40
5
 406 LET X=200: LET Y=75: GO SUB
 2000
 407 LET T1=2*X
 408 PRINT AT 0,0;"Io value in m
V (usually 880mV) ?
                          ": INPUT A(4
)
 409 PRINT AT 0,0;"Time per cm i
n ms ?                    "
: INPUT A(5)
 410 FLASH 1: PRINT AT 0,0;"CALC
ULATING OPTICAL DENSITIES
                                ": F
LASH 0
 411 LET A(5)=A(5)/40100: REM Co
nverts ms/cm to s/point for 401
points in 10cm
 412 FOR N=T0 TO T1
 413 PRINT AT 1,15;N
 414 LET B(1,N)=S*((PEEK (R+N))-
BASELINE)/25.5: LET B(5,N)=(N-T0
)*A(5): LET X=A(4)/(A(4)-B(1,N))
: LET B(2,N)=0.434294*LN (X): LE
T B(3,N)=LN (ABS B(2,N))
 415 NEXT N
 416 REM B(5,N)=Time from T0 in
seconds
 420 RETURN
 500 REM Plot LN ABS(Delta OD)
 501 CLS : PLOT 10,10: DRAW 230,
0: PLOT 10,10: DRAW 0,160: PRINT
 AT 21,5;"Time ";1000*A(5);" ms/
point": PRINT AT 0,0;"LN(OD/ODma
x)": PRINT AT 2,10;a$
 503 FOR N=T0 TO T1
 504 LET P=B(3,N)-B(3,T1): LET P
=P*165/(B(3,T0)-B(3,T1)): LET P=
10+ABS (P)
 505 IF P>175 THEN NEXT N: IF P<
10 THEN NEXT N
 507 PLOT 10+N/2,P
 508 NEXT N
 510 RETURN
 550 REM Set START1,2 and END1,2
 551 PRINT AT 0,0;"Set START1 wi
th U,D,L and R keys": PRINT "Pre
ss S when complete."
 552 LET X=25: LET Y=25: GO SUB
2000
 553 LET START1=(X-10)*2
 554 PRINT AT 0,0;"Set END1 with
 U,D,L and R keys      ": PRINT "P
ress S when complete."
 555 LET X=100: LET Y=25: GO SUB
 2000
 556 LET END1=(X-10)*2
 557 PRINT AT 0,0;"Set START2 wi
th U,D,L and R keys": PRINT "Pre
ss S when complete."
 558 LET X=100: LET Y=25: GO SUB
 2000
 559 LET START2=2*(X-10)
 560 PRINT AT 0,0;"Set END2 with
 U,D,L and R keys      ": PRINT "P
ress S when complete."
 561 LET X=200: LET Y=25: GO SUB
 2000
 562 LET END2=2*(X-10)
 563 RETURN
```

```
 600 REM Calculate K2 and interc
ept
 601 FLASH 1: PRINT AT 0,0;"CALC
ULATING K2
                      FLASH 0
 602 LET A=0: LET B=0: LET C=0:
LET D=0: LET E=0: LET V=1+END2-S
TART2
 603 FOR N=START2 TO END2
 604 PRINT AT 1,15;N
 605 LET A=A+B(3,N)*B(3,N)
 606 LET B=B+B(5,N)*B(5,N)
 607 LET C=C+B(3,N)
 608 LET D=D+B(5,N)
 609 LET E=E+B(3,N)*B(5,N)
 610 NEXT N
 619 LET K2 = -(V*E-D*C)/(V*B-D*
D)
 620 PRINT AT 0,0;"K2 = ";K2;" s
-1"
 630 PRINT "CC = ";(V*E-D*C)/SQR
 ((V*B-D*D)*(V*A-C*C))
 634 LET INTERCEPT2=(B*C-D*E)/(V
*B-D*D)
 635 LET OD2=EXP (INTERCEPT2)*AB
S (B(2,T0))/B(2,T0)
 640 PRINT "OD2 = ";OD2
 650 PRINT : PRINT : PRINT "COPY
 ? (Y/N)": INPUT a$
 655 IF a$="y" THEN LPRINT "K2=
",K2;"s-1","OD2 =",OD2,"CC =",(V
*E-D*C)/SQR ((V*B-D*D)*(V*A-C*C)
)
 660 RETURN
 700 REM Recalculate OD for fast
 section
 701 LET B=0: LET C=0: LET D=0:
LET E=0: LET F=0: LET OD2=EXP (I
NTERCEPT2)*ABS (B(2,T0))/B(2,T0)
 705 FOR N=START1 TO END1
 706 LET DELTA=OD2*EXP (-K2*B(5,
N)): LET B(4,N)=LN ((B(2,N)-DELT
A)*(ABS (B(2,T0))/B(2,T0)))
 719 FLASH 1: PRINT AT 0,0;"CALC
ULATING K1": FLASH 0: PRINT "


"
 720 LET F=F+B(4,N)*B(4,N): LET
B=B+B(5,N)*B(5,N): LET C=C+B(4,N
): LET D=D+B(5,N): LET E=E+B(4,N
)*B(5,N)
 725 NEXT N
 726 LET V=1+END1-START1
 730 LET K1=-(V*E-D*C)/(V*B-D*D)
: LET INTERCEPT1=(B*C-D*E)/(V*B-
D*D)
 731 LET OD1=EXP (INTERCEPT1)*AB
S (B(2,T0))/B(2,T0)
 734 PRINT "k1 = ";K1;"(s-1)": P
RINT "OD1 = ";OD1: PRINT "Corr.
Coef. = ";(V*E-D*C)/SQR ((V*B-D*
D)*(V*F-C*C))
 735 PRINT "COPY ? (y/n)": INPUT
 a$
 736 IF a$="y" THEN GO TO 738
 737 RETURN
 738 LPRINT "k1 = ";K1;"(s-1)":
PRINT "OD1 = ";OD1: LPRINT "Corr
. Coef. = ";(V*E-D*C)/SQR ((V*B-
D*D)*(V*F-C*C))
 739 REM B(4,N) now equals LN AB
S(Corrected OD)
 740 RETURN
```

```
 800 REM Plot calculated curves
and data
 801 GO SUB 500
 810 FOR N=T0 TO T1
 811 LET Y=OD1*EXP (-K1*B(5,N))+
OD2*EXP (-K2*B(5,N)): LET B(4,N)
=LN ABS (Y)
 815 PRINT AT 10,10;N
 820 NEXT N
 830 REM B(4,N) now equals LN AB
S(Calc. OD)
 835 FOR N=T0 TO T1
 836 PRINT AT 10,10;N  .
 840 LET P=B(4,N)-B(4,T1): LET P
=P*165/(B(4,T0)-B(4,T1)): LET P=
10+ABS (P)
 841 IF P>175 THEN NEXT N: IF P<
10 THEN NEXT N
 842 PLOT 10+N/2,P
 845 NEXT N
 850 PRINT AT 0,0;"Copy data (y=
1 n=2) ?

": INPUT A(1)
 851 IF A(1)=2 THEN RETURN
 852 IF A(1)=1 THEN GO TO 854
 853 GO TO 850
 854 LPRINT "OD = ODmax*[A*exp(-
k1*t)+(1-A)*exp(-k2*t)]": LPRINT
 : LPRINT "k1 = ";K1;" s-1": LPR
INT "k2 = ";K2;" s-1": LPRINT "A
  = ";INTERCEPT1/(INTERCEPT1+INT
ERCEPT2): LPRINT : LPRINT : COPY
 : LPRINT : LPRINT
 860 RETURN
 900 REM Calculate Reduced Chisq
uare
 901 LET CHI=0
 905 FOR N=T0 TO T1
 906 PRINT AT 0,10;N
 910 LET Y=OD1*EXP (-K1*B(5,N))+
OD2*EXP (-K2*B(5,N))
 915 LET CHI=CHI+(B(2,N)-Y)*(B(2
,N)-Y)/(0.0025*(T1-T0+1))
 920 NEXT N
 930 REM Assumes sigma=0.05 henc
e sigma squared=0.0025
 931 PRINT "Reduced Chi = ";CHI
 935 PRINT "Print CHI ? (Y=1 N=2
)": INPUT q
 936 IF q=1 THEN GO TO 940
 937 IF q=2 THEN GO TO 950
 938 GO TO 935
 940 LPRINT "Reduced Chi =";CHI:
 LPRINT : LPRINT
 950 REM Residuals
 955 CLS : PLOT 0,0: DRAW 0,175:
 PLOT 0,80: DRAW 255,0: PRINT AT
 5,10;"RESIDUAL PLOT": PRINT AT
0,0;"10000*R": PRINT AT 14,16;"T
ime"
 960 FOR N=T0 TO T1
 961 LET R=(B(2,N)-OD1*EXP (-K1*
B(5,N))-OD2*EXP (-K2*B(5,N)))
 962 LET R=80+10000*R
 963 IF R>175 THEN NEXT N
 964 IF R<0 THEN NEXT N
 965 PLOT (N-T0)/2,R
 966 PRINT AT 0,13;N
 970 NEXT N
 975 FLASH 1: PRINT AT 20,2;"COP
Y (y=1 n=2) ?": FLASH 0: INPUT A
(1)
 976 IF A(1)=2 THEN RETURN
 977 IF A(1)=1 THEN GO TO 980
 978 GO TO 975
 980 PRINT AT 20,2;"
                                ": COP
Y
 999 RETURN
```

```
1000 REM Synthesise data - if ti
me per cm=1ms then k1=2005 and k
2=200.5
1001 FLASH 1: PRINT AT 0,0;"GENE
RATING DATA": FLASH 0
1002 FOR n=0 TO 400
1003 POKE (R+n),(25+(150*(0.4*EX
P (-0.05*n)+0.6*EXP (-0.005*n)))
: PRINT AT 1,0;N
1004 NEXT N
1005 RETURN
1999 REM Move Start and Stop
2000 IF INKEY$="3" THEN GO TO 30
00
2001 PLOT X,Y
2002 IF INKEY$="" THEN GO TO 200
2
2003 IF INKEY$="r" THEN GO TO 21
00
2005 IF INKEY$="l" THEN GO TO 22
00
2006 IF INKEY$="s" THEN RETURN
2007 IF INKEY$="u" THEN GO TO 23
00
2008 IF INKEY$="d" THEN GO TO 24
00
2010 GO TO 2002
2100 PLOT INVERSE 1;X,Y: LET X=X
+1: GO TO 2001
2200 PLOT INVERSE 1;X,Y: LET X=X
-1: GO TO 2001
2300 PLOT INVERSE 1;X,Y: LET Y=Y
+1: GO TO 2001
2400 PLOT INVERSE 1;X,Y: LET Y=Y
-1: GO TO 2001
5000 STOP
```

APPENDIX 3

Homogeneous Dimer Equilibrium Case (Transport Model).

In the case of homogeneous dimer, $(MV^+)_2$, equilibrium with monomer MV^+, we can write:

$$D_{soln} \rightleftharpoons 2M_{soln} \qquad (A3.1)$$

Let the total number of moles generated per particle be C, where

$$C = 2D + M \qquad (A3.2)$$

As D and M is diffusing away in an expanding sphere of radius $\sim (D_o t)^{1/2}$ (from second law of Diffusion), then we have:

$$[M] + 2[D] \sim \frac{C}{(D_o t)^{3/2}} \qquad (A3.3)$$

Where D and M are dimer and monomer and D_o is diffusion coefficient. Here assumed $(D_o t)^{1/2} >> r_{particle}$.

By using equation (A3.1) we can write:

$$[D] = K[M]^2 \qquad (A3.4)$$

and we suppose that [D] << [M] and K is equilibrium constant.

We can also write:

$$OD_\infty = \frac{n_p \int_o^\infty 4\pi r^2 \varepsilon_M [M] dr}{V} = \frac{n_p \varepsilon_M C}{V} \qquad (A3.6)$$

We suppose that at t = 0 (at start) we have all dimers, then

$$OD_{max} = \frac{n_p \int_o^\infty 4\pi r^2 \varepsilon_D [D] dr}{V} = \frac{n_p \varepsilon_D C}{2V} \qquad (A3.7)$$

Equation A3.3 can be written as:

$$2 \int_o^\infty 4\pi r^2 [D] dr + \int_o^\infty 4\pi r^2 [M] dr = C \qquad (A3.8)$$

putting $[M] = [M]_\infty - 2[D]$ in equation (A3.5) yields

$$OD = \frac{n_p \varepsilon_M C}{V} + \frac{n_p (\varepsilon_D - 2\varepsilon_M)}{V} \int_o^\infty 4\pi r^2 [D] dr \qquad (A4.9)$$

Then

$$OD - OD_\infty = \frac{n_p (\varepsilon_D - 2\varepsilon_M)}{V} \int_o^\infty 4\pi r^2 [D] dr \qquad (A4.10)$$

and

$$OD_{max} - OD_\infty = \frac{n_p (\varepsilon_D - 2\varepsilon_M) C}{2V} \qquad (A4.11)$$

Dividing equation to (A4.10) gives:

$$y = \frac{OD - OD_\infty}{OD_{max} - OD_\infty} = \frac{2 \int_o^\infty 4\pi r^2 [D] dr}{C} \qquad (A4.12)$$

If the concentration of monomer around the particle supposed to be

$$[M] = \frac{C}{4\pi (D_o' t)^{3/2}} \qquad (A3.13)$$

then using equation (A4.4) we have

$$[D] = \frac{KC^2}{[4\pi (D_o' t)^{3/2}]^2} \qquad (A3.14)$$

where D_o' is diffusion coefficient in non-expanding sphere

$(D't)^{1/2} \perp\!\!\!\sim r_{particle}$.

Substitution of equation (A3.14) into (A3.12) gives

$$y = \frac{\frac{2}{3} KC}{4\pi(D_o't)^{3/2}} = \frac{0.7\ KC}{4\pi(D_o't)^{3/2}} \qquad (A3.15)$$

Full analytical treatment in case of $(D_o t)^{1/2} >> r_{particle}$ shows that

$$y = \frac{0.20\ KC}{4\pi(D_o t)^{3/2}} \qquad (A3.16)$$

Comparison of equation (A3.15) and (A3.16), and ploting log y against log t shows that the gradient is -1.5 and deviation occurs when $(D_o't)^{1/2} \sim r_{particle}$. This gives the radius of particle about 10^{-5}cm, while the radii of real particles measured by high resolution electron microscopy was about 10^{-7}cm. This appendix shows that the formation of dimer and its homogeneous equilibrium with monomer could be possible if the radius of particle were about 100 times bigger than that of measured. Therefore there is no dimer at equilibrium at all.

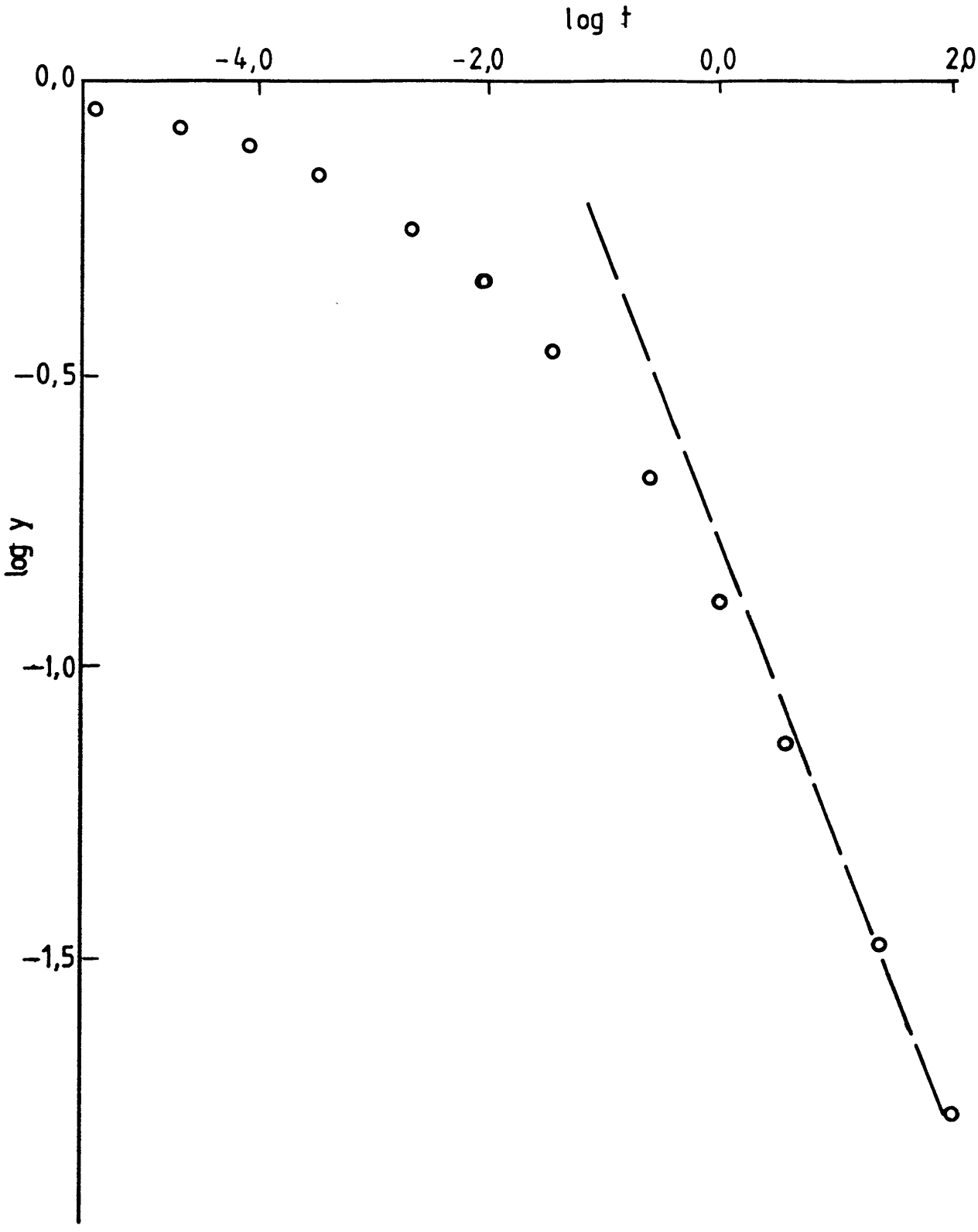


Fig. A 3.1

APPENDIX 4

Homogeneous Dimer Case

By using the 485nm and 605nm transient traces (Fig. 4.7) we can write

$$OD = \varepsilon_D[D] - \varepsilon_M[M] \qquad (A4.1) \qquad \text{for} \quad 485nm$$

and

$$OD' = \varepsilon'_D[D] + \varepsilon'_M[M] \qquad (A4.2) \qquad \text{for} \quad 605nm$$

It is assumed

$$2[D] + [M] = [M]_\infty \qquad (A4.3)$$

and

$$\varepsilon'_D[D] << \varepsilon'_M[M] \qquad (A4.4)$$

Therefore

$$\frac{[M]}{[M]_\infty} = \frac{OD'}{OD'_\infty} \qquad (A4.5)$$

and, from equation (A4.3)

$$\frac{[D]}{[M]_\infty} = \frac{1}{2}\left(1 - \frac{OD'}{OD'_\infty}\right) \qquad (A4.6)$$

Equation (A4.1) can be rewritten as

$$OD = \varepsilon_D[D] + OD_\infty \frac{[M]}{[M]_\infty} \qquad (A4.7)$$

Assuming that $OD_\infty = \varepsilon_M[M]_\infty$. Subtraction of equation (A4.5) from (A4.7) and using [D] from equation (A4.6) gives

$$\frac{OD}{OD_\infty} - \frac{OD'}{OD'_\infty} = \frac{\varepsilon_D [M]_\infty}{2OD_\infty} \left(1 - \frac{OD'}{OD_\infty}\right) \qquad (A4.8)$$

If the assumption of equation (A4.4) is not made, then we have

$$\frac{[M]}{[M]_\infty} = \frac{OD' - \varepsilon'_D [D]}{OD'_\infty} \qquad (A4.9)$$

and

$$\frac{[M]}{[M]_\infty} = \frac{1}{2} \left(1 - \frac{OD'}{OD'_\infty} + \frac{\varepsilon'_D [D]}{OD'_\infty}\right)$$

or

$$\frac{[D]}{[M]_\infty} \left(1 - \frac{1}{2} \frac{\varepsilon'_D}{\varepsilon'_M}\right) = \frac{1}{2} \left(1 - \frac{OD'}{OD'_\infty}\right)$$

or

$$\frac{[D]}{[M]_\infty} = \frac{\frac{1}{2} \left(1 - \frac{OD'}{OD'_\infty}\right)}{\left(1 - \frac{1}{2} \varepsilon'_D / \varepsilon'_M\right)} \qquad (A4.10)$$

From equation (A4.3) we have

$$\frac{[M]}{[M]_\infty} = 1 - \frac{2[D]}{[M]_\infty} \qquad (A4.11)$$

Substitution of equation (A4.10) into (A4.11) gives

$$\frac{[M]}{[M]_\infty} = 1 - \left(1 - \frac{OD'}{OD'_\infty}\right) / \left(1 - \frac{1}{2} \varepsilon'_D / \varepsilon'_M\right)$$

$$= \frac{\frac{OD'}{OD\infty} - \frac{1}{2} \frac{\varepsilon' D}{\varepsilon' M}}{1 - \frac{1}{2} \varepsilon'_D / \varepsilon'_M} \qquad (A4.12)$$

By substituting equations (A4.10) and (A4.12) into equation (A4.7) are obtained

$$\frac{OD}{OD_\infty} = \frac{\varepsilon_D}{2\varepsilon_M} \frac{(1-\frac{OD'}{OD'_\infty})}{(1-\frac{1}{2}\frac{\varepsilon'_D}{\varepsilon'_M})} + \frac{(\frac{OD'}{OD'_\infty} - \frac{1}{2}\frac{\varepsilon'_D}{\varepsilon'_M})}{(1-\frac{1}{2}\frac{\varepsilon'_D}{\varepsilon'_M})}$$

or

$$\frac{OD}{OD_\infty}(1-\frac{1}{2}\frac{\varepsilon'_D}{\varepsilon'_M}) - \frac{OD'}{OD'_\infty} = \frac{\varepsilon_D}{2\varepsilon_M}(1-\frac{OD'}{OD'_\infty}) - \frac{1}{2}\frac{\varepsilon'_M}{\varepsilon'_M}$$

$$\frac{OD}{OD_\infty} - \frac{OD'}{OD'_\infty} = \frac{\varepsilon_D}{2\varepsilon_M}(1-\frac{OD'}{OD'_\infty}) - \frac{1}{2}\frac{\varepsilon'_D}{\varepsilon'_M}(1-\frac{OD}{OD_\infty}) \qquad (A4.13)$$

Dividing both sides of equation (A4.13), by $(1- OD'/OD'_\infty)$ gives

$$\frac{\frac{OD}{OD\infty} - \frac{OD'}{OD'\infty}}{1-\frac{OD'}{OD'\infty}} = \frac{\varepsilon_D}{2\varepsilon_M} + \frac{\varepsilon'_D}{2\varepsilon'_M}\frac{\frac{OD}{OD\infty}-1}{1-\frac{OD'}{OD'\infty}}$$

or

$$Y = \frac{\varepsilon_D}{2\varepsilon_M} + \frac{\varepsilon'_D}{2\varepsilon'_M} X \qquad (A4.14)$$

A plot of Y against X for different concentrations of MV^{2+} is shown in Fig. A4.1. This figure shows that the data at all concentrations of MV^{2+} were well fitted by equation (A4.14). The slope in this figure is about one. That means

$$\frac{\varepsilon'_D}{2\varepsilon'_M} \sim 1 \qquad \text{or} \qquad \varepsilon_D' = 2\varepsilon_M'$$

As we know[81, 165] the extinction coefficient of dimer at 605nm should be less than that of its monomer ($\varepsilon'_D << \varepsilon'_M$). While our

calculation suggests convese. In this case we may say that the transients in Fig. 4.7 not belong to the equilibrium dimer case but belong to the desorption of dimer $(MV^{+})_2$, from the surface of CdS particle to the solution.

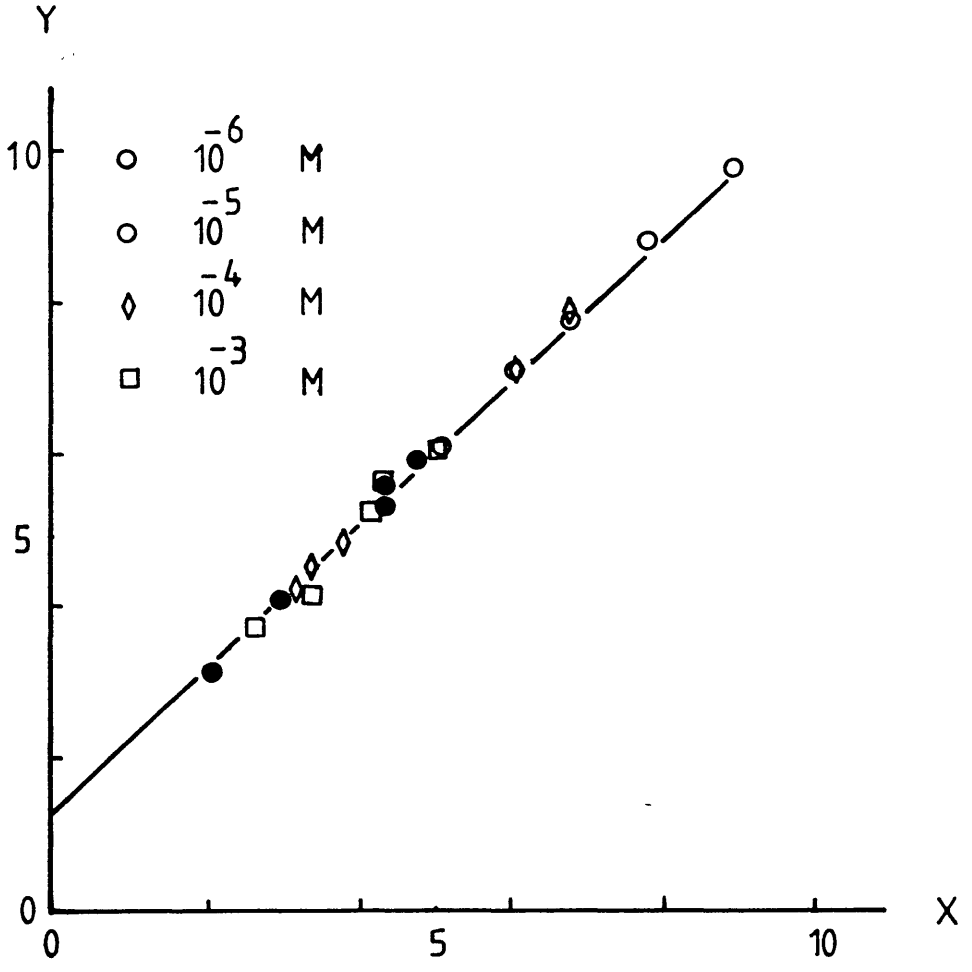


Fig. A4-1

APPENDIX 5

Calculation of the concentration of surface dimer, d_s.

By using the transient traces (Fig. 4.3) we can write

$$OD = \varepsilon_D d_s + OD_\infty \frac{m_s}{m_\infty} \qquad (A5.1)$$

where d_s and m_s are the surface concentrations of dimers and monomers respectively and m_∞ is the concentration of monomer at the end.

m_s can be written as

$$m_s = m_\infty - 2d_s \qquad (A5.2)$$

Substitution m_s in equation (A6.1) gives

$$OD = \varepsilon_D d_s + OD_\infty - 2d_s \varepsilon_M$$

or

$$d_s = \frac{(OD - OD_\infty)}{\varepsilon_{eff}} \qquad (A5.3)$$

where

$$\varepsilon_{eff} = 2\varepsilon_M \left(\frac{\varepsilon_D}{2\varepsilon_M} - 1\right) \quad \text{and} \quad \varepsilon_M = \frac{OD_\infty}{M_\infty}$$

REFERANCE

These papers are classified according to the subject:

a,b,c	represents the n-type semiconductors of CdS, TiO_2, ZnS respectively
P	indicates polymer
PPy	deals with polypyrrole
Q	means quantised effect due to small particle size
*	means H_2/O_2 evolution

Where more than one of these abbreviations are present, this indicates that more than one subject is dealt with in the paper.

1. Meinel, A.B., Meind, M.P. **Applied Solar Energy** - An Introduction (Reading, M.A.: Addison - Wesley Publishing Co. (1976).

2. Leheny, A.R., Rossetti, R., Brus, L.E. **J. Phys. Chem.** (1985), 89, 211.

3. Fendler, J.H. **J. Chem. Educ.** (1983), 60, 872

4. Gerischer, H., Bressel, B. **Ber. Bunsenges. Phys. Chem. Int. Ed. Engl.** (1979), 18, 624.

5. Lume-Percira, C., Baral, S., Henglein, A., Janata, E. **J. Phys. Chem.** (1985), 89, 5772.

6. Ibid, (1985), 89, 5779.

7. Darwent, J.R. **J. Chem. Soc. Chem. Commun.** (1982), 798.

8. Ebbesen, T.W. **J. Phys. Chem.** (1984), 88, 4131.

9. Fendler, J.H. **J. Phys. Chem.** (1985), 89, 2730.

10. Amougal, E., Grand, D., Moradpour, A., Keller, P. **Nouv. J. Chim.** (1982), 6, 241.

11. Kiwi, J., Gratzel, M. **Angew. Chem. Int. Ed. Engl.** (1979), 18, 624.

12. Henglein, A. Angew. Chem. Int. Ed. Engl. (1979), 18, 418.

13. Henglein, A. **J. Phys. Chem.** (1979), 83, 2209.

14. Henglein, A., Lilie, J. **J. Phys. Chem.** (1981), 85, 1246.

15. Chandrasekaran, K., Foreman, T.K., Whitten, D.G. **Nouv. J. Chim.** (1981), 5, 275.

16. Neumann-Spallart, M. **J. Chem. Soc. Faraday Trans 1** (1985), 81, 601.

17. Oswald, W.O., "Di Welt der Vernachlasslichten Dimensionen", 8th ed., Steinkopf, Dresden, Leipzig, (1922); translated by Fischer, M.H. as "**An Introduction to Theoretical and Applied Colloid Chemistry, The World of Neglected Dimensions**", 2nd ed. Wiley, New York, (1922).

18. Shaw, D.J. '**Introduction to Colloid and Surface Chemistry**' Third edition, Butterworths (1983).

19. Goodwin, J.W., Ed. "**Colloidal Dispersion**", Special Publication/Royal Society of Chemistry, Colloid-Congress (1982).

20. Laidler, K.J., Meiser, J.B. (editor) "**Physical Chemistry**" Chapter 13, The Benjamin/Cummings Publishing Co. Inc. (1982).

21. Weissberger, A. and Rossiter, B.W. (editors), **Physical Methods of Chemistry**, Vol. 1., Part 1-6 of **Techniques of Chemistry**, Wiley-Interscience (1971-1977).

22. Graham, Th, **Phil. Trans. Royal Soc.** (1811), 15, 183.

23. Faraday, M. **Phil. Trans. Royal Soc.** (1857), 147, 145.

24. La Mer, V.K., Barnes, M.D. **J. Colloid Sci.** (1946), 1, 71; La Mer, V.K. **J. Phys. Colloid Chem.** (1948), 52, 65, Sinclair, D, La Mer, V.K. **Chem. Revs.** (1949), 44, 245, La Mer, V.K., Gruen, R. **Trans. Faraday Soc.** (1952), 48, 410.

25. Matijeric, E. **Acc. Chem. Res.** (1981), 14, 22.

26. Ref. 18 Part 3 pp. 44-59.

27. Pusey, P.N. See Ref. 19 Part 6, pp. 129-142 and references therein.

28. Tyndall, J. **Phil Mag.** (1869), 37, 384.

29. Strutt, J.W. (Rayleigh, L), **Phil, Mag** (1871), 41, 447.

30. Mie, G. **Ann. Physik** (4), (1908), 25, 377.

31. Zimm, B.H. **J. Chem. Phys.** (1948), 16, 1093.

32. Holzer, A.M., Benoit, H. and Doty, P. **J. Phys. Chem.** (1954), 58, 624.

33. Cummins, H.Z. and Pike, E.R. eds. **Photon correlation spectroscopy and velocimetry.** NATO Advanced Study Institutes Series B: Plenum (1977).

34. Cummins, H.Z. and Pike, E.R. eds. "**Photon correlation and light beating spectroscopy**". NATO Advanced Study Institutes Series B: Plenum (1977).

35. Chu, B, "**Laser light scattering**", New York: Academic Press, (1974).

36. Chu, B, "**Dynamics of macromolecular solutions**" **Phys. Sci.** (1979), 19, 458.

37. Berne, B.J. and Pecorn, R. "**Dynamic light scattering**", New York: Wiley Interscience (1975).

38. Randle, K.J. **Chem. and Indust.** (1980), pp.74-81.

39. Helmholtz, H.L.F., **Wiss Abhandl. Physik Tech.** Reichsanstalt

(1879), 1, 925.

40. Gouy, G. J. Phys. (1910), 9, 457.

41. Chapman, D.L. Phil. Mag. (1913), 25, 475.

42. Stern, O. Z. Electrochem. (1924), 30, 508.

43. Tilselius, A. Novu Acta Reg. Soc. Sci. Upsaliensis, 7 No. 4 (1930), Trans. Faraday Soc., (1937), 33, 524.

44. Albery, W.J., Bartlett, P.N., Wildes, C.P., Darwent, J.R.

J. Am. Chem. Soc., Faraday Trans. 1, (1985), 107, 1859.

a) CdS

45. Albery, W.J., Brown, G.T., Darwent, J.R., Saievar-Iranizad, E. J. Chem. Soc. Faraday, Trans. 1. (1985), 81, 1999.

46. Albery, W.J., Bartlett, P.N., Porter, J.D. J. Electrochem. Soc. (1984), 131, 2892.

47. ibid, (1984), 131, 2896.

48. Rossetti, R., Beck, S.M., Brus, L.E. J. Am. Chem. Soc. (1984), 106, 980.

49. Rossetti, R., Brus, L.E. J. Phys. Chem. (1986), 90, 558.

50. Rossetti, R., Brus, L.E. J. Phys. Chem. (1982), 86, 4470.

51. Borgarello, E., Ramseden, J., Grätzel, M. Helv. Chim. Acta (1983), 66, 1827.

52. Dounghong, D., Ramseden, J., Grätzel, M. J. Am. Chem. Soc. (1982), 104, 2977.

53. Ramseden, J. Grätzel, M. J. Chem. Soc., Faraday Trans. 1, (1984), 80, 919.

54. Ramseden, J., Webber, S.E., Grätzel, M. J. Phys. Chem. (1985), 89, 2740.

55. Grätzel, M., Frank, A.J. J. Phys. Chem. (1982), 86, 2964.

56. Henglein, A. Bor. Bunsenges. Phys. Chem. (1982), 86, 301.

57. Gutierrez, M., Henglein, A. Ber. Bunsenges. Phys. Chim. (1983), 87, 474.

58. Henglein, A., Gutierrez, M. Ber. Bunsenges. Phys. Chim.

(1983), 87, 852.

59. Alfassi, Z., Bahnemann, D., Henglein, A. J. Phys. Chem. (1982), 86, 4656.

60. Henglein, A. Pure and Appl. Chem. (1984), 56, 1215.

61. Kuczynski, J., Thomas, J.K. Chem. Phys. Lett (1982), 88, 445.

62. Kuczynski, J., Milosavijevic, B.H., Thomas, J.K. J. Phys. Chem. (1983), 87, 3368.

63. Kuczynski, J., Thomas, J.K. J. Phys. Chem. (1983), 87, 5498.

64. Metcalfe, K., Hester, R.E. J. Chem. Soc. Chem. Commun. (1983), 133.

65. Evenor, M., Gottesfeld, S., Harzion, Z., Huppert, D., Feldberg, S.W. J. Phys. Chem. (1984), 88, 6213.

a*) CdS

66. Tricot, Y-M., Emeren, A., Fendler, J.H. J. Phys. Chem. (1985), 89, 4721.

67. Rafaeloft, R., Tricot, Y.-M., Nome, F., Tundo, P., Fendler, J.H. J. Phys. Chem. (1985), 89, 1236.

68. Rafaeloff, R., Tricot, Y.-M., Nome, F., Fendler, J.H. J. Phys. Chem. (1985), 89, 533.

*

69. Meyer, M., Wallberg, C., Kurihara, K., Fendler, J.H. J. Chem. Soc. Chem. Commun. (1984), 90.

70. Tricot, Y.-M., Fendler, J.H. J. Am. Chem. Soc. (1984), 106, 7359.

71. Gratzel, M. Acc. Chem. Res. (1981), 14, 376.

72. Kalyansundaram, K., Borgarello, E., Duonghong, D., Gratzel, M. Angew. Chem. Int. Ed. Engl. (1981), 20, 987.

73. Kalyansundaram, K., Borgarello, E., Gratzel, M. Helv. Chim. Acta (1981), 64, 362.

74. Borgarello, E., Kalyansundaram, K., Gratzel, M. Helv. Chim. Acta (1982), 65, 243.

*

75. Henglein, A. J. Phys. Chem. (1982), 86, 2291.

b) TiO_2

76. Brown, G.T., Darwent, J.R. J. Chem. Soc. Chem. Commun. (1985), 98.

77. Brown, G.T., Darwent, J.R. J. Chem. Soc. Faraday Trans. 1, (1984), 80, 1631.

78. Brown, G.T., Darwent, J.R. J. Phys. Chem. (1984), 88, 4955.

79. Duonghong, D., Serpone, N., Gratzel, M. Helv. Chim. Acta (1984), 67, 1012.

80. Moser, J., Gratzel, M. J. Am. Chem. Soc. (1984), 106, 6557.

81. Nakahira, T., Gratzel, M. J. Phys. Chem. (1984), 88, 4006.

82. Moser, J., Gratzel, M. J. Am. Chem. Soc. (1983), 105, 6547.

83. Henglein, A. Ber Bunsenges. Phys. Chem. (1982), 86, 241.

84. Bahnemann, D., Henglein, A., Lilie, J., Spanhel, L. J. Phys. Chem. (1984), 88, 709.

85. Kamat, D.V. J. Chem. Soc., Faraday Trans. 1, (1985), 81, 509.

86. Kamat, D.V. J. Photochem (1985), 28, 513.

87. Kamat, D.V. Langmuir, (1985), 1, 608.

b*) TiO_2

88. Cuendel, P., Gratzel, M. J. Am. Chem. Soc. (1983), 105, 6547.

89. Duonghong, D. Borgarello, E., Gratzel, M. J. Am. Chem. Soc. (1981), 103, 4685.

90. Furlong, D.N., Wells, D., Sasse, W.H.F. J. Phys. Chem. (1985), 89, 1922.

91. Myamlin, V.A., Pleskov, Y.V. "Electrochemistry of Semiconductors", Plenum Press, New York (1967).

92. Schokleg, W. "Electrons and Holes in Semiconductors", D. Van Nostrand, Princeton, N.J. (1950).

93. Gerischer, H. **Adv. Electrochem. Electrochem. Engs.** (1961), 1, 139.

94. Gerischer, H. in "**Physical Chemistry - An Advanced Treatise**", Vol. IXA, Eyring, H., Henderson, D., Jost, W. Eds. Academic Press, New York, (1970), p. 463.

95. Memming, R. in "**Topics in Surface Chemistry**", ed. by Kay E., Bayus, P.S. Plenum Press, New York (1978).

96. Vetter, K.J. "**Electrochemical Kinetics**", p. 73, Academic Press, New York, (1967).

97. Albery, W.J., Bartlett, P.N. **J. Electrochem. Soc.** (1984), 131, 2892.

98. Memming, R. in "**Electroanals Chem. Adv. Series**", Bard, A.J. (ed) Marcel Oekker, New York, (1976), 11, 1.

99. Butler, M.A., Ginley, D.S. In "**Semiconductor Liquid-Junction Solar Cells, Proceedings of Conference on Electrochemistry and Physics of Semiconductor-Liquid Interfaces Under Illumination, Airlie, Va.**" ed. Heller, A. **Electrochem. Soc.** Princeton, N.J. (1977), pp. 290-93.

100. Sanderson, R.T. "**Chemical Periodicity**", New York, Reintold (1960). pp. 37-38.

101. Nethercot, A.H. **Phys. Rev. Lett** (1974), 33, 1088.

102. Sze, S.M. "**Physics of Semiconductors Devices**, New York, Wiley, (1980), pp. ....

103. McCaldin, J.O., McGill, T.C. In "**Electrochem. Soc. Monogs. Thin Film Interdfissuion and Interfacial Reactions**", ed. by Poate, J. New York, Wiley-Intersci (1977).

104. Gomes, W.P., Cardon, F. (1977). See ref. 99, pp. 120-31.

105. Watanabe, T., Fujishima, A., Tatsuoki, O., Honda, K. **Bull Chem. Soc. Jpn** (1976), 49, 8.

106. "**Solar Power and Fuels**", Bolton, J.R. (ed), Academic Press, N.Y. (1977).

107. "**Solar Energy: Chemical Conversion and Storage**", Hautala, R.R. King, R.B., Kutal, C. (eds), Humana Press, Clifton, N.J. (1979).

108. "**Photochemical Conversion and Storage of Solar Energy**", Connolly, J.S. (ed). Academic Press, N.Y. (1981).

109. "**Photoelectrochemistry, Photocatalysis and Photoreactors**", Schiavello, N. (ed)., D. Reidal Publishing Co., Holland (1984).

110. "Energy Resources Through Photochemistry and Catalysis", Gratzel, M. (ed)., Academic Press, N.Y. (1983).

111. "Photogeneration of Hydrogen", Harrison, A., West. M. (eds)., Academic Press, London (1982).

112. "Solar Hydrogen Energy Systems", Ohta, T. (ed)., Pergamon Press, U.K. (1979).

113. "Photochem. Convers. Storage Sol. Energy (Proc. III, Int. Conf), Connolly, J.S. (ed), Academic Press, N.Y. (1981).

114. Kiwi, J., Kalyansundaram, K., Gratzel, M. Struc. and Bonding. (1981), 49, 37.

115. Borgarella, E., Kiwi, J., Pelizetti, E., Visca, M., Gratzel, M. J. Am. Chem. Soc., (1981), 103, 6324, ibid, (1982), 104, 2996.

116. Yesodharan, E., Gratzel, M. Helv. Chem. Acta. (1983), 66, 2145.

117. Mills, A., Porter, G. J. Chem. Soc. Faraday Trans. 1. (1982), 78, 3659.

118. Blondeel, G., Harriman, A., Williams, D. Solar Energy Mater.,(1983), 9, 217.

119. Lehn, J.-M., Sauvage, J.-P., Ziessel, R. Nouv. J. Chim. (1984), 4, 623.

120. Maggliozu, R., Krasna, A.I. Photochem. Photobiol. (1983), 38, 15.

121. Mette, H., Otoves, J.W., Calvin, M. Solar Energy Mater (1981), 4, 443, Domen, K., Naito, S., Onishi, T., Tamaru, K. Chem. Phys. Lett. (1982), 94, 433.

122. Albery, W.J., Bartlett, P.N. J. Electroanal. Chem. (1982), 139 57.

123. Albery, W.J. Acc. Chem. Res. (1982), 15, 142.

124. Kalyansundaram, K., Kiwi, J., Gratzel, M. Helv. Chim. Acta (1978), 61, 2720.

125. Kiwi, J., Gratzel, M. J. Am. Chem. Soc. (1979), 101, 7219.

126. Loferski, J.J. J. Appl. Phys., (1956), 27, 277.

127. Archer, M.D. J. Appl. Electrochem, (1975), 5, 17.

128. Archer, M.D. Solar Energy, (1978), 20, 167.

129. Bolton, J.R. **Solar Energy**, (1978), 20, 181.

130. Mathews, C.D. **J. Appl. Phys.** (1977), 48, 3181.

131. Scharf, H.D., Fleischhouer, J., Leismann, H., Ressler, I., Schleker, W.,Weitz, R., **Angew. Chem. Int. Ed. Engl.** (1979), 18, 652.

132. Thekaekara, M.P., **Supplement to Proc. 20th Annual Meeting of Inst. Environ. Sci.**, (1974), 21.

133. Gerischer, H. In **"Photovoltaic and Photoelectrochemical Solar Energy Conversion"** (eds Cardon, F., Gomes, W.P., Dekeyser) Nato Advanced Study Inst. Series B.69, Plenum Press, N.Y. (1980), pp. 190-261.

134. Memming, R. **Electrochemical Acta** (1980), 77.

135. Nozik, A.J. See ref. 54 (1977), pp.272-89.

136. Porter, G. **Disc. Faraday. Soc.**, (1950), 9, 60.

137. Darwent, J.R. **J. Chem. Soc., Faraday Trans. 1** (1984), 80, 183.

138. Mills, A. **J. Chem. Soc. Chem. Commun.** (1982), 367.

139. Wilde, C.P. **PhD Thesis** (1985), Imperial College, London.

140. FSA Laboratory Supplies, Loughborough Leics., U.K.

141. Butler, M.A. **J. Appl. Phys.** (1977), 48, 1914.

142. Streckert, H., Tony, J., Carpenter, M., Ellis, A. **J. Electrochem. Soc.** (1982), 129, 772.

143. Kuczynski, J., Thomas, J.K. **J. Phys. Chem.** (1985), 89, 2720.

144. Smith, R.A. **"Semiconductors"**, 2nd ed., Cambridge Press London (1979), 2720.

145. Frank, S.N., Bard, A.J. **J. Phys. Chem.** (1977), 81, 1484.

146. Izumi, I., Fan, F.F., Bard, A.J. **ibid.** (1981), 85, 218.

147. Gerischer, H. **J. Chem. Soc. Faraday Discuss.** (1981), 70, 137.

148. Bard, A., Wrighton, M. **J. Electrochem. Soc.** (1977), 124, 1706.

149. Streeman, D.G. **"Solid State Electronic Devices"**

(Prentice-Hall, Inc), (1980).

150. Van der Zeil, A. "Solid State Physical Electronics" (Prentice-Hall, Inc) (1968).

151. Kuczynski, J.P., Milosavljevic, B.H., Thomas, J.K. J. Phys. Chem. (1984), 88, 980.

152. Thomas, J.K. Chem. Rev. (1980), 80, 283.

153. Albery, W.J., Calvo, E.J. J. Chem. Soc. Faraday Trans. 1., (1983), 79, 2583.

154. Prybyla, S., Struve, W.S., Parkinson, B.A. J. Electrochem. Soc. (1984), 131, 1587.

155. Weller, H., Koch, U., Guttierrez, M., Henglein, A. Ber. Bunsenges. Phys. Chem. (1984), 88, 649.

156. Koppel, D.E. J. Chem. Phys. (1972), 57, 4814.

157. Brown, J.C. Pusey, P.N., Dietz, R. J. Chem. Phys. (1975), 62 1136.

158. Robinson, R.A., Stokes, R.H. "Electrolyte Solutions" (Butterworths, London, 1959), p.12.

159. Darwent, J.R., Porter, G. J. Chem. Soc., Chem. Commun. (1981), 145.

160. Darwent, J.R. J. Chem. Soc., Faraday Trans. 2. (1981), 77, 1703.

161. Harbour, J.R., Hair, M.L. J. Phys. Chem. (1977), 81, 1791.

162. Watanabe, T., Fujishima, A., Tatsouki, O., Honda, K., Bull. Chem. Soc. Japan (1976), 49, 8.

163. Brown, G.T., Darwent, J.R., Fletcher, P.D.I. J. Am. Chem. Soc. (1985), 107, 23.

164. Darwent, J.R. J. Chem. Soc. Faraday Trans. 1, (1984), 80, 183.

165. Kosower, E.M.; Cotter,J.L. J. Am. Chem. Soc. (1964), 86, 5524.

166. Henglein, A. J. Phys. Chem. (1982), 86, 2291.

167. - 169. Have not been used in the text.

c) ZnS

170. Tributsch, H., Bennett, J.C. J. Chem. Tech. Biotechnol. (1981), 31, 565.

171. Platz, H., Schenk, P.W. Angew. Chem. (1936), 49, 822.

172. Gloor, K. Helv. Chim. Acta (1937), 20, 853.

173. Bücheler, J., Zeug, N., Kisch, H. Angew. Chem. Int. Ed. Engl. (1982), 21, 783.

174. Becker, W.G., Bard, A.J. J. Phys. Chem. (1983), 87, 4888.

175. Bryant, F.J., Hogg, J.H.C., Faffery, P.R. J. Phys. Chem. Solids (1983), 44, 595.

176. Wilhelmy, D.M., Matiievic, E. J. Chem. Soc., Faraday Trans. 1. (1984), 80, 563.

177. Weller, H., Koch, U., Gutierrez, M., Henglein, A. Ber. Bunsenges. Phys. Chem. (1984), 88, 649.

178. Henglein, A., Gutierrez, M. Fischer, Ch.-H., Ber Bunsenges. Phys. Chem. (1984), 88, 170.

179. Bücheler, J., Kisch, H. J. Am Chem. Soc. (1985), 107, 1459.

180. Kakuta, N., Park, K.H., Finlayson, M.F., Ueno, A., Bard, A.J., Campion, A., Fox, M.A., Webber, S.E. J. Phys. Chem. (1985), 89, 732.

181. Enea, O., Bard, A.J. J. Phys. Chem. (1986), 90, 301.

182. Yanagida, S., Azuma, T., Sakurai, H. Chem. Lett. (1982), 1069.

183. Curie, D., "Luminescence in Crystals", Methuen, London (1963), Chapt. 4 and 5.

184. Curie, D., Prener, J.J. in "Physics and Chemistry of II-VI Compounds", pp. 434-485 eds. Aven, M., Prener, J.J. North Holland Publishing Company, Amsterdam, (1967).

185. Shionoya, S. in "Luminescence of Inorganic Solids", Goldberg, P.G. Ed., Academic Press, N.Y., Chapter 4 (1966).

186. Henglein, A. J. Phys. Chem. (1982), 86, 2291.

187. Harbour,m J.R., Wolkow, R., Hair, M.L. J. Phys. Chem. (1981), 85, 4026.

188. Henglein, A., Lindig, B., Westerhausen, J. J. Phys. Chem. (1981), 85, 1627.

189. Uchida, I. J. Phys. Soc. Jpn. (1964), 19, 670.

190. Hoshina, T., Kawai, H. Jpn. J. Appl. Phys. (1980), 19, 267.

191. Reber, J.-F., Meier, K. J. Phys. Chem. (1984), 88, 5903.

*

192. Fox, M.A. Ed. "Organic Phototransformations in Non-homogeneous Media", American Chemical Society, Washington DC, (1985), ACS Symp. Ser. No. 278.

193. Enea, O., Bard, A.J. J. Phys. Chem. (1986), 90, 301.

194. Nozaka, Y., Fox, M.A. J. Phys. Chem. (1986), 90, 6521.

195. Furlong, D.N., Grieser, F., Hayes, D., Sasse, W., Wells, D. J. Phys. Chem. (1986), 90, 2388.

196. Tricot, Y.-M., Fendler, J.H. J. Phys. Chem. (1986), 90, 3369.

197. Young, H.-C., Tricot, Y.-M., Fendler, J.H. J. Phys. Chem. (1987), 91, 581.

198. Kamat, P.V., Dimitrijevic, N.M., Fessenden, R.W. J. Phys. Chem. (1987), 91, 396.

Q) Quantised effect

199. Rossetti, R., Nakahara, S., Brus, L.E. J. Chem. Phys. (1983), 79, 1086.

200. Brus, L.E. J. Chem. Phys. (1983), 79, 5566.

201. Brus, L.E. J. Chem. Phys. (1984), 80, 4403.

202. Rossetti, R., Ellison, J.L., Gibson, J.M., Brus, L.E. J. Chem. Phys. (1984), 80, 4464.

203. Rossetti, R., Hull, R., Gibson, J.M., Brus, L.E. J. Chem. Phys. (1985), 82, 552.

204. Chestony, N., Harris, T.D., Hull, R., Brus, L.E. J. Phys. Chem. (1986), 90, 33.

205. Chestony, N., Hull, R., Brus, L.E. J. Chem. Phys. (1986), 85, 2237.

206. Fojtik, A., Weller, H., Koch, U., Henglein, A. Ber. Bunsenyes. Phys. Chem. (1984), 88, 969.

207. Baral, S., Fojtik, A., Weller, H., Henglein, A. J. Am. Chem. Soc. (1986), 108, 375.

208. Weler, H., Schmidt, H.M., Koch, U., Fojtik, A., Baral, S., Henglein, A., Kunath, W., Weiss, K., Deman, E. Chem. Phys. Lett, (1986), 124, 557.

209. Nozik, A.J., Williams, F., Nenadovic, M.T., Rajh, T., Micic, O.I. J. Phys. Chem. (1985), 89, 397.

210. Nedeljkovic, J.M., Nenadoric, M.T., Micic, O.I., Nozik, A.J. J. Phys. Chem. (1986), 90, 12.

211. Ramsden, J.J., Webber, S.E., Gratzel, M. J. Phys. Chem. (1985), 89, 2740.

212. Fox, M.A. Acc. Chem. Res. (1983), 16, 314.

213. Ekimov, A.I., Onushchenko, A.A. JETP Lett (Engl. Transl) (1984), 40, 1137.

214. Sandroff, C.J., Hwang, D.M., Chung, W.M. Phys. Rev. B. Condens. Matter (1986), 33, 5953.

215. Wang, Y., Herron, N. J. Phys. Chem. (1987), 91, 257.

P) Polymer

216. Krishnan, M., White, J.R., Fox, M.A., Bard, A.J. J. Am. Chem. Soc. (1983), 105, 7002.

217. Meissner, D., Memming, R., Kastening, B. Chem. Phys. Lett. (1983), 96, 34.

218. Fendler, J.H. "Membrane mimetic chemistry", Wiley Interscience, N.Y. (1982).

219. Fendler, J.H. Chem. Eng. News. (1984), 62, 25.

220. Kakuta, N., white, J.M., Campion, A., Bard, A.J., Fox, M.A., Webber, S.E. J. Phys. Chem. (1985), 89, 48.

221. Mau, A. W.-H., Huang, C.-B., Kakuta, N., Bard, A.J., Campion, A., Fox, M.A., White, J.M., Webber, S.E. J. Am. Chem. Soc., (1984), 106, 6537.

222. Tricot, Y.M., Fendler, J.H. J. Am. Chem. Soc. (1984), 106, 2475.

223. Tricot, Y.M., Emeren, A., Fendler, J.A. J. Phys. Chem.

(1985), 89, 4721.

224. Watzke, H.J., Fendler, J.H. J. Phys. Chem. (1987), 91, 854.

225. Kakuta, N., Park, K.H., Finlayson, M.F., Bard, A.J., Campion, A., Fox, M.A., Webber, S.E., White, J.M. J. Phys. Chem. (1985), 89, 5028.

226. Lopes, M., Kipling, B., Yeager, H.L. Anal. Chem. (1976), 48, 1120.

227. Yeo, R.S. Polymer (1980), 21, 432.

228. Serpone, N., Sharma, D.K., Gratzel, M., Ramseden, J. Chem. Phys. Lett. (1985), 115, 473.

229. Lee, P.C., Meisel, D. J. Am. Chem. Soc. (1980), 102, 5477.

230. Moser, J., Gratzel, M. Helv. Chim. Acta (1982), 65, 1436.

231. Calderbank, A., Charlton, D.F., Farrington, J.A., James, R., J. Chem. Soc., Perkin Trans. (1972), 1, 138.

232. Henglein, A., Fojtik, A., Weller, H. Ber. Bunsenges. Phys. Chem. (1987), 91, 441.

233. Henglein, A. Pure Appl. Chem. (1984), 56, 1215.

234. Meissner, D., Memming, R., Kastening, B., Bahnemann, D. Chem Phys. Lett. (1986), 127, 419.

235. Weller, H., Fojtik, A., Henglein, A. Chem. Phys. Lett, (1985), 117 485.

236. Darwent, J.R., Lepre, A. J. Chem. Soc. Faraday Trans 2, (1986), 82, 1457.

237. Griffiths, J. Chem. Soc. Rev. (1972), 1, 481.

238. Laitinen, H.A., Boyer, K.W. Anal. Chem. (1972), 44, 920.

239. Gorner, H., Gruen, H., Schulte-Frohlinde, D. J. Phys. Chem. (1980), 84, 3031.

240. Albery, W.J. Hillman, A.R. Chem. Soc. Annu. Rep. C. (1981), 377.

PPy) POlypyrrol

241. Noufi, R., Frank, A.J., Nozik, A.J. J. Am. Chem. Soc. (1981), 103, 1849.

242. Cooper, G., Noufi, R., Frank, A.J., Nozik, A.J. Nature

(London) (1982), 295, 578.

243. Noufi, R., Tench, D., Warren, L.F. J. Electrochem. Soc. (1980), 127, 2310.

244. Noufi, R., Tench, D., Warren, L.F. ibid (1981), 128, 2596.

245. Skotheim, T., Lundstrom, I., Prejza, J. J. Electrochem. Soc. (1981), 128, 1625.

246. Skotheim, T., Lundstrom, I., Delahoy, A.E., Kampas, F.J., Vanier, P.E. Appl. Phys. Lett. (1982), 40, 281.

247. Fan, F-.R.F., Wheeler, B.L., Bard, A.J., Noufi, R. J. Electrochem. Soc. (1981), 128, 2042.

248. Simon, Q.A., Ricco, A.J., Wrighton, M.S. J. Am. Chem. Soc. (1982), 104, 2031.

249. Frank, A.J., Honda, K. J. Phys. Chem. (1982), 86, 1933.

250. Labes, M.M., Love, P., Nichol, L.F. Chem. Rev. (1979), 7, 79.

251. Mac Diarmid, A.G., Heeger, A.J. Proceedings of the NATO ASI on Molecular Metals, Les Arcs, France, (1979), Plenum Press.

252. Dall'Olio, A., Dascola, Y., Varacca, V., Bocchi, C.R. Acad. Sci. Ser. C, (1968), 267, 433.

253. Gardini, G.P. Adv. Heterocycl. Chem. (1973), 15, 67.

254. Jones, R.A., Been, G.P. The Chemistry of Pyrroles, Academic Press, San Francisco, (1977).

255. Diaz, A.F., Kanazawa, K.K. J.C.S. Chem. Comm. (1979), 635.

256. Kanazawa, K.K., Diaz, A.F., Geiss, R.H., Gill, W.D., Kwak, J.F., Logan, J.A., Rabol, J.F., Street, G.B. ibid (1979), 854.

257. Kanazawa, K.K., Diaz, A.F., Gill, W.D., Grant, P.M., Street, G.B., Gardini, G.P., Kwak, J.K. Synth. Met. (1979/80), 1 329.

258. Diaz, A.F., Logan, J.A. J. Electrochem. Chem. (1980), 111 111.

259. Diaz, A.F., Castillo, J.I. J.C.S. Chem. Comm. (1980), 397.

260. Diaz, A.F. Chem. Scripta, (1981), 17, 145.

261. Diaz, A.F., Martinez, A., Kanazawa, K.K., Salmon, M. J. Electroanal. Chem. (1981), 129, 115.

262. Bull, R.A., Fan. F., Bard, A.J. J. Electrochem. Soc. (1982), 129, 1009.

263. Salmon, M., Diaz, A.F., Logan, A.J., Krounbi, M., Bargon, J. **Mol. Cryst.** (1982), 83, 265.

264. Kanazawa, K.K., Diaz, A.F., Krounbi, M., Salmon, M. J. **Polymer Sci. Polymer Lett.** (1982), 20, 187.

265. Wynne, K.J., Street, J.B. **Ind. Eng. Chem. Prod. Res. Rev.** (1982), 21, 23.

266. Genies, E.M., Bidan, G., Diaz, A.F. **J. Eklectroanal. Chem.** (1983), 149, 101.

267. Kaneto, K., Yoshino, K., Inuishi, Y. **Jap. Appl. Phys.** (1983), 22, L412.

268. Diaz, A.F., Hall, B. **IBM Res. Dev.** (1983), 27, 342.

269. Santhanam, K.S.V., O'Brien, R.N. **J. Electroanal. Chem.** (1984), 160, 377.

270. Mengoli, G., Musiani, M.M., Fleischmann, Pletcher, D. **J. Appl. Electroanal. Chem.** (1984), 14, 285.

271. Honda, K., Frank, A. **J. Phys. Chem.** (1984), 88, 5577.

272. Asavapiriyanont, S., Chandler, G.K., Gunawardena, G.A., Pletcher, D. **J. Electroanal. Chem.** (1984), 117, 229, **ibid**, (1984), 117, 245.

273. Albery, W.J., Jones, C.C., **Faraday Discuss. Chem Soc.** (1984), 78, 193.

274. Genies, E.M., Pernant, J.M. **J. Electroanal. Chem.** (1985), 191, 111.

275. Kaneko, M., Okuzumi, K., Yamada, A. **J. Electroanal. Chem.** (1985), 183, 407.

276. Bredas, J.L., Street, G.B., Themans, B., Andre, J.M. **J. Chem. Phys.** (1985), 83, 1323.

277. Rosenthal, M.V., Skotheim, T., Warren, J. **J. Chem. Soc. Chem. Commun.** (1985), 342.

278. Yanagida, S., Kabumoto, A., Mizumoto, K., Pac, C., Yoshino, K., **Ibid** (1985), 474.

279. Skotheim, T., Rosenthal, M.V., Linkous, C.A. **Ibid.** (1985), 612.

280. Villemin, D. **Ibid** (1985), 870.

281. Mizutani, F., Iijima, S.-I., Tanabe, Y., Tsuda, K. **Ibid**,

(1985), 1728.

282. Audebert, P., Bidan, G., Lapkowski, M. Ibid (1986), 887.

283. Saraceno, R.A., Pack, J.G. Ewing, A.G. J. Electroanal. Chem. (1986), 197, 265.

284. Foos, J.S., Erker, S.M. J. Electrochem. Accelerated Brief Commun. (1986), 1983.

285. Nagasubramanian, G., Di-Stefano, S., Moacanin, J. J. Electrochem. Soc. (1986), 133, 305.

286. Mohammadi, A., Inganas, O., Lundstrom, I. Ibid, (1986), 133 947.

287. Compton, R.G., Day, M.J., Ledworth, A., Abu-Abdounc, I.I. J. Chem. Soc. Chem. Commun. (1986), 328.

288. Hamnett, A., Hillman, A.R., Ber. Bunsenges. Phys. Chem. (1987), 91, 329.

289. Gningue, D., Horowitz, G., Garnier, F. Ibid, (1987), 91, 402.

290. Hagemeister, M.P., White, H.S. J. Phys. Chem. (1987), 91, 150.

291. Brown, A.P., Koval, C., Anson, F.C. J. Electroanal. Chem. (1976, 72, 379.

292. Hagal, J.H. J. Electroanal. Chem. (1980), 109, 389.

293. Merz, A., Bard, A.J. J. Am. Chem. Soc. (1978), 100, 3222.

294. Oyama, N., Anson, F.C. J. Am. Chem. Soc. (1979), 101, 739.

295. Abruna, H.D., Denisevich, P., Umana, M., Meyer, T.J., Murray, R.W. J. Am. Chem. Soc. (1981), 103, 1.

296. Daum, P., Murray, R.W. J. Phys. Chem. (1981), 85, 389.

297. Peerce, P.J., Bard, A.J. J. Electroanal. Chem. (1980), 114, 89.

298. Bard, A.J. J. Chem. Educ. (1983), 60, 302.

299. Kittelesen, G.P., White, H.S., Wrighton, M.S. J. Am. Chem. Soc. (1984), 106, 7389.

300. Sammells, A.F., Ang. P.G.P. J. Electrochimi Soc. (1984), 131, 617.

301. Sammells, A.F., Schmidt, S.R. J. Electrochemi. Soc. (1985), 132, 520.

302. Cooke, R.L., Sammells, A.F. **Ibid** (1985), 132 2429.

303. Skotheim, T.A., Inganas, O. **Ibid** (1985), 132, 2116.

304. Nigery, P.S. Mac Innes, Jr., Nairns, D.P., MacDiarmid, A.G., Heeger, A.J. **J. Electrochem.** (1981), 128, 1651.

305. Chiang, C.K. **Polymer**, (1981), 22, 1454.

306. Beck, F., Drub, A. **Electrochim. Acta**, (1983), 28, 1847.

307. Kaneto, K., Yoshino, K., Inuishi, Y. **Jpn. J. Appl. Phys.** (1983), 22, L567.

308. Farrington, G.C., Scrosati, B., Frydrych, D., De Nuzzio, J. **J. ElectroChem.** (1984), 131, 7.

309. Matsuda, Y., Morita, M., Katsuma, H. **Ibid**, (1984), 131, 104.

310. Chein, J.C.W., Schlenoff, J.B. **Nature**, (1984), 311 362.

311. Murray, R.W., Pickup, P.G., Kuo, K.N. **J. Electrochem. Soc.** (1983), 130, 2205.

312. Tourillon, G., Dartyge, E., Dexport, H., Fontaine, A., Jucha, A., Legarde, P., Sayers. D.E. **J. Electroanal. Chem.** (1984), 178, 357.

313. Tourillon, G., Garnier, F. **J. Phys. Chem.** (1984), 88, 5281.